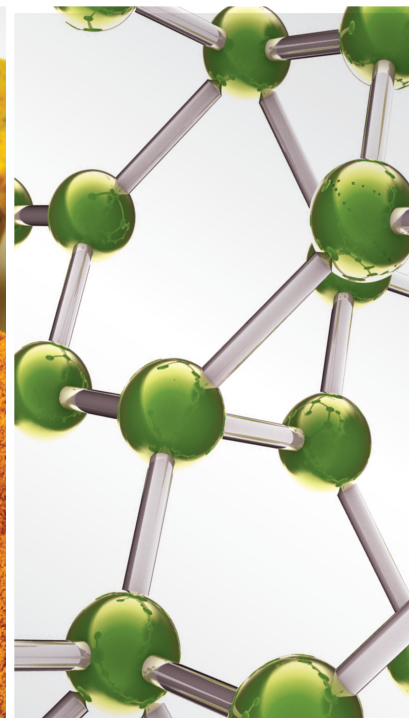
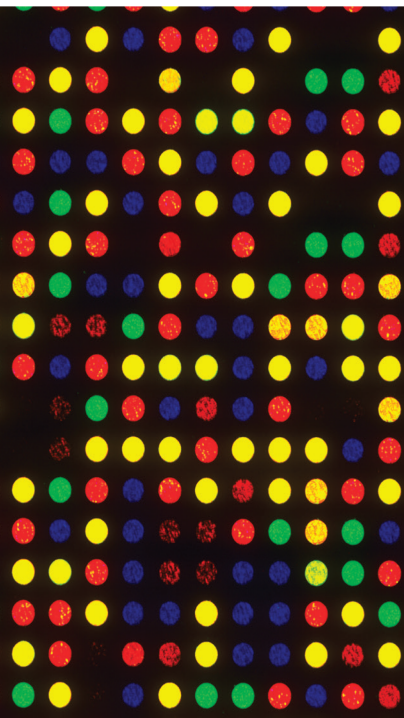


Complementary and Alternative Medicine for Liver Fibrosis

Lead Guest Editor: Chan#Yen Kuo

Guest Editors: Chih-Yuan Ko and Chih-Wei Chou





Complementary and Alternative Medicine for Liver Fibrosis

Evidence-Based Complementary and Alternative Medicine

Complementary and Alternative Medicine for Liver Fibrosis

Lead Guest Editor: Chan#Yen Kuo

Guest Editors: Chih-Yuan Ko and Chih-Wei Chou



Copyright © 2021 Hindawi Limited. All rights reserved.

This is a special issue published in "Evidence-Based Complementary and Alternative Medicine." All articles are open access articles distributed under the Creative Commons Attribution License, which permits unrestricted use, distribution, and reproduction in any medium, provided the original work is properly cited.

Chief Editor

Jian-Li Gao , China






Associate Editors

Hyunsu Bae , Republic of Korea
Raffaele Capasso , Italy
Jae Youl Cho , Republic of Korea
Caigan Du , Canada
Yuewen Gong , Canada
Hai-dong Guo , China
Kuzhuvelil B. Harikumar , India
Ching-Liang Hsieh , Taiwan
Cheorl-Ho Kim , Republic of Korea
Victor Kuete , Cameroon
Hajime Nakae , Japan
Yoshiji Ohta , Japan
Olumayokun A. Olajide , United Kingdom
Chang G. Son , Republic of Korea
Shan-Yu Su , Taiwan
Michał Tomczyk , Poland
Jenny M. Wilkinson , Australia

Academic Editors

Eman A. Mahmoud , Egypt
Ammar AL-Farga , Saudi Arabia
Smail Aazza , Morocco
Nahla S. Abdel-Azim, Egypt
Ana Lúcia Abreu-Silva , Brazil
Gustavo J. Acevedo-Hernández , Mexico
Mohd Adnan , Saudi Arabia
Jose C Adsuar , Spain
Sayeed Ahmad, India
Touqeer Ahmed , Pakistan
Basiru Ajiboye , Nigeria
Bushra Akhtar , Pakistan
Fahmida Alam , Malaysia
Mohammad Jahoor Alam, Saudi Arabia
Clara Albani, Argentina
Ulysses Paulino Albuquerque , Brazil
Mohammed S. Ali-Shtayeh , Palestinian Authority
Ekram Alias, Malaysia
Terje Alraek , Norway
Adolfo Andrade-Cetto , Mexico
Letizia Angiolella , Italy
Makoto Arai , Japan

Daniel Dias Rufino Arcanjo , Brazil
Duygu AĞAGÜNDÜZ , Turkey
Neda Baghban , Iran
Samra Bashir , Pakistan
Rusliza Basir , Malaysia
Jairo Kenupp Bastos , Brazil
Arpita Basu , USA
Mateus R. Beguelini , Brazil
Juana Benedí, Spain
Samira Boulbaroud, Morocco
Mohammed Bourhia , Morocco
Abdelhakim Bouyahya, Morocco
Nunzio Antonio Cacciola , Italy
Francesco Cardini , Italy
María C. Carpinella , Argentina
Harish Chandra , India
Guang Chen, China
Jianping Chen , China
Kevin Chen, USA
Mei-Chih Chen, Taiwan
Xiaojia Chen , Macau
Evan P. Cherniack , USA
Giuseppina Chianese , Italy
Kok-Yong Chin , Malaysia
Lin China, China
Salvatore Chirumbolo , Italy
Hwi-Young Cho , Republic of Korea
Jeong June Choi , Republic of Korea
Jun-Yong Choi, Republic of Korea
Kathrine Bisgaard Christensen , Denmark
Shuang-En Chuang, Taiwan
Ying-Chien Chung , Taiwan
Francisco José Cidral-Filho, Brazil
Daniel Collado-Mateo , Spain
Lisa A. Conboy , USA
Kieran Cooley , Canada
Edwin L. Cooper , USA
José Otávio do Amaral Corrêa , Brazil
Maria T. Cruz , Portugal
Huantian Cui , China
Giuseppe D'Antona , Italy
Ademar A. Da Silva Filho , Brazil
Chongshan Dai, China
Laura De Martino , Italy
Josué De Moraes , Brazil

Arthur De Sá Ferreira , Brazil
Nunziatina De Tommasi , Italy
Marinella De leo , Italy
Gourav Dey , India
Dinesh Dhamecha, USA
Claudia Di Giacomo , Italy
Antonella Di Sotto , Italy
Mario Dioguardi, Italy
Jeng-Ren Duann , USA
Thomas Efferth , Germany
Abir El-Alfy, USA
Mohamed Ahmed El-Esawi , Egypt
Mohd Ramli Elvy Suhana, Malaysia
Talha Bin Emran, Japan
Roger Engel , Australia
Karim Ennouri , Tunisia
Giuseppe Esposito , Italy
Tahereh Eteraf-Oskouei, Iran
Robson Xavier Faria , Brazil
Mohammad Fattahi , Iran
Keturah R. Faurot , USA
Piergiorgio Fedeli , Italy
Laura Ferraro , Italy
Antonella Fioravanti , Italy
Carmen Formisano , Italy
Hua-Lin Fu , China
Liz G Müller , Brazil
Gabino Garrido , Chile
Safoora Gharibzadeh, Iran
Muhammad N. Ghayur , USA
Angelica Gomes , Brazil
Elena González-Burgos, Spain
Susana Gorzalczany , Argentina
Jiangyong Gu , China
Maruti Ram Gudavalli , USA
Jian-You Guo , China
Shanshan Guo, China
Narcís Gusi , Spain
Svein Haavik, Norway
Fernando Hallwass, Brazil
Gajin Han , Republic of Korea
Ihsan Ul Haq, Pakistan
Hicham Harhar , Morocco
Mohammad Hashem Hashempur , Iran
Muhammad Ali Hashmi , Pakistan

Waseem Hassan , Pakistan
Sandrina A. Heleno , Portugal
Pablo Herrero , Spain
Soon S. Hong , Republic of Korea
Md. Akil Hossain , Republic of Korea
Muhammad Jahangir Hossen , Bangladesh
Shih-Min Hsia , Taiwan
Changmin Hu , China
Tao Hu , China
Weicheng Hu , China
Wen-Long Hu, Taiwan
Xiao-Yang (Mio) Hu, United Kingdom
Sheng-Teng Huang , Taiwan
Ciara Hughes , Ireland
Attila Hunyadi , Hungary
Liaqat Hussain , Pakistan
Maria-Carmen Iglesias-Osma , Spain
Amjad Iqbal , Pakistan
Chie Ishikawa , Japan
Angelo A. Izzo, Italy
Satveer Jagwani , USA
Rana Jamous , Palestinian Authority
Muhammad Saeed Jan , Pakistan
G. K. Jayaprakasha, USA
Kyu Shik Jeong, Republic of Korea
Leopold Jirovetz , Austria
Jeeyoun Jung , Republic of Korea
Nurkhalida Kamal , Saint Vincent and the
Grenadines
Atsushi Kameyama , Japan
Kyungsu Kang, Republic of Korea
Wenyi Kang , China
Shao-Hsuan Kao , Taiwan
Nasiara Karim , Pakistan
Morimasa Kato , Japan
Kumar Katragunta , USA
Deborah A. Kennedy , Canada
Washim Khan, USA
Bonglee Kim , Republic of Korea
Dong Hyun Kim , Republic of Korea
Junghyun Kim , Republic of Korea
Kyungho Kim, Republic of Korea
Yun Jin Kim , Malaysia
Yoshiyuki Kimura , Japan

Nebojša Kladar , Serbia
Mi Mi Ko , Republic of Korea
Toshiaki Kogure , Japan
Malcolm Koo , Taiwan
Yu-Hsiang Kuan , Taiwan
Robert Kubina , Poland
Chan-Yen Kuo , Taiwan
Kuang C. Lai , Taiwan
King Hei Stanley Lam, Hong Kong
Faniel Lampiao, Malawi
Ilaria Lampronti , Italy
Mario Ledda , Italy
Harry Lee , China
Jeong-Sang Lee , Republic of Korea
Ju Ah Lee , Republic of Korea
Kyu Pil Lee , Republic of Korea
Namhun Lee , Republic of Korea
Sang Yeoup Lee , Republic of Korea
Ankita Leekha , USA
Christian Lehmann , Canada
George B. Lenon , Australia
Marco Leonti, Italy
Hua Li , China
Min Li , China
Xing Li , China
Xuqi Li , China
Yi-Rong Li , Taiwan
Vuanghao Lim , Malaysia
Bi-Fong Lin, Taiwan
Ho Lin , Taiwan
Shuibin Lin, China
Kuo-Tong Liou , Taiwan
I-Min Liu, Taiwan
Suhuan Liu , China
Xiaosong Liu , Australia
Yujun Liu , China
Emilio Lizarraga , Argentina
Monica Loizzo , Italy
Nguyen Phuoc Long, Republic of Korea
Zaira López, Mexico
Chunhua Lu , China
Ângelo Luís , Portugal
Anderson Luiz-Ferreira , Brazil
Ivan Luzardo Luzardo-Ocampo, Mexico

Michel Mansur Machado , Brazil
Filippo Maggi , Italy
Juraj Majtan , Slovakia
Toshiaki Makino , Japan
Nicola Malafrente, Italy
Giuseppe Malfa , Italy
Francesca Mancianti , Italy
Carmen Mannucci , Italy
Juan M. Manzanque , Spain
Fatima Martel , Portugal
Carlos H. G. Martins , Brazil
Maulidiani Maulidiani, Malaysia
Andrea Maxia , Italy
Avijit Mazumder , India
Isac Medeiros , Brazil
Ahmed Mediani , Malaysia
Lewis Mehl-Madrona, USA
Ayikoé Guy Mensah-Nyagan , France
Oliver Micke , Germany
Maria G. Miguel , Portugal
Luigi Milella , Italy
Roberto Miniero , Italy
Letteria Minutoli, Italy
Prashant Modi , India
Daniel Kam-Wah Mok, Hong Kong
Changjong Moon , Republic of Korea
Albert Moraska, USA
Mark Moss , United Kingdom
Yoshiharu Motoo , Japan
Yoshiki Mukudai , Japan
Sakthivel Muniyan , USA
Saima Muzammil , Pakistan
Benoit Banga N'guessan , Ghana
Massimo Nabissi , Italy
Siddavaram Nagini, India
Takao Namiki , Japan
Srinivas Nammi , Australia
Krishnadas Nandakumar , India
Vitaly Napadow , USA
Edoardo Napoli , Italy
Jorddy Neves Cruz , Brazil
Marcello Nicoletti , Italy
Eliud Nyaga Mwaniki Njagi , Kenya
Cristina Nogueira , Brazil




Sakineh Kazemi Noureini , Iran
Rômulo Dias Novaes, Brazil
Martin Offenbaecher , Germany
Oluwafemi Adeleke Ojo , Nigeria
Olufunmiso Olusola Olajuyigbe , Nigeria
Luís Flávio Oliveira, Brazil
Mozaniel Oliveira , Brazil
Atolani Olubunmi , Nigeria
Abimbola Peter Oluyori , Nigeria
Timothy Omara, Austria
Chiagoziem Anariochi Otuechere , Nigeria
Sokcheon Pak , Australia
Antônio Palumbo Jr, Brazil
Zongfu Pan , China
Siyaram Pandey , Canada
Niranjan Parajuli , Nepal
Gunhyuk Park , Republic of Korea
Wansu Park , Republic of Korea
Rodolfo Parreira , Brazil
Mohammad Mahdi Parvizi , Iran
Luiz Felipe Passero , Brazil
Mitesh Patel, India
Claudia Helena Pellizzon , Brazil
Cheng Peng, Australia
Weijun Peng , China
Sonia Piacente, Italy
Andrea Pieroni , Italy
Haifa Qiao , USA
Cláudia Quintino Rocha , Brazil
DANIELA RUSSO , Italy
Muralidharan Arumugam Ramachandran,
Singapore
Manzoor Rather , India
Miguel Rebollo-Hernanz , Spain
Gauhar Rehman, Pakistan
Daniela Rigano , Italy
José L. Rios, Spain
Francisca Rius Diaz, Spain
Eliana Rodrigues , Brazil
Maan Bahadur Rokaya , Czech Republic
Mariangela Rondanelli , Italy
Antonietta Rossi , Italy
Mi Heon Ryu , Republic of Korea
Bashar Saad , Palestinian Authority
Sabi Saheed, South Africa
Mohamed Z.M. Salem , Egypt
Avni Sali, Australia
Andreas Sandner-Kiesling, Austria
Manel Santafe , Spain
José Roberto Santin , Brazil
Tadaaki Satou , Japan
Roland Schoop, Switzerland
Sindy Seara-Paz, Spain
Veronique Seidel , United Kingdom
Vijayakumar Sekar , China
Terry Selfe , USA
Arham Shabbir , Pakistan
Suzana Shahar, Malaysia
Wen-Bin Shang , China
Xiaofei Shang , China
Ali Sharif , Pakistan
Karen J. Sherman , USA
San-Jun Shi , China
Insop Shim , Republic of Korea
Maria Im Hee Shin, China
Yukihiro Shoyama, Japan
Morry Silberstein , Australia
Samuel Martins Silvestre , Portugal
Preet Amol Singh, India
Rajeev K Singla , China
Kuttulebbai N. S. Sirajudeen , Malaysia
Slim Smaoui , Tunisia
Eun Jung Sohn , Republic of Korea
Maxim A. Solovchuk , Taiwan
Young-Jin Son , Republic of Korea
Chengwu Song , China
Vanessa Steenkamp , South Africa
Annarita Stringaro , Italy
Keiichiro Sugimoto , Japan
Valeria Sulsen , Argentina
Zewei Sun , China
Sharifah S. Syed Alwi , United Kingdom
Orazio Tagliatela-Scafati , Italy
Takashi Takeda , Japan
Gianluca Tamagno , Ireland
Hongxun Tao, China
Jun-Yan Tao , China
Lay Kek Teh , Malaysia
Norman Temple , Canada

Kamani H. Tennekoon , Sri Lanka
Seong Lin Teoh, Malaysia
Menaka Thounaojam , USA
Jinhui Tian, China
Zipora Tietel, Israel
Loren Toussaint , USA
Riaz Ullah , Saudi Arabia
Philip F. Uzor , Nigeria
Luca Vanella , Italy
Antonio Vassallo , Italy
Cristian Vergallo, Italy
Miguel Vilas-Boas , Portugal
Aristo Vojdani , USA
Yun WANG , China
QIBIAO WU , Macau
Abraham Wall-Medrano , Mexico
Chong-Zhi Wang , USA
Guang-Jun Wang , China
Jinan Wang , China
Qi-Rui Wang , China
Ru-Feng Wang , China
Shu-Ming Wang , USA
Ting-Yu Wang , China
Xue-Rui Wang , China
Youhua Wang , China
Kenji Watanabe , Japan
Jintanaporn Wattanathorn , Thailand
Silvia Wein , Germany
Katarzyna Winska , Poland
Sok Kuan Wong , Malaysia
Christopher Worsnop, Australia
Jih-Huah Wu , Taiwan
Sijin Wu , China
Xian Wu, USA
Zuoqi Xiao , China
Rafael M. Ximenes , Brazil
Guoqiang Xing , USA
JiaTuo Xu , China
Mei Xue , China
Yong-Bo Xue , China
Haruki Yamada , Japan
Nobuo Yamaguchi, Japan
Junqing Yang, China
Longfei Yang , China

Mingxiao Yang , Hong Kong
Qin Yang , China
Wei-Hsiung Yang, USA
Swee Keong Yeap , Malaysia
Albert S. Yeung , USA
Ebrahim M. Yimer , Ethiopia
Yoke Keong Yong , Malaysia
Fadia S. Youssef , Egypt
Zhilong Yu, Canada
RONGJIE ZHAO , China
Sultan Zahiruddin , USA
Armando Zarrelli , Italy
Xiaobin Zeng , China
Y Zeng , China
Fangbo Zhang , China
Jianliang Zhang , China
Jiu-Liang Zhang , China
Mingbo Zhang , China
Jing Zhao , China
Zhangfeng Zhong , Macau
Guoqi Zhu , China
Yan Zhu , USA
Suzanna M. Zick , USA
Stephane Zingue , Cameroon


Contents

Alleviative Effect of *Ruellia tuberosa* L. on Insulin Resistance and Abnormal Lipid Accumulation in TNF- α -Treated FL83B Mouse Hepatocytes

Hong-Jie Chen , Chih-Yuan Ko , Jian-Hua Xu, Yu-Chu Huang, James Swi-Bea Wu, and Szu-Chuan Shen 


Research Article (8 pages), Article ID 9967910, Volume 2021 (2021)

Wild Bitter Melon Extract Regulates LPS-Induced Hepatic Stellate Cell Activation, Inflammation, Endoplasmic Reticulum Stress, and Ferroptosis

Chang-Hsun Ho, Jen-Hsuan Huang, Maw-Sheng Sun, I-Shiang Tzeng, Yi-Chiung Hsu, and Chan-Yen Kuo 



Research Article (11 pages), Article ID 6671129, Volume 2021 (2021)

Lower Somatic Mutation Levels in the λ Light-Chain Repertoires with Chronic HBV Infection

Binbin Hong , Qiaoling Liu, Qiulan Li, Lili Su, and Lizhi Wang



Research Article (9 pages), Article ID 5525369, Volume 2021 (2021)

Quantitative Profiling of Oxylipin Reveals the Mechanism of Pien-Tze-Huang on Alcoholic Liver Disease

Ziye Zhu, Wenjun Zhou, Yang Yang, Kai Wang, Fenghua Li , and Yanqi Dang 

Research Article (14 pages), Article ID 9931542, Volume 2021 (2021)

Jian-Gan-Xiao-Zhi Decoction Alleviates Inflammatory Response in Nonalcoholic Fatty Liver Disease Model Rats through Modulating Gut Microbiota

Jiabao Liao, Xuehua Xie, Jinmei Gao, Zhaiyi Zhang, Fei Qu, Huantian Cui, Yongjun Cao, Xue Han, Jie Zhao, Weibo Wen , and Hongwu Wang 



Research Article (13 pages), Article ID 5522755, Volume 2021 (2021)

***Astragali Radix* Contributes to the Inhibition of Liver Fibrosis via High-Mobility Group Box 1-Mediated Inflammatory Signaling Pathway**

Jianxia Wen , Dan Wang , Jian Wang , Ruilin Wang, Shizhang Wei, and Yanling Zhao 



Research Article (11 pages), Article ID 5574010, Volume 2021 (2021)

Hepatocardiac or Cardiohepatic Interaction: From Traditional Chinese Medicine to Western Medicine

Yaxing Zhang  and Xian-Ming Fang 









Review Article (14 pages), Article ID 6655335, Volume 2021 (2021)

Network Pharmacology-Based Study on the Molecular Biological Mechanism of Action for Qingdu Decoction against Chronic Liver Injury

Chongyang Ma, Mengpei Zhao, Yuqiong Du , Shuang Jin, Xiaoyi Wu, Haiyan Zou, Qiuyun Zhang, and Lianyin Gao 



Research Article (12 pages), Article ID 6661667, Volume 2021 (2021)

The Association between Metabolic Syndrome and Elevated Alanine Aminotransferase Levels in an Indigenous Population in Northern Taiwan: A Community-Based and Cross-Sectional Study

Yi-Fang Chen , Yen-An Lin , Wei-Chung Yeh , Yu-Chung Tsao , Wen-Cheng Li , Wei-Ching Fang , I-Ju Chen , and Jau-Yuan Chen 

Research Article (9 pages), Article ID 6612447, Volume 2020 (2020)



Identification of Bioactive Components from *Ruellia tuberosa* L. on Improving Glucose Uptake in TNF- α -Induced Insulin-Resistant Mouse FL83B Hepatocytes

Jian-Hua Xu, Yangming Martin Lo, Wen-Chang Chang, Da-Wei Huang, James Swi-Bea Wu, Yu-Yuan Jhang, Wen-Chung Huang, Chih-Yuan Ko , and Szu-Chuan Shen 

Research Article (7 pages), Article ID 6644253, Volume 2020 (2020)

Research Article

Alleviative Effect of *Ruellia tuberosa* L. on Insulin Resistance and Abnormal Lipid Accumulation in TNF- α -Treated FL83B Mouse Hepatocytes

Hong-Jie Chen ¹, Chih-Yuan Ko ^{2,3,4,5}, Jian-Hua Xu,⁶ Yu-Chu Huang,⁷
James Swi-Bea Wu,⁸ and Szu-Chuan Shen ⁷

¹Department of Nutrition, People's Hospital of Leshan, Leshan 614000, China

²Department of Clinical Nutrition, The Second Affiliated Hospital of Fujian Medical University, Quanzhou 362000, China

³Department of Respiratory and Critical Care Medicine, The Second Affiliated Hospital of Fujian Medical University, Quanzhou 362000, China

⁴School of Public Health, Fujian Medical University, Fuzhou, Fujian 350122, China

⁵Respiratory Medicine Center of Fujian Province, Quanzhou 362000, China

⁶Department of Tumor Surgery, The Second Affiliated Hospital of Fujian Medical University, Quanzhou 362000, China

⁷Graduate Program of Nutrition Science, National Taiwan Normal University, Taipei 11677, Taiwan

⁸Graduate Institute of Food Science and Technology, National Taiwan University, Taipei 10672, Taiwan

Correspondence should be addressed to Szu-Chuan Shen; scs@ntnu.edu.tw

Received 24 March 2021; Accepted 8 June 2021; Published 24 June 2021

Academic Editor: Ying-Chien Chung

Copyright © 2021 Hong-Jie Chen et al. This is an open access article distributed under the Creative Commons Attribution License, which permits unrestricted use, distribution, and reproduction in any medium, provided the original work is properly cited.

Type 2 diabetes mellitus (T2DM) is a chronic metabolic disease, and most patients with T2DM develop nonalcoholic fatty liver disease (NAFLD). Both diseases are closely linked to insulin resistance (IR). Our previous studies demonstrated that *Ruellia tuberosa* L. (RTL) extract significantly enhanced glucose uptake in the skeletal muscles and ameliorated hyperglycemia and IR in T2DM rats. We proposed that RTL might be via enhancing hepatic antioxidant capacity. However, the potent RTL bioactivity remains unidentified. In this study, we investigated the effects of RTL on glucose uptake, IR, and lipid accumulation *in vitro* to mimic the T2DM accompanied by the NAFLD paradigm. FL83B mouse hepatocytes were treated with tumor necrosis factor- α (TNF- α) to induce IR, coincubated with oleic acid (OA) to induce lipid accumulation, and then, treated with RTL fractions, fractionated with n-hexane or ethyl acetate (EA), from column chromatography, and analyzed by thin-layer chromatography. Our results showed that the ethyl acetate fraction (EAF2) from RTL significantly increased glucose uptake and suppressed lipid accumulation in TNF- α plus OA-treated FL83B cells. Western blot analysis showed that EAF2 from RTL ameliorated IR by upregulating the expression of insulin-signaling-related proteins, including protein kinase B, glucose transporter-2, and peroxisome proliferator-activated receptor alpha in TNF- α plus OA-treated FL83B cells. The results of this study suggest that EAF2 from RTL may improve hepatic glucose uptake and alleviate lipid accumulation by ameliorating and suppressing the hepatic insulin signaling and lipogenesis pathways, respectively, in hepatocytes.

1. Introduction

Type 2 diabetes mellitus (T2DM) is a metabolic disorder characterized by chronic hyperglycemia, insufficient insulin secretion or action, or insulin resistance (IR). These conditions cause abnormalities in lipid, carbohydrate, protein, water, and electrolyte functions. Long-term hyperglycemic

conditions increase both oxidative stress and inflammatory responses, leading to an increased risk of chronic inflammatory systemic diseases and their respective complications [1–3].

Interestingly, approximately 70% of patients with T2DM present with nonalcoholic fatty liver disease (NAFLD), which is a bidirectional relationship [4, 5]. The main

pathological feature of NAFLD is lipid overaccumulation in liver cells, and it is associated mainly with obesity and dyslipidemia. There is a strong relationship between IR and hepatocyte abnormal lipid accumulation. Normally, insulin promotes assimilation, stimulates glycogen synthesis in liver and muscle cells, and synthesizes and stores fat as adipocytes. If IR occurs, the lipolysis rate of visceral fat cells increases, which leads to an increased content of free fatty acids (FFAs) in the blood. When glycerol and fatty acids enter the liver, this results in increased lipogenesis and excess lipid accumulation in liver cells, eventually causing fatty liver disease. Taken together, the pathophysiology of NAFLD and T2DM is related to IR, and they are mutually vicious interrelated risk factors [4, 5], although their pathological mechanisms have not been fully elucidated. Current T2DM- or NAFLD-related studies follow combined approaches, and these researchers' paradigm is more in line with the actual condition of such patients.

Oleic acid (OA) is a monounsaturated fatty acid that is naturally found widely in animals and plants and is one of the most abundant fatty acids in human fat tissue. In fact, OA has been demonstrated to induce hepatic cell steatosis in established *in vitro* steatosis models [6, 7].

Our previous study has demonstrated that *Ruellia tuberosa* L. (RTL) aqueous or ethanolic extracts significantly improved glucose uptake in C2C12 myoblasts, alleviated tumor necrosis factor- α - (TNF- α -) induced IR in skeletal muscles, and ameliorated hyperglycemia and IR indices in high-fat-diet-fed plus streptozotocin-induced T2DM rats [8]. Additionally, we demonstrated that RTL ameliorated abnormal hepatic detoxification by enhancing hepatic antioxidant capacity [9]. However, the potent bioactivities of RTL and mechanism on improving NAFLD remain uncertain. Hence, in the present study, we aimed to utilize the TNF- α -induced IR combined with the OA-induced steatosis paradigm to identify the active ingredients of RTL extracts through thin-layer chromatography (TLC), to improve glucose intake and inhibit lipogenesis, and to clarify the underlying mechanisms of metabolism in FL83B cells.

2. Materials and Methods

2.1. Preparation of RTL Extracts. RTL was purchased in July 2017 from Wanhua, Taipei County, Taiwan, identified by Prof. Wei-Jan Huang in the College of Pharmacy, Taipei Medical University. A voucher specimen (TMU27449) was deposited in the herbarium of College of Pharmacy, Taipei Medical University. The extraction protocol was based on our previous methods, with slight modifications [8]. RTL stems and leaves together were freeze-dried into a powder (4160.9 g), subsequently extracted with 6 mL distilled water or methanol (1:6, w/v) at 4°C for 72 h, and filtered using a cheese cloth. The filtrate was filtered twice through Whatman No. 1 filter paper and centrifuged at 7,000 \times g for 20 min. The supernatant was vacuum-concentrated using a rotary evaporator below 40°C. The concentrated methanol extract was dissolved in 400 mL water and subsequently extracted with an equal volume of hexane and ethyl acetate (EA) solvent, and the n-hexane and EA layers were divided

through column chromatography using a Sephadex LH-20 column with 200 mL of 50–100% alcohol sequentially. The different fractions were then collected from the n-hexane layer (Hf1, Hf2, Hf3, and Hf4) and the EA layer (Eaf1, Eaf2, Eaf3, and Eaf4), as shown in Figure 1.

2.2. TLC. The supernatants were placed onto a silica gel precoated plate (Kieselgel 60 F254, 0.20 mm, Merck, Darmstadt, Germany). The TLC plates were added with a solvent mixture of dichloromethane: methanol: H₂O: acetic acid (10:1:0.1:0.2, v/v), followed by immersion into 10% sulfuric acid, and then, the mixture was heated. Using the color distribution state of TLC, similar effluents were collected, and the solvent was drained through a rotary evaporator. Different concentrates were freeze-dried into a powder and kept at -80°C until use.

2.3. Cell Culture. The experiments were performed on FL83B mouse hepatocytes (ATCC, Rockville, MD, USA) incubated in an F12K medium containing 10% fetal bovine serum (Invitrogen Corporation, Camarillo, CA, USA) in 10 cm Petri dishes at 37°C and 5% CO₂. The experiments were performed on cells that were 80–90% confluent.

2.4. TNF- α Induction of IR in FL83B Cells. The IR-induced paradigm was described as the previous method with slight modifications [10]. FL83B cells were seeded in 10 cm dishes and incubated at 37°C for 48 h to reach 80% confluence. The serum-free medium containing recombinant mouse TNF- α and different RTL fractions (25 μ g/mL) was incubated for 2 h at 37°C to induce IR.

2.5. TNF- α Induction of IR with OA-Induced Lipid Accumulation in FL83B Cells. FL83B cells (5×10^5) were seeded in six-well plates and incubated in a serum-free medium containing 20 ng/mL TNF- α , 1 mM OA, and 2% bovine serum albumin for 24 h. The cells were then transferred to a serum-free medium containing 25 μ g/mL of the samples and 100 nM of insulin, followed by incubation at 37°C.

Lipid accumulation was measured by using Oil Red O staining. Cells were placed on a plate, washed in PBS, and then, fixed in 10% formalin for 1 h. PBS was washed twice, and 0.5 g Oil Red O stain was added for 15 min. The stained cells were washed in distilled water, subsequently washed in 1 ml isopropanol. Taking 100 μ l to a plate, the absorbance was measured at 492 nm. The value represented the total fat content in the cell.

2.6. Uptake of Fluorescent 2-[N-(7-nitrobenz-2-oxa-1,3-diazol-4-yl) amino]-2-deoxy-d-glucose (2-NBDG) in FL83B Cells. The FL83B cells were seeded in 10 cm dishes and then incubated at 37°C for 48 h to achieve 80% confluence. The serum-free medium containing 20 ng/mL recombinant mouse TNF- α was added before incubating for 2 h to induce IR. The cells were then transferred to another F12K medium containing 5 mM glucose, without (basal) or with 200 μ M insulin and

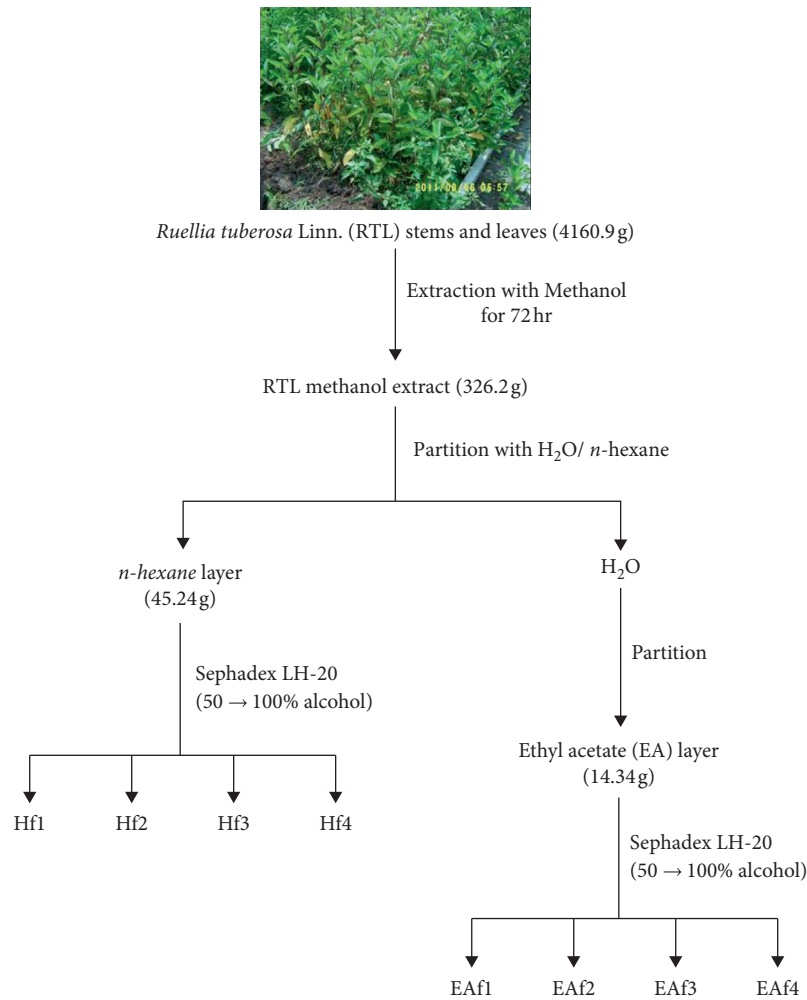


FIGURE 1: The flow chart for fractionation of *Ruellia tuberosa* Linn. extraction.

10 μ L different RTL fractions and incubated for 30 min at 37°C. An assay of glucose uptake was then performed as described previously [10]. The fluorescence intensity of the cell suspension was evaluated by flow cytometry (FACScan, Becton Dickinson, Bellport, NY, USA) at an excitation wavelength of 488 nm and an emission wavelength of 542 nm. Fluorescence intensity reflected the cellular uptake of 2-NBDG.

2.7. Western Blot Analysis. The protein extraction methods used in this study were adopted from our previous protocol [11]. The protein concentration in the cell extract was determined using a Bio-Rad protein assay dye reagent (Richmond, VA, USA). Aliquots of the supernatant containing 50 μ g protein were separated through standard SDS-PAGE and electrophoretically transferred to polyvinylidene difluoride membranes. The membranes were incubated with anti-insulin receptor β (IR β ; 1:1000; Cell Signaling Technology, Beverly, MA, USA), anti-PI3-kinase p85 (1:1000; Cell Signaling Technology), anti-phospho-Akt (Ser473) (1:1000; Cell Signaling Technology), anti-Akt (1:500; Cell Signaling Technology, Danvers, MA, USA), antiglucose transporter (GLUT)2 (1:500; Millipore, Billerica, MA,

USA), anti-PPAR α (1:1000; GeneTex, Irvine, CA, USA), or anti β -actin (1:4000; GeneTex) antibodies at 4°C overnight. The membranes were incubated with anti-mouse IgG or anti-rabbit IgG secondary antibodies and washed thrice for 5 min each time. Protein band images were detected and captured using the UVP Biospectrum image system (Level, Cambridge, UK). Finally, all relevant protein expressions were normalized with β -actin.

2.8. Statistical Analyses. Values are presented as the mean \pm standard deviation using SPSS version 22.0 (SPSS Inc., Chicago, IL, USA) analysis by one-way analysis of variance (ANOVA) and Duncan's new multiple-range tests. $p < 0.05$ was considered statistically significant.

3. Results

3.1. RTL Fractions Collection and Analysis by TLC. The different RTL fractions from the n-hexane layer (Hf1, Hf2, Hf3, and Hf4) and the EA layer (EAf1, EAf2, EAf3, and EAf4) were collected through TLC analysis (Supplementary Figure 1).

3.2. Effect of Different RTL Fractions on Glucose Uptake in FL83B Mouse Hepatocytes. An evaluation of the 2-NBDG uptake was performed to assess the improvement of glucose uptake in FL83B cells. The EAF4 fraction improved glucose uptake of FL83B mouse hepatocytes compared with the control group ($p = 0.030$) or compared with the TNF- α -induced IR group ($p = 0.013$). In addition, the fluorescence level of the EAF2 fraction group was 1.3 times greater than that of the TNF- α -induced IR group ($p = 0.014$) (Figure 2).

3.3. Effect of EAF2 Fraction on TNF- α plus OA-Induced IR and Lipid Accumulation in FL83B Cells. Both the OA-induced and the TNF- α plus OA-induced groups showed a significant increase in intracellular lipid accumulation (Figure 3). There was no difference between the groups administered EAF2 at 20, 30, and 60 min and the OA-induced group/TNF- α plus OA-induced group. However, a decrease in intracellular lipid accumulation was significantly observed 10 min after EAF2 administration, compared with the TA20 group ($p = 0.005$), TA30 group ($p = 0.008$), and TA60 group ($p = 0.012$), respectively (Figure 4). After 120 min of EAF2 administration, the significantly decreased lipid accumulation was observed, compared with the TNF- α -induced IR group ($p = 0.045$) (Figure 4).

3.4. Effect of EAF2 Fraction on TNF- α plus OA-Induced IR and Lipid Accumulation in Enhancing FL83B Cell Insulin Signaling Pathway Protein Expression. Western blot analyses of hepatic insulin-signaling-related proteins were conducted, including IR β , PI3K, p-Akt/Akt, GLUT2, and PPAR α (Figure 5(a)). PPAR α protein expression was increased after the EAF2 fraction administration to the OA-induced group and TNF- α plus OA-induced group, compared with the control group, which increased by 108% and 138%, respectively (Figure 5(b)). The expression of the GLUT2 protein increased after the administration of the EAF2 fraction to the TNF- α -induced, OA-induced, and TNF- α plus OA-induced groups (Figure 5(c)). The expression of the p-Akt/Akt protein increased after the administration of the EAF2 fraction to the TNF- α -induced and TNF- α plus OA-induced groups (Figure 5(d)). The administration of the EAF2 fraction increased PI3K protein expression in the OA-induced group (Figure 5(e)). The EAF2 fraction can regulate IR β protein expression in the TNF- α -induced and OA-induced groups (Figure 5(f)).

4. Discussion

In the present study, EA fractions from RTL, especially in EAF2, showed the best improved glucose uptake in IR mouse FL83B hepatocytes. Additionally, the EAF2 fraction from RTL also attenuated IR plus lipid accumulation in FL83B cells. RTL may have possibly regulated and enhanced hepatic insulin-signaling-related metabolic protein expressions, including those of GLUT2, p-Akt/Akt, and PPAR α (Figure 6), suggesting that the possible underlying mechanisms of RTL extract were to improve glucose intake and inhibit lipogenesis in FL83B cells.

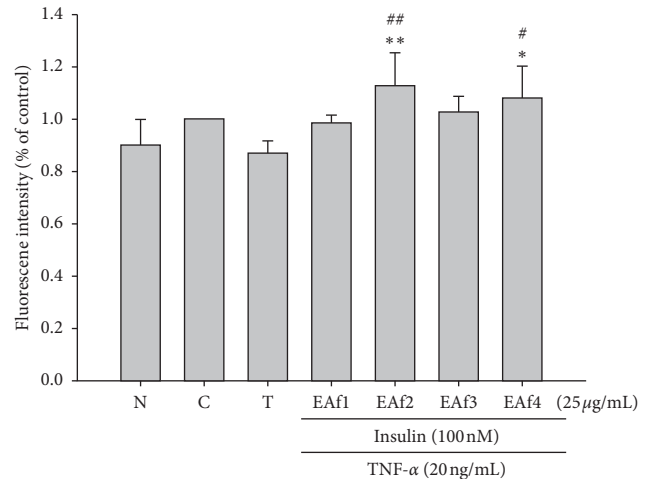


FIGURE 2: Effects of fractions from RTL extracts on glucose uptake in insulin-resistant FL83B cells. N cells incubated with the F12K medium group. C cells incubated with the F12K medium containing the 100 nM insulin group. T: TNF- α induced for the insulin resistance group. * $p < 0.05$ and ** $p < 0.01$ vs. control group; # $p < 0.05$ and ## $p < 0.01$ vs. TNF- α group.

In this study, TNF- α inhibits glucose uptake in FL83B hepatocytes. OA increases lipid accumulation in TNF- α -treated FL83B hepatocytes. We postulated that the EAF2 fraction increased glucose uptake and suppressed lipid accumulation may be attributed by alleviating the IR in TNF- α and OA-treated FL83B hepatocytes. When adipocytes develop IR, insulin signaling is blocked. Lipogenesis is inhibited, lipolysis is increased, and FFA concentration is increased in the blood. The absorption rate of FFAs in other organs is increased, thereby stimulating hepatocytes for gluconeogenesis, fat synthesis, and synthesis of very-low-density lipoprotein (VLDL). No study has confirmed the lipotoxicity of liver fat and visceral fat in the IR of muscle cells, although obesity is associated with IR [12–14]. Individuals with higher liver and visceral fat who develop IR in muscle, liver, and fat cells show increased concentrations of lipoprotein in the blood, whereas individuals with obesity and higher visceral fat content have a significant increase in lipogenesis compared with individuals of normal weight [15]. The fat accumulated in liver cells reflects the balance of lipolysis, lipid peroxidation, lipogenesis, and VLDL production and elimination. When regulating fat metabolism dysfunction, hepatic fat decomposition is reduced, fat accumulation is increased, and fatty acid oxidation and VLDL production reach saturation, resulting in the accumulation of lipid in hepatocytes, which eventually leads to a fatty liver [4].

In the present study, IR β , PI3K, and p-Akt/Akt expressions were decreased in TNF- α -induced cells, compared with untreated cells, indicating that TNF- α induced IR in hepatocytes through this pathway. Moreover, TNF- α plus OA-induced cells were also altered through the same signaling pathway, which showed a decrease in the expression of both GLUT2 and PPAR α , illustrating that this model can induce IR in normal liver cells when combined with the fatty liver model.

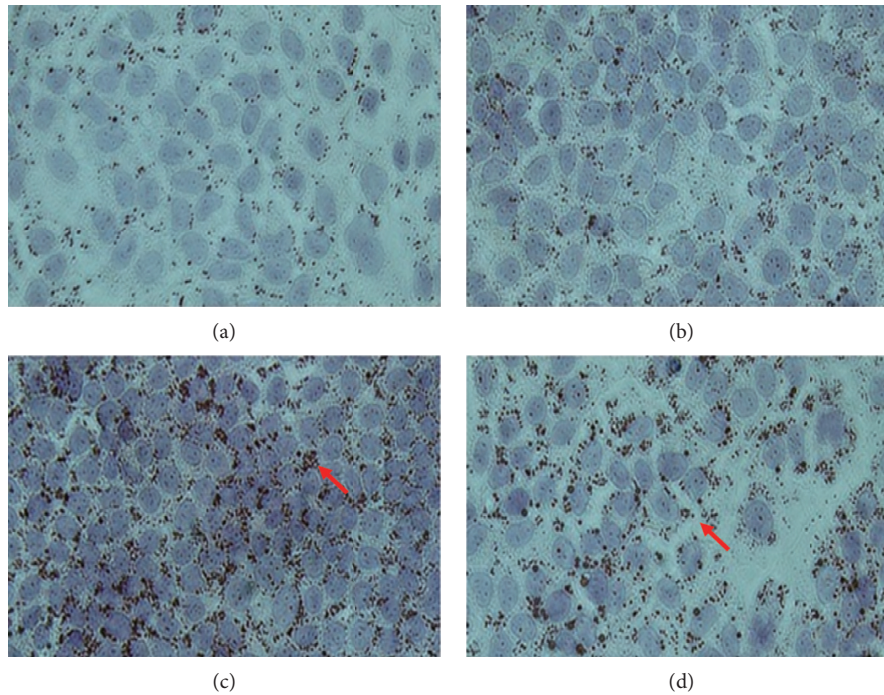


FIGURE 3: Lipid accumulation in FL83B cells by oil red O staining. (a) C: cells incubated with the F12K medium group. (b) T: TNF- α induced for the insulin resistance group. (c) OA: oleic acid induced for the lipid accumulation group. (d) TA: TNF- α and oleic acid induced insulin resistance for the fatty liver cells group.

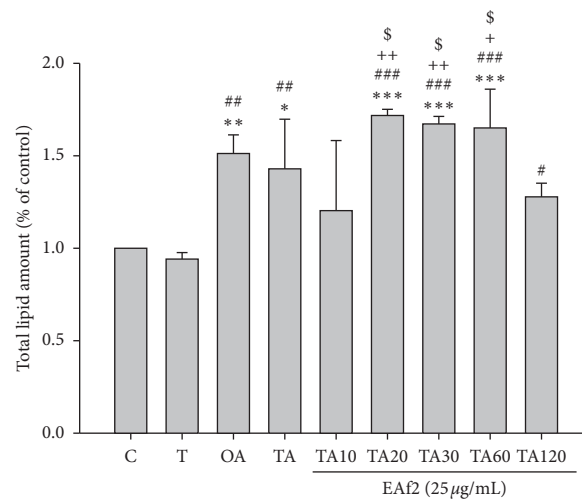
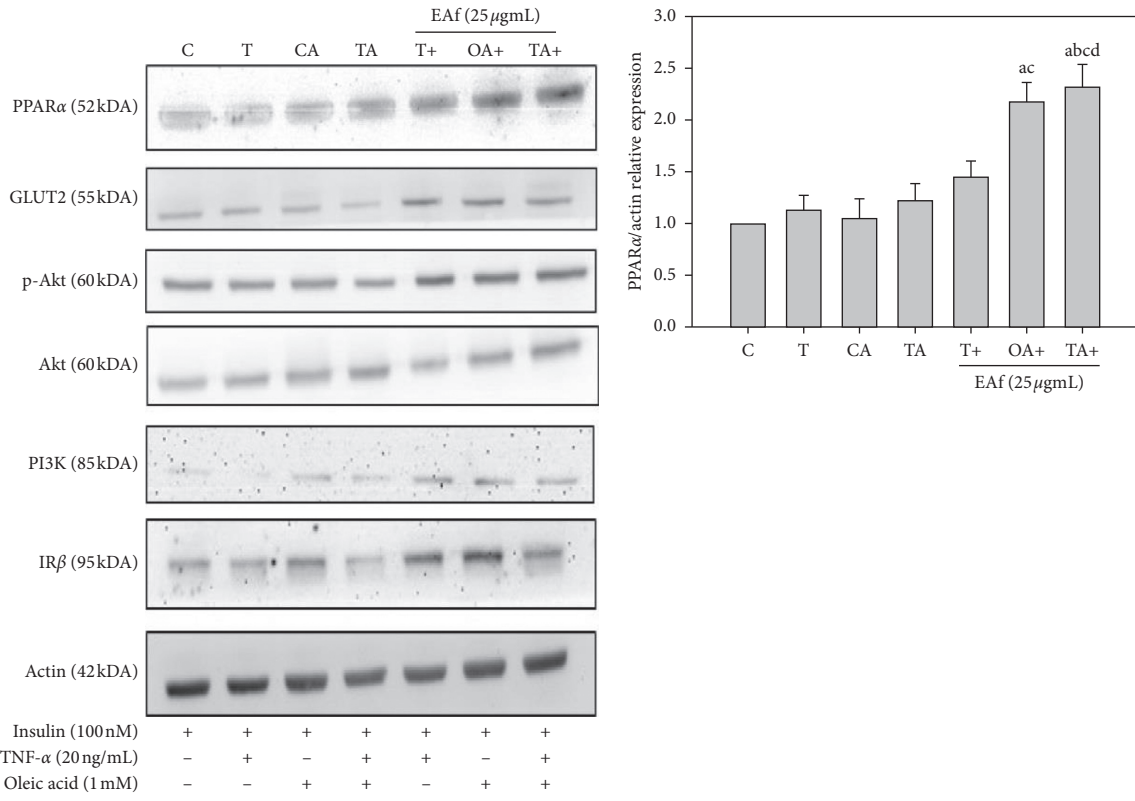


FIGURE 4: Effects of ethyl acetate fraction 2 (EAF2) on lipid accumulation in FL83B cells. C: cells incubated with the F12K medium containing the 100 nM insulin group. T: TNF- α induced for the insulin resistance group. OA: oleic acid induced for the fatty liver cells group. TA: TNF- α and oleic acid induced insulin resistance for the fatty liver cells group. * $p < 0.05$, ** $p < 0.01$, and *** $p < 0.001$ vs. control group; # $p < 0.05$, ## $p < 0.01$, and ### $p < 0.001$ vs. TNF- α group; + $p < 0.05$ and ++ $p < 0.01$ vs. TA10 group; and \$ $p < 0.05$ vs. TA120 group.

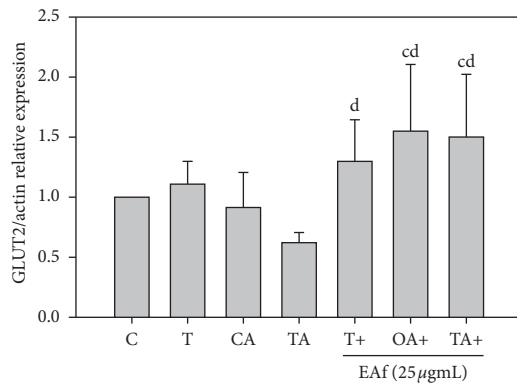
Glucose uptake evaluation showed that the EAF2 fraction increased glucose uptake in IR FL83B cells, indicating that it can alleviate cellular IR and recover normal cellular insulin-related functions. The EAF2 fraction can enhance insulin receptor protein expression and stimulate PI3K expression, as well as promote the activation of downstream pathways. PI3K is a downstream molecule of the insulin receptor substrate (IRS), and when insulin binds to insulin receptors,

IRS phosphorylation activation is promoted and the signaling of the PI3K pathway is activated. PI3K is a secondary signal transduction factor that subsequently promotes downstream Akt/PKB protein activation, and the glucose channel protein GLUT2 is moved from the cytoplasm to the surface of the cell membrane, thus enhancing cellular glucose uptake [16]. The EAF2 fraction has the effect of increasing intracellular phosphorylated Akt reaction,

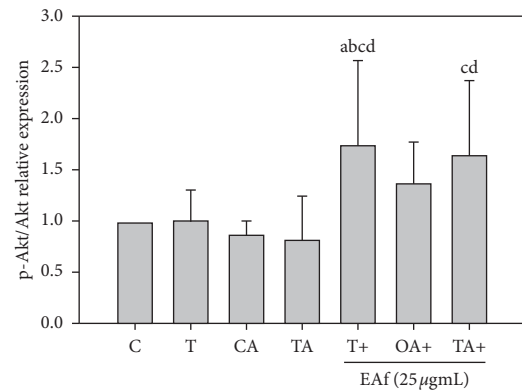


(a)

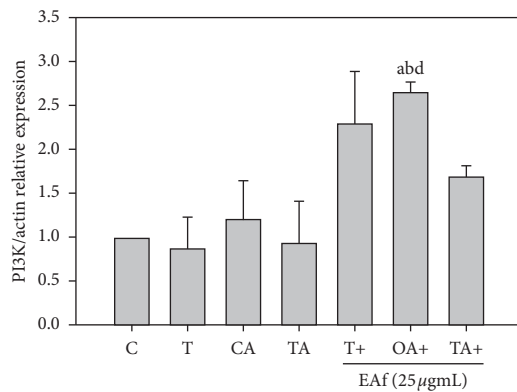
(b)



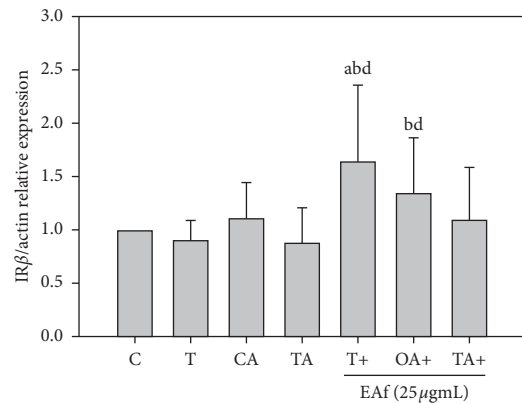
(c)



(d)



(e)



(f)

FIGURE 5: Effects of EAF2 on the expression of peroxisome proliferator-activated receptor alpha (PPAR α), glucose transporter-2 (GLUT2), phosphorylation of protein kinase B (PKB/Akt), phosphatidylinositol-3 kinase (PI3K), and insulin receptor-beta (IR β) in FL83B cells. C: cells incubated with the F12K medium containing the 100 nM insulin group. T TNF- α induced for the insulin resistance group. OA: oleic acid induced for the fatty liver cells group. TA :TNF- α and oleic acid induced insulin resistance for the fatty liver cells group. ^a $p < 0.05$ vs. control group, ^b $p < 0.05$ vs. TNF- α group, ^c $p < 0.05$ vs. OA group, and ^d $p < 0.05$ vs. TA group.

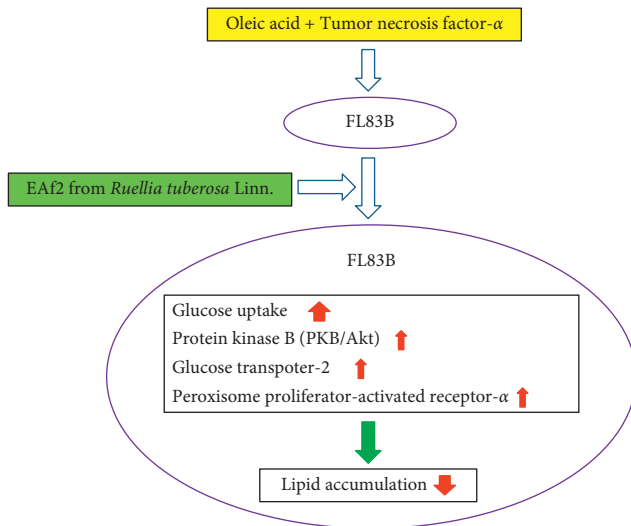


FIGURE 6: The postulated mechanism of EAF2 from RTL on improving glucose intake and inhibiting lipogenesis in FL83B mouse hepatocytes.

suggesting that the degree of phosphorylated Akt increases because of increased PI3K expression. When Akt is stimulated by upstream signaling, such as PI3K signaling, it activates Ser473 and Thr308 phosphorylation, which promotes downstream proteins, such as glycogen synthase kinase 3, forkhead box O, and mammalian target of rapamycin, to regulate glucose transport and glycogen synthesis [17]. The activation of Akt moves GLUT4 from the cytoplasm to the cell membrane, thereby increasing cellular glucose uptake. When insulin stimulation disappears, GLUT4 returns to the cytoplasm for standby. GLUT2 is glucose sensitive and has a bidirectional transport direction. It is present widely in the liver, islet beta cells, kidneys, and small intestine cells and is different from GLUT4. GLUT2 is regulated by insulin and glucose levels in the blood, which regulate the cellular glucose output or input [18].

IR combined with fatty liver results in reduced GLUT2 protein expression in liver cells. In the present study, the EAF2 fraction ameliorated IR combined with fatty liver by enhancing the expression of GLUT2 and PPAR α , thereby reducing intracellular lipid accumulation and ameliorating fatty liver. Indeed, the increased PPAR α protein expression reduced intracellular lipid accumulation [19]. PPAR α is abundant in the liver, muscle, and kidney. It is used to promote fat oxidation and remove FFAs in the blood, which has protective and preventive effects on fatty liver [19].

The administration of RTL fractions of n-hexane and EA in diabetic rabbits lowered the animals' blood sugar level [20]. Moreover, the best evaluation of antioxidant activity resulted from RTL extraction using methanol and EA [21]. Here, our findings showed that n-hexane and EA fractions of RTL have better effects on improving the glucose uptake capacity of IR cells, which is consistent with the results of other studies. EA fractions of RTL can effectively improve the blood sugar level in diabetes through their antioxidant capacity, as EA fractions speculatively contain high amounts of polyphenols and triterpenoids [20]. Another study

indicated that the active compound of the EA fraction may be a polyphenol called cirsimaritin [22]. Although this compound is speculated, the components are quite complicated. Our recent study indicated the possible bioactive compounds of EA from RTL identified by high-performance liquid chromatography assay, including phenolic acids (syringic acid and p-coumaric acid) and flavanoid (cirsimaritin) on improving glucose uptake in hepatocytes [10].

5. Conclusions

Our results showed that EAF2 from RTL significantly increased glucose uptake and suppressed lipid accumulation in TNF- α plus OA-induced FL83B cells. The possible alleviating mechanism happens by enhancing the expression of the insulin signaling pathway protein, including Akt and GLUT2, to ameliorate the glucose uptake capacity, which may have been due to the increased Akt phosphorylation and GLUT2 expression that attenuated IR and the increased PPAR α expression that reduced lipid accumulation in TNF- α plus OA-induced FL83B cells. The further separation and identification of bioavailability contributor on alleviating abnormal lipid accumulation from RTL EA fractions using mouse hepatocyte models is currently on process in our laboratory.

Data Availability

All the data used to support the findings of this study are included in the article.

Conflicts of Interest

The authors declare that they do not have any conflicts of interest.

Authors' Contributions

Hong-Jie Chen and Chih-Yuan Ko contributed equally to this work.

Acknowledgments

The authors would like to thank the Ministry of Science and Technology of the Republic of China (ROC), Taiwan, for financially supporting this research under contract no. MOST 107-2320-B-003-004-MY3, and the Second Affiliated Hospital of Fujian Medical University (serial no. BS201902), for academic funding. Special thanks are due to Professor W. J. Huang of the College of Pharmacy at Taipei Medical University for his guidance in column chromatography analysis.

Supplementary Materials

Supplementary Figure 1. Thin-layer chromatography profiles of different column fractions from RTL. (A) Hf1: n-hexane layer fraction 1, (B) Hf2: n-hexane layer fraction 2, (C) Hf3: n-hexane layer fraction 3, (D) Hf4: n-hexane layer fraction 4, (E) EAF1: ethyl acetate fraction 1, (F) EAF2: ethyl

acetate fraction 2, (G) EAF3: ethyl acetate fraction 3, and (H) EAF4: ethyl acetate fraction 4. (*Supplementary Materials*)

References

- [1] G. Boden, P. She, M. Mozzoli et al., "Free fatty acids produce insulin resistance and activate the proinflammatory nuclear factor- κ B pathway in rat liver," *Diabetes*, vol. 54, no. 12, pp. 3458–3465, 2005.
- [2] V. T. Samuel and G. I. Shulman, "Mechanisms for insulin resistance: common threads and missing links," *Cell*, vol. 148, no. 5, pp. 852–871, 2012.
- [3] G. L. King, K. Park, and Q. Li, "Selective insulin resistance and the development of cardiovascular diseases in diabetes: the 2015 edwin Bierman award lecture," *Diabetes*, vol. 65, no. 6, pp. 1462–1471, 2016.
- [4] M. Gaggini, M. Morelli, E. Buzzigoli, R. DeFronzo, E. Bugianesi, and A. Gastaldelli, "Non-alcoholic fatty liver disease (NAFLD) and its connection with insulin resistance, dyslipidemia, atherosclerosis and coronary heart disease," *Nutrients*, vol. 5, no. 5, pp. 1544–1560, 2013.
- [5] W. Mu, X.-f. Cheng, Y. Liu et al., "Potential nexus of non-alcoholic fatty liver disease and type 2 diabetes mellitus: insulin resistance between hepatic and peripheral tissues," *Frontiers in Pharmacology*, vol. 9, p. 1566, 2019.
- [6] W. Cui, S. L. Chen, and K. Q. Hu, "Quantification and mechanisms of oleic acid-induced steatosis in HepG2 cells," *American Journal of Translational Research*, vol. 1, no. 2, pp. 95–104, 2010.
- [7] D.-D. Zhang, J.-G. Zhang, X. Wu et al., "Nuciferine down-regulates Per-Arnt-Sim kinase expression during its alleviation of lipogenesis and inflammation on oleic acid-induced hepatic steatosis in HepG2 cells," *Frontiers in Pharmacology*, vol. 6, p. 238, 2015.
- [8] C.-Y. Ko, R.-H. Lin, Y.-M. Zeng et al., "Ameliorative effect of *Ruellia tuberosa* L. on hyperglycemia in type 2 diabetes mellitus and glucose uptake in mouse C2C12 myoblasts," *Food Science & Nutrition*, vol. 6, no. 8, pp. 2414–2422, 2018.
- [9] W.-C. Chang, D.-W. Huang, J.-A. Chen, Y.-F. Chang, J. Swi-Bea Wu, and S.-C. Shen, "Protective effect of *Ruellia tuberosa* L. extracts against abnormal expression of hepatic detoxification enzymes in diabetic rats," *RSC Advances*, vol. 8, no. 38, pp. 21596–21605, 2018.
- [10] J. H. Xu, Y. M. Lo, W. C. Chang et al., "Identification of bioactive components from *Ruellia tuberosa* L. on improving glucose uptake in TNF- α -induced insulin-resistant mouse FL83B hepatocytes," *Evidence-Based Complementary and Alternative Medicine*, vol. 2020, Article ID 6644253, 2020.
- [11] S.-C. Shen, W.-C. Chang, and C.-L. Chang, "An extract from wax apple (*Syzygium Samarangense* (blume) merrill and perry) effects glycogenesis and glycolysis pathways in tumor necrosis factor- α -treated fl83b mouse hepatocytes," *Nutrients*, vol. 5, no. 2, pp. 455–467, 2013.
- [12] E. Bugianesi, A. Gastaldelli, E. Vanni et al., "Insulin resistance in non-diabetic patients with non-alcoholic fatty liver disease: sites and mechanisms," *Diabetologia*, vol. 48, no. 4, pp. 634–642, 2005.
- [13] A. Gastaldelli, K. Cusi, M. Pettiti et al., "Relationship between hepatic/visceral fat and hepatic insulin resistance in nondiabetic and type 2 diabetic subjects," *Gastroenterology*, vol. 133, no. 2, pp. 496–506, 2007.
- [14] A. Kotronen, L. Juurinen, A. Hakkarainen et al., "Liver fat is increased in type 2 diabetic patients and underestimated by serum alanine aminotransferase compared with equally obese nondiabetic subjects," *Diabetes Care*, vol. 31, no. 1, pp. 165–169, 2008.
- [15] B. L. Wajchenberg, "Subcutaneous and visceral adipose tissue: their relation to the metabolic syndrome," *Endocrine Reviews*, vol. 21, no. 6, pp. 697–738, 2000.
- [16] M. P. Czech and S. Corvera, "Signaling mechanisms that regulate glucose transport," *Journal of Biological Chemistry*, vol. 274, no. 4, pp. 1865–1868, 1999.
- [17] X. Huang, G. Liu, J. Guo, and Z. Su, "The PI3K/AKT pathway in obesity and type 2 diabetes," *International Journal of Biological Sciences*, vol. 14, no. 11, pp. 1483–1496, 2018.
- [18] A. Leturque, E. Brot-Laroche, and M. Le Gall, "GLUT2 mutations, translocation, and receptor function in diet sugar managing," *American Journal of Physiology. Endocrinology and Metabolism*, vol. 296, no. 5, pp. E985–E992, 2009.
- [19] J.-J. Chang, M.-J. Hsu, H.-P. Huang, D.-J. Chung, Y.-C. Chang, and C.-J. Wang, "Mulberry anthocyanins inhibit oleic acid induced lipid accumulation by reduction of lipogenesis and promotion of hepatic lipid clearance," *Journal of Agricultural and Food Chemistry*, vol. 61, no. 25, pp. 6069–6076, 2013.
- [20] D. Shahwara, S. Ullah, M. Ahmad, S. Ullah, N. Ahmad, and M. A. Khan, "Hypoglycemic activity of *Ruellia tuberosa* linn (Acanthaceae) in normal and alloxan-induced diabetic rabbits," *Indian Journal of Pharmaceutical Sciences*, vol. 7, pp. 107–115, 2011.
- [21] F.-A. Chen, A.-B. Wu, P. Shieh, D.-H. Kuo, and C.-Y. Hsieh, "Evaluation of the antioxidant activity of *Ruellia tuberosa*," *Food Chemistry*, vol. 94, no. 1, pp. 14–18, 2006.
- [22] D. R. Wulan, E. P. Utomo, and C. Mahdi, "Antidiabetic activity of *Ruellia tuberosa* L., role of α -amylase inhibitor: in silico, in vitro, and in vivo approaches," *Biochemistry Research International*, vol. 2015, Article ID 349261, 2015.

Research Article

Wild Bitter Melon Extract Regulates LPS-Induced Hepatic Stellate Cell Activation, Inflammation, Endoplasmic Reticulum Stress, and Ferroptosis

Chang-Hsun Ho,¹ Jen-Hsuan Huang,¹ Maw-Sheng Sun,^{1,2} I-Shiang Tzeng,³ Yi-Chiung Hsu,⁴ and Chan-Yen Kuo³

¹Department of Anesthesiology, Show Chwan Memorial Hospital, Changhua, Taiwan

²Department of Nursing, Meiho University, Pingtung, Taiwan

³Department of Research, Taipei Tzu Chi Hospital, Buddhist Tzu Chi Medical Foundation, New Taipei City, Taiwan

⁴Department of Biomedical Sciences and Engineering, National Central University, Taoyuan, Taiwan

Correspondence should be addressed to Chan-Yen Kuo; cykuo863135@gmail.com

Received 5 October 2020; Accepted 17 June 2021; Published 22 June 2021

Academic Editor: Shagufta Perveen

Copyright © 2021 Chang-Hsun Ho et al. This is an open access article distributed under the Creative Commons Attribution License, which permits unrestricted use, distribution, and reproduction in any medium, provided the original work is properly cited.

The activation of hepatic stellate cells (HSCs) is a key component of liver fibrosis. Two antifibrosis pathways have been identified, the reversion to quiescent-type HSCs and the clearance of HSCs through apoptosis. Lipopolysaccharide- (LPS-) induced HSCs activation and proliferation have been associated with the development of liver fibrosis. We determined the pharmacological effects of wild bitter melon (WM) on HSC activation following LPS treatment and investigated whether WM treatment affected cell death pathways under LPS-treated conditions, including ferroptosis. WM treatment caused cell death, both with and without LPS treatment. WM treatment caused reactive oxygen species (ROS) accumulation without LPS treatment and reversed the decrease in lipid ROS production in HSCs after LPS treatment. We examined the effects of WM treatment on fibrosis, endoplasmic reticulum (ER) stress, inflammation, and ferroptosis in LPS-activated HSCs. The western blotting analysis revealed that the WM treatment of LPS-activated HSCs induced the downregulation of the connective tissue growth factor (CTGF), α -smooth muscle actin (α -SMA), integrin- β 1, phospho-JNK (p-JNK), glutathione peroxidase 4 (GPX4), and cystine/glutamate transporter (SLC7A11) and the upregulation of CCAAT enhancer-binding protein homologous protein (CHOP). These results support WM as an antifibrotic agent that may represent a potential therapeutic solution for the management of liver fibrosis.

1. Introduction

Chronic liver fibrosis is a health problem, characterized by severe morbidity and significant mortality [1–3]. The underlying physiology of chronic liver fibrosis has been associated with the rapid activation and transdifferentiation of quiescent HSCs fibrogenic myofibroblast-like cells following liver injury or the development of liver fibrosis [4, 5], resulting in cell proliferation, migration, extracellular matrix (ECM) accumulation [6], contraction, chemotaxis, and inflammatory signaling [7]. ECM accumulation has been associated with the increased expression of α -smooth muscle

actin (α -SMA), type I and III collagens, and tissue inhibitor of metalloproteinase-1 (TIMP-1), following the development of liver fibrosis [5, 8–10]. The contraction of HSCs has been proposed to mediate fibrosis by regulating sinusoidal blood flow and ECM remodeling [11]. Recent studies have shown that HSCs are activated by external signals, contributing to liver inflammation or liver injury by producing inflammatory cytokines and directing T lymphocytes into the parenchyma [12]. Multiple cellular and molecular signaling pathways are involved in the regulation of HSC activation: (1) the release of mitogenic (transforming growth factor- α (TGF- α [13]), platelet-derived growth factor

(PDGF [14, 15]), interleukin-1 (IL-1 [16]), tumor necrosis factor- α (TNF- α [17]), and insulin-like growth factor (IGF-1)) and fibrogenic (transforming growth factor- β (TGF- β [18]) and interleukin-6 (IL-6)) cytokines; (2) receptor activation, including Toll-like receptors (TLRs [19]), collagen receptors [20], liver X receptor [21], the nuclear receptor Rev-erb α [22], the orphan nuclear receptor NR4A1 [23], vitamin D receptor [24], and G protein-coupled receptors, such as succinate dehydrogenase-G protein-coupled receptor 91 (GPR91) [25, 26]; (3) autophagy, endoplasmic reticulum (ER) stress, and oxidative stress [27–31]; and (4) inflammatory cells, including macrophages, natural killer cells, hepatocytes, and B cells [5, 16, 17, 32–34].

The resolution of hepatic fibrosis requires the clearance of activated HSCs, via apoptosis, or the reversion of HSCs an inactivated phenotype [7–9]. Therefore, HSCs represent an attractive target for antifibrotic therapy [35, 36]. The differentiation of HSCs into proliferative, fibrogenic myofibroblasts is well-known to play a critical role during hepatic fibrosis, as demonstrated by both experimental and clinical human liver injuries [7]. Existing antifibrotic strategies include decreasing the number of activated HSCs via the inhibition of proliferation, the induction of apoptosis, and the inhibition of excessive ECM deposition [37]. Thus, the suppression of HSC growth and/or the induction of HSC apoptosis by natural products are considered to be effective options for the amelioration of liver fibrosis.

Wild bitter melon (WM; *Momordica charantia* L. var. *Abbreviata* Seringe) is a wild variety of bitter melon (*Momordica charantia*) [38, 39]. The ethyl acetate (EA) fraction from WM has been reported to exhibit strong antioxidant activity, via the scavenging activity of 1, 1-diphenyl-2-picryl-hydrazyl (DPPH), which can reduce H₂O₂-induced DNA damage. Moreover, the EA fraction effectively inhibited α -amylase activity and suppressed the production of the proinflammatory mediator nitric oxide (NO) in LPS-stimulated murine macrophage RAW 264.7 cells [40]. Similar results indicated that the EA extract of WM suppressed *Propionibacterium acnes*-induced inflammation in THP-1 cells [41]. WM has been demonstrated to have anticancer activities in various cancers types, in vitro, including breast cancer [42–44], colon cancer [45, 46], pancreatic cancer [47], liver cancer [48, 49], prostate cancer [50, 51], cervical cancer [52], and others [53]. However, the full impact of WM on human health has not been thoroughly demonstrated, and systematic clinical studies remain necessary to establish the efficacy and safety of WM extract use in patients. Both in vitro and in vivo studies have demonstrated that bitter melon may elicit toxic or adverse effects under various conditions [53].

This study aimed to investigate whether WM extracts attenuated HSC T6 cell activation induced by LPS treatment. Our data indicated that WM treatments increased ROS and lipid ROS accumulation, induced ER stress, and triggered ferroptosis in LPS-treated HSC T6 cells. We proposed that WM treatment attenuated the LPS-induced HSC activation via ER stress and ferroptosis.

2. Materials and Methods

2.1. Reagents. WM extract (WM) was purchased from License Biotec, Co., Ltd. (Taipei, Taiwan). The total phenolic extract (TPE) was obtained as described by Huang et al. [54].

2.2. Antibodies. The following antibodies were used for immunofluorescence staining and Western blotting: rabbit polyclonal antibodies against CHOP (#A0854, 1:1000 dilution, ABclonal, MA, USA), p-JNK (#AP0808, 1:1000 dilution, ABclonal, MA, USA), JNK (#A4867, 1:1000 dilution, ABclonal, MA, USA), CTGF (#A11456, 1:1000 dilution, ABclonal, MA, USA), α -SMA (#A1011, 1:1000 dilution, ABclonal, MA, USA), integrin- β 1 (#A11060, 1:1000 dilution, ABclonal, MA, USA), GPX4 (#A1933, 1:1000 dilution, ABclonal, MA, USA), SLC7A11 (#A13685, 1:1000 dilution, ABclonal, MA, USA), and β -actin (#AC026, 1:5000 dilution, ABclonal, MA, USA).

2.3. Cell Culture. HSC-T6, a rat HSC cell line, was purchased from Millipore (MA, USA). HSC-T6 cells were cultured at 37°C in Dulbecco's minimum essential medium (DMEM; Gibco, NY, USA), supplemented with 10% fetal bovine serum (FBS) and antibiotics (100 U/ml penicillin, 100 μ g/ml streptomycin, and 2.5 μ g/ml amphotericin B), in a humidified atmosphere containing 5% CO₂. The culture medium was replaced every other day. Once the cells reached 70–80% confluency, they were trypsinized and seeded into 6-well or 24-well plastic dishes for further experiments.

2.4. Analysis of Cell Viability. Cell viability was measured using WST-1 assay. Cells were seeded at a density of 5×10^4 cells/mL in 24-well plates and cultured in phenol red-free DMEM, containing 0.5% heat-inactivated FBS, for 24 h. Cells were then incubated with 20 μ g/ml of WM or 10 μ g/ml of LPS, as indicated, for 24 h. WST-1 reagent was then added to the medium and incubated at 37°C for 2 h. The absorbance was measured at 450 nm using a microplate reader (Thermo LabSystems, Waltham, MA, USA).

2.5. Western Blotting. Sodium dodecyl sulfate-polyacrylamide gel electrophoresis (SDS-PAGE) was performed using 10% acrylamide gels, with 20 μ g of protein loaded into each lane. After electrophoresis, the proteins were transferred from the gel to a polyvinylidene fluoride (PVDF) membrane, at 350 mA for 2 hours, and the membrane was then blocked with 5% nonfat milk for 1 hour. The membranes were incubated with primary antibodies, diluted 1:1,000 in 5% nonfat milk, overnight at 4°C. Membranes were washed in TBST buffer (20 mM Tris-HCl, pH 7.4, 137 mM NaCl, and 0.1% Tween-20) 3 times, for 10 minutes each time, incubated with secondary antibodies conjugated to horseradish peroxidase (HRP), at 1:10,000 dilution, for 1 hour at room temperature, washed again, and stained with a Western HRP substrate. Protein bands were visualized on X-ray film using an enhanced chemiluminescence system (Kodak).

2.6. Lipid ROS Detection. Cells were incubated with 2 μ M C11-BODIPY 581/591 (Thermo Fisher Scientific), in culture medium for 1 h and then washed with phosphate-buffered saline. After trypsinization, cells were collected and used for flow cytometry (BD Biosciences, San Jose, CA, USA), using an excitation wavelength of 488 nm and an emission wavelength of 517–527 nm.

2.7. Statistical Analysis. Continuous data were expressed as the mean \pm standard error of the mean. Statistical differences among means from different groups were determined by one-way or a two-way analysis of variance, followed by a Bonferroni post hoc test for continuous variables. *P* values <0.05 were considered significant differences.

3. Results

3.1. WM Treatment Caused ROS Accumulation and Cell Death. The acceleration ROS accumulation has been shown to disrupt redox homeostasis and cause severe damage in cancer cells, resulting in cancer cell death via the activation of apoptosis, autophagic cell death, and necroptosis [55]. The induction of apoptosis on HSCs via the stimulation of ROS accumulation represents a potential strategy for addressing liver fibrosis [56]. Our results showed that WM treatment induced ROS overproduction in HSCs relative to untreated cells (Figures 1(a) and 1(b)). Decreased HSC viability was detected after treatment with 20 μ g/ml WM for 24 h compared with untreated cells (Figure 1(c)). These results indicated that WM treatment induced ROS accumulation and cell death.

3.2. WM Treatment Resulted in Lipid ROS Accumulation and Cell Death in LPS-Activated HSCs. LPS is a well-known activator of HSCs and LPS treatment results in the activation of a proinflammatory, myofibroblast phenotype [57]. ROS-induced lipid peroxidation and lipid ROS accumulation has been reported to play critical roles in cell death pathways, including apoptosis, autophagy, and ferroptosis [58]. As shown in Figure 2, the results indicated that lipid ROS accumulation decreased in LPS-activated HSCs compared with untreated HSCs (Figures 2(a) and 2(b), column 1 vs. column 2 but increased after the WM treatment of LPS-activated HSCs (WM treatment in LPS-activated HSCs, Figures 2(a) and 2(b), column 2 vs. column 4). In contrast, cell viability significantly decreased after WM treatment in quiescent HSCs compared with untreated cells (Figure 2(c), column 1 vs. column 3). Interestingly, WM treatment caused cell death in LPS-activated HSCs (Figure 2(c), column 2 vs. column 4). Therefore, we proposed that WM treatment resulted in lipid ROS accumulation and cell death in LPS-activated HSCs.

3.3. WM Treatment Enhanced ER Stress, Attenuated Inflammation, and Triggered Ferroptosis in LPS-Activated HSCs. CHOP plays a critical role in ER stress-induced apoptosis [59]. Oyadomari and Mori demonstrated that when severe

ER stress conditions persist, apoptotic signaling pathways become activated, resulting in the induction of CHOP [60]. Our results showed that CHOP expression levels decreased in LPS-activated HSCs (Figures 3(a) and 3(b), column 1 vs. column 2) but increased following the WM treatment of LPS-activated HSCs (WM treatment in LPS-activated HSCs, Figures 3(a) and 3(b), column 2 vs. column 4). Additionally, JNK is a well-known regulator of the inflammatory response [61]. As shown in Figures 3(a) and 3(b), the expression levels of p-JNK increased in LPS-activated HSCs, compared with quiescent HSCs (Figures 3(a) and 3(b), column 1 vs. column 2) and decreased after the WM treatment of LPS-activated HSCs (WM treatment in LPS-activated HSCs, Figures 3(a) and 3(b), column 2 vs. column 4).

Ferroptosis is a newly identified cell death pathway, which occurs in an iron-dependent manner and is characterized by iron accumulation and lipid peroxidation during the cell death process [62]. SLC7A11 is a key regulator of the antioxidant system Xc⁻, which mediates the exchange of cysteine and glutamate, and is widely distributed in the phospholipid bilayer [63]. GPX4 (glutathione peroxidase 4) activity decreases with increasing system Xc⁻ activity, resulting in decreased antioxidant capacity, lipid ROS accumulation, and ultimately, oxidative damage and ferroptosis [62]. Friedmann Angeli et al. reported that knockout of GPX4 caused cell death via ferroptosis, both in vitro and in vivo [64]. In the present study, the results showed that the expression levels of GPX4 and SLC7A11 increased in LPS-activated HSCs, compared with untreated HSCs (Figures 3(c) and 3(d), column 1 vs. column 2), but decreased after the WM treatment of LPS-activated HSCs (WM treatment in LPS-activated HSCs, Figures 3(c) and 3(d), column 2 vs. column 4). Altogether, these results indicated that WM treatment sensitized LPS-activated HSCs ER stress, attenuated inflammation, and triggered ferroptosis.

3.4. WM Treatment Has Antifibrotic Effects on LPS-Activated HSCs. Activated HSCs are well-known as potential therapeutic targets in liver fibrosis [65]. We investigated whether WM treatments have any antifibrotic effects in LPS-activated HSCs. As shown in Figures 4(a) and 4(b), the expression levels of CTGF, α -SMA, and integrin- β 1 increased in LPS-activated HSCs, compared with untreated HSCs (Figures 4(a) and 4(b), column 1 vs. column 2), but decreased after WM treatment (WM treatment in LPS-activated HSCs, Figures 4(a) and 4(b), column 2 vs. column 4). Therefore, we suggested that WM treatment has great potential for use to treat and prevent liver fibrosis through effects on activated HSCs.

4. Discussion

Activated HSCs play major roles in the pathogenesis of liver fibrosis [66]. Growing evidence has suggested that the induction of HSC cell death and the inhibition of HSC growth may represent potential strategies for the treatment and/or prevention of liver fibrosis [9, 33, 67–70]. Furthermore, natural fruits may be used as additional therapeutic

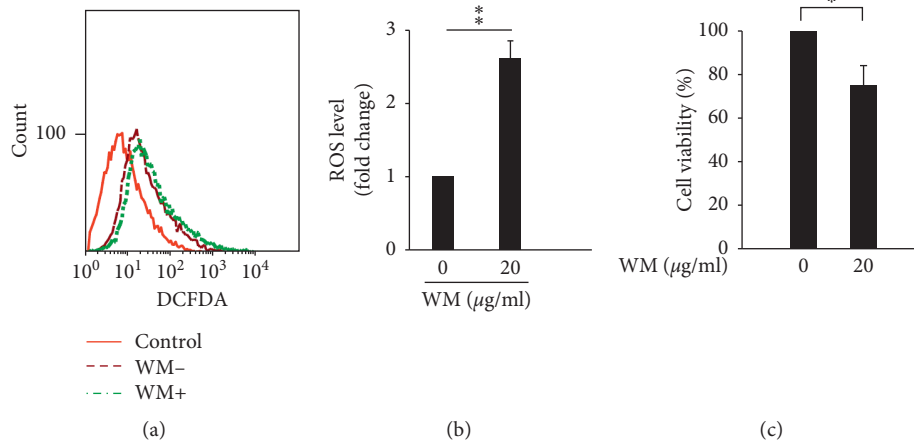


FIGURE 1: WM treatment induced ROS production and decreased cell viability. (a) Cells treated with (WM+) or without (WM-) 20 μg/ml WM for 24 h. The levels of intracellular ROS were determined using DCF-DA, and fluorescence was detected using FACS Calibur analysis. Control samples refer to cells without DCF-DA. (b) ROS levels are expressed as the mean fluorescence intensity. (c) Cells treated with either the vehicle (0 μg/ml WM) or WM (20 μg/ml) for 24 h. After the incubation period, cell viability was determined using WST-1 assay. All data are presented as the mean ± SD. **p* < 0.05, ***p* < 0.01, *n* = 3.

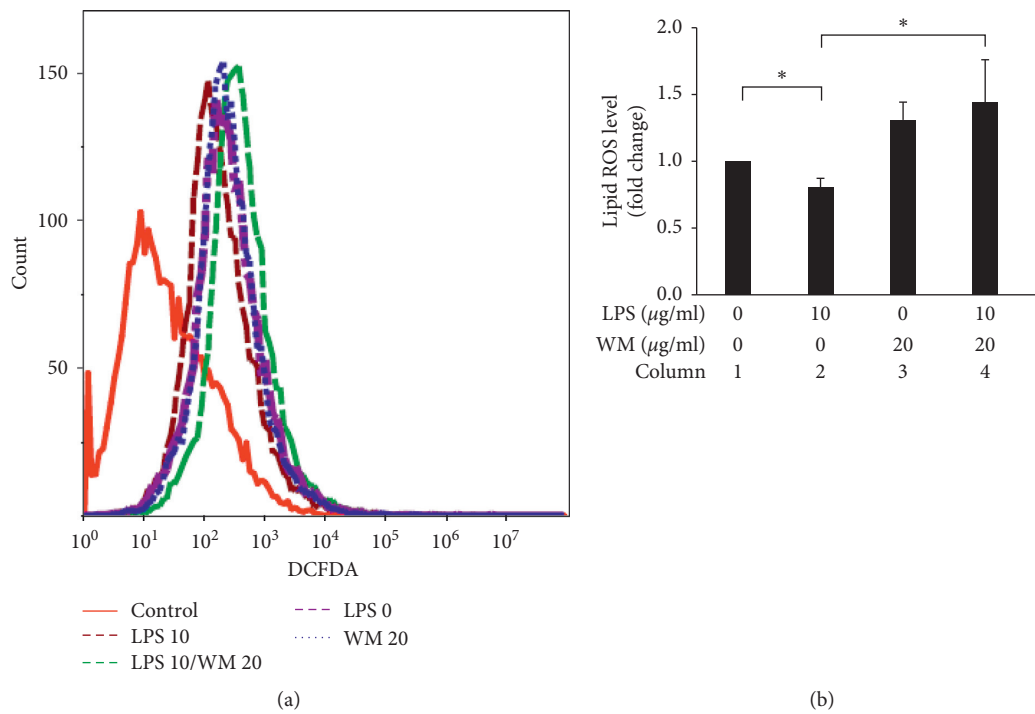


FIGURE 2: Continued.

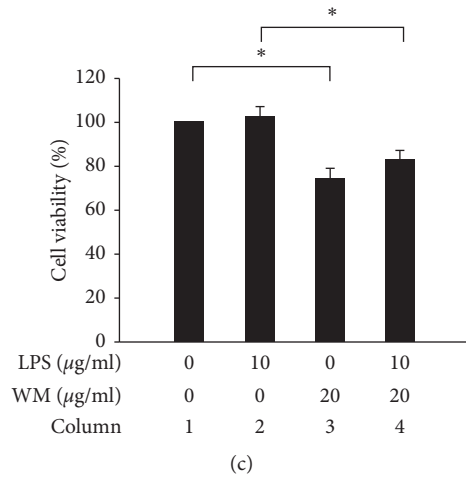


FIGURE 2: WM treatment reversed the decrease in lipid ROS production and increased cell viability in LPS-activated HSCs. (a) Changes in cellular lipid ROS levels, associated with the indicated conditions in HSC-T6 cells. (b) ROS levels are expressed as mean fluorescence intensity. (c) Cells cultured using the indicated conditions, for 24 h. After the incubation period, cell viability was determined using WST-1 assay. Controls refer cells without $2\ \mu\text{M}$ C11-BODIPY 581/591. LPS 0 indicates cells without LPS treatment. LPS 10 indicates cells treated with $10\ \mu\text{g/ml}$ LPS. WM 20 indicates cells treated with $20\ \mu\text{g/ml}$ WM. All data are presented as the mean \pm SD. $*p < 0.05$, $n = 3$.

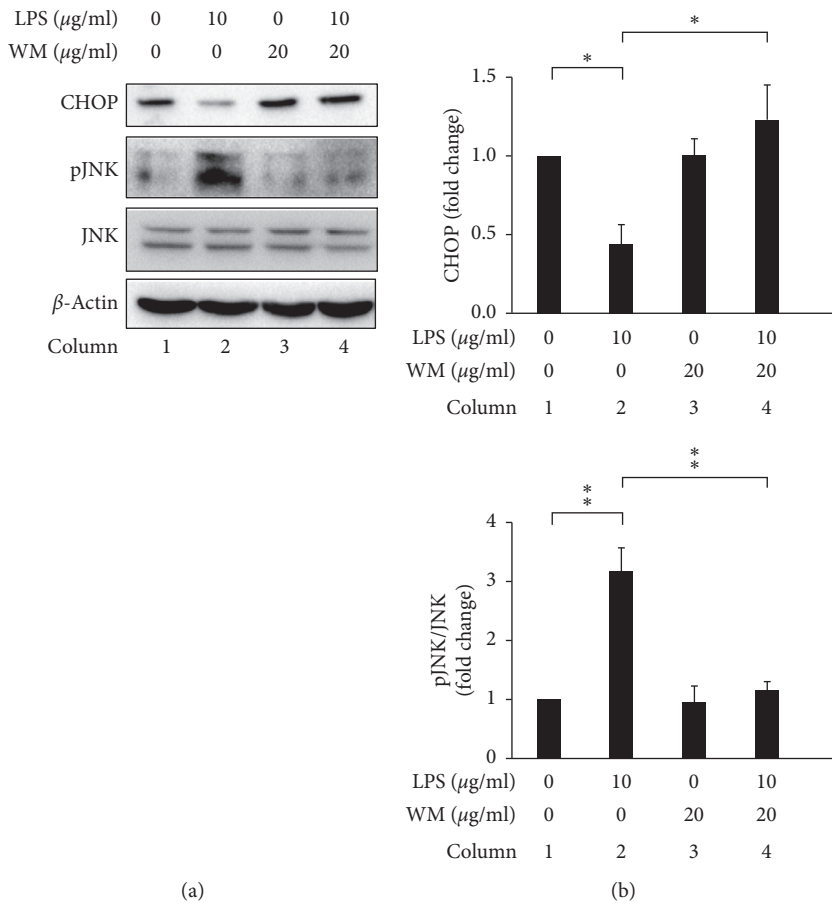


FIGURE 3: Continued.

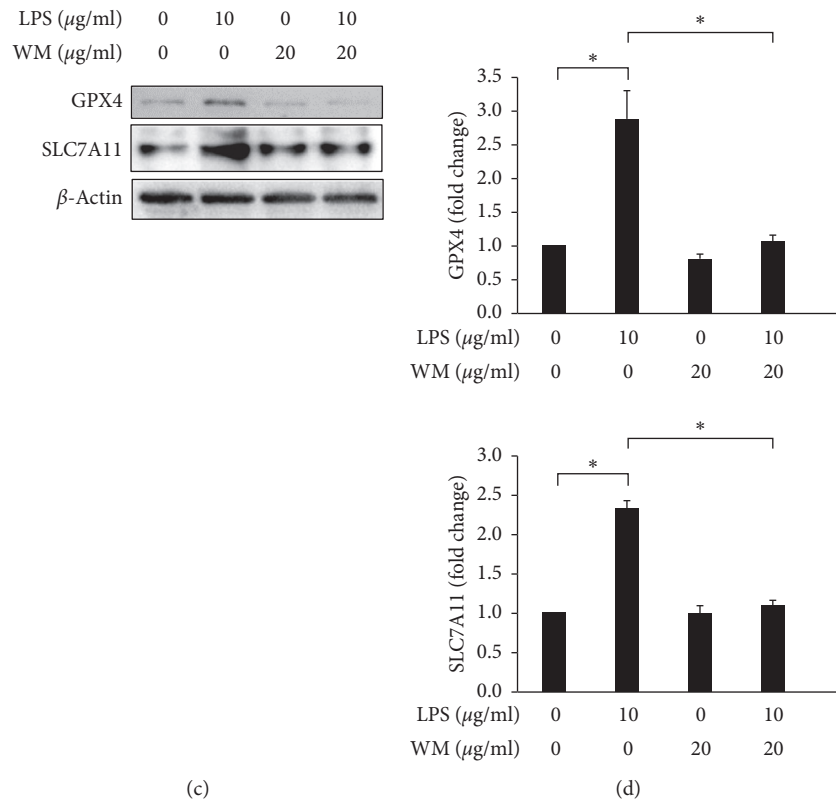


FIGURE 3: WM treatment induced ER stress, alleviated inflammation, and triggered ferroptosis in LPS-activated HSCs. (a) Changes in the expression levels of CHOP and p-JNK. β -Actin was used as an internal control. (b) Quantitative evaluation of the levels of specific proteins, assessed by ImageJ. All data are presented as the mean \pm SD. $n = 3$, $*p < 0.05$. (c) Changes in the expression levels of GPX4 and SLC7A11. β -Actin was used as an internal control. (d) Quantitative evaluation of the levels of specific proteins, assessed by ImageJ. All data are presented as the mean \pm SD. $n = 3$, $*p < 0.05$.

approaches to inhibit hepatic fibrogenesis. To our knowledge, this study demonstrated, for the first time, that an extract from the natural fruit WM could attenuate LPS-induced HSC activation via the regulation of ER stress and ferroptosis. However, the pharmacological effects of WM treatments in HSCs remain unclear. Our results indicated that WM treatment caused ROS accumulation, lipid ROS accumulation, and cell death in LPS-activated HSCs (Figures 1 and 2). WM treatment also increased ER stress-induced apoptosis and attenuated inflammation and ferroptosis in LPS-activated HSCs (Figure 3). We also detected the effects of WM treatment on the expression of the following proteins: α -SMA, a critical marker of HSC activation [71]; CTGF, a maker of liver fibrosis [72, 73]; and integrin- β 1, a hallmark of hepatic fibrosis [74]. As shown in Figure 4, WM treatment decreased the expression levels of these proteins (Figure 4). Therefore, these data demonstrated that WM treatment may protect against liver fibrosis via HSC inactivation or death.

Astaxanthin was shown to inhibit liver fibrosis via HSC inactivation and the decreased formation of ECM in carbon tetrachloride (CCL_4) and bile duct ligation mouse models [75]. Similar results were also reported for treatments with curcumin [76], blueberry [77], silymarin [78], 3, 5-diethoxy-3'-hydroxyresveratrol [79], quercetin [80], epigallocatechin-3-gallate [81], coffee [82], and vitamins [83]. Additionally, Kuo et al. suggested that the marine extract from a

gorgonian coral *Pinnigorgia* sp. (Pin) could induce apoptosis in HSC-T6 cells via ROS-ERK/JNK-caspase-3 signaling and may exhibit therapeutic potential for the clearance of HSCs [84]. Other studies have reported similar results [85–87]. These studies further strengthen the evidence for the use of bioactive food components and natural products with potential antifibrotic effects in therapeutic approaches designed to slow or reverse the development of liver fibrosis.

Huang et al. reported that the quantitative high-performance liquid chromatography analysis of WM TPE revealed gallic, chlorogenic, caffeic, ferulic, and cinnamic acids, myricetin, quercetin, luteolin, apigenin, and thymol and that WM TPE displayed an anti-inflammatory response against *Propionibacterium acnes*-induced skin inflammation, in vivo [54]. Chen et al. showed that gallic acids attenuated dimethylnitrosamine-induced fibrosis via the regulation of Smad phosphorylation [88]. Chlorogenic acids protect against CCL_4 -induced liver fibrosis through the suppression of oxidative stress in the liver and HSCs [89]. Caffeic and ferulic acids have been shown to prevent liver damage and ameliorate liver fibrosis in CCL_4 -treated rats [90, 91]. Wang et al. demonstrated that trans-cinnamic acid has antiobesity effects in oleic acid- (OA-) induced HepG2 cells and high-fat diet- (HFD-) fed mice [92]; however, the role played by trans-cinnamic acid in HSCs remains unclear. Myricetin modulated the polarization of macrophages via

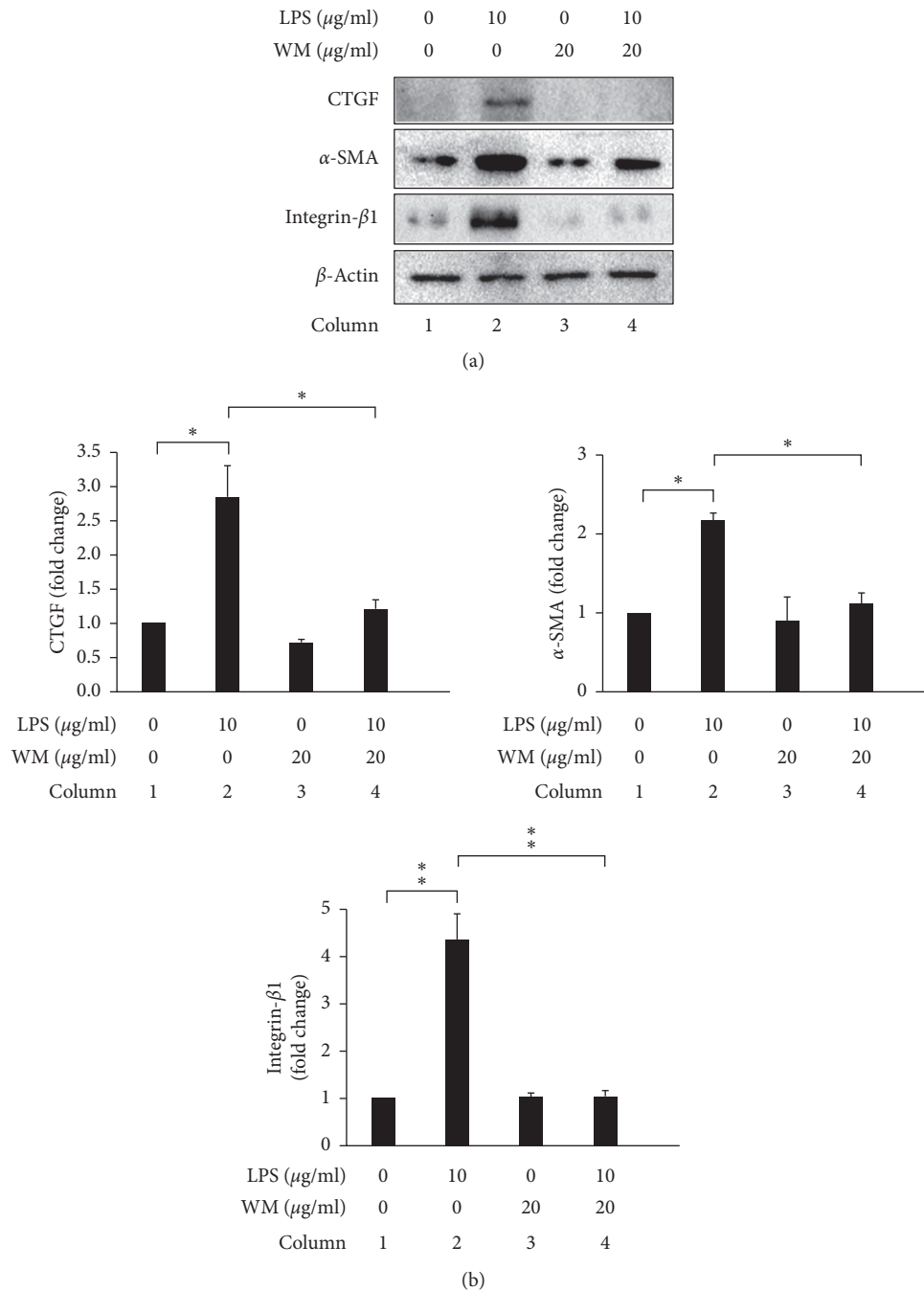


FIGURE 4: WM treatment attenuated fibrosis in LPS-activated HSCs. (a) Changes in the expression levels of CTGF, α -SMA, and integrin- β 1. β -Actin was used as an internal control. (b) Quantitative evaluation of the levels of specific proteins, assessed by ImageJ. All data are presented as the mean \pm SD. $n = 3$, $*p < 0.05$, $**p < 0.01$.

the inhibition of TREM-1-TLR2/4-MyD88 signaling molecules in macrophages and attenuated liver inflammation and fibrosis in a choline-deficient, L-amino acid-defined, high-fat diet-induced nonalcoholic steatohepatitis model [93]. Quercetin caused decreased oxidative stress and inflammation and prevented liver fibrosis via the induction of HSC apoptosis [94]. Li et al. speculated that luteolin exhibits antifibrotic effects in HSCs and liver fibrosis by targeting the

AKT/mTOR/p70S6K and TGF β /Smad signaling pathways in CCl₄, dimethylnitrosamine, and bile duct ligation induced animal models of fibrosis and rat HSCs and HSC-T6 cells [95]. A computational approach indicated that apigenin was predicted to have antifibrotic activity [96]. Thymol significantly ameliorated liver injury due to endotoxicity in gastric ulcer rat models [97]; however, the role played by thymol in liver fibrosis remains uncertain.

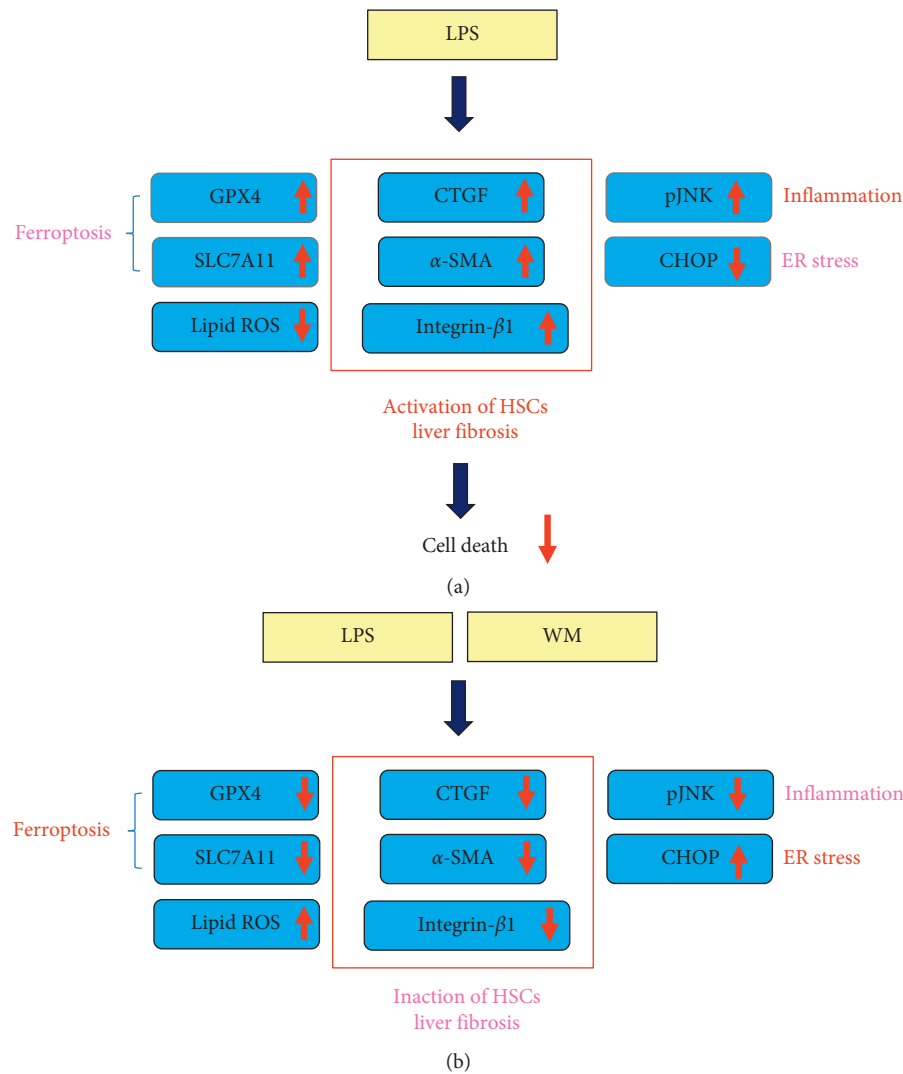


FIGURE 5: A summary diagram outlines the working mechanisms of WM in LPS-activated HSCs. (a) LPS decreased ER stress and ferroptosis via downregulations of CHOP and GPX4/SLC7A11, respectively. LPS reduced lipid ROS production and cell death, but induced inflammation. On the other hand, LPS promoted liver fibrosis via HSCs activation determined by CTGF, α -SMA, and integrin- β 1 upregulation. (b) WM induced ER stress and ferroptosis via upregulations of CHOP and GPX4/SLC7A11, respectively. WM also caused increases in ROS, lipid ROS production, and cell death, but reduced inflammation. Moreover, WM prevented liver fibrosis via HSCs inactivation determined by CTGF, α -SMA, and integrin- β 1 downregulation.

5. Conclusions

In summary, the present study demonstrated that the pretreatment of HSCs with WM prevented LPS-induced HSC-T6 cell activation (as demonstrated by CTGF, α -SMA, and integrin- β 1 levels) and inflammation (as indicated by p-JNK levels). WM treatment caused ROS/lipid ROS overproduction, cell death, ER stress activation (as indicated by CHOP expression), and ferroptosis (as indicated by GPX4 and SLC7A11 expression) in LPS-activated HSC-T6 cells (Figure 5). These novel findings deepen our understanding of the mechanistic actions underlying WM treatments. Because WM showed potential antifibrotic effects in activated HSCs, further *in vivo* studies should be performed to determine the potential effects of WM treatment on various liver fibrosis models.

Data Availability

The data used to support the findings of this study are included within the article.

Conflicts of Interest

The authors declare that there are no conflicts of interest.

Acknowledgments

The authors appreciate the research assistants, Mrs. Yi-Ying Lin and Ming-Cheng Lee, for the troubleshooting of flow cytometry and Western blot, respectively, and acknowledge the Core Laboratory, Department of Research, Taipei Tzu Chi Hospital, Buddhist Tzu Chi Medical Foundation, New

Taipei City, Taiwan. Thanks to all the authors for their contribution to this article. This work was supported by the Show Chwan Memorial Hospital, Changhua, Taiwan (SRD-109027).

References

- [1] P. A. Bonis, S. L. Friedman, and M. M. Kaplan, "Is liver fibrosis reversible?" *New England Journal of Medicine*, vol. 344, pp. 452–454, 2001.
- [2] S. L. Friedman, "Hepatic fibrosis-overview," *Toxicology*, vol. 254, pp. 120–129, 2008.
- [3] S. L. Friedman, "Mechanisms of hepatic fibrogenesis," *Gastroenterology*, vol. 134, pp. 1655–1669, 2008.
- [4] S. L. Friedman, "Hepatic stellate cells: protean, multifunctional, and enigmatic cells of the liver," *Physiological Reviews*, vol. 88, pp. 125–172, 2008.
- [5] W. Hou and W. K. Syn, "Role of metabolism in hepatic stellate cell activation and fibrogenesis," *Frontiers in Cell and Developmental Biology*, vol. 6, p. 150, 2018.
- [6] R. Bataller and D. A. Brenner, "Liver fibrosis," *Journal of Clinical Investigation*, vol. 115, pp. 209–218, 2005.
- [7] T. Tsuchida and S. L. Friedman, "Mechanisms of hepatic stellate cell activation," *Nature Reviews Gastroenterology & Hepatology*, vol. 14, pp. 397–411, 2017.
- [8] F. R. Murphy, R. Issa, X. Zhou et al., "Inhibition of apoptosis of activated hepatic stellate cells by tissue inhibitor of metalloproteinase-1 is mediated via effects on matrix metalloproteinase inhibition," *Journal of Biological Chemistry*, vol. 277, no. 13, pp. 11069–11076, 2002.
- [9] S. L. Friedman, "Evolving challenges in hepatic fibrosis," *Nature Reviews Gastroenterology & Hepatology*, vol. 7, pp. 425–436, 2010.
- [10] P. Bedossa and V. Paradis, "Liver extracellular matrix in health and disease," *Journal of Pathology*, vol. 200, pp. 504–515, 2003.
- [11] R. K. Soon Jr. and H. F. Yee Jr., "Stellate cell contraction: role, regulation, and potential therapeutic target," *Clinical Liver Disease*, vol. 12, pp. 791–803, 2008.
- [12] T. Fujita and S. Narumiya, "Roles of hepatic stellate cells in liver inflammation: a new perspective," *Inflammation and Regeneration*, vol. 36, p. 1, 2016.
- [13] H. Tsukamoto, "Cytokine regulation of hepatic stellate cells in liver fibrosis," *Alcoholism: Clinical and Experimental Research*, vol. 23, pp. 911–916, 1999.
- [14] L. Wong, G. Yamasaki, R. J. Johnson, and S. L. Friedman, "Induction of beta-platelet-derived growth factor receptor in rat hepatic lipocytes during cellular activation in vivo and in culture," *Journal of Clinical Investigation*, vol. 94, pp. 1563–1569, 1994.
- [15] M. Pinzani, "PDGF and signal transduction in hepatic stellate cells," *Frontiers in Bioscience*, vol. 7, pp. d1720–d1726, 2002.
- [16] R. G. Gieling, K. Wallace, and Y. P. Han, "Interleukin-1 participates in the progression from liver injury to fibrosis," *American Journal of Physiology-Gastrointestinal and Liver Physiology*, vol. 296, pp. G1324–G1331, 2009.
- [17] H. L. Reeves and S. L. Friedman, "Activation of hepatic stellate cells—a key issue in liver fibrosis," *Frontiers in Bioscience*, vol. 7, pp. d808–d826, 2002.
- [18] B. Dewidar, C. Meyer, S. Dooley, and A. N. Meindl-Beinker, "TGF-beta in hepatic stellate cell activation and liver fibrogenesis—updated 2019," *Cells*, vol. 8, 2019.
- [19] M. H. Chou, Y. H. Huang, T. M. Lin et al., "Selective activation of toll-like receptor 7 in activated hepatic stellate cells may modulate their profibrogenic phenotype," *Biochemical Journal*, vol. 447, pp. 25–34, 2012.
- [20] H. Liu, X. Pan, H. Cao et al., "IL-32gamma promotes integrin alphavbeta6 expression through the activation of NF-kappaB in HSCs," *Experimental and Therapeutic Medicine*, vol. 14, pp. 3880–3886, 2017.
- [21] S. W. Beaven, K. Wroblewski, J. Wang et al., "Liver X receptor signaling is a determinant of stellate cell activation and susceptibility to fibrotic liver disease," *Gastroenterology*, vol. 140, pp. 1052–1062, 2011.
- [22] T. Li, A. L. Eheim, S. Klein et al., "Novel role of nuclear receptor rev-erba in hepatic stellate cell activation: potential therapeutic target for liver injury," *Hepatology*, vol. 59, no. 6, pp. 2383–2396, 2014.
- [23] K. Palumbo-Zerr, P. Zerr, A. Distler et al., "Orphan nuclear receptor NR4A1 regulates transforming growth factor-beta signaling and fibrosis," *Nature Medicine*, vol. 21, pp. 150–158, 2015.
- [24] A. Duran, E. D. Hernandez, M. Reina-Campos et al., "p62/SQSTM1 by binding to vitamin D receptor inhibits hepatic stellate cell activity, fibrosis, and liver cancer," *Cancer Cell*, vol. 30, pp. 595–609, 2016.
- [25] Y. H. Li, D. H. Choi, E. H. Lee, S. R. Seo, S. Lee, and E.-H. Cho, "Sirtuin 3 (SIRT3) regulates alpha-smooth muscle actin (alpha-SMA) production through the succinate dehydrogenase-G protein-coupled receptor 91 (GPR91) pathway in hepatic stellate cells," *Journal of Biological Chemistry*, vol. 291, no. 19, pp. 10277–10292, 2016.
- [26] Y. H. Li, S. H. Woo, D. H. Choi, and E. H. Cho, "Succinate causes alpha-SMA production through GPR91 activation in hepatic stellate cells," *Biochemical and Biophysical Research Communications*, vol. 463, pp. 853–858, 2015.
- [27] L. F. Thoen, E. L. Guimaraes, L. Dolle et al., "A role for autophagy during hepatic stellate cell activation," *Journal of Hepatology*, vol. 55, pp. 1353–1360, 2011.
- [28] V. Hernández-Gea and S. L. Friedman, "Autophagy fuels tissue fibrogenesis," *Autophagy*, vol. 8, no. 5, pp. 849–850, 2012.
- [29] V. Hernandez-Gea, Z. Ghiassi-Nejad, R. Rozenfeld et al., "Autophagy releases lipid that promotes fibrogenesis by activated hepatic stellate cells in mice and in human tissues," *Gastroenterology*, vol. 142, pp. 938–946, 2012.
- [30] V. Hernández-Gea, M. Hilscher, R. Rozenfeld et al., "Endoplasmic reticulum stress induces fibrogenic activity in hepatic stellate cells through autophagy," *Journal of Hepatology*, vol. 59, no. 1, pp. 98–104, 2013.
- [31] Q. Ou, Y. Weng, S. Wang et al., "Silybin alleviates hepatic steatosis and fibrosis in NASH mice by inhibiting oxidative stress and involvement with the NF-kappaB pathway," *Digestive Diseases and Sciences*, vol. 63, pp. 3398–3408, 2018.
- [32] J. Li, Y. R. Zhao, and Z. Tian, "Roles of hepatic stellate cells in acute liver failure: from the perspective of inflammation and fibrosis," *World Journal of Hepatology*, vol. 11, pp. 412–420, 2019.
- [33] J. P. Pradere, J. Kluwe, S. De Minicis et al., "Hepatic macrophages but not dendritic cells contribute to liver fibrosis by promoting the survival of activated hepatic stellate cells in mice," *Hepatology*, vol. 58, pp. 1461–1473, 2013.
- [34] A. Wehr, C. Baeck, F. Heymann et al., "Chemokine receptor CXCR6-dependent hepatic NK T cell accumulation promotes inflammation and liver fibrosis," *Journal of Immunology*, vol. 190, pp. 5226–5236, 2013.

- [35] J. A. Fallowfield, "Therapeutic targets in liver fibrosis," *American Journal of Physiology: Gastrointestinal and Liver Physiology*, vol. 300, pp. G709–G715, 2011.
- [36] S. L. Friedman, "Preface," *Clinics in Liver Disease*, vol. 12, no. 4, pp. xiii–xiv, 2008.
- [37] H. N. Fan, H. J. Wang, C. R. Yang-Dan et al., "Protective effects of hydrogen sulfide on oxidative stress and fibrosis in hepatic stellate cells," *Molecular Medicine Reports*, vol. 7, pp. 247–253, 2013.
- [38] J. Saengsai, S. Kongtunjanphuk, N. Yoswatthana, T. Kummalue, and W. Jiratchariyakul, "Antibacterial and antiproliferative activities of plumericin, an iridoid isolated from *Momordica charantia* vine," *Evidence-Based Complementary and Alternative Medicine*, vol. 2015, Article ID 823178, 10 pages, 2015.
- [39] T. H. Tsai, W. C. Huang, H. T. Ying et al., "Wild bitter melon leaf extract inhibits *Porphyromonas gingivalis*-induced inflammation: identification of active compounds through bioassay-guided isolation," *Molecules*, vol. 21, p. 454, 2016.
- [40] T. M. H. Pham, D.-H. Ngo, D.-N. Ngo, and T. S. Vo, "Investigation of biological activities of wild bitter melon (*Momordica charantia* linn. Var. *Abbraviata* ser.)," *Biomolecules*, vol. 9, no. 6, p. 211, 2019.
- [41] C. Hsu, T. H. Tsai, Y. Y. Li, W. H. Wu, C. J. Huang, and P. J. Tsai, "Wild bitter melon (*Momordica charantia* Linn. var. *abbraviata* Ser.) extract and its bioactive components suppress *Propionibacterium acnes*-induced inflammation," *Food Chemistry*, vol. 135, pp. 976–984, 2012.
- [42] J. R. Weng, L. Y. Bai, C. F. Chiu, J. L. Hu, S. J. Chiu, and C. Y. Wu, "Cucurbitane triterpenoid from *Momordica charantia* induces apoptosis and autophagy in breast cancer cells, in part, through peroxisome proliferator-activated receptor gamma activation," *Evidence-Based Complementary and Alternative Medicine*, vol. 2013, Article ID 935675, 12 pages, 2013.
- [43] E. F. Fang, C. Z. Zhang, W. P. Fong, and T. B. Ng, "RNase MC2: a new *Momordica charantia* ribonuclease that induces apoptosis in breast cancer cells associated with activation of MAPKs and induction of caspase pathways," *Apoptosis*, vol. 17, pp. 377–387, 2012.
- [44] R. B. Ray, A. Raychoudhuri, R. Steele, and P. Nerurkar, "Bitter melon (*Momordica charantia*) extract inhibits breast cancer cell proliferation by modulating cell cycle regulatory genes and promotes apoptosis," *Cancer Research*, vol. 70, pp. 1925–1931, 2010.
- [45] Y. Li, L. Yin, L. Zheng et al., "Application of high-speed counter-current chromatography coupled with a reverse micelle solvent system to separate three proteins from *Momordica charantia*," *Journal of chromatography. B, Analytical Technologies in the Biomedical and Life Sciences*, vol. 895–896, pp. 77–82, 2012.
- [46] D. Kwatra, A. Venugopal, D. Standing et al., "Bitter melon extracts enhance the activity of chemotherapeutic agents through the modulation of multiple drug resistance," *Journal of Pharmaceutical Sciences*, vol. 102, pp. 4444–4454, 2013.
- [47] M. Kaur, G. Deep, A. K. Jain et al., "Bitter melon juice activates cellular energy sensor AMP-activated protein kinase causing apoptotic death of human pancreatic carcinoma cells," *Carcinogenesis*, vol. 34, pp. 1585–1592, 2013.
- [48] E. F. Fang, C. Z. Zhang, J. H. Wong, J. Y. Shen, C. H. Li, and T. B. Ng, "The MAP30 protein from bitter melon (*Momordica charantia*) seeds promotes apoptosis in liver cancer cells in vitro and in vivo," *Cancer Letters*, vol. 324, pp. 66–74, 2012.
- [49] C. Z. Zhang, E. F. Fang, H. T. Zhang, L. L. Liu, and J. P. Yun, "Momordica charantia lectin exhibits antitumor activity towards hepatocellular carcinoma," *Investigational New Drugs*, vol. 33, pp. 1–11, 2015.
- [50] P. Pitchakarn, S. Suzuki, K. Ogawa et al., "Induction of G1 arrest and apoptosis in androgen-dependent human prostate cancer by Kuguacin J, a triterpenoid from *Momordica charantia* leaf," *Cancer Letters*, vol. 306, pp. 142–150, 2011.
- [51] S. D. Xiong, K. Yu, X. H. Liu et al., "Ribosome-inactivating proteins isolated from dietary bitter melon induce apoptosis and inhibit histone deacetylase-1 selectively in premalignant and malignant prostate cancer cells," *International Journal of Cancer*, vol. 125, pp. 774–782, 2009.
- [52] P. Pitchakarn, S. Ohnuma, K. Pintha, W. Pompimon, S. V. Ambudkar, and P. Limtrakul, "Kuguacin J isolated from *Momordica charantia* leaves inhibits P-glycoprotein (ABCB1)-mediated multidrug resistance," *Journal of Nutritional Biochemistry*, vol. 23, pp. 76–84, 2012.
- [53] M. Bortolotti, D. Mercatelli, and L. Polito, "Momordica charantia, a nutraceutical approach for inflammatory related diseases," *Frontiers in Pharmacology*, vol. 10, p. 486, 2019.
- [54] W. C. Huang, T. H. Tsai, C. J. Huang et al., "Inhibitory effects of wild bitter melon leaf extract on *Propionibacterium acnes*-induced skin inflammation in mice and cytokine production in vitro," *Food Functions*, vol. 6, pp. 2550–2560, 2015.
- [55] S. J. Kim, H. S. Kim, and Y. R. Seo, "Understanding of ROS-inducing strategy in anticancer therapy," *Oxidative Medicine and Cellular Longevity*, vol. 2019, Article ID 5381692, 12 pages, 2019.
- [56] A. M. Brunati, M. A. Pagano, A. Bindoli, and M. P. Rigobello, "Thiol redox systems and protein kinases in hepatic stellate cell regulatory processes," *Free Radical Research*, vol. 44, pp. 363–378, 2010.
- [57] F. J. Bohanon, X. Wang, C. Ding et al., "Oridonin inhibits hepatic stellate cell proliferation and fibrogenesis," *Journal of Surgical Research*, vol. 190, pp. 55–63, 2014.
- [58] L. J. Su, J. H. Zhang, H. Gomez et al., "Reactive oxygen species-induced lipid peroxidation in apoptosis, autophagy, and Ferroptosis," *Oxidative Medicine and Cellular Longevity*, vol. 2019, Article ID 5080843, 13 pages, 2019.
- [59] H. Hu, M. Tian, C. Ding, and S. Yu, "The C/EBP homologous protein (CHOP) transcription factor functions in endoplasmic reticulum stress-induced apoptosis and microbial infection," *Frontiers in Immunology*, vol. 9, p. 3083, 2018.
- [60] S. Oyadomari and M. Mori, "Roles of CHOP/GADD153 in endoplasmic reticulum stress," *Cell Death & Differentiation*, vol. 11, pp. 381–389, 2004.
- [61] R. J. Davis, "Signal transduction by the JNK group of MAP kinases," *Cell*, vol. 103, pp. 239–252, 2000.
- [62] J. Li, F. Cao, H. L. Yin et al., "Ferroptosis: past, present and future," *Cell Death and Disease*, vol. 11, p. 88, 2020.
- [63] S. J. Dixon, K. M. Lemberg, M. R. Lamprecht et al., "Ferroptosis: an iron-dependent form of nonapoptotic cell death," *Cell*, vol. 149, pp. 1060–1072, 2012.
- [64] J. P. Friedmann Angeli, M. Schneider, B. Proneth et al., "Inactivation of the ferroptosis regulator Gpx4 triggers acute renal failure in mice," *Nature Cell Biology*, vol. 16, pp. 1180–1191, 2014.
- [65] R. K. Moreira, "Hepatic stellate cells and liver fibrosis," *Archives of Pathology & Laboratory Medicine*, vol. 131, pp. 1728–1734, 2007.
- [66] J. S. Troeger, I. Mederacke, G. Y. Gwak et al., "Deactivation of hepatic stellate cells during liver fibrosis resolution in mice," *Gastroenterology*, vol. 143, pp. 1073–1083, 2012.

- [67] R. Franco and J. A. Cidowski, "Glutathione efflux and cell death," *Antioxidants & Redox Signaling*, vol. 17, pp. 1694–1713, 2012.
- [68] K. Ray, "Hepatic stellate cells hold the key to liver fibrosis," *Nature Reviews Gastroenterology & Hepatology*, vol. 11, no. 2, p. 74, 2014.
- [69] J. E. Puche, Y. Saiman, and S. L. Friedman, "Hepatic stellate cells and liver fibrosis," *Comprehensive Physiology*, vol. 3, pp. 1473–1492, 2013.
- [70] L. M. Kuo, C. Y. Kuo, C. Y. Lin, M. F. Hung, J. J. Shen, and T. L. Hwang, "Intracellular glutathione depletion by oridonin leads to apoptosis in hepatic stellate cells," *Molecules*, vol. 19, pp. 3327–3344, 2014.
- [71] J. J. Tomasek, G. Gabbiani, B. Hinz, C. Chaponnier, and R. A. Brown, "Myofibroblasts and mechano-regulation of connective tissue remodelling," *Nature Reviews Molecular Cell Biology*, vol. 3, pp. 349–363, 2002.
- [72] G. Huang and D. R. Brigstock, "Regulation of hepatic stellate cells by connective tissue growth factor," *Frontiers in Bioscience (Landmark Ed.)*, vol. 17, pp. 2495–2507, 2012.
- [73] V. Paradis, D. Dargere, M. Vidaud et al., "Expression of connective tissue growth factor in experimental rat and human liver fibrosis," *Hepatology*, vol. 30, pp. 968–976, 1999.
- [74] G. Huang and D. R. Brigstock, "Integrin expression and function in the response of primary culture hepatic stellate cells to connective tissue growth factor (CCN2)," *Journal of Cellular and Molecular Medicine*, vol. 15, pp. 1087–1095, 2011.
- [75] M. Shen, K. Chen, J. Lu et al., "Protective effect of astaxanthin on liver fibrosis through modulation of TGF-beta1 expression and autophagy," *Mediators of Inflammation*, vol. 2014, Article ID 954502, 14 pages, 2014.
- [76] Y. Zhao, X. Ma, J. Wang et al., "Curcumin protects against CCl4-induced liver fibrosis in rats by inhibiting HIF-1alpha through an ERK-dependent pathway," *Molecules*, vol. 19, pp. 18767–18780, 2014.
- [77] Y. Wang, M. Cheng, B. Zhang, F. Nie, and H. Jiang, "Dietary supplementation of blueberry juice enhances hepatic expression of metallothionein and attenuates liver fibrosis in rats," *PLoS One*, vol. 8, p. e58659, 2013.
- [78] S. Gharbia, C. Balta, H. Herman et al., "Enhancement of silymarin anti-fibrotic effects by complexation with hydroxypropyl (HPBCD) and randomly methylated (RAMEB) beta-cyclodextrins in a mouse model of liver fibrosis," *Frontiers in Pharmacology*, vol. 9, p. 883, 2018.
- [79] P. J. Lee, H. J. Park, N. Cho, and H. P. Kim, "3, 5-Diethoxy-3'-Hydroxyresveratrol (DEHR) ameliorates liver fibrosis via Caveolin-1 activation in hepatic stellate cells and in a mouse model of bile duct ligation injury," *Molecules*, vol. 23, 2018.
- [80] X. Li, Q. Jin, Q. Yao et al., "The flavonoid quercetin ameliorates liver inflammation and fibrosis by regulating hepatic macrophages activation and polarization in mice," *Frontiers in Pharmacology*, vol. 9, p. 72, 2018.
- [81] K. Shen, X. Feng, R. Su, H. Xie, L. Zhou, and S. Zheng, "Epigallocatechin 3-gallate ameliorates bile duct ligation induced liver injury in mice by modulation of mitochondrial oxidative stress and inflammation," *PLoS One*, vol. 10, p. e0126278, 2015.
- [82] M. Wadhawan and A. C. Anand, "Coffee and liver disease," *Journal of Clinical and Experimental Hepatology*, vol. 6, pp. 40–46, 2016.
- [83] M. Bae, Y. K. Park, and J. Y. Lee, "Food components with antifibrotic activity and implications in prevention of liver disease," *Journal of Nutritional Biochemistry*, vol. 55, pp. 1–11, 2018.
- [84] L. M. Kuo, P. J. Chen, P. J. Sung et al., "The bioactive extract of *Pinnigorgia* sp. induces apoptosis of hepatic stellate cells via ROS-ERK/JNK-caspase-3 signaling," *Marine Drugs*, vol. 16, 2018.
- [85] Y. Jia, F. Wang, Q. Guo et al., "Curcumol induces RIPK1/RIPK3 complex-dependent necroptosis via JNK1/2ROS signaling in hepatic stellate cells," *Redox Biology*, vol. 19, pp. 375–387, 2018.
- [86] Y. Y. Tao, X. C. Yan, T. Zhou, L. Shen, Z. L. Liu, and C. H. Liu, "Fuzheng Huayu recipe alleviates hepatic fibrosis via inhibiting TNF-alpha induced hepatocyte apoptosis," *BMC Complementary and Alternative Medicine*, vol. 14, p. 449, 2014.
- [87] Y. H. Yeh, C. Y. Liang, M. L. Chen et al., "Apoptotic effects of hsian-tsoa (*Mesona procumbens* Hemsley) on hepatic stellate cells mediated by reactive oxygen species and ERK, JNK, and caspase-3 pathways," *Food Science & Nutrition*, vol. 7, no. 5, pp. 1891–1898, 2019.
- [88] Y. Chen, Z. Zhou, Q. Mo, G. Zhou, and Y. Wang, "Gallic acid attenuates dimethylnitrosamine-induced liver fibrosis by alteration of Smad phosphoisoform signaling in rats," *BioMed Research International*, vol. 2018, Article ID 1682743, 14 pages, 2018.
- [89] H. Shi, A. Shi, L. Dong et al., "Chlorogenic acid protects against liver fibrosis in vivo and in vitro through inhibition of oxidative stress," *Clinical Nutrition*, vol. 35, pp. 1366–1373, 2016.
- [90] N. Yang, S. Dang, J. Shi et al., "Caffeic acid phenethyl ester attenuates liver fibrosis via inhibition of TGF-beta1/Smad3 pathway and induction of autophagy pathway," *Biochemical and Biophysical Research Communications*, vol. 486, pp. 22–28, 2017.
- [91] M. Mu, S. Zuo, R. M. Wu et al., "Ferulic acid attenuates liver fibrosis and hepatic stellate cell activation via inhibition of TGF-beta/Smad signaling pathway," *Drug Design, Development and Therapy*, vol. 12, pp. 4107–4115, 2018.
- [92] Z. Wang, S. Ge, S. Li, H. Lin, and S. Lin, "Anti-obesity effect of trans-cinnamic acid on HepG2 cells and HFD-fed mice," *Food and Chemical Toxicology*, vol. 137, Article ID 111148, 2020.
- [93] Q. Yao, S. Li, X. Li, F. Wang, and C. Tu, "Myricetin modulates macrophage polarization and mitigates liver inflammation and fibrosis in a murine model of nonalcoholic steatohepatitis," *Frontiers in Medicine (Lausanne)*, vol. 7, p. 71, 2020.
- [94] L. D. Hernández-Ortega, B. E. Alcántar-Díaz, L. A. Ruiz-Corro et al., "Quercetin improves hepatic fibrosis reducing hepatic stellate cells and regulating pro-fibrogenic/anti-fibrogenic molecules balance," *Journal of Gastroenterology and Hepatology*, vol. 27, no. 12, pp. 1865–1872, 2012.
- [95] J. Li, X. Li, W. Xu et al., "Antifibrotic effects of luteolin on hepatic stellate cells and liver fibrosis by targeting AKT/mTOR/p70S6K and TGFbeta/Smad signalling pathways," *Liver International*, vol. 35, pp. 1222–1233, 2015.
- [96] D. F. Hicks, N. Goossens, A. Blas-García et al., "Transcriptome-based repurposing of apigenin as a potential anti-fibrotic agent targeting hepatic stellate cells," *Science Reports*, vol. 7, p. 42563, 2017.
- [97] F. Geyikoglu, E. G. Yilmaz, H. S. Erol et al., "Hepatoprotective role of thymol in drug-induced gastric ulcer model," *Annals of Hepatology*, vol. 17, pp. 980–991, 2018.

Research Article

Lower Somatic Mutation Levels in the λ Light-Chain Repertoires with Chronic HBV Infection

Binbin Hong ¹, Qiaoling Liu,¹ Qiulan Li,¹ Lili Su,¹ and Lizhi Wang²

¹Central Laboratory, Second Affiliated Hospital of Fujian Medical University, Quanzhou 362000, China

²Traditional Chinese Medicine Department, Rehabilitation Hospital, Nan'an, Quanzhou 362300, China

Correspondence should be addressed to Binbin Hong; bbh.0329@163.com

Received 7 January 2021; Accepted 27 May 2021; Published 7 June 2021

Academic Editor: Woon-Man Kung

Copyright © 2021 Binbin Hong et al. This is an open access article distributed under the Creative Commons Attribution License, which permits unrestricted use, distribution, and reproduction in any medium, provided the original work is properly cited.

To investigate the characteristics of the immunoglobulin light-chain repertoires with chronic HBV infection, the high-throughput sequencing and IMGT/HighV-QUEST were adapted to analyze the κ (IgK) and λ (IgL) light-chain repertoires from the inactive HBV carriers (IHB) and the healthy adults (HH). The comparative analysis revealed high similarity between the κ light-chain repertoires of the HBV carriers and the healthy adults. Nevertheless, the proportion of IGLV genes with $\geq 90\%$ identity as the germline genes was higher in the IgL light-chain repertoire of the IHB library compared with that of HH library (74.6% vs. 69.1%). Besides, the frequency of amino acid mutations in the CDR1 regions was significantly lower in the IgL light-chain repertoire of the IHB library than that of the HH library (65.52% vs. 56.0%). These results suggested the lower somatic mutation level in the IgL repertoire of IHB library, which might indicate the biased selection of IGLV genes in the IgL repertoire with chronic HBV infection. These findings might lead to a better understanding of the characteristics of the light-chain repertoires of HBV chronically infected individuals.

1. Introduction

Hepatitis B virus infection is the major global health problem, despite the existence of hepatitis B vaccination [1, 2]. Most primary HBV infections are self-limiting with virus clearance and lifelong protective immunity; however, an estimated 3% to 5% of adults and up to 95% of children develop chronic HBV infection [3]. Chronic HBV infection greatly increases the risk of terminal liver disease, but current therapies could rarely achieve a cure. An extensive body of research suggested the neutralizing antibodies can not only prevent acute HBV infection but also have a possibility to modulate the development of chronic HBV infection [4, 5].

Recently, high-throughput sequencing technologies have been advanced and are improving our understanding of humoral immune responses [6–8]. Some characteristics of the antibody repertoire before and after HBV vaccination have been demonstrated using high-throughput sequencing [9–11]. B-cell receptors (BCRs) are formed by pairing of

heavy chains and light chains that together specify the effector functions [12]. Unfortunately, very few studies investigate the antibody repertoire of individuals with chronic HBV infection, and even less attention has been paid to the light-chain repertoire with HBV infection. Thus, the characteristics of the light-chain repertoires with chronic HBV infection are less clear.

In this study, we analyzed the light-chain repertoires of κ (IgK) and λ (IgL) isotypes with chronic HBV infection. The characteristics of the IgK repertoires demonstrated no significant difference between the healthy and the HBV carriers. Conversely, the characteristics of the IgL repertoires showed some difference between the healthy adults and the HBV carriers, although most of the characteristics in the IgL repertoires showed no significant difference. We found that the somatic hypermutation level in the IgL repertoire of the HBV carriers was lower than that of healthy adults. Moreover, the preferred used variable (V) and joining (J) genes also showed some difference in the IgL repertoires of the healthy and the HBV carriers.

2. Methods and Materials

2.1. Samples. Totally, twenty adults were included in this study that comprised 10 inactive HBV carriers with serum HBsAg but without serum virus load increased (IHB) and 10 healthy adults (HH) who underwent a routine health check with no history of HBV infection or known major diseases. The included HBV carriers did not have active hepatitis or received antiviral treatment. The basic characteristics of the study population are summarized in Table 1.

2.2. Establishment of the Antibody Repertoires for Deep Sequencing. Peripheral blood mononuclear cells (PBMCs) were prepared according to the published protocols [13]. Total RNA was extracted and then reverse-transcribed to the first-strand cDNA that was used as the template to amplify the antibody sequences. The PCR amplifications were performed using a set of sense primers highly aligned to the first seven codons of the V regions and antisense primers that exhibit specificity for the last eight codons at the 3' ends of the constant domains corresponding to the numbering schemes of the IMGT database. Two rounds of PCR amplifications were performed to produce the special isotype antibody fragments with the proper length for sequencing. Finally, the PCR amplicons were purified and subjected to high-throughput sequencing based on the Illumina HiSeq platform according to the manufacturer's protocol.

2.3. Sequence Processing. A series of stringent quality control criteria were applied in the data processing as published in our previous report [14]. To exclude biologically implausible sequences, IMGT/HighV-QUEST (version 1.5.1) was used for sequence annotation to identify insertion and deletion (indels) errors and classify the sequencing data into productive and unproductive sequences [15, 16]. The unproductive VJ rearrangements were eliminated from the dataset. Then, the productive sequences that contained stop codons, indel errors, and substitutions or mutations in the conserved amino acids at specified positions were excluded. Furthermore, the redundant sequences were eliminated to avoid the accumulation of one single sequence due to PCR amplification. Finally, the unique sequences with unique VJ genes, or unique CDR3 amino acid sequences defined as the unique clones, were selected for further analysis. The number of sequences after each step of processing is listed in Table 2.

2.4. Statistical Analyses. The clone diversity in each library was described by the Margalef index (D) that was defined and given by the function $D = (S-1)/\ln N$, with S being species richness and N being the total number of all specimens in a sample [17]. Student's t -test, Pearson's chi-square test, and logistic regression analysis were used in statistical analysis. In comparative analyses, the difference significance was determined by the parameter of the effect sizes: *Cohen's d* value and the *odds ratio* (OR) were used to measure the standardized difference between two means and between two rates, respectively [18, 19]. When $p < 0.05$ (two sided),

$d \geq 0.20$, and $OR \geq 1.50$ or ≤ 0.60 , the difference was considered to be significant. The data analyses were performed using the R, Perl, and GraphPad Prism programs. The sequencing data have been deposited in the NCBI SRA database (PRJNA578033).

2.5. Ethics Statement. The blood samples were provided by the Second Affiliated Hospital of Fujian Medical University (Quanzhou, Fujian, China) with the approval of the institutional research board and the donors' consent. Procedures followed in this study were under the ethical standards of concerned institutional policies.

3. Results

3.1. The Clone Diversity. In this study, we analyzed the antibody light-chain repertoires of inactive HBV carriers (IHB) and compared them with that of healthy adults (HH). Approximately 1.0×10^7 PBMCs from each group were input to analyses, and totally 28,083,374 raw sequences were obtained from IgK repertoires and 25,839,997 sequences obtained from IgL repertoires after the sequencing. After a series of data cleaning procedures, a total of 385,825 unique clones were identified in the IgK repertoire of IHB library and 329,688 unique clones were found in the HH library (Figure 1(a)). Besides, 129,453 and 182,727 unique clones were found in the IgL repertoires of the IHB and HH library, respectively (Figure 1(a)). Interestingly, we found that the HH and IHB library shared 66,653 IgK clones, accounting for 17.28% in the IHB and 20.22% in the HH library, respectively (Figure 1(a)); and 18,466 clones shared between the IgL repertoires of the two libraries, constituting 14.26% of the IHB and 10.11% of the HH library (Figure 1(a)). Additionally, the Margalef index was calculated and suggested that the clone diversity demonstrated no significant difference between the HH and IHB library in both the IgK and IgL repertoires (Figure 1(b)).

Among the unique clones, 179,734 unique CDR3 sequences were found in the IgK repertoire of the IHB and 161,443 sequences were found in the HH library (Figure 1(c)); as well as 89,434 unique CDR3 sequences were found in the IgL repertoire of IHB library, and 125,014 sequences were found in the HH library (Figure 1(c)). Similarly, 40,260 convergent CDR3 sequences were found between the IgK repertoires of HH and IHB library (22.40% in IHB and 24.94% in HH); and 14,323 convergent CDR3s were found between IgL repertoires of the two libraries (16.02% in IHB and 11.46% in HH) (Figure 1(c)). Next, the VJ gene rearranged patterns were analyzed to describe the diversity of rearrangements. In IgK repertoires, 450 VJ gene rearranged patterns were found in the IHB library and 459 patterns in the HH library. We found 437 shared rearranged patterns between the two libraries that accounted for more than 95% in both the two libraries (Figure 1(d)). In IgL repertoires, 320 VJ gene rearranged patterns were found in the IHB library and 353 patterns in the HH library; and the two libraries shared 289 rearranged patterns that constituted 90.31% in the IHB and 81.87% in the HH library

TABLE 1: The basic characteristics of study population.

Group	Gender (F/M) ^a	Average age ^b	HBsAg ^c	HBsAb ^c	HBeAg ^c	HBeAb ^c	HBcAb ^c	Average HBV DNA load ^d (IU/mL)
Inactive HBV carriers (IHB)	2/8	44.3 ± 9.27	+	—	—	+	+	<500 ^e
Healthy adults (HH)	0/10	37.0 ± 9.55	—	—	—	—	—	0

^a(F/M): female/male; ^b the average age had no significant difference in the three groups (Student's *t*-test, $p > 0.005$); ^cfive serological markers of HBV were tested by ELISA; ^dHBV DNA load was tested by the real-time fluorescent quantitative PCR; ^ethe detection limit is 500 IU/mL.

TABLE 2: The number of input cells and sequencing data.

Repertoires	Healthy human (HH)		Inactive HBV carriers (IHB)	
	IgK	IgL	IgK	IgL
Total input cells		1.0×10^7		1.0×10^7
Raw sequences	13,067,133	14,491,757	15,016,241	11,348,240
Productive sequences*	10,782,027	10,991,517	12,484,862	8,278,375
Productive unique aa sequences	5,164,247	3,686,212	5,756,099	2,869,219
Unique clones	329,688	182,727	385,825	129,453

*seqs: sequences.

(Figure 1(d)). Taken together, these results demonstrated the limited diversity of unique clones in the light-chain repertoires. A small portion of unique clones and CDR3 sequences shared between the library of healthy adults and the inactive HBV carriers, but the majority of the VJ gene rearranged patterns were shared between the two libraries.

3.2. The Usage of VJ Genes. The IgK repertoire contains 6 IGKV gene families. IGKV1, IGKV2, IGKV3, and IGKV4 were frequently used in the two libraries, accounting for more than 98% altogether in both libraries, but IGKV5 and IGKV6 families were rarely used with a frequency less than 1.5% (Figure 2(a)). The IGKV genes usage preference was very similar between the two libraries: IGKV4-1, IGKV3-20, and IGKV2-30 were most frequently used (Figures 2(b) and 2(c), Supplementary Table 1). Besides, five IGKJ gene families were observed, all of which were frequently used. The biased used IGKJ alleles also showed no significant differences between the two libraries that were IGKJ4*01, IGKJ5*01, and IGKJ1*01 (Figures 2(b) and 2(c), Supplementary Table 2). For the IgL repertoire, there are 10 IGLV gene families and 7 IGLJ gene families. The IGLV3 family was extremely biased used in both libraries accounting for 47.65% in HH and 54.58% in IHB. In both the libraries, IGLV3-1 and IGLV3-21 were frequently used. Interestingly, IGLV9-49 and IGLV10-54 were equally used in the HH library with a rate about 10%; but in the IHB library, the usage of IGLV9-49 was almost three times more than IGLV10-54 with a rate of 15.71% and 5.18%, respectively (Supplementary Table 3). For the IGLJ gene usage, IGLJ2 and IGLJ3 families were frequently used in both the IHB and HH libraries, together consisting more than 70% of all IGLJ families. The most frequently used IGLJ allele was IGLJ2*01 in the HH library at a rate of 41.24%, but it was IGLJ3*01 in the IHB library with a rate of 37.38% (Supplementary Table 4). Together, these results might indicate a different selection of IGLV and IGLJ genes in the IgL repertoire of IHB library, but which were not observed in the IgK repertoire.

3.3. The Somatic Hypermutation in V Regions. The somatic hypermutations (SHM) in the V gene segments were analyzed by comparing the sequencing data with the germline genes from the IMGT database. There were approximately 70% sequences in the IgL repertoires and more than 80% sequences in the IgK repertoires with $\geq 90\%$ V gene identity as the germline genes (Figure 3(a)). The proportion of sequences with high V gene identity as the germline genes did not show significant difference in the IgK repertoires of HH and IHB library (HH vs. IHB: 87.6% vs. 86.9%; Figure 3(a), Supplementary Table 5). However, slight difference was found between the IgL repertoires of these two libraries (HH vs. IHB: 69.2% vs. 74.6%; $p < 2.2E - 16$, OR = 1.312, 95% CI: 1.291–1.333; Figure 3(a)), suggesting the IGLV genes in the IHB library carried less mutations.

Then, the frequency of amino acid mutations in CDR1 and CDR2 were further calculated. In IgL repertoires, it was interestingly to find that the frequency of amino acid mutations in CDR1 was lower in IHB than HH (IHB vs. HH: 56.0% vs. 65.5%; Figure 3(b)); the difference was significant since the OR value was close to the threshold level ($p < 2.2E - 16$, OR = 1.493 \approx 1.50, 95% CI: 1.472–1.515). The frequency of amino acid mutations in CDR2 was also lower in the IHB library (IHB vs. HH: 52.6% vs. 56.8%; Figure 3(b)), although the difference was not significant ($p < 2.2E - 16$, OR = 1.183, 95% CI: 1.166–1.20). In the IgK repertoires, the frequency of amino acid mutations in CDR1 and CDR2 also showed no significant difference between the two libraries (Figure 3(c), Supplementary Table 5).

3.4. The Characteristics of CDR3 Regions. The characteristics of the CDR3 regions were analyzed, including the length of distribution, the amino acid usage, and the occurrence and mean length of junctional modifications. In our datasets, the length distribution of CDR3 ranged from 2 to 40 amino acids in light-chain repertoires. The average length of CDR3 was approximately 9 amino acids for the IgK repertoires and 11 amino acids for the IgL repertoires in the HH and IHB library

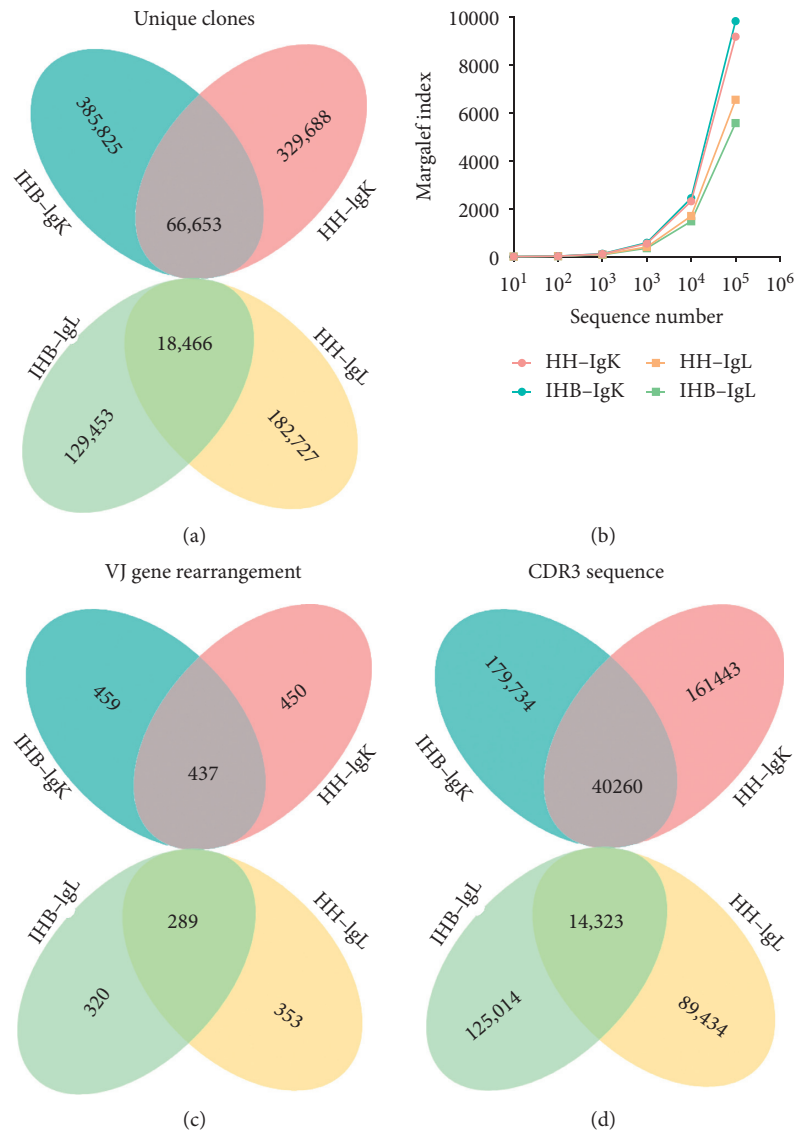


FIGURE 1: The diversity of κ (IgK) and λ (IgL) light-chain repertoires of the healthy human (HH) and inactive HBV carriers (IHB). (a) The diversity of unique clones in the IgK and IgL repertoires from the HH and IHB library. (b) The Margalef index was calculated to describe the repertoire diversity that was calculated, respectively, when 10, 100, 1000, 10000, 100000, and 1000000 sequences were randomly selected using the randomized table generated by R program. (c) The diversity of VJ gene rearrangements in the IgK and IgL repertoires from the HH and IHB library. (d) The diversity of unique CDR3 sequences in the IgK and IgL repertoires from the HH and IHB library.

(Figure 4(a)). For the amino acid usage in CDR3 regions, glutamine, threonine, and proline were the most frequently used amino acids in IgK repertoires (Figure 4(b)). But in IgL repertoires, the top frequently used amino acids were serine, valine, and aspartic acid (Figure 4(c)). Overall, the average CDR3 length and the amino acid usage showed little difference between the two libraries (data not shown). The junctional modifications are the main mechanisms contributing to the CDR3 diversity, including additions of the palindromic nucleotides (P) and the nontemplate randomized nucleotides (N), as well as the deletion of nucleotides caused by exonuclease trimming (T). The occurrences of these modifications were analyzed, but no significant difference was found between the two libraries in both IgK and IgL repertoires (Figures 4(d) and 4(e), Supplementary Table 6).

4. Discussion

In this study, the high-throughput sequencing method was adapted to analyze the light-chain repertoires of chronic HBV-infected individuals and healthy adults. Totally, 53,923,371 raw sequences were obtained from 20 individuals. After the analyses, we found that the characteristics in the IgK repertoires were highly similar between the healthy adults and the HBV carriers, including the somatic mutations in V regions, the average CDR3 length, and the occurrence of junctional modifications. Although most of the characteristics in the IgL repertoires were similar between the two groups of investigated population, we still found that the SHM level in V regions was lower in the IgL repertoire of inactive HBV carriers compared with that of healthy adults.

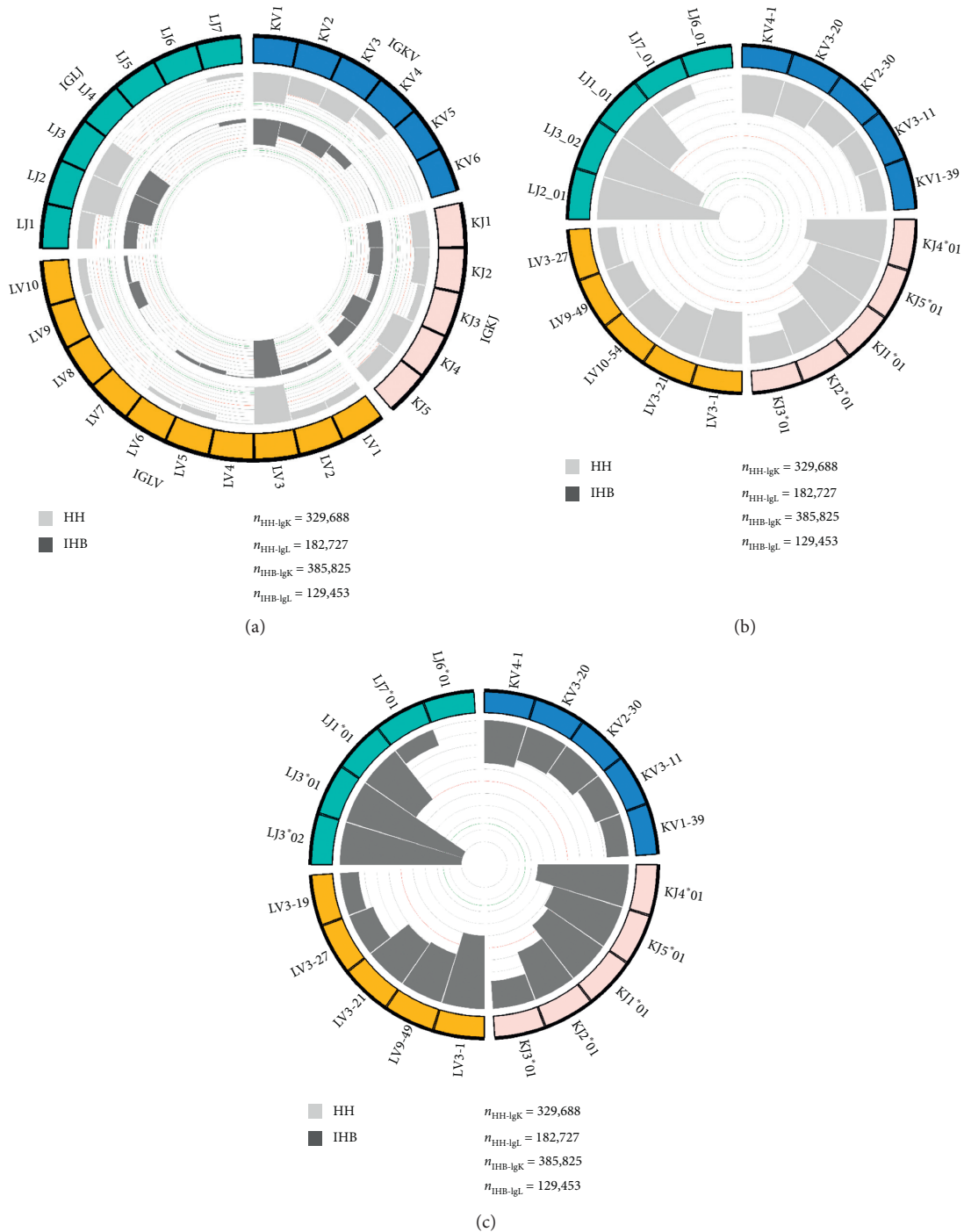


FIGURE 2: (a) The usage of VJ gene families in IgK and IgL repertoires of the HH and IHB library. The outsider arcs represent the IGKV (blue arc), IGKJ (pink arc), IGLV (orange arc), and IGLJ (cyan arc) gene families, and the histograms inside the circle represent the usage of each gene family in the IgK and IgL repertoires of HH (gray) and IHB library (dark gray). (b) The top 5 most frequently used VJ genes in the IgK and IgL repertoires of HH library. (c) The top 5 most frequently used VJ genes in the IgK and IgL repertoires of IHB library.

Human immunoglobulin consists of a pair of identical heavy chains and a pair of identical light chains, κ or λ alternatively. The heavy chains are the primary factor in forming the functional paratopes to realize foreign antigens [20, 21]. A number of research studies suggested that the rearrangements of the light chains aimed to silence the self-reactivity [22, 23]. Thus, the diversity of the light-chain

repertoire was constrained. Despite the lack of clone diversity, the high portion of shared clones between individuals in light-chain repertoires has been reported recently [23–26]. In this study, we included 1×10^7 PBMC initially and only obtained $1 \sim 3 \times 10^6$ unique clones in the light-chain repertoire from each library. The shared portion of the unique clones was approximately 10% to 20% in IgK or IgL

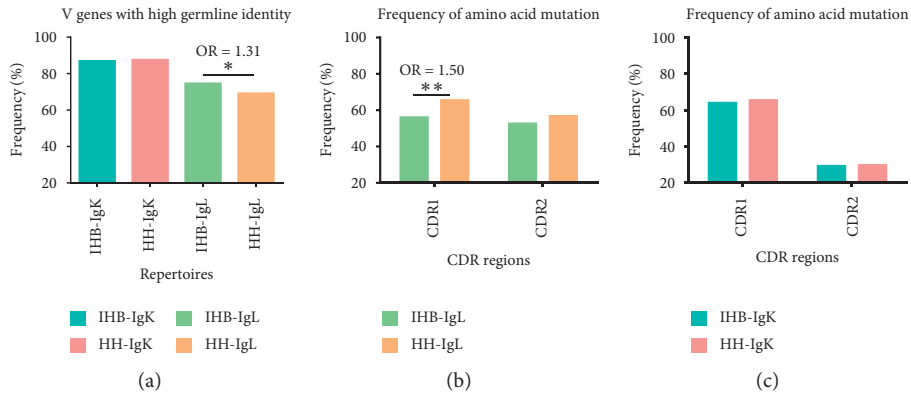


FIGURE 3: The somatic hypermutation level in the light-chain repertoires. (a) The proportion of sequences with more than 90% V gene identity as the germline genes from the IMGT database. (b) The frequencies of amino acid mutations in CDR1 and CDR2 regions of the IgL repertoires. (c) The frequencies of amino acid mutations in CDR1 and CDR2 regions of the IgK repertoires.

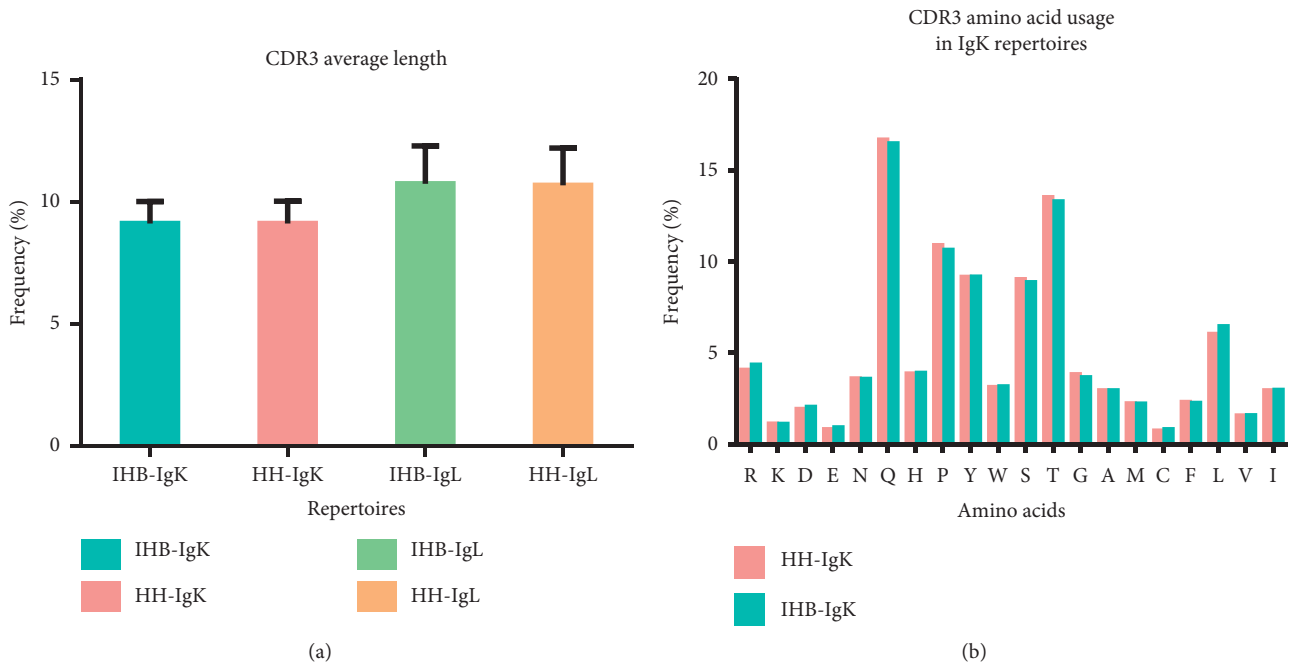


FIGURE 4: Continued.

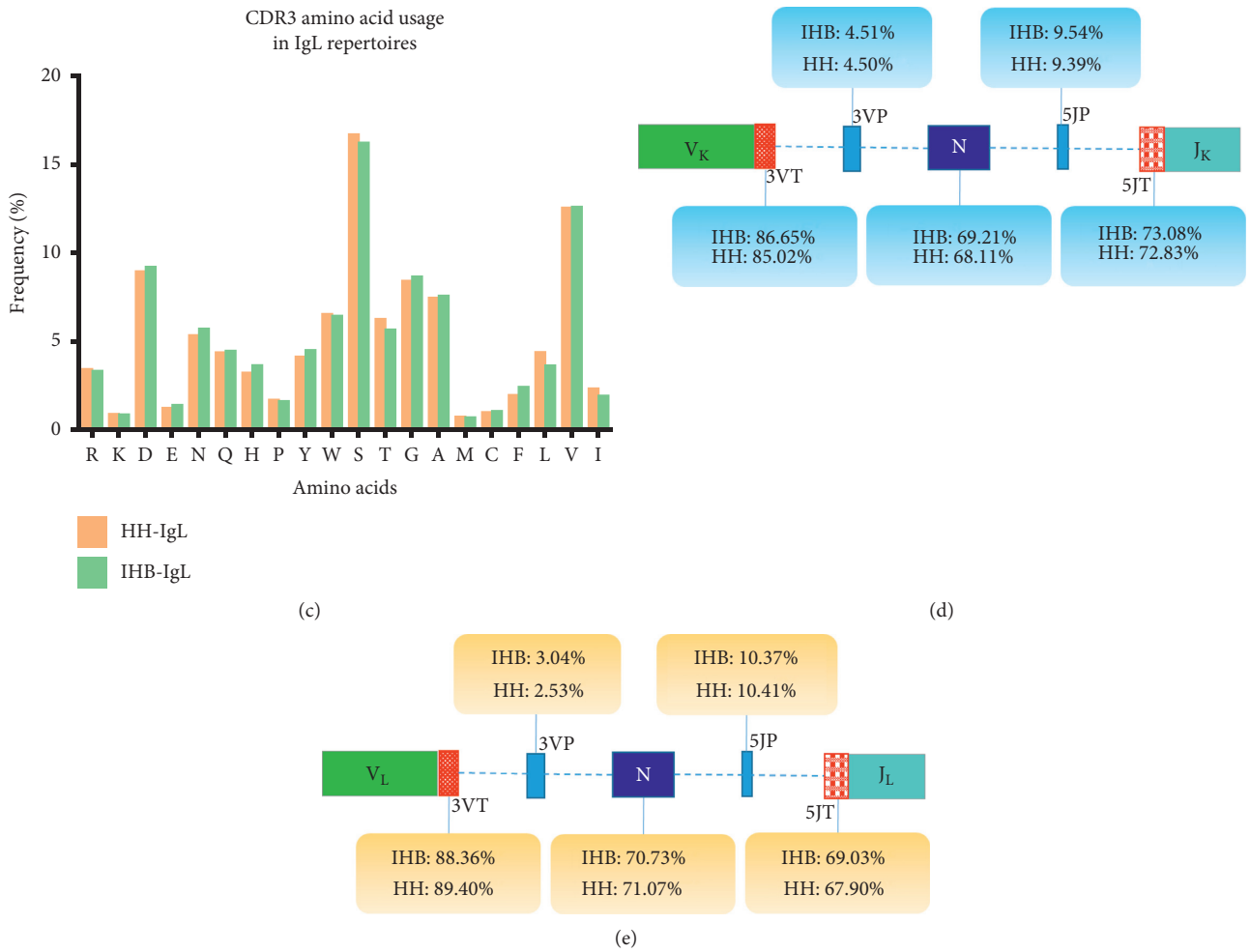


FIGURE 4: The characteristics of CDR3 regions. (a) The average length of CDR3 regions in the IgK and IgL repertoires from the HH and IHB library. (b) The usage of amino acids in the CDR3 regions of IgK repertoires from the HH and IHB library. (c) The usage of amino acids in the CDR3 regions of IgL repertoires from the HH and IHB library. (d) The occurrence of junctional modifications in the CDR3 regions of the IgK repertoires. (e) The occurrence of junctional modifications in the CDR3 regions of the IgL repertoires.

repertoires between the two groups of investigated population. In addition, the diversity of VJ rearranged patterns was extremely limited due to the lack of the diversity (D) genes. Only hundreds of rearranged patterns were observed in both IgK and IgL repertoires, and more than 80% of the VJ gene rearrangements shared between the healthy adults and inactive HBV carriers in both IgK and IgL repertoires.

SHM is a critical mechanism to diversify the BCR repertoires [27–29]. High levels of SHM were commonly seen in the antibody repertoires after virus infection and vaccinations [10, 30–33], although the reduced mutation level was also observed in the IgG repertoire with acute dengue virus infection and the IgG repertoire after pandemic H1N1 influenza monovalent inactivated vaccine [34, 35]. In this study, we found the SHM level was lower in the IgL repertoire of HBV carriers compared with that of the healthy

adults. However, the lower mutation level did not result in the decrease of the clone diversity in this study since the clone diversity showed no significant difference between the IgL repertoires of healthy adults and inactive HBV carriers. Thus, it could be inferred that the lower mutation level in the IgL repertoire of inactive HBV carriers might result from the biased selection of the germline-like IGLV genes under the influence of HBV infection.

5. Conclusions

In this study, we analyzed the light-chain repertoires with chronic HBV infection by the high-throughput sequencing. The repertoire characteristics were similar between the κ light-chain repertoires of the HBV carriers and healthy adults. Nevertheless, lower SHM levels in V regions were

observed in the λ light-chain repertoire of the individuals with chronic HBV infection, which might indicate the biased selection of IGLV genes under the influence of chronic HBV infection. The findings in this study were relevant for understanding of the characteristics of the light-chain repertoire during chronic HBV infection.

Data Availability

The sequencing data have been deposited in the NCBI SRA database (PRJNA578033).

Conflicts of Interest

The authors declare that they have no conflicts of interest.

Authors' Contributions

BH conceived and designed the project. LS, Q Li, and Q Liu carried out the experiments. BH and LW analyzed the data. BH wrote the paper with input from all coauthors.

Acknowledgments

This work was supported by the Scientific Research Starting Foundation for Doctors from the Second Affiliated Hospital of Fujian Medical University (BS201801), the Grants Programs from the Health Commission of Fujian Province, China (2019-ZQN-67), and the Fujian Provincial Natural Science Foundation Projects (2020J05053).

Supplementary Materials

Table 1 and Table 2: the usage of IGKV and IGKJ genes in the HH and IHB library. Table 3 and Table 4: the usage of IGLV and IGLJ genes in the HH and IHB library. Table 5: the comparisons of the somatic hypermutation levels between the HH and IHB library. Table 6: the comparisons of the occurrence of junctional modifications in IgK and IgL repertoires. (*Supplementary Materials*)

References

- [1] H. B. El-Serag, "Epidemiology of viral hepatitis and hepatocellular carcinoma," *Gastroenterology*, vol. 142, no. 6, pp. 1264–1273, 2012.
- [2] C. Trépo, H. L. Y. Chan, and A. Lok, "Hepatitis B virus infection," *The Lancet*, vol. 384, no. 9959, pp. 2053–2063, 2014.
- [3] C. Q. Pan and J. X. Zhang, "Natural history and clinical consequences of hepatitis B virus infection," *International Journal of Medical Sciences*, vol. 2, no. 1, pp. 36–40, 2005.
- [4] A. Bertoletti and C. Ferrari, "Adaptive immunity in HBV infection," *Journal of Hepatology*, vol. 64, no. 1, pp. S71–S83, 2016.
- [5] B. Hong, Y. Wen, and T. Ying, "Recent progress on neutralizing antibodies against hepatitis B virus and its implications," *Infectious Disorders—Drug Targets*, vol. 19, no. 3, pp. 213–223, 2019.
- [6] G. Georgiou, G. C. Ippolito, J. Beausang, C. E. Busse, H. Wardemann, and S. R. Quake, "The promise and challenge of high-throughput sequencing of the antibody repertoire," *Nature Biotechnology*, vol. 32, no. 2, pp. 158–168, 2014.
- [7] S. Friedensohn, T. A. Khan, and S. T. Reddy, "Advanced methodologies in high-throughput sequencing of immune repertoires," *Trends in Biotechnology*, vol. 35, no. 3, pp. 203–214, 2017.
- [8] W. H. Robinson, "Sequencing the functional antibody repertoire—diagnostic and therapeutic discovery," *Nature Reviews Rheumatology*, vol. 11, no. 3, pp. 171–182, 2015.
- [9] A. Miyasaka, Y. Yoshida, T. Wang, and Y. Takikawa, "Next-generation sequencing analysis of the human T-cell and B-cell receptor repertoire diversity before and after hepatitis B vaccination," *Human Vaccines & Immunotherapeutics*, vol. 15, no. 11, pp. 2738–2753, 2019.
- [10] L. Ma, X. Wang, X. Bi et al., "Characteristics peripheral blood IgG and IgM heavy chain complementarity determining region 3 repertoire before and after immunization with recombinant HBV vaccine," *PLoS One*, vol. 12, no. 1, Article ID e0170479, 2017.
- [11] Y.-H. Chang, H.-C. Kuan, T. C. Hsieh et al., "Network signatures of IgG immune repertoires in hepatitis B associated chronic infection and vaccination responses," *Scientific Reports*, vol. 6, no. 1, Article ID 26556, 2016.
- [12] H. W. Schroeder Jr. and L. Cavacini, "Structure and function of immunoglobulins," *Journal of Allergy and Clinical Immunology*, vol. 125, no. 2, pp. S41–S52, 2010.
- [13] W. Chen, Z. Zhu, X. Xiao, and D. S. Dimitrov, "Construction of a human antibody domain (VH) library," *Therapeutic Antibodies*, vol. 525, pp. 81–99, 2009.
- [14] B. Hong, Y. Wu, W. Li et al., "In-depth analysis of human neonatal and adult IgM antibody repertoires," *Frontiers in Immunology*, vol. 9, p. 128, 2018.
- [15] M.-P. Lefranc, "IMGT unique numbering for the variable (V), constant (C), and groove (G) domains of IG, TR, MH, IgSF, and MhSF," *Cold Spring Harbor Protocols*, vol. 2011, no. 6, pp. 633–642, 2011, Epub 2011/06/03.
- [16] F. Ehrenmann, V. Giudicelli, P. Duroux, and M.-P. Lefranc, "IMGT/Collier de Perles: IMGT standardized representation of domains (IG, TR, and IgSF variable and constant domains, MH and MhSF groove domains)," *Cold Spring Harbor Protocols*, vol. 2011, no. 6, pp. 726–736, 2011.
- [17] P. Li, Z. Wu, T. Liu, and Y. Wang, "Biodiversity, phylogeny, and antifungal functions of endophytic fungi associated with *zanthoxylum bungeanum*," *International Journal of Molecular Sciences*, vol. 17, no. 9, p. 1541, 2016.
- [18] J. Cohen, *Statistical Power Analysis for the Behavioral Sciences*, Lawrence Erlbaum Associates, Mahwah, NJ, USA, 2nd edition, 1988.
- [19] J. Muth, *Basic Statistics and Pharmaceutical Statistical Applications*, BChapman & Hall/CRC Press, Boca Raton, FL, USA, 2006.
- [20] S. Muyldermans, "Nanobodies: natural single-domain antibodies," *Annual Review of Biochemistry*, vol. 82, no. 1, pp. 775–797, 2013.
- [21] S. C. Clarke, B. Ma, N. D. Trinklein et al., "Multispecific antibody development platform based on human heavy chain antibodies," *Frontiers in Immunology*, vol. 9, p. 3037, 2018.
- [22] H. Wardemann, J. Hammersen, and M. C. Nussenzweig, "Human autoantibody silencing by immunoglobulin light chains," *Journal of Experimental Medicine*, vol. 200, no. 2, pp. 191–199, 2004.
- [23] A. M. Collins and C. T. Watson, "Immunoglobulin light chain gene rearrangements, receptor editing and the development of a self-tolerant antibody repertoire," *Frontiers in Immunology*, vol. 9, p. 2249, 2018.

- [24] C. Soto, R. G. Bombardi, A. Branchizio et al., “High frequency of shared clonotypes in human B cell receptor repertoires,” *Nature*, vol. 566, no. 7744, pp. 398–402, 2019.
- [25] K. H. Hoi and G. C. Ippolito, “Intrinsic bias and public rearrangements in the human immunoglobulin V λ light chain repertoire,” *Genes & Immunity*, vol. 14, no. 4, pp. 271–276, 2013.
- [26] K. J. L. Jackson, Y. Wang, B. A. Gaeta et al., “Divergent human populations show extensive shared IGK rearrangements in peripheral blood B cells,” *Immunogenetics*, vol. 64, no. 1, pp. 3–14, 2012.
- [27] K. Kitaura, H. Yamashita, H. Ayabe, T. Shini, T. Matsutani, and R. Suzuki, “Different somatic hypermutation levels among antibody subclasses disclosed by a new next-generation sequencing-based antibody repertoire analysis,” *Frontiers in Immunology*, vol. 8, p. 389, 2017.
- [28] J. M. Di Noia and M. S. Neuberger, “Molecular mechanisms of antibody somatic hypermutation,” *Annual Review of Biochemistry*, vol. 76, no. 1, pp. 1–22, 2007.
- [29] J. K. Hwang, F. W. Alt, and L. S. Yeap, “Related mechanisms of antibody somatic hypermutation and class switch recombination,” *Mobile DNA III*, vol. 3, no. 1, pp. 325–348, 2015.
- [30] J. D. Galson, J. Trück, A. Fowler et al., “Analysis of B Cell repertoire dynamics following hepatitis B vaccination in humans, and enrichment of vaccine-specific antibody sequences,” *EBioMedicine*, vol. 2, no. 12, pp. 2070–2079, 2015.
- [31] C. Wang, Y. Liu, L. T. Xu et al., “Effects of aging, cytomegalovirus infection, and EBV infection on human B cell repertoires,” *The Journal of Immunology*, vol. 192, no. 2, pp. 603–611, 2014.
- [32] B. S. Wendel, C. He, M. Qu et al., “Accurate immune repertoire sequencing reveals malaria infection driven antibody lineage diversification in young children,” *Nature Communications*, vol. 8, no. 1, p. 531, 2017.
- [33] J. D. Galson, J. Trück, E. A. Clutterbuck et al., “B-cell repertoire dynamics after sequential hepatitis B vaccination and evidence for cross-reactive B-cell activation,” *Genome Medicine*, vol. 8, no. 1, p. 68, 2016.
- [34] E. E. Godoy-Lozano, J. Téllez-Sosa, G. Sánchez-González et al., “Lower IgG somatic hypermutation rates during acute dengue virus infection is compatible with a germinal center-independent B cell response,” *Genome Medicine*, vol. 8, no. 1, p. 23, 2016.
- [35] B. Cortina-Ceballos, E. E. Godoy-Lozano, J. Téllez-Sosa et al., “Longitudinal analysis of the peripheral B cell repertoire reveals unique effects of immunization with a new influenza virus strain,” *Genome Medicine*, vol. 7, no. 1, p. 124, 2015.

Research Article

Quantitative Profiling of Oxylipin Reveals the Mechanism of Pien-Tze-Huang on Alcoholic Liver Disease

Ziye Zhu,^{1,2} Wenjun Zhou,¹ Yang Yang,² Kai Wang,² Fenghua Li^{ID},² and Yanqi Dang^{ID}¹

¹*Institute of Digestive Diseases, Longhua Hospital, China-Canada Center of Research for Digestive Diseases (ccCRDD), Shanghai University of Traditional Chinese Medicine, Shanghai 200032, China*

²*Experiment Center for Science and Technology, Shanghai University of Traditional Chinese Medicine, Shanghai 200032, China*

Correspondence should be addressed to Fenghua Li; lfh@hotmail.com and Yanqi Dang; dangyanqi9022@126.com

Received 10 March 2021; Revised 30 April 2021; Accepted 6 May 2021; Published 1 June 2021

Academic Editor: Chan-Yen Kuo

Copyright © 2021 Ziye Zhu et al. This is an open access article distributed under the Creative Commons Attribution License, which permits unrestricted use, distribution, and reproduction in any medium, provided the original work is properly cited.

Alcoholic liver disease (ALD) is a liver disease caused by long-term alcohol consumption. ROS-mediated oxidative stress is the leading cause of ALD. Pien-Tze-Huang (PZH), a traditional formula, is famous in China. This study was designed to evaluate the effects and explore the potential mechanisms of PZH in ALD. Forty mice were randomly divided into five groups: control group (normal diet + vehicle), model group (ethanol diet + vehicle), PZH-L group (ethanol diet + PZH (0.125 g/kg)), PZH-M group (ethanol diet + PZH (0.25 g/kg)), and PZH-H group (ethanol diet + PZH (0.5 g/kg)). The mice were sacrificed, and their liver and blood samples were preserved. Liver steatosis, triglyceride (TG), total cholesterol, serum alanine aminotransferase (ALT), and aspartate aminotransferase (AST) levels were assayed. Malondialdehyde (MDA), glutathione peroxidase (GSH-PX), and total superoxide dismutase were identified using commercial kits. Oxylipins were profiled, and the data were analyzed. The AMPK/ACC/CPT1A pathway was identified using real-time polymerase chain reaction and western blotting. The PZH-H intervention significantly alleviated hepatic steatosis and injury and reduced the levels of liver TG and serum ALT and AST. In addition, MDA levels were markedly reduced, and GSH-PX activity significantly increased after PZH-H intervention. Finally, PZH-H increased the levels of 17-HETE, 15-HEPE, 9-HOTrE, 13-HOTrE, and 5,6-dihydroxy-8Z,11Z,14Z,17Z-eicosatetraenoic acid, and reduced PGE2 levels. PZH-H intervention also promoted the phosphorylation of AMPK and ACC, and the expression of CPT1A. In conclusion, PZH reduced oxidative stress and alleviated hepatic steatosis and injury. The mechanism was correlated with the oxylipin metabolites/AMPK/ACC/CPT1A axis.

1. Introduction

Alcoholic liver disease (ALD) is a liver disease caused by long-term alcohol consumption. It is one of the most common types of chronic liver diseases globally and is currently one of the major chronic liver diseases in China [1–3]. Heavy drinkers (ethanol consumption of ≥ 40 g/day for men and ≥ 20 g/day for women over 5 years; or ethanol consumption of >80 g/day and binge drinking within 2 weeks) develop fatty liver, and about 20%–40% of them develop more severe ALD [1, 4]. According to the International Classification of Diseases (ICD-10), ALD is classified as alcoholic fatty liver, alcoholic hepatitis, alcoholic liver fibrosis, alcoholic cirrhosis, and alcoholic liver failure. Studies have found that the prevalence of

ALD in China is 4.5%, which is similar to that in European and American countries, among which the prevalence of ALD in people aged 40–49 years is the highest, accounting for more than 10% [5]. At present, the effective ways to reduce or terminate alcoholic liver injury are nutritional support and abstinence from alcohol, but some patients still need to undergo combined treatment with drug intervention. The guidelines for the prevention and treatment in 2018 included glucocorticoid, metadoxine, S-adenosylmethionine, polyene phosphatidylcholine, glycyrrhizic acid preparation, and silymarin. Although these drugs show some improvement in patients with ALD, strict and extensive sample data supporting effective treatment and improvement of ALD are still lacking in clinical trials.

Alcohol consumption can induce the generation of reactive oxygen species (ROS), which cause oxidative stress. ROS can change the structure and function of the protein by binding to them and finally generate host antigens that can induce immune responses [6, 7]. ROS can also lead to lipid peroxidation and generate lipid peroxidation products, such as 4-hydroxynonenal (4-HNE) and malondialdehyde (MDA). Studies have found that these products can bind to DNA bases and induce apoptosis and autophagy in cells [8–10]. Therefore, ROS-mediated oxidative stress is the leading cause of ALD.

Oxylipins are produced by the oxidation of polyunsaturated fatty acids (PUFAs), including arachidonic acid (AA), linoleic acid (LA), eicosapentaenoic acid (EPA), and docosahexaenoic acid (DHA). Oxylipins play an important role in inflammatory response [11, 12], immune defense [13, 14], and oxidative stress [13, 15]. Studies have found that AA can inhibit inflammatory responses and oxidative stress to protect against brain injury [15]. LA attenuates acrolein-induced oxidative stress [16]. EPA can decrease ROS to attenuate oxidative stress [17–19]. In addition, DHA protects photoreceptors from oxidative stress [20]. These studies have shown that oxylipins can attenuate oxidative stress.

The traditional formula, Pien-Tze-Huang (PZH), is famous in China and is mainly composed of four traditional Chinese medicines, namely, *Panax notoginseng* (85%), Musk (3%), *Calculus bovis* (5%), and snake's gall bladder (7%). Studies have found that PZH has the functions of clearing away heat and detoxification, reducing swelling and relieving pain, anti-inflammatory effects, and liver protection [21–23]. Clinically, it is widely used in various inflammatory diseases, such as viral hepatitis, alcoholic hepatitis, and fatty liver [24]. Currently, the mechanism of PZH in ALD remains unclear. Therefore, in this study, we explored the protective effect of PZH on ALD and its potential mechanism.

2. Materials and Methods

2.1. Animals. C57BL/6 male mice (22–25 g) were obtained from Beijing Vital River Laboratory Animal Technology Co. Ltd, China. Mice were maintained under a specific pathogen-free environment (23–25°C, relative humidity: 40%–70%) with a 12-hour light/dark cycle.

2.2. Experimental Design and Administration of PZH. Mice were randomly divided into five groups: control group (normal diet + vehicle), model group (ethanol diet + vehicle), PZH-L group (ethanol diet + PZH (0.125 g/kg)), PZH-M group (ethanol diet + PZH (0.25 g/kg)), and PZH-H group (ethanol diet + PZH (0.5 g/kg)). Mice fed an ethanol diet were fed an ethanol Lieber-DeCarli diet (Trophic Animal Feed High-tech Co. Ltd, China) containing 5% (v/v) ethanol for 10 days. Mice with a normal diet were pair-fed with an equicaloric normal Lieber-DeCarli diet for 10 days. PZH was exclusively produced and certified by Zhangzhou Pien Tze Huang Pharmaceutical Co., Ltd., and the fingerprint spectrum was determined by HPLC-MS in a previous

study [22]. PZH-treated mice were gavaged with PZH aqueous solution simultaneously as they were fed an ethanol diet for 10 days. On day 11, mice fed an ethanol diet were gavaged with a single dose of 31.5% (v/v) ethanol (20 μ L/g body weight), and mice fed a normal diet were gavaged with equicaloric 45% (w/v) maltose dextrin (20 μ L/g body weight). All mice were euthanized after 9 hours, and blood and liver samples were collected for further study.

2.3. Biochemical Analysis. The blood was centrifuged for 20 min at 4000 rpm at 4°C, and serum was collected for analysis. Liver tissue was homogenized in propanone/ethanol (1:1) and incubated overnight at 4°C. Homogenates were centrifuged for 10 min at 4000 rpm at 4°C, and the supernatant was collected for testing. Serum alanine aminotransferase (ALT) and aspartate aminotransferase (AST) levels, liver triglyceride (TG), and total cholesterol (TC) levels were measured using an automatic biochemistry analyzer (TBA-40FR, Toshiba, Japan).

2.4. Histological Analysis. The left lobe of the liver was cut in half. One half was fixed in 10% buffered formalin, and the other was frozen in liquid nitrogen. The fixed liver sections were dehydrated, embedded, and sectioned into 4 μ m sections for staining with hematoxylin and eosin (H&E). The frozen liver sections were embedded and sectioned into 10 μ m thick sections using a frozen microtome (Leica, Germany) for staining with Oil Red O, according to previous studies [25, 26].

2.5. Measurement of MDA, GSH-PX, and T-SOD Levels in the Liver. Liver tissue was homogenized and centrifuged for 10 min at 4000 rpm at 4°C, and the supernatant was collected. The levels of MDA, glutathione peroxidase (GSH-PX), and total superoxide dismutase (T-SOD) in liver tissue were measured using commercial kits (Nanjing Jiancheng Bioengineering Institute, Nanjing, China).

2.6. Sample Preparation and the Detection of Oxylipins Profile. Tissue (20 mg) was weighed and homogenized with 200 μ L of oxylipin extract (BB24, Next Advance, Inc., Averill Park, NY, USA) for 3 min. The mixture was centrifuged for 10 min at 5000 rpm at 4°C. The supernatant was concentrated, dried, and then redissolved in 100 μ L methanol/water (1:1, v/v). Seventy-one oxylipin metabolites were determined at the Metabo-Profile R & D Laboratory (Shanghai, China). Ultra-performance liquid chromatography-tandem mass spectrometry (UPLC-MS/MS) (ExionLC™ AD, QTRAP® 6500+) was used to detect them according to manufacturer's instructions.

2.7. Oxylipins Data Analysis. The raw data generated by UPLC-MS/MS were extracted, integrated, identified, and quantitatively analyzed for each metabolite using AB Sciex's Analyst software (V1.6.3, AB Sciex, Boston, MA, USA). Principal component analysis (PCA), partial least squares

discriminant analysis (PLS-DA), and variable importance of projection (VIP) were performed to analyze the data. The formula used for calculating the Z-score was $Z\text{-scores} = (x - \text{mean}) / \text{SD}$. The Euclidean distance of Z-scores was clustered with the method in the heatmap. Kyoto Encyclopedia of Genes and Genomes (KEGG) pathways were enriched using Metaboanalyst 4.0.

2.8. Real-Time Polymerase Chain Reaction (RT-PCR).

Total RNA was isolated from liver tissue using RNAiso Reagent (Takara, Japan) and reverse-transcribed using PrimeScript™ RT Master Mix (Takara, Japan). RT-PCR was performed using TB Green® Premix Ex Taq™ according to the manufacturer's instructions. Target gene expression was analyzed using the $2^{-\Delta\Delta C_t}$ method by normalization to β -actin. The primers used are listed in Table 1.

2.9. Western Blot Analysis. Liver tissue was lysed and centrifuged for 10 min at 4000 rpm at 4°C, and the supernatant was collected and denatured. Denatured proteins were separated by SDS-PAGE and transferred to polyvinylidene fluoride membranes (Millipore, USA). The membranes were blocked using 5% skim milk and then incubated at 4°C overnight with the primary antibodies, including AMP-activated protein kinase alpha (AMPK α) (CST, USA), phospho-AMPK α (CST, USA), acetyl-CoA carboxylase (ACC) (CST, USA), phospho-ACC (CST, USA), carnitine palmitoyltransferase 1A (CPT1A) (Gene Tex), peroxisome proliferator-activated receptor alpha (PPAR α) (ABclonal, China), sterol regulatory element-binding transcription factor 1 (SREBP1) (Santa Cruz, USA), and HRP-conjugated β -actin (HUABIO, China). After the overnight incubation, the membranes were incubated with HRP-conjugated secondary antibody (Jackson Immuno). Blots were visualized with ECL luminescence reagent (Meilunbio, China) and quantified using ImageJ software.

2.10. Statistical Analysis. Data are presented as mean \pm standard deviation ($\bar{x} \pm s$). Statistical significance was analyzed using one-way ANOVA in SPSS 24.0. Qualitative data among the three groups were assessed using one-way ANOVA, the Kruskal–Wallis test, or the chi-square test based on data distribution. Differences between the two groups were analyzed using Student's *t*-test. The values were considered statistically significant at $P < 0.05$.

3. Results

3.1. PZH-H Alleviated Hepatic Steatosis in ALD-Mice. Hepatic steatosis was significantly higher in the model group than in the control group, and the PZH-M and PZH-H interventions significantly improved hepatic steatosis (Figures 1(a) and 1(b)). In addition, liver TG and TC levels were markedly increased in the model group compared with those in the control group. The PZH-H intervention significantly reduced liver TG levels, but liver TC was increased in the PZH-H group compared with that in the model group

(Figures 1(c) and 1(d)). Furthermore, serum ALT and AST levels were markedly increased in the model group compared with those in the control group. The PZH-H intervention markedly reduced ALT and AST levels, and the PZH-M intervention also markedly reduced ALT levels (Figures 1(e) and 1(f)). These results indicated that PZH-M and PZH-H alleviated hepatic steatosis and injury in ALD mice, and the effect of PZH-H was better than that of PZH-M.

3.2. Effect of PZH on MDA, GSH-PX, and SOD. Oxidative stress is one of the main pathogenesises of ALD; MDA, GSH-PX, and T-SOD are the primary biomarkers of oxidative stress. Thus, we tested the levels of MDA, GSH-PX, and T-SOD in the livers of ALD-mice. Compared with the control group, the level of MDA in the model group was significantly increased, while the activities of GSH-PX and T-SOD were significantly decreased. Compared with the model group, the level of MDA in the three PZH groups was significantly decreased (Figure 2(a)), and the activity of GSH-PX in the PZH-H group was significantly increased (Figure 2(b)). Although T-SOD activity in the PZH-H group was not different, its activity was significantly increased in the PZH-M group (Figure 2(c)). These results indicate that PZH-H could improve oxidative stress.

3.3. Analysis of Oxylipin Metabolites among Three Groups.

Our results showed that PZH could alleviate hepatic steatosis, liver injury, and oxidative stress, and the effect of PZH-H was better than that of the PZH-L and PZH-M groups. Thus, we chose the PZH-H group to explore the mechanism of oxidative stress improvement. Previous studies have proved that oxylipins play an important role in oxidative stress [13, 15]. Therefore, the profiling of oxylipins was performed and analyzed. The results indicated that the proportion of DHA was the highest, followed by that of LA (Figure 3(a)). DHA, LA, and EPA levels were significantly different among the three groups (Figure 3(b)). Fifty-eight oxylipin metabolites were detected in the liver tissue of the mice (Figure 3(c), Supplementary file 1). The PCA and PLS-DA analyses yielded clear distinctions among the three groups (Figures 3(d) and 3(e)).

3.4. Effect of PZH on Different Oxylipin Metabolites. First, using values of $P < 0.05$, the sets of 24 and 16 different oxylipin metabolites were obtained in the model group compared with the control group, and the PZH-H group compared with the model group (Figures 4(a) and 4(c)), respectively. Furthermore, combined with the value of VIP > 1 , only 22 and 16 different oxylipin metabolites were obtained in the model group compared with the control group, and the PZH-H group compared with the model group (Figures 4(b) and 4(d), Supplementary file 2), respectively. KEGG pathway analysis revealed that the main pathways included carnitine O-acetyltransferase, carnitine-acetylcarnitine carrier, fatty acyl-CoA desaturase, linoleic acid (n-C18:2) transport via diffusion, carnitine

TABLE 1: The sequence of primers in the study.

Primer name	Forward primer sequence (5'→3')	Reverse primer sequence (5'→3')
β -Actin	GGCTGTATTCCCCTCCATCG	CCAGTTGGTAACAATGCCATGT
ACC1	GATGAACCATCTCCGTTGGC	GACCCAATTATGAATCGGGAGTG
ACC2	CCTTTGGCAACAAGCAAGGTA	AGTCGTACACATAGGTGGTCC
CPT1A	CTCCGCCTGAGCCATGAAG	CACCAGTGATGATGCCATTCT
PPAR α	AGAGCCCCATCTGTCCTCTC	ACTGGTAGTCTGAAAACCAAA
SREBP-1	GCAGCCACCATCTAGCCTG	CAGCAGTGAGTCTGCCTTGAT

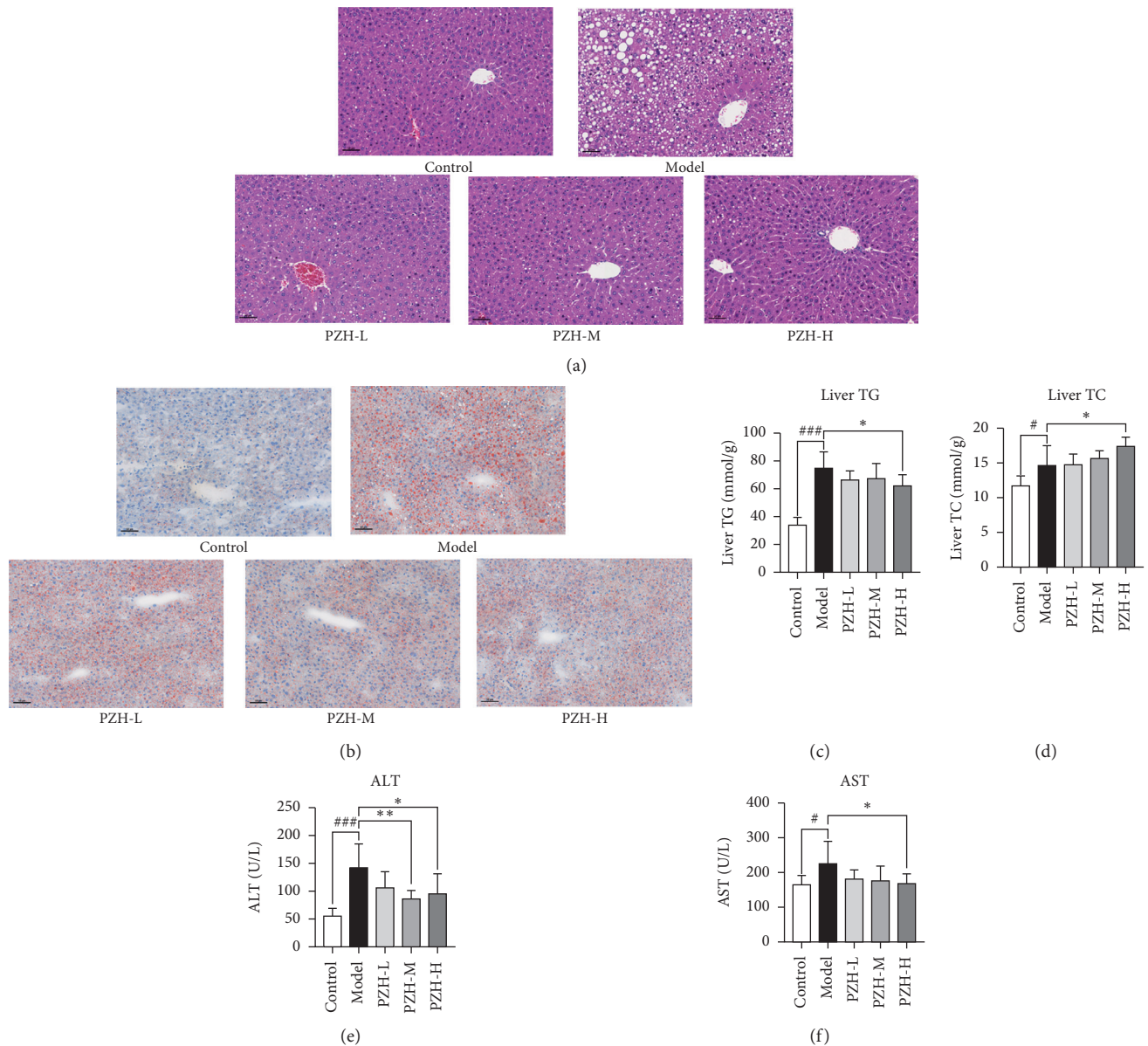


FIGURE 1: PZH-H alleviated hepatic steatosis in ALD-mice. (a) HE staining in liver sections was presented. (b) Oil Red O in liver sections was presented. (c) Liver TG and (d) TC were analyzed ($n=8$); (e) Serum ALT and (f) AST were analyzed ($n=8$). Data were presented as means \pm SD. # $P < 0.05$, ## $P < 0.01$, and ### $P < 0.001$ in the model group vs the control group; * $P < 0.05$ and ** $P < 0.01$ in the PZH groups vs the model group.

O-palmitoyltransferase, and beta-oxidation of fatty acids (Figures 4(e) and 4(f)). We further identified six overlapping oxylipin metabolites among the three groups using a Venn

diagram (Figure 5(a)), including two EPAs (17-HETE and 15-HEPE), three LAs (9-HOTrE, 13-HOTrE, 5,6-dihydroxy-8Z, 11Z, 14Z, 17Z-eicosatetraenoic acid), and one DGLA

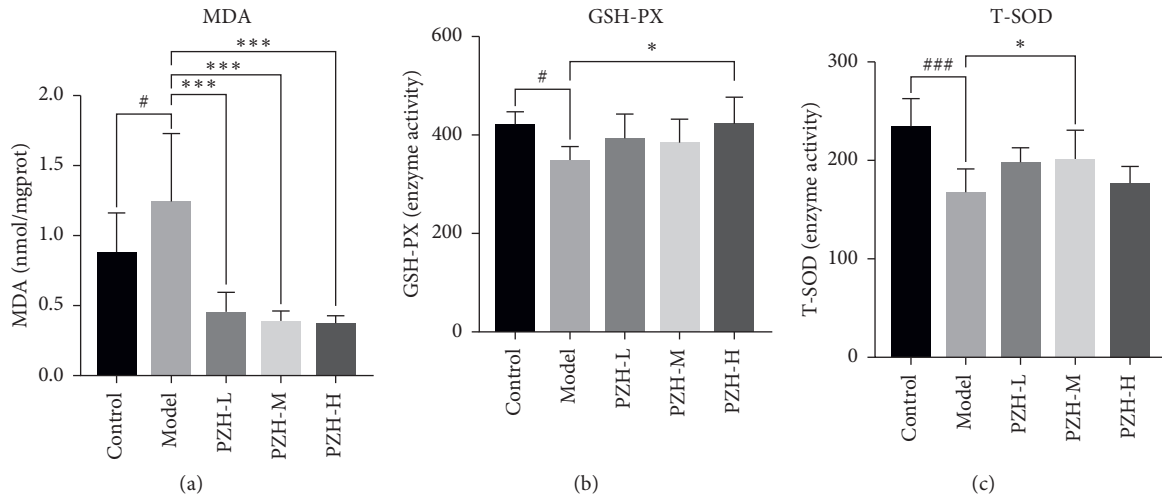


FIGURE 2: Effect of PZH on MDA, GSH-PX, and T-SOD. (a) The content of MDA, (b) the activity of GSH-PX, and (c) T-SOD was measured using kits ($n=8$). Data were presented as means \pm SD. # $P < 0.05$ and ### $P < 0.001$ in the model group vs the control group; * $P < 0.05$ and *** $P < 0.001$ in the PZH groups vs the model group.

(PGE2). The levels of 17-HETE, 15-HEPE, 5,6-dihydroxy-8Z, 11Z, 14Z, 17Z-eicosatetraenoic acid, 9-HOTrE, and 13-HOTrE were markedly increased, and PGE2 levels were significantly reduced in the model group compared with the control group. PZH-H intervention further increased the levels of 17-HETE, 15-HEPE, 9-HOTrE, 13-HOTrE, and 5,6-dihydroxy-8Z, 11Z, 14Z, 17Z-eicosatetraenoic acid, and reduced PGE2 levels (Figures 5(b)–5(g), Table 2).

3.5. Oxylipin Metabolites Were Negatively Correlated with MDA. PZH-H reduced MDA levels and promoted the activity of GSH-PX (Figure 2). Profiling of oxylipins indicated that PZH-H could also increase the levels of 17-HETE, 15-HEPE, 5,6-dihydroxy-8Z, 11Z, 14Z, 17Z-eicosatetraenoic acid, 9-HOTrE, 13-HOTrE, and reduced PGE2 levels (Figure 4). Therefore, Spearman correlation analysis was performed to evaluate the correlation of oxylipin metabolites, MDA, and GSH-PX. The results showed that 15-HEPE, 5,6-dihydroxy-8Z, 11Z, 14Z, 17Z-eicosatetraenoic acid, 9-HOTrE, and 13-HOTrE were negatively correlated with MDA, and there was no correlation among the other indices (Figure 6).

3.6. Effect of PZH on AMPK-ACC-CPT1A Pathway. Previous studies have indicated that oxylipin metabolites can regulate the AMPK signaling pathway [27–30]. The results showed that although the phosphorylation of AMPK was not significantly different in the model group compared with the control group, PZH-H intervention markedly promoted the phosphorylation of AMPK (Figure 7(a)). In addition, compared with the control group, the phosphorylation of ACC was significantly reduced in the model group, and PZH-H intervention markedly promoted the phosphorylation of ACC. However, the mRNA levels of ACC1 and ACC2 in the model group were significantly increased, the mRNA levels of ACC1 were significantly decreased, and

ACC2 levels were significantly increased after PZH-H intervention (Figures 7(a)–7(c)). Compared with the control group, the mRNA and protein levels of CPT1A were significantly decreased in the model group, and PZH-H intervention significantly promoted CPT1A expression (Figures 7(a) and 7(d)). Although the phosphorylation of PPAR α was not significantly different in the model group compared with the control group, the PZH-H intervention markedly promoted the phosphorylation of PPAR α . Moreover, the expression of SREBP1 was not significantly different among the three groups (Figures 7(e)–7(g)).

4. Discussion

In the present study, we showed that PZH could improve hepatic steatosis and injury in ALD mice, consistent with previous studies. In addition, PZH reduced the level of MDA and increased the activity of GSH-PX, ultimately ameliorating oxidative stress, which is consistent with a previous study [31]. Through the analysis of oxylipin profiling, we found that PZH promoted the levels of 17-HETE, 15-HEPE, 5,6-dihydroxy-8Z, 11Z, 14Z, 17Z-eicosatetraenoic acid, 9-HOTrE, and 13-HOTrE, and reduced PGE2 levels, further activating the AMPK pathway. Previous studies have also shown that PZH can reduce tumor necrosis factor- α and interleukin-1 β secretion to ameliorate hepatic inflammation [31] and can ameliorate hepatic injury by inhibiting the PERK/eIF2 α pathway [22]. In addition, PZH could also ameliorate hepatic fibrosis by suppressing the NF- κ B pathway [21]. Panax notoginseng saponins and polysaccharides have hepatoprotective effects against alcoholic liver damage [32, 33], but the mechanism is not precise. Our study is the first to demonstrate that PZH regulates the oxylipin-metabolites/AMPK pathway to reduce oxidative stress and improve hepatic steatosis and injury in ALD-mice. This study fully confirmed the mechanism of action of PZH on ALD through the quantitative profiling of oxylipin.

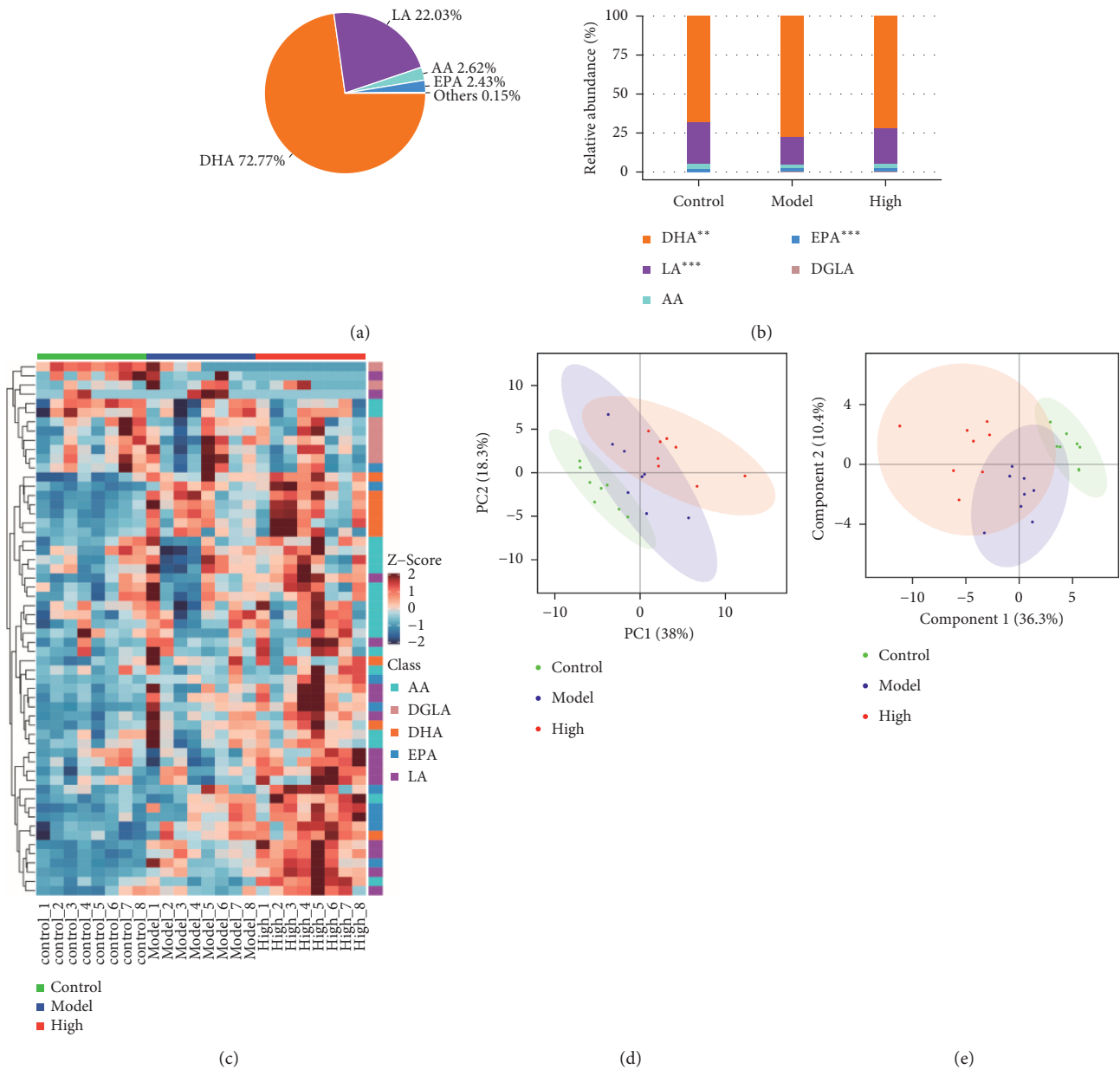


FIGURE 3: Analysis of oxylipin metabolites among three groups. (a) The proportion of identified metabolite classes in all groups was shown. (b) The relative abundance of each metabolite class in different groups was shown. (c) Fifty-eight oxylipin metabolites were detected in the liver tissue of mice. (d) PCA and (e) PLS-DA were analyzed and shown. High: PZH-H group.

Oxidative stress is one of the main pathogenesis of ALD. As a primary biomarker of oxidative stress, MDA was markedly increased in ALD and promoted the generation of etheno-DNA adducts to induce damage to the liver [9, 10]. In the present study, MDA levels were also markedly increased in the ALD mice, and PZH intervention significantly reduced MDA levels. In addition, the activity of GSH-PX, an antioxidant enzyme, was significantly reduced in ALD-mice, consistent with a previous study [34], and PZH increased the activity. These results indicated that PZH could attenuate oxidative stress.

Oxylipins play an essential role in oxidative stress [13, 15]. Studies have shown that EPA, as an oxylipin, can

decrease oxidative stress and placental lipid deposition in a sirtuin-1-independent manner [17]. The EPA could also decrease oxidative stress and attenuate cardiomyoblast apoptosis by activating autophagy [35]. EPA supplementation attenuates HFD-induced oxidative stress and steatosis [36]. In this study, PZH promoted the levels of EPA (17-HETE, 15-HEPE). Furthermore, LA is also an oxylipin, and studies have shown that LA can attenuate acrolein-induced oxidative stress [16]. Clinical trials have confirmed that LA can improve oxidative stress in obese patients with non-alcoholic fatty liver disease [37]. In our study, PZH increased LA levels, including 9-HOTrE, 13-HOTrE, and 5,6-dihydroxy-8Z, 11Z, 14Z, 17Z-eicosatetraenoic acid. Studies have also

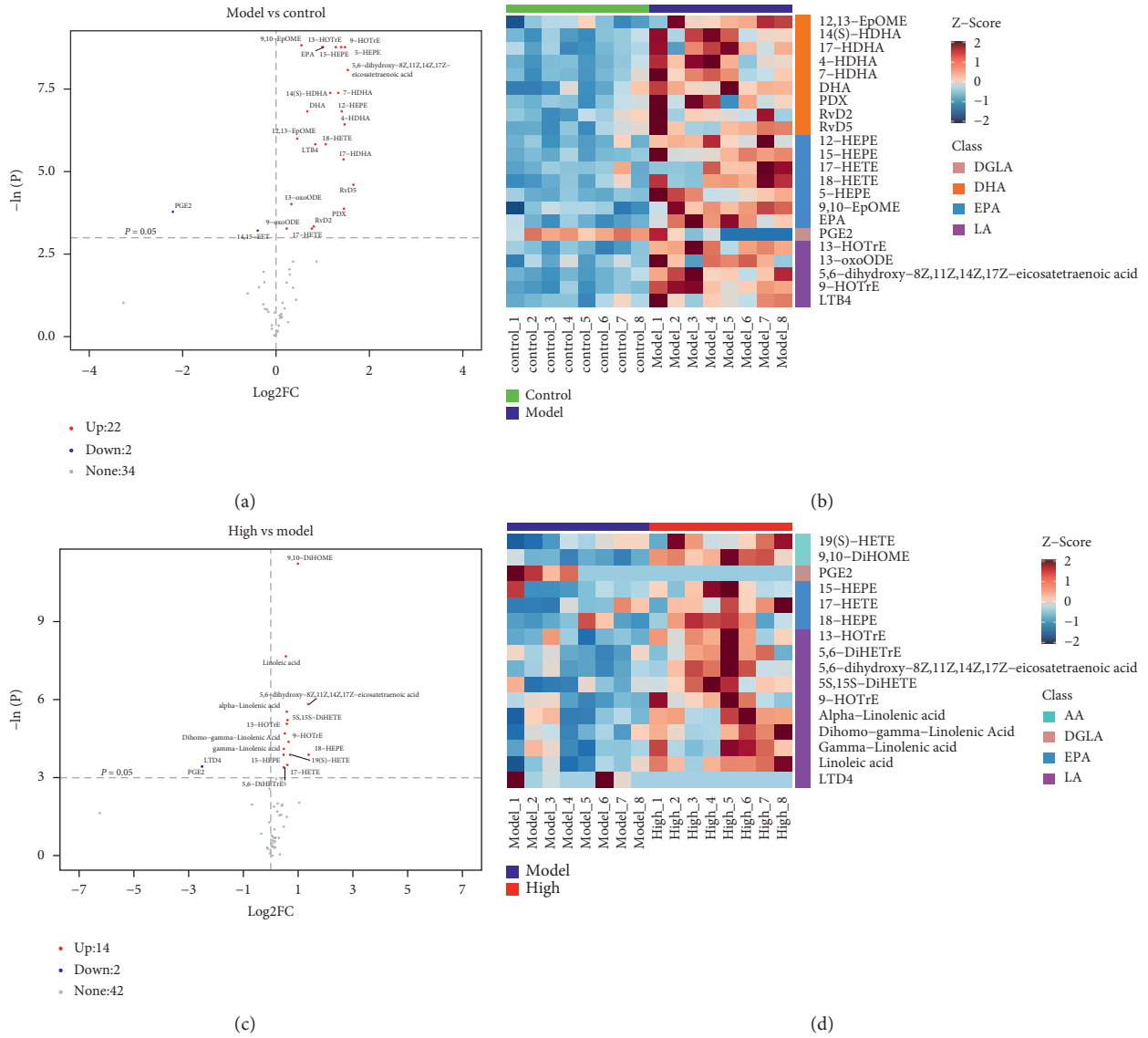


FIGURE 4: Continued.

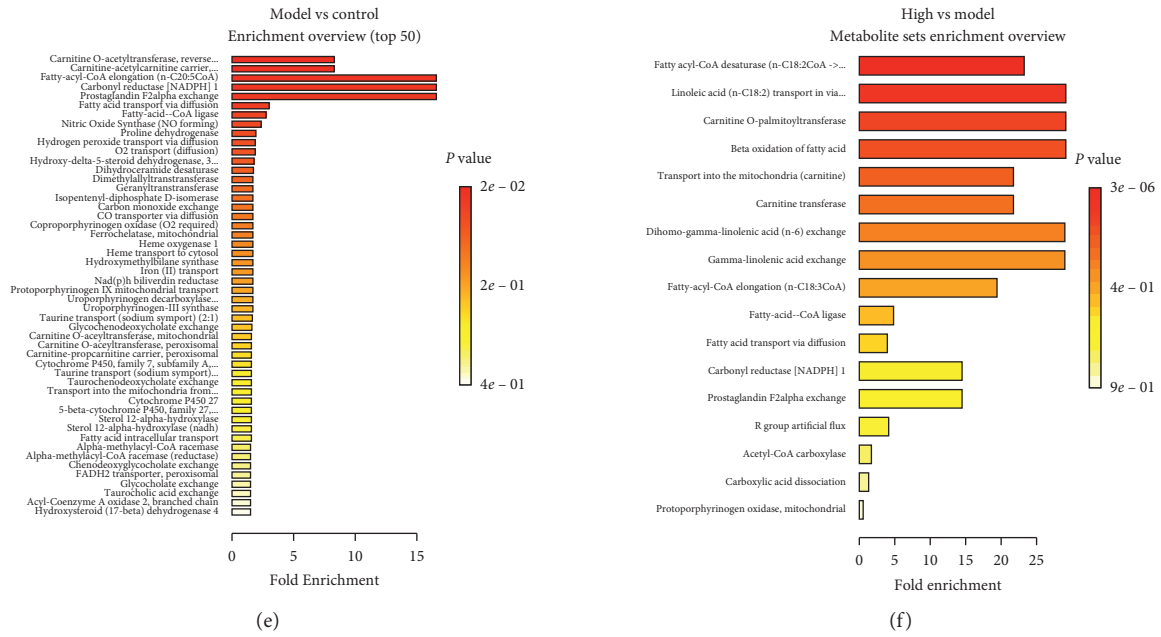


FIGURE 4: Effect of PZH on different oxylipin metabolites. (a) At $P < 0.05$, 24 different oxylipin-metabolites were obtained in the model group compared with the control group. (b) Combined with the value of VIP > 1 , 22 different oxylipin metabolites were obtained in the model group compared with the control group. (c) At $P < 0.05$, 16 different oxylipin-metabolites were obtained in the PZH-H group compared with the model group. (d) Combined with the value of VIP > 1 , 16 different oxylipin metabolites were obtained in the PZH-H group compared with the model group. The KEGG pathway was shown in (e) the model group compared with the control group and (f) the PZH-H group compared with the model group. High: PZH-H group.

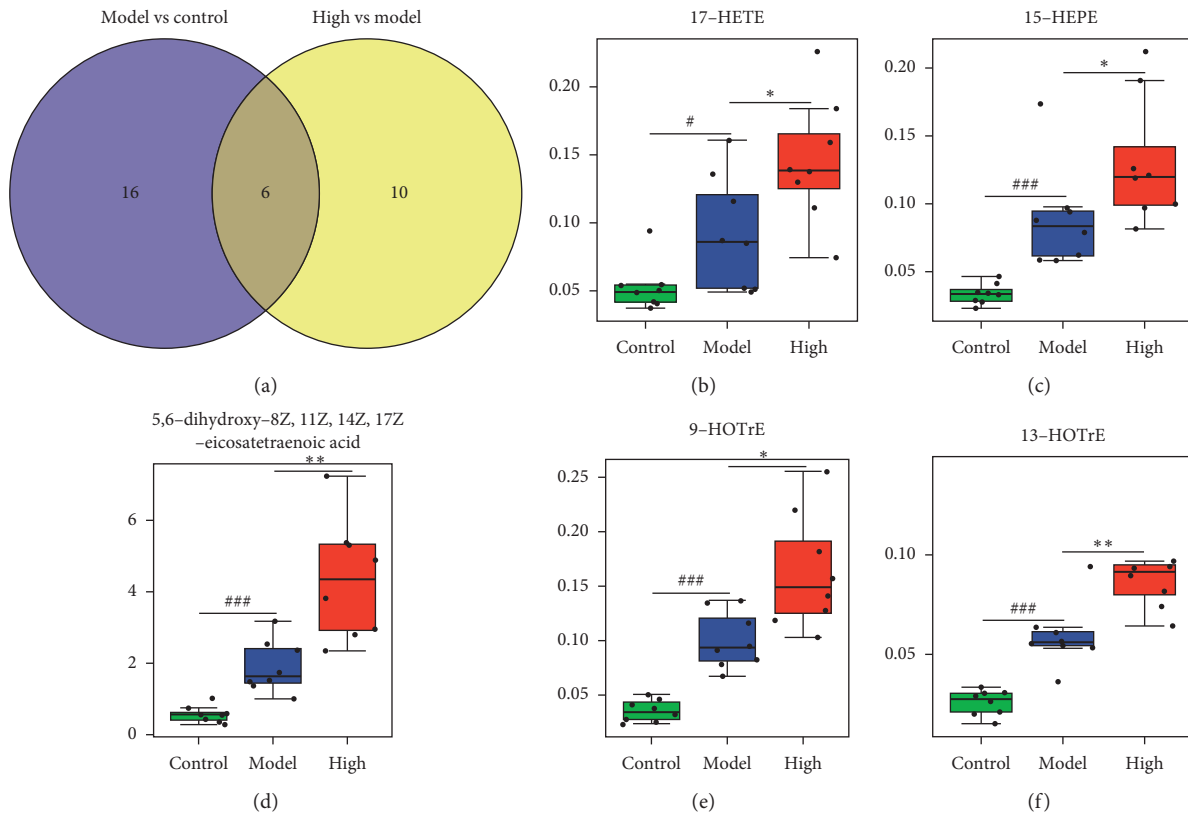


FIGURE 5: Continued.

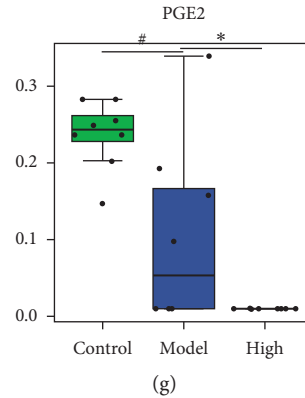


FIGURE 5: Effect of PZH on 6 overlapping oxylipin metabolites. (a) 6 overlapping oxylipin metabolites were showed among three groups. (b) 17-HETE, (c) 15-HEPE, (d) 5,6-dihydroxy-8Z,11Z,14Z,17Z-eicosatetraenoic acid, (e) 9-HOTrE, (f) 13-HOTrE, and (g) PGE2 levels were shown. # $P < 0.05$ and ### $P < 0.001$ in the model group vs the control group; * $P < 0.05$ and ** $P < 0.01$ in the PZH group vs the model group. High: PZH-H group.

TABLE 2: Six overlapping oxylipin metabolites among three groups.

Class	Metabolite	Model vs. control			PZH-H vs. model		
		Fold change	P value	VIP	Fold change	P value	VIP
EPA	17-HETE	1.735887097	0.037917638	1.059880581	1.574488	0.030620	1.438892
EPA	15-HEPE	2.479289941	0.0001554	1.470827013	1.431981	0.020668	1.013007
LA	5,6-Dihydroxy-8Z, 11Z, 14Z, 17Z-eicosatetraenoic acid	2.960944596	0.0003108	1.678973419	2.665644	0.002953	1.914047
LA	9-HOTrE	2.685344828	0.0001554	1.810016764	1.625732	0.012600	1.562081
LA	13-HOTrE	2.027124774	0.0001554	1.770831487	1.554011	0.006302	1.812153
DGLA	PGE2	0.220679012	0.022819743	1.13067223	0.181818	0.032474	1.211364

shown that high DGLA levels could be a biomarker for hepatic steatosis [38]. PGE2 can promote hepatic fibrosis and lead to insulin resistance [39]. Green tea extract attenuated PGE2 accumulation and protected against liver injury in an HFD-feeding NASH model [40], and meloxicam reduced PGE2 level and modulated oxidative stress to protect against liver injury [41]. Moreover, *Panax notoginseng* saponins attenuated gastric injury by modulating the metabolism of PGE2 [42]. In the present study, we found that PZH reduced PGE2 levels. In addition, our results further proved that 15-HEPE, 9-HOTrE, 13-HOTrE, and 5,6-dihydroxy-8Z, 11Z, 14Z, 17Z-eicosatetraenoic acid were negatively correlated with MDA. Further analysis showed that the upregulated metabolites (15-HEPE, 5,6-dihydroxy-8Z, 11Z, 14Z, 17Z-eicosatetraenoic acid, 9-HOTrE, and 13-HOTrE) were negative correlated with T-SOD, and downregulated PGE2 were positively correlated with T-SOD (Supplementary Figure 1), indicating that PZH could reduce oxidative stress through non-SOD dependent approach. Finally, the results showed that PZH may improve oxidative stress by oxylipin metabolites, including EPA, LA, and PGE2. On the basis of a previous study [42], we speculated that *Panax notoginseng* of PZH may mainly enhance oxylipin metabolites.

The AMPK-ACC-CPT1A pathway is involved in the regulation of oxidative stress and ALD [43–47]. Previous

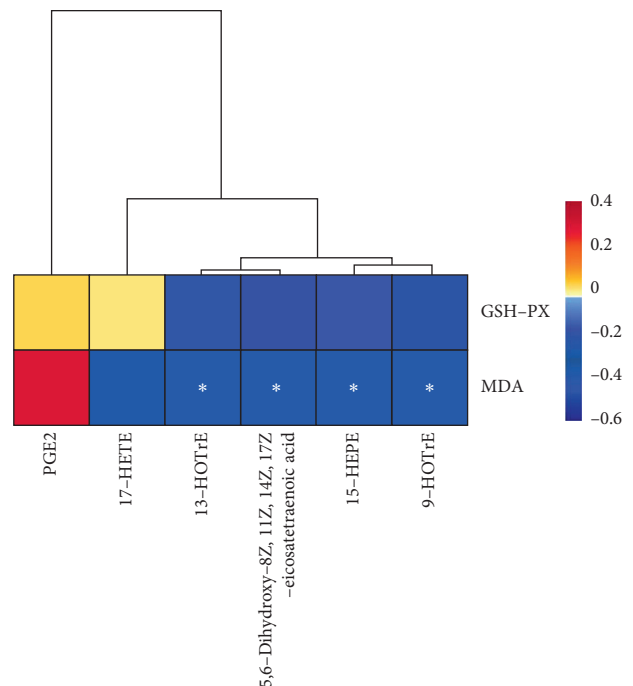


FIGURE 6: The correlation of oxylipin-metabolites, MDA, and GSH-PX was analyzed by the Spearman correlation analysis.

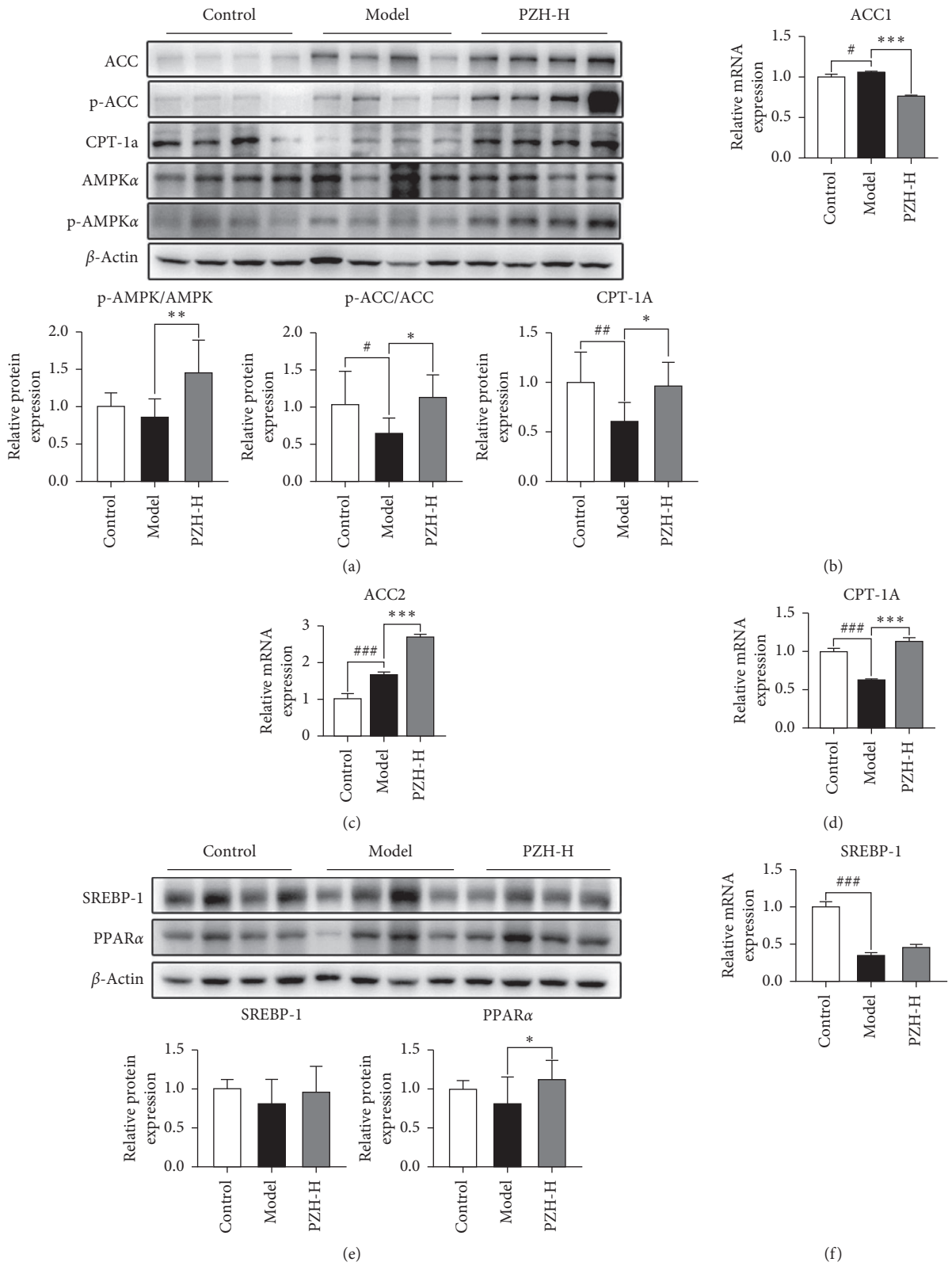


FIGURE 7: Continued.

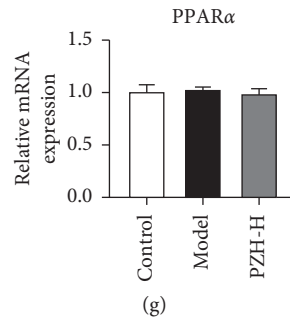


FIGURE 7: Effect of PZH on AMPK-ACC-CPT1A pathway. (a) The levels of p-AMPK, AMPK, p-ACC, ACC, and CPT-1A were shown ($n=8$). The mRNA expression of (b) ACC1, (c) ACC2, and (d) CPT-1A was detected by RT-PCR ($n=8$). (e) The protein expression of SREBP-1 and PPAR α was shown ($n=8$). (f) SREBP-1 mRNA expression and (g) PPAR α mRNA expression were detected ($n=8$). Data were presented as means \pm SD. # $P < 0.05$, ## $P < 0.01$, and ### $P < 0.001$ in the model group vs the control group; * $P < 0.05$, ** $P < 0.01$, and *** $P < 0.001$ in the PZH-H group vs the model group.

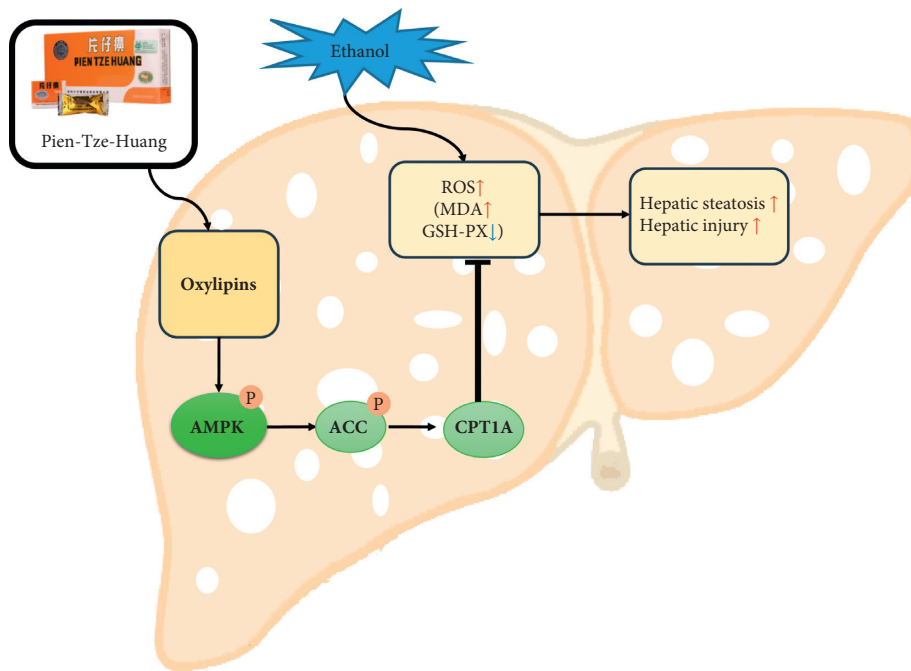


FIGURE 8: Summary of the study. Traditional Chinese formulae PZH increased the levels of oxylipin metabolites, activated AMPK-ACC-CPT1A pathway, and finally alleviated oxidative stress and hepatic steatosis.

studies have proved that EPA could improve palmitate-induced endothelial dysfunction and lipotoxicity by activating AMPK pathway [28, 48]. In addition, LA can reduce hepatic lipid metabolism [29, 30], insulin resistance, and adiposity [49, 50] via the AMPK pathway. PGE2 can negatively regulate the AMPK pathway [51, 52]. In this study, we found that PZH increased the levels of EPA and LA and reduced PGE2 levels. In addition, PZH can activate AMPK and promote the phosphorylation of ACC, which reduces the ACC activity [53] and finally promotes the expression of CPT1A. Although studies have shown that PPAR α and SREBP-1 could improve oxidative stress [54–56], PZH did not regulate their expression in our study, indicating that PZH did not play a regulatory role in ALD through PPAR α

and SREBP-1. However, in this study, we found that the levels of 9-HOTrE, 13-HOTrE, 5,6-dihydroxy-8Z, 11Z, 14Z, 17Z-eicosatetraenoic acid, 17-HETE, and 15-HEPE were increased in the liver of ALD-mice, and PZH further increased their levels. PGE2 levels were decreased in the liver of ALD-mice, and PZH further decreased this level. We speculated that oxylipin metabolites may need to reach certain concentrations in vivo and activate the AMPK/ACC/CPT1A pathway to protect against hepatic injury. However, further studies are required to elucidate the underlying mechanism. Although our results showed that PZH could regulate oxylipin metabolites and speculated that Panax notoginseng may mainly enhance oxylipin metabolites, further studies are also needed.

5. Conclusions

In summary, PZH reduced oxidative stress and alleviated hepatic steatosis and injury. The mechanism was correlated with the oxylipin metabolites/AMPK/ACC/CPT1A pathway (Figure 8).

Data Availability

The data used to support the findings of this study are available from the corresponding author upon request.

Ethical Approval

This study (PZSHUTCM200703007) was approved by the Animal Experiment Ethics Committee of Shanghai University of Traditional Chinese Medicine.

Conflicts of Interest

The authors declare that they have no conflicts of interest.

Authors' Contributions

Ziye Zhu and Wenjun Zhou contributed equally to this work. Fenghua Li and Yanqi Dang conceived, designed, and supervised the study. Ziye Zhu, Wenjun Zhou, Yang Yang, and Kai Wang performed the experiments. Yanqi Dang, Ziye Zhu, and Wenjun Zhou analyzed the data; and Yanqi Dang and Ziye Zhu wrote the paper. Fenghua Li and Wenjun Zhou revised the manuscript. All authors reviewed and approved the final manuscript.

Acknowledgments

The authors thank Metabo-Profile R&D Laboratory (Shanghai, China) for the profiling of oxylipins. This work was supported by the National Natural Science Foundation of China (81804018 and 81808397).

Supplementary Materials

Supplementary file 1. The levels of oxylipin-metabolites are shown among three groups. *Supplementary file 2.* 22 and 16 different oxylipin-metabolites are shown in the model group compared with the control group, and the PZH-H group compared with the model group, respectively. *Supplementary Figure 1.* The correlation of oxylipin-metabolites and T-SOD was analyzed by the Spearman correlation analysis. (*Supplementary Materials*)

References

- [1] J. Rehm and K. D. Shield, "Global burden of alcohol use disorders and alcohol liver disease," *Biomedicines*, vol. 7, no. 4, 2019.
- [2] S. K. Asrani, H. Devarbhavi, J. Eaton, and P. S. Kamath, "Burden of liver diseases in the world," *Journal of Hepatology*, vol. 70, no. 1, pp. 151–171, 2019.
- [3] A. K. Singal, R. Bataller, J. Ahn, P. S. Kamath, and V. H. Shah, "ACG clinical guideline: alcoholic liver disease," *The American Journal of Gastroenterology*, vol. 113, no. 2, pp. 175–194, 2018.
- [4] Y. M. Li and J. G. Fan, "Guidelines of prevention and treatment for alcoholic liver disease (2018, China)," *Journal of Digestive Diseases*, vol. 20, no. 4, pp. 174–180, 2019.
- [5] F. S. Wang, J. G. Fan, Z. Zhang, B. Gao, and H. Y. Wang, "The global burden of liver disease: the major impact of China," *Hepatology*, vol. 60, no. 6, pp. 2099–2108, 2014.
- [6] H. K. Seitz and F. Stickel, "Molecular mechanisms of alcohol-mediated carcinogenesis," *Nature Reviews Cancer*, vol. 7, no. 8, pp. 599–612, 2007.
- [7] E. Albano, P. Clot, M. Morimoto, A. Tomasi, M. Ingelman-Sundberg, and S. W. French, "Role of cytochrome P4502E1-dependent formation of hydroxyethyl free radical in the development of liver damage in rats intragastrically fed with ethanol," *Hepatology*, vol. 23, no. 1, pp. 155–163, 1996.
- [8] L. J. Su, J. H. Zhang, H. Gomez et al., "Reactive oxygen species-induced lipid peroxidation in apoptosis, autophagy, and ferroptosis," *Oxidative Medicine and Cellular Longevity*, vol. 2019, Article ID 5080843, 13 pages, 2019.
- [9] Y. Wang, G. Millonig, J. Nair et al., "Ethanol-induced cytochrome P4502E1 causes carcinogenic etheno-DNA lesions in alcoholic liver disease," *Hepatology*, vol. 50, no. 2, pp. 453–461, 2009.
- [10] S. Mueller, T. Peccerella, H. Qin et al., "Carcinogenic etheno DNA adducts in alcoholic liver disease: correlation with cytochrome P-4502E1 and fibrosis," *Alcoholism: Clinical and Experimental Research*, vol. 42, no. 2, pp. 252–259, 2018.
- [11] J. F. Ferguson, K. Roberts-Lee, C. Borcea, H. M. Smith, Y. Midgette, and R. Shah, "Omega-3 polyunsaturated fatty acids attenuate inflammatory activation and alter differentiation in human adipocytes," *Journal of Nutritional Biochemistry*, vol. 64, pp. 45–49, 2019.
- [12] C. Colson, R. A. Ghandour, O. Dufies et al., "Diet supplementation in omega3 polyunsaturated fatty acid favors an anti-inflammatory basal environment in mouse adipose tissue," *Nutrients*, vol. 11, no. 2, 2019.
- [13] C. Hunsche, O. Hernandez, A. Gheorghe, L. E. Diaz, A. Marcos, and M. De la Fuente, "Immune dysfunction and increased oxidative stress state in diet-induced obese mice are reverted by nutritional supplementation with monounsaturated and n-3 polyunsaturated fatty acids," *European Journal of Nutrition*, vol. 57, no. 3, pp. 1123–1135, 2018.
- [14] F. Gottrand, "Long-chain polyunsaturated fatty acids influence the immune system of infants," *Journal of Nutrition*, vol. 138, no. 9, pp. 1807S–1812S, 2008.
- [15] Y. Qu, H. L. Zhang, X. P. Zhang, and H. L. Jiang, "Arachidonic acid attenuates brain damage in a rat model of ischemia/reperfusion by inhibiting inflammatory response and oxidative stress," *Human & Experimental Toxicology*, vol. 37, no. 2, pp. 135–141, 2018.
- [16] B. Aydin, Z. Atli Sekeroglu, and V. Sekeroglu, "Effects of whey protein and conjugated linoleic acid on acrolein-induced cardiac oxidative stress, mitochondrial dysfunction and dyslipidemia in rats," *Biomedicine & Pharmacotherapy*, vol. 107, pp. 901–907, 2018.
- [17] M. Vara-Messler, J. H. Mukdsi, N. I. Osieki et al., "Eicosapentaenoic acid prevents salt sensitivity in diabetic rats and decreases oxidative stress," *Nutrition*, vol. 72, Article ID 110644, 2020.
- [18] J. Peng, J. Xiong, C. Cui et al., "Maternal eicosapentaenoic acid feeding decreases placental lipid deposition and improves the

- homeostasis of oxidative stress through a sirtuin-1 (SIRT1) independent manner,” *Molecular Nutrition & Food Research*, vol. 63, no. 21, Article ID e1900343, 2019.
- [19] K. Palanisamy, R. Krishnaswamy, P. Paramasivan, H. Chih-Yang, and V. P. Vishwanadha, “Eicosapentaenoic acid prevents TCDD-induced oxidative stress and inflammatory response by modulating MAP kinases and redox-sensitive transcription factors,” *British Journal of Pharmacology*, vol. 172, no. 19, pp. 4726–4740, 2015.
- [20] M. V. Simon, D. L. Agnolazza, O. L. German et al., “Synthesis of docosahexaenoic acid from eicosapentaenoic acid in retina neurons protects photoreceptors from oxidative stress,” *Journal of Neurochemistry*, vol. 136, no. 5, pp. 931–946, 2016.
- [21] H. Zheng, X. Wang, Y. Zhang, L. Chen, L. Hua, and W. Xu, “Pien-Tze-Huang ameliorates hepatic fibrosis via suppressing NF-kappaB pathway and promoting HSC apoptosis,” *Journal of Ethnopharmacology*, vol. 244, Article ID 111856, 2019.
- [22] Y. Yang, Z. Chen, L. Deng et al., “Pien Tze Huang ameliorates liver injury by inhibiting the PERK/eIF2alpha signaling pathway in alcohol and high-fat diet rats,” *Acta Histochema*, vol. 120, no. 6, pp. 578–585, 2018.
- [23] Y. Deng, H. Luo, J. Shu et al., “Pien Tze Huang alleviate the joint inflammation in collagen-induced arthritis mice,” *Chinese Medicine*, vol. 15, p. 30, 2020.
- [24] L. Huang, Y. Zhang, X. Zhang et al., “Therapeutic potential of pien-tze-huang: a review on its chemical composition, pharmacology, and clinical application,” *Molecules*, vol. 24, no. 18, 2019.
- [25] Y. Dang, J. Xu, Y. Yang et al., “Ling-gui-zhu-gan decoction alleviates hepatic steatosis through SOCS2 modification by N6-methyladenosine,” *Biomedicine & Pharmacotherapy*, vol. 127, Article ID 109976, 2020.
- [26] Y. Dang, J. Xu, M. Zhu, W. Zhou, L. Zhang, and G. Ji, “Gan-Jiang-Ling-Zhu decoction alleviates hepatic steatosis in rats by the miR-138-5p/CPT1B axis,” *Biomedicine & Pharmacotherapy*, vol. 127, Article ID 110127, 2020.
- [27] N. Kim, M. S. Kang, M. Nam, S. A. Kim, G. S. Hwang, and H. S. Kim, “Eicosapentaenoic acid (EPA) modulates glucose metabolism by targeting AMP-activated protein kinase (AMPK) pathway,” *International Journal of Molecular Sciences*, vol. 20, no. 19, 2019.
- [28] A. Sakamoto, M. Saotome, P. Hasan et al., “Eicosapentaenoic acid ameliorates palmitate-induced lipotoxicity via the AMP kinase/dynamin-related protein-1 signaling pathway in differentiated H9c2 myocytes,” *Experimental Cell Research*, vol. 351, no. 1, pp. 109–120, 2017.
- [29] C. Fu, Y. Zhang, Q. Yao et al., “Maternal conjugated linoleic acid alters hepatic lipid metabolism via the AMPK signaling pathway in chick embryos,” *Poultry Science*, vol. 99, no. 1, pp. 224–234, 2020.
- [30] T. Y. Zhang, J. T. Huang, H. B. Tian et al., “Trans-10,cis-12 conjugated linoleic acid alters lipid metabolism of goat mammary epithelial cells by regulation of de novo synthesis and the AMPK signaling pathway,” *Journal of Dairy Science*, vol. 101, no. 6, pp. 5571–5581, 2018.
- [31] J. Zhao, H. Hu, Y. Wan, Y. Zhang, L. Zheng, and Z. Hong, “Pien Tze Huang Gan Bao ameliorates carbon tetrachloride-induced hepatic injury, oxidative stress and inflammation in rats,” *Experimental and Therapeutic Medicine*, vol. 13, no. 5, pp. 1820–1826, 2017.
- [32] C. Wang, L. Zheng, S. Liu et al., “A novel acidic polysaccharide from the residue of Panax notoginseng and its hepatoprotective effect on alcoholic liver damage in mice,” *International Journal of Biological Macromolecules*, vol. 149, pp. 1084–1097, 2020.
- [33] F. Liu, X. Bai, R. B. Ding, Y. J. Hu, H. Su, and J. B. Wan, “UPLC/Q-TOFMS-based metabolomics studies on the protective effect of panax notoginseng saponins on alcoholic liver injury,” *The American Journal of Chinese Medicine*, vol. 43, no. 4, pp. 695–714, 2015.
- [34] X. Lin, D. Bai, Z. Wei et al., “Curcumin attenuates oxidative stress in RAW264.7 cells by increasing the activity of antioxidant enzymes and activating the Nrf2-Keap1 pathway,” *PLoS One*, vol. 14, no. 5, Article ID e0216711, 2019.
- [35] H. C. Hsu, C. Y. Chen, C. H. Chiang, and M. F. Chen, “Eicosapentaenoic acid attenuated oxidative stress-induced cardiomyoblast apoptosis by activating adaptive autophagy,” *European Journal of Nutrition*, vol. 53, no. 2, pp. 541–547, 2014.
- [36] F. Echeverria, R. Valenzuela, A. Bustamante et al., “Attenuation of high-fat diet-induced rat liver oxidative stress and steatosis by combined hydroxytyrosol- (HT-) eicosapentaenoic acid supplementation mainly relies on HT,” *Oxidative Medicine and Cellular Longevity*, vol. 2018, Article ID 5109503, 2018.
- [37] M. Ebrahimi-Mameghani, H. Jamali, R. Mahdavi, F. Kakaei, R. Abedi, and B. Kabir-Mamdooh, “Conjugated linoleic acid improves glycemic response, lipid profile, and oxidative stress in obese patients with non-alcoholic fatty liver disease: a randomized controlled clinical trial,” *Croatian Medical Journal*, vol. 57, no. 4, pp. 331–342, 2016.
- [38] M. Matsuda, T. Kawamoto, and R. Tamura, “Predictive value of serum dihomo-gamma-linolenic acid level and estimated Delta-5 desaturase activity in patients with hepatic steatosis,” *Obesity Research & Clinical Practice*, vol. 11, no. 1, pp. 34–43, 2017.
- [39] T. Inazumi, K. Yamada, N. Shirata et al., “Prostaglandin E2-EP4 Axis promotes lipolysis and fibrosis in adipose tissue leading to ectopic fat deposition and insulin resistance,” *Cell Reports*, vol. 33, no. 2, Article ID 108265, 2020.
- [40] M. Y. Chung, E. Mah, C. Masterjohn et al., “Green tea lowers hepatic COX-2 and prostaglandin E2 in rats with dietary fat-induced nonalcoholic steatohepatitis,” *Journal of Medicinal Food*, vol. 18, no. 6, pp. 648–655, 2015.
- [41] M. Edfawy, M. H. Hassan, A. Mansour, A. A. Hamed, and H. A. Amin, “Meloxicam modulates oxidative stress status, inhibits prostaglandin E2, and abrogates apoptosis in carbon tetrachloride-induced rat hepatic injury,” *International Journal of Toxicology*, vol. 31, no. 3, pp. 276–286, 2012.
- [42] W. Wang, L. Yang, L. Song et al., “Combination of Panax notoginseng saponins and aspirin potentiates platelet inhibition with alleviated gastric injury via modulating arachidonic acid metabolism,” *Biomedicine & Pharmacotherapy*, vol. 134, Article ID 111165, 2021.
- [43] J. Yu, W. N. Wang, N. Matei et al., “Ezetimibe attenuates oxidative stress and neuroinflammation via the AMPK/Nrf2/TXNIP pathway after MCAO in rats,” *Oxidative Medicine and Cellular Longevity*, vol. 2020, Article ID 4717258, 14 pages, 2020.
- [44] X. Han, H. Tai, X. Wang et al., “AMPK activation protects cells from oxidative stress-induced senescence via autophagic flux restoration and intracellular NAD (+) elevation,” *Aging Cell*, vol. 15, no. 3, pp. 416–427, 2016.
- [45] R. Hu, M. Q. Wang, S. H. Ni et al., “Salidroside ameliorates endothelial inflammation and oxidative stress by regulating the AMPK/NF-kappaB/NLRP3 signaling pathway in AGEs-

- induced HUVECs,” *European Journal of Pharmacology*, vol. 867, Article ID 172797, 2020.
- [46] Y. You, Y. L. Liu, Z. Y. Ai et al., “Lactobacillus fermentum KP-3-fermented ginseng ameliorates alcohol-induced liver disease in C57BL/6N mice through the AMPK and MAPK pathways,” *Food Function*, vol. 11, no. 11, pp. 9801–9809, 2020.
- [47] A. Nagappan, J. H. Kim, D. Y. Jung, and M. H. Jung, “Cryptotanshinone from the salvia miltiorrhiza bunge attenuates ethanol-induced liver injury by activation of AMPK/SIRT1 and Nrf2 signaling pathways,” *International Journal of Molecular Sciences*, vol. 21, no. 1, 2019.
- [48] C. H. Lee, S. D. Lee, H. C. Ou, S. C. Lai, and Y. J. Cheng, “Eicosapentaenoic acid protects against palmitic acid-induced endothelial dysfunction via activation of the AMPK/eNOS pathway,” *International Journal of Molecular Sciences*, vol. 15, no. 6, pp. 10334–10349, 2014.
- [49] H. Qin, Y. Liu, N. Lu, Y. Li, and C. H. Sun, “Cis-9,trans-11-Conjugated linoleic acid activates AMP-activated protein kinase in attenuation of insulin resistance in C2C12 myotubes,” *Journal of Agricultural and Food Chemistry*, vol. 57, no. 10, pp. 4452–4458, 2009.
- [50] S. Jiang, Z. Wang, J. J. Riethoven, Y. Xia, J. Miner, and M. Fromm, “Conjugated linoleic acid activates AMP-activated protein kinase and reduces adiposity more effectively when used with metformin in mice,” *Journal of Nutrition*, vol. 139, no. 12, pp. 2244–2251, 2009.
- [51] C. Wang, Y. Gao, Z. Zhang et al., “Safflower yellow alleviates osteoarthritis and prevents inflammation by inhibiting PGE2 release and regulating NF-kappaB/SIRT1/AMPK signaling pathways,” *Phytomedicine*, vol. 78, Article ID 153305, 2020.
- [52] K. Funahashi, X. Cao, M. Yamauchi, Y. Kozaki, N. Ishiguro, and F. Kambe, “Prostaglandin E2 negatively regulates AMP-activated protein kinase via protein kinase a signaling pathway,” *Prostaglandins & Other Lipid Mediators*, vol. 88, no. 1-2, pp. 31–35, 2009.
- [53] Y. Minokoshi, Y. B. Kim, O. D. Peroni et al., “Leptin stimulates fatty-acid oxidation by activating AMP-activated protein kinase,” *Nature*, vol. 415, no. 6869, pp. 339–343, 2002.
- [54] H. Yaribeygi, M. T. Mohammadi, and A. Sahebkar, “PPAR-alpha agonist improves hyperglycemia-induced oxidative stress in pancreatic cells by potentiating antioxidant defense system,” *Drug Research*, vol. 68, no. 6, pp. 355–360, 2018.
- [55] Y. Zhou, W. Yang, Z. Li et al., “Moringa oleifera stem extract protect skin keratinocytes against oxidative stress injury by enhancement of antioxidant defense systems and activation of PPARalpha,” *Biomedicine & Pharmacotherapy*, vol. 107, pp. 44–53, 2018.
- [56] A. Sharma, S. K. Anand, N. Singh, U. N. Dwivedi, and P. Kakkar, “Berbamine induced AMPK activation regulates mTOR/SREBP-1c axis and Nrf2/ARE pathway to allay lipid accumulation and oxidative stress in steatotic HepG2 cells,” *European Journal of Pharmacology*, vol. 882, Article ID 173244, 2020.

Research Article

Jian-Gan-Xiao-Zhi Decoction Alleviates Inflammatory Response in Nonalcoholic Fatty Liver Disease Model Rats through Modulating Gut Microbiota

Jiabao Liao,¹ Xuehua Xie,^{2,3} Jinmei Gao,⁴ Zhaiyi Zhang,⁵ Fei Qu,¹ Huantian Cui,⁶ Yongjun Cao,⁷ Xue Han,³ Jie Zhao,³ Weibo Wen ,³ and Hongwu Wang ⁵

¹Jiaxing Hospital of Traditional Chinese Medicine, Zhejiang Chinese Medical University, Jiaxing, Zhejiang, China

²Nanjing University of Traditional Chinese Medicine, Nanjing, Jiangsu, China

³Yunnan Provincial Hospital of Chinese Medicine, Kunming, Yunnan, China

⁴Fujian People's Hospital of Traditional Chinese Medicine, Fuzhou, Fujian, China

⁵Tianjin University of Traditional Chinese Medicine, Tianjin, China

⁶Shandong Provincial Key Laboratory of Animal Cell and Developmental Biology, School of Life Sciences, Shandong University, Qingdao, China

⁷Nantong Hospital of Traditional Chinese Medicine, Nantong, Jiangsu, China

Correspondence should be addressed to Weibo Wen; wenweibo2020@163.com and Hongwu Wang; whw2009@tjutc.edu.cn

Received 9 January 2021; Revised 1 March 2021; Accepted 11 March 2021; Published 22 March 2021

Academic Editor: Chih-Yuan Ko

Copyright © 2021 Jiabao Liao et al. This is an open access article distributed under the Creative Commons Attribution License, which permits unrestricted use, distribution, and reproduction in any medium, provided the original work is properly cited.

Background. Jian-Gan-Xiao-Zhi decoction (JGXZ), composed of *Salvia miltiorrhiza* Bunge, *Panax notoginseng*, *Curcuma zedoaria*, and other 9 types of herbs, has demonstrated beneficial effects on nonalcoholic fatty liver disease (NAFLD). However, the mechanisms behind JGXZ's impact on NAFLD remain unknown. **Methods.** In this study, a NAFLD rat model induced by a high-fat diet (HFD) received oral treatment of JGXZ (8 or 16 g crude herb/kg) for 12 weeks. The therapeutic effects of JGXZ on NAFLD model rats were investigated through blood lipid levels and pathological liver changes. 16S rRNA analysis was used to study the changes in gut microbiota after JGXZ treatment. The expressions of occludin and tight junction protein 1 (ZO-1) in the colon were investigated using immunostaining to study the effects of JGXZ on gut permeability. The anti-inflammatory effects of JGXZ were also studied through measuring the levels of IL-1 β , IL-6, and TNF- α in the serum and liver. **Results.** JGXZ treatment could decrease body weight and ameliorate dyslipidemia in NAFLD model rats. H&E and Oil Red O staining indicated that JGXZ reduced steatosis and infiltration of inflammatory cells in the liver. 16S rRNA analysis showed that JGXZ impacted the diversity of gut microbiota, decreasing the *Firmicutes*-to-*Bacteroidetes* ratio, and increasing the relative abundance of probiotics, such as *Alloprevotella*, *Lactobacillus*, and *Turicibacter*. Gut permeability evaluation found that the expressions of ZO-1 and occludin in the colon were increased after JGXZ treatment. Moreover, JGXZ treatment could decrease the levels of IL-1 β , IL-6, and TNF- α in the serum and liver. **Conclusions.** Our study illustrated that JGXZ could ameliorate NAFLD through modulating gut microbiota, decreasing gut permeability, and alleviating inflammatory response.

1. Background

Nonalcoholic fatty liver disease (NAFLD) is a chronic disease characterized by hepatic steatosis and dyslipidemia that can lead to type 2 diabetes, atherosclerosis, hepatic fibrosis, and even hepatic carcinoma [1]. With lifestyles and diets changing for the worse in recent years, the morbidity of NAFLD is on the rise [2]. Currently, few therapeutic

approaches have demonstrated a definite effect on NAFLD [3]. As such, there is a critical need to develop novel therapies to treat NAFLD.

Traditional Chinese medicine has been widely used in the treatment of NAFLD, with accumulating numbers of studies highlighting its lipid-lowering effects [4]. For instance, researchers were able to utilize Jiang-Zhi-Ning to ameliorate high-fat-diet (HFD)-induced dyslipidemia

through modulating the synthesis and translation of cholesterol and inhibiting oxidative stress [5]. Additionally, Zhixiong capsules have shown lipid-lowering effects on atherosclerosis model rats [6]; and Da-Huang-Ze-Xie decoction can improve dyslipidemia and hepatic steatosis in NAFLD rats through modulating gut microbiota and inhibiting the inflammatory response in the liver [7].

Jian-Gan-Xiao-Zhi decoction (JGXZ), composed of *Salvia miltiorrhiza* Bunge, *Panax notoginseng*, *Curcuma zedoaria*, hawthorn, *Astragalus membranaceus*, *Vatica mangachapoi* Blanco, *Radix Paeoniae Rubra*, *Curcuma longa*, *Rhizoma Alismatis*, *Dendranthema morifolium*, lotus leaf, and *Glycyrrhiza uralensis* Fisch., has been used for the treatment of NAFLD in clinics. Furthermore, our previous study demonstrated that JGXZ could improve dyslipidemia and insulin resistance in a NAFLD rat model [8]. However, the mechanisms behind JGXZ's beneficial impact on NAFLD remain elusive.

Part of the difficulty is that the mechanisms of pathogenesis for NAFLD itself remain unclear. An imbalance between energy consumption and intake, inflammatory responses in the liver, and hereditary factors have all been implicated in NAFLD [9]. Recent studies have also indicated a critical role for gut microbiota in the progression of NAFLD, with the diversity of gut microbiota altered significantly in NAFLD patients [10, 11]. Studies have also demonstrated that the dysfunction of the gut microbiota could impair the tight junction of intestinal epithelial cells and cause an increase in gut permeability [12]; whereupon metabolites derived from gut microbiota, such as lipopolysaccharide (LPS), could enter circulation through the impaired intestinal mucosal barrier and trigger inflammatory responses in the liver [13]. Modulating gut microbiota to improve gut permeability and reduce inflammatory response has been proposed as a potential method to alleviate NAFLD [14].

Based on the dysfunction in gut microbiota and the inflammatory response in the liver about the potential pathogenesis of NAFLD, as well as our previous results regarding the improvement in dyslipidemia and insulin resistance of JGXZ, our present study was aimed to illustrate the regulatory effects of JGXZ on inflammatory response and gut permeability and correlated gut microbiota in a rat model. An NAFLD rat model was induced via HFD and orally treated with JGXZ (8 or 16 g crude herb/kg) for 12 weeks. The therapeutic effects of JGXZ on NAFLD model rats were investigated through blood lipid levels and pathological liver changes. 16S rRNA analysis was used to study the changes in gut microbiota after JGXZ treatment. Gut permeability was investigated via occludin and tight junction protein 1 (ZO-1) colon immunostaining. Lastly, the anti-inflammatory effects of JGXZ were examined by quantification of IL-1 β , IL-6, and TNF- α in rat serum and livers.

2. Material and Methods

2.1. Reagents. HFD (17.7% sucrose, 17.7% fructose, 19.4% protein, and 40% fat) was purchased from Beijing Huafukang Bioscience Co., Ltd. (Beijing, China). Total DNA and

RNA extraction kits (cat. no. DP419), first-stand cDNA reverse transcription kits (cat. no. KR106-02), polymerase chain reaction (PCR) kits (cat. no. FP205-02), and primers were obtained from Tiangen Biotechnology Co., Ltd. (Beijing, China). Rat IL-6 (cat. no. E02I0006), IL-1 β (cat. no. E02I0010), and TNF- α (cat. no. E02T0008) ELISA kits were obtained from Shanghai BlueGene Biotech CO., Ltd. (Shanghai, China). Aspartate aminotransferase (AST; cat. no. C010-2-1), alanine aminotransferase (ALT; cat. no. C009-2-1), triglyceride (TG; cat. no. A110-1-1), and total cholesterol (TC; cat. no. A111-1-1) test kits were purchased from Nanjing Jiancheng Bioengineering Institute (Nanjing, China). The Oil Red O staining kit (cat. no. G1261) was obtained from Solarbio Biotechnology Co., Ltd. (Beijing, China). Primary antibodies of ZO-1 (cat. no. 61-7300) and occludin (cat. no. 71-1500) were purchased from Invitrogen (USA).

2.2. Animals. Male Sprague-Dawley rats (180–220 g) were purchased from Beijing Huafukang Bioscience Co., Ltd. All animals were handled using experimental protocols outlined by the National Institutes of Health regulations and approved by the Ethics Committee and Use Committee of the Yunnan University of Traditional Chinese Medicine (approval no. 2020-0016). Throughout the acclimatization and study periods, all animals had access to food and water *ad libitum* and were maintained on a 12-h light/dark cycle ($21 \pm 2^\circ\text{C}$ with a relative humidity of $45 \pm 10\%$).

2.3. Preparation of JGXZ. JGXZ contained 15 g of *Salvia miltiorrhiza* Bunge, 6 g of *Panax notoginseng*, 15 g of *Curcuma zedoaria*, 20 g of hawthorn, 20 g of *Astragalus membranaceus*, 10 g of *Vatica mangachapoi* Blanco, 20 g of *Radix Paeoniae Rubra*, 12 g of *Curcuma longa*, 15 g of *Rhizoma Alismatis*, 15 g of *Dendranthema morifolium*, 15 g of lotus leaf, and 6 g of *Glycyrrhiza uralensis* Fisch. All herbs were purchased from the Department of Pharmacy of Yunnan Provincial Hospital of Traditional Chinese Medicine. The above herbs were soaked in 300 mL of water for 30 min and decocted for 30 min to obtain a JGXZ extract. The water extract of JGXZ was then filtered and concentrated to a density of 4 g crude herb/mL.

2.4. Animal Grouping. After acclimatization to laboratory conditions for 1 week, 40 rats were weight-matched and randomized into four groups ($n=10$ per group): control, model, JGXZ low-dose, and JGXZ high-dose groups. Rats in the control group received standard chow containing 59.4% total carbohydrate, 20% protein, and 4.8% fat. Rats in the model, JGXZ low-dose, and JGXZ high-dose groups received HFD for 12 weeks to induce NAFLD [15]. Rats in the JGXZ low-dose and JGXZ high-dose groups received an oral gavage of JGXZ (8 or 16 g crude herb/kg rat weight, respectively) [8], whereas rats in the control and model groups received an oral treatment of 2 mL saline once per day for 12 weeks. Rats in each group were weighed every two weeks.

At the end of 12 weeks of JGXZ treatment, rat livers were removed and weighed under anesthesia. The liver index was calculated using the following formula: liver index (%) = liver weight (g)/body weight (g) × 100. The timeline for experimental design is shown in Figure 1.

2.5. Serum Biochemical Markers Assay. After 12 weeks of JGXZ treatment, serum samples were collected for the biochemical assays. Briefly, rats were anaesthetized and blood was harvested by syringe from the aorta abdominalis. Then, blood was centrifuged at 3,000 rpm for 15 min to obtain the serum. The levels of TG, TC, ALT, and AST in the serum were assayed according to the manufacturer's instructions provided by Nanjing Jiancheng Biological Engineering Institute (Nanjing, China), and the absorbance value was detected using a microplate reader (Varioskan Flash; Thermo Fisher, Massachusetts, USA).

2.6. Histology. After 12 weeks of JGXZ treatment, rat livers were removed, fixed in paraffin, and cut into 5 μm sections. Hematoxylin and eosin (H&E) staining was performed using standard protocols. Briefly, after dewaxing, rehydration, staining, dehydration, transparency, and sealing, the pathological changes were visualized under a light microscope (BX50; Olympus America, Melville, NY, USA).

2.7. Oil Red O Staining. Oil Red O staining on liver were based on Cui et al. 2020 [16]. Briefly, rat livers were embedded in Tissue-Tek OCT compound (Sakura Finetek) for frozen block preparation. Frozen tissue sections were stained with Oil Red O for lipid detection following the manufacturer's instructions. The staining of lipid drops by Oil Red O was quantified using Image J to obtain the integrated optical density (IOD). The mean optical density (MOD) was calculated based on the ratio of IOD to the sum area.

2.8. Fecal 16S rRNA Sequencing. After 12 weeks of JGXZ treatment, feces from the control, model, JGXZ low-dose, and JGXZ high-dose groups were simultaneously obtained under sterile conditions in a laminar flow hood. 16S rRNA sequencing was conducted as described previously [17]. Briefly, total DNAs were extracted from fecal samples using the CTAB/SDS method. DNA purity and quantity were evaluated on 1% agarose gels and subsequently diluted to 1 ng/μL with sterile water. The PCR was carried out with diluted template DNA using specific barcoded primers (515F: GTGCCAGCMGCCGCGGTAA 806R:GGACTACHVGG GTWTCTAAT). The PCR products were visualized after electrophoresis and purified with the GeneJET™ Gel Extraction Kit (Qiagen, Germany). Sequencing libraries were generated using TruSeq® DNA PCR-Free Sample Preparation Kit (Illumina, United States). After library detection, the IlluminaHiSeq2500 platform was used for sequencing. Then, paired-end reads were generated from 16S rRNA sequencing and assigned to samples, truncated using trimming the barcode and primer sequence, and merged based on FLASH V1.2.7 analysis tool (a) to derive raw tags, which were

subsequently rarified to obtain the clean tags according to the QIIME V1.9.1 quality controlled process (b). The effective tags were obtained through detecting and removing the chimera sequences in clean tags using the UCHIME algorithm (c). The sequences of effective tags with ≥97% similarity were assigned to the same OTUs via Uparse V7.0.1001 software (d). Then representative sequences for each OTU were selected for further annotation using the SILVA database (e). The relative abundances of OTUs were normalized using a standard of sequence number corresponding to the sample with the least sequences. Ultimately, the normalized data were applied for alpha diversity and beta diversity analysis.

- (a) <http://ccb.jhu.edu/software/FLASH/>
- (b) http://qiime.org/scripts/split_libraries_fastq.html
- (c) http://www.drive5.com/usearch/manual/uchime_algo.html
- (d) <http://drive5.com/uparse/>
- (e) <http://www.arb-silva.de/>

2.9. Cytokine Quantification by Enzyme-Linked Immunoassay (ELISA). The levels of IL-6, IL-1β, and TNF-α in the serum were measured by ELISA according to the manufacturer's instructions (Shanghai BlueGene Biotech Co., Ltd. China).

2.10. RNA Isolation and Real-Time Reverse Transcription Quantitative Polymerase Chain Reaction (qPCR). We followed the methods of Wang et al. 2020 [18]. Total RNAs were isolated from livers using the RNA extraction kit, and first-strand cDNAs were synthesized from 1 μg of total RNAs according to the manufacturer's instructions. qPCR was used to detect the expression of *Il6*, *Il1b*, and *Tnfa* in the livers. All samples were run in triplicate and detected using a BIORAD iQ5 detection system. *Actb* was used as the loading control. Quantification was done using the $2^{-\Delta\Delta CT}$ method [19]. The sequences of all primers are listed in Table 1.

2.11. Immunostaining. We followed the methods of Wang et al. 2020 [18]. Briefly, rat colons were removed and fixed in paraffin, and the expression of occludin and tight junction protein-1 (ZO-1) in the colon was accessed via immunostaining. The ratio of positive expressed area to sum area was analyzed and quantified using Image J based on the IOD.

2.12. Statistics. All data are reported as the mean ± standard deviation (mean ± SD) for independent experiments. Statistical differences between the experimental groups were examined by analysis of variance (ANOVA) using SPSS, version 20.0. A *P* value < 0.05 was considered statistically significant. Curve fitting was carried out using the graphical package GraphPad Prism5.

3. Results

3.1. Effects of JGXZ on Body Weight Gain, Dyslipidemia, and Liver Pathology in NAFLD Model Rats. During the 12 weeks of HFD treatment, the body weight in the model group

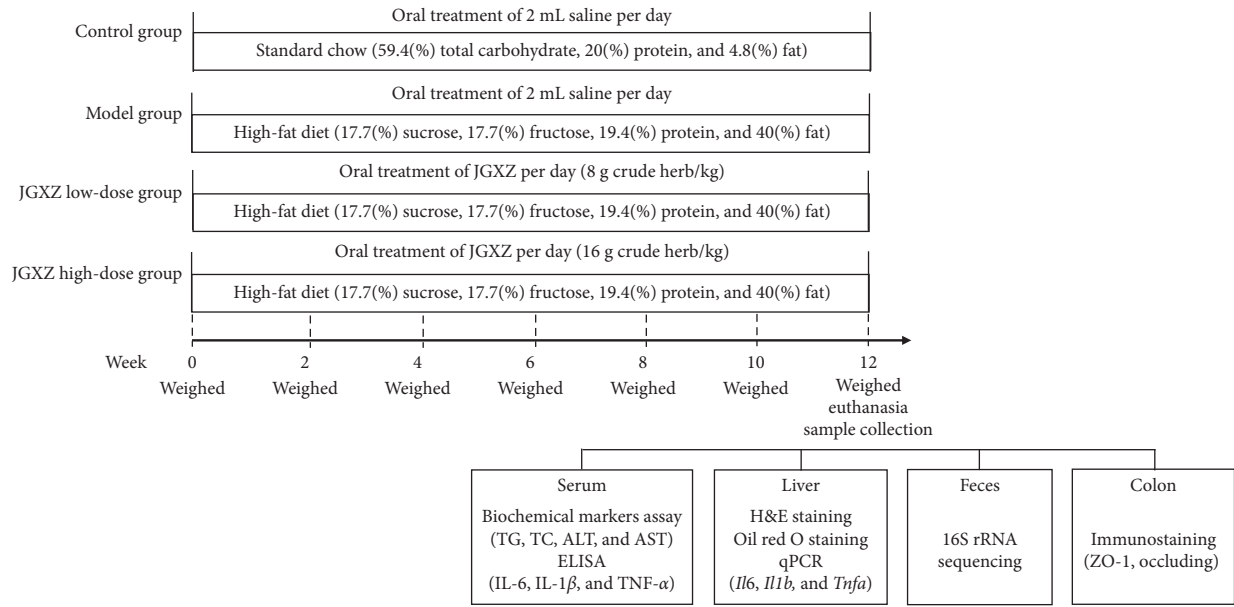


FIGURE 1: The timeline for experimental design.

TABLE 1: Primer sequences used for the target rat genes.

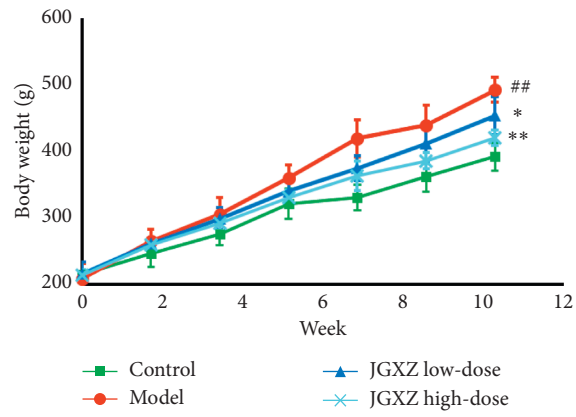
Genes	Primer sequence (5'–3')
<i>Actb</i>	Forward: TCTTCCAGCCTTCCTTCCTG Reverse: CACACAGAGTACTTGCGCTC
<i>Il6</i>	Forward: CTCATTCTGTCTCGAGCCCA Reverse: TGAAGTAGGGAAGGCAGTGG
<i>Il1b</i>	Forward: GGGATGATGACGACCTGCTA Reverse: TGTCGTTGCTTGTCTCTCCT
<i>Tnfa</i>	Forward: GAGCACGGAAGCATGATCC Reverse: TAGACAGAAGAGCGTGGTGG

increased significantly compared with the control group ($P < 0.01$). Both low-dose and high-dose JGXZ treatment inhibited the body weight gain in HFD-treated rats ($P < 0.05$ and $P < 0.01$, respectively; Figure 2(a)). After JGXZ treatment for 12 weeks, the liver index was significantly higher in the model group than the control group ($P < 0.05$), whereas the liver index was significantly decreased in the JGXZ high-dose group compared with the model group ($P < 0.05$, Figure 2(b)). Compared with the control group, the serum levels of ALT, AST, TG, and TC were significantly increased in the model group ($P < 0.01$). Low-dose JGXZ-treated rats exhibited significantly lower serum ALT and TG compared with rats in the model group ($P < 0.05$). Accordingly, the serum levels of ALT, AST, TG, and TC were significantly lower in the JGXZ high-dose group compared with the model group ($P < 0.01$, $P < 0.01$, $P < 0.01$, and $P < 0.05$, respectively; Table 2). *H&E* staining indicated extensive steatosis of hepatocytes in the model group, whereas JGXZ treatment alleviated hepatocyte steatosis in NAFLD model rats (Figure 2(c)). Likewise, Oil Red O staining showed increased lipid contents in the model group compared with the control group ($P < 0.01$, Figures 2(d), 2(e)), JGXZ (8 and 16 g crude herb/kg) treatment decreased the lipid contents in the liver ($P < 0.01$; Figure 2(d), 2(e)).

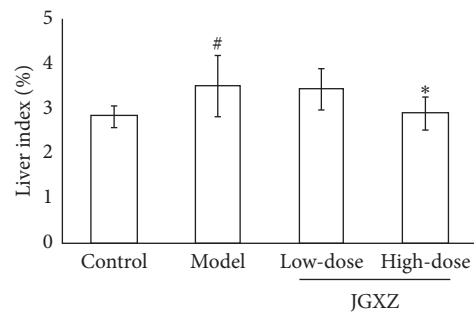
3.2. Effects of JGXZ on Gut Dysbiosis in NAFLD Model Rats.

We next examined whether JGXZ could improve the dysbiosis of gut microbiota using 16S rRNA sequencing. The Shannon index was calculated to determine the alpha diversity of gut microbiota in each group. The Shannon index was higher in the model group compared with the control ($P < 0.01$) and was lower in JGXZ high-dose group compared with the model group ($P < 0.05$, Figure 3(a)). Venn diagram analysis indicated that there were 442 OTUs overlapped among the groups; 544 OTUs present in the control and model groups; 685 in the model and JGXZ low-dose groups; 695 in the model and JGXZ high-dose groups; and 651 in JGXZ low-dose and JGXZ high-dose groups (Figure 3(b)). The beta diversity of gut microbiota was also studied using principle coordinate analysis (PCoA) and system clustering tree. PCoA and system clustering tree indicated a significant variance of beta diversity between the control and model groups. Both low-dose and high-dose JGXZ treatment changed the beta diversity in NAFLD model rats, with the distances between JGXZ-treated groups (both 8 and 16 g crude herb/kg) and the model group in PCA shorter than that between the model and control groups. Additionally, the distances between the high-dose JGXZ-treated rats and the control group showed more similar beta diversities than that between the control group and low-dose JGXZ-treated rats (Figures 3(c), 3(d)).

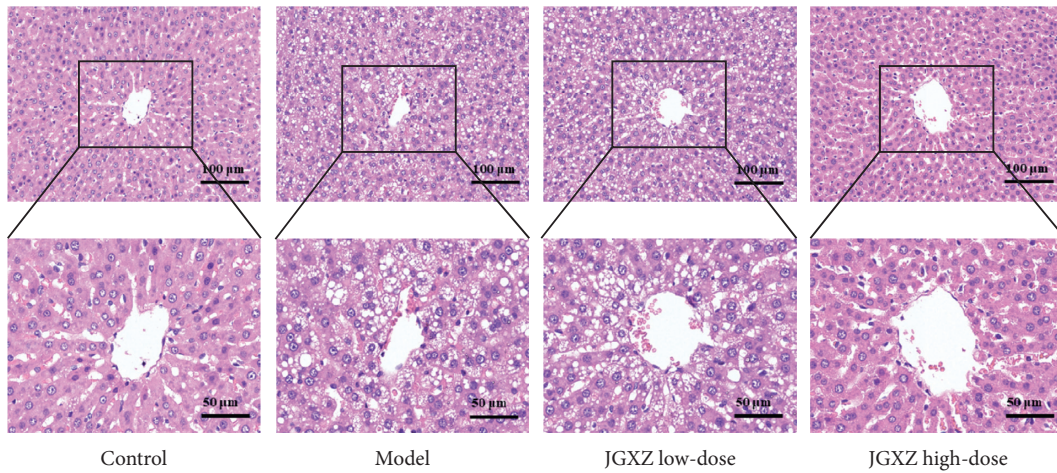
We then investigated the changes in abundances of gut microbiota in each group. At the phylum level, *Firmicutes* and *Bacteroidetes* were the most abundant phyla in all samples (Figure 4(a)). The *Firmicutes*-to-*Bacteroidetes* (*F*-to-*B*) ratio was higher in the model group than that in the control group ($P < 0.01$), whereas the *F*-to-*B* ratio was lower in the JGXZ-treated groups (8 and 16 g crude herb/kg) than that in the model group ($P < 0.05$ and $P < 0.01$, respectively; Figure 4(b)). At the genus level, the abundances of *Lactobacillus* ($P < 0.01$) and *Blautia* ($P < 0.05$) were decreased and



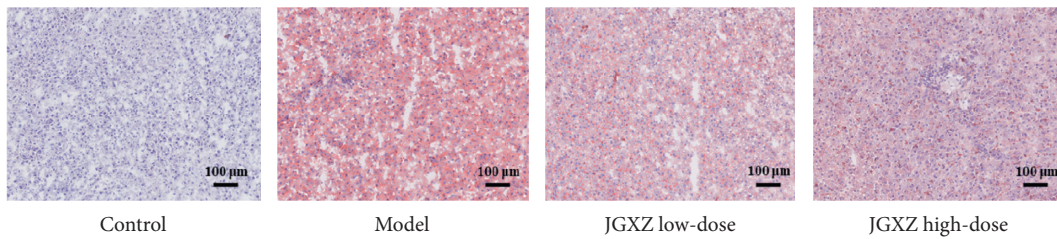
(a)



(b)



(c)



(d)

FIGURE 2: Continued.

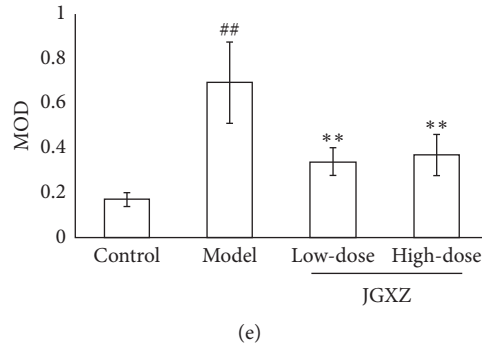


FIGURE 2: JGXZ treatment reduced body weight gain and improved liver steatosis in NAFLD model rats. (a) Body weight gain was reduced in NAFLD model rats after treatment with JGXZ. (b) JGXZ treatment decreased the liver index in NAFLD model rats. (c) H&E staining indicated that JGXZ treatment ameliorated liver steatosis in NAFLD model rats (200× and 400×). (d, e) The liver lipid contents were decreased in NAFLD model rats after JGXZ treatment (100×). Control, model, JGXZ low-dose, and JGXZ high-dose groups (*n* = 10 per group). Data are presented as the mean ± SD. **P* < 0.05 compared to the control group; ##*P* < 0.01 compared to the control group; **P* < 0.05 compared to the experimental model group; and ***P* < 0.01 compared to the experimental model group.

TABLE 2: Changes in serum ALT, AST, TG, and TC levels in NAFLD model rats.

Group	ALT (U/L)	AST (U/L)	TG (mmol/L)	TC (mmol/L)
Control	36.87 ± 8.61	81.33 ± 16.15	2.06 ± 0.49	4.46 ± 1.26
Model	77.02 ± 18.80##	166.82 ± 41.02##	10.67 ± 2.07##	6.82 ± 1.51##
JGXZ low-dose	53.12 ± 21.33*	145.19 ± 38.16	7.25 ± 2.60*	6.05 ± 2.08
JGXZ high-dose	45.80 ± 9.97**	129.81 ± 17.02**	6.37 ± 1.57**	4.69 ± 1.49*

Control, model, JGXZ low-dose, and JGXZ high-dose groups (*n* = 10 per group). Data are presented as the mean ± SD. ##*P* < 0.01 compared to the control group. **P* < 0.05 compared to the experimental model group. ***P* < 0.01 compared to the experimental model group.

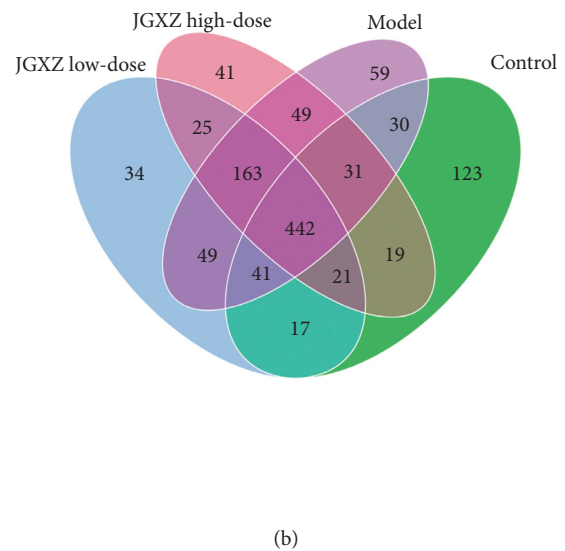
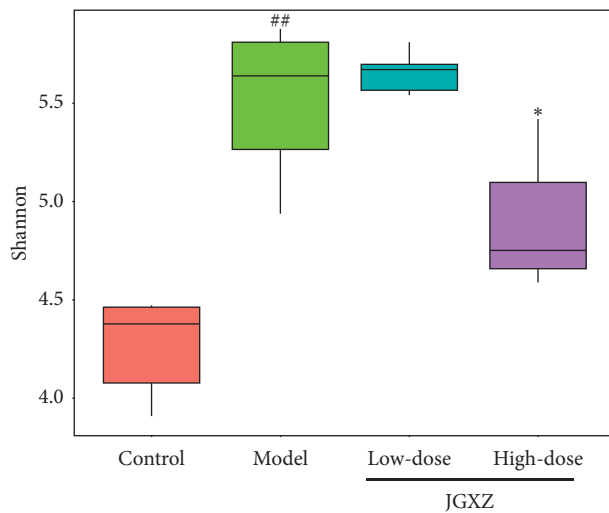


FIGURE 3: Continued.

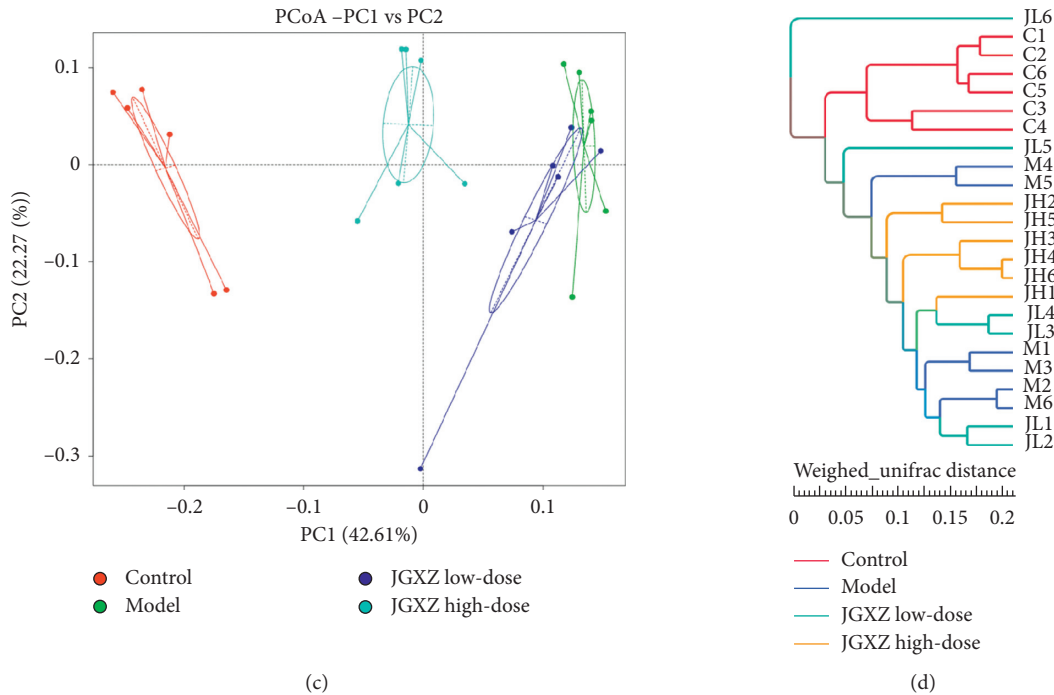


FIGURE 3: JGXZ treatment improved the diversity of gut microbiota in NAFLD model rats. (a) The Shannon index was decreased in NAFLD model rats after JGXZ treatment. (b) The different numbers of OTUs were visualized via a Venn diagram. (c), (d) PCoA and system clustering tree showed more similar beta diversity between the JGXZ high-dose and control groups than that between the model and control groups. Control, model, JGXZ low-dose, and JGXZ high-dose groups ($n = 6$ per group). $^{##}P < 0.01$ compared to the control group and $^*P < 0.05$ compared to the experimental model group.

the abundances of *Turicibacter* ($P < 0.01$), *Collinsella* ($P < 0.01$), *Faecalibaculum* ($P < 0.05$), and *Roseburia* ($P < 0.01$) were increased in the model group compared with the control group (Figure 4(c)). Low-dose JGXZ treatment increased the abundance of *Lactobacillus* ($P < 0.05$) and decreased the abundances of *Collinsella* ($P < 0.05$) and *Roseburia* ($P < 0.05$). High-dose JGXZ treatment increased the abundances of *Lactobacillus* ($P < 0.01$) and *Blautia* ($P < 0.01$) and decreased the abundances of *Turicibacter* ($P < 0.05$), *Collinsella* ($P < 0.01$), and *Roseburia* ($P < 0.05$, Figure 4(c)).

3.3. Effects of JGXZ on Gut Permeability and Inflammatory Response in NAFLD Model Rats. Immunostaining indicated that ZO-1 and occludin were expressed in all colonic epithelial cells. The expressions of ZO-1 and occludin were decreased in the model group compared with the control ($P < 0.01$; Figures 5(a)–5(d)). JGXZ treatment (8 and 16 g crude herb/kg) increased the expressions of ZO-1 ($P < 0.05$ and $P < 0.01$, respectively; Figures 5(a) and 5(c)) and occludin ($P < 0.01$; Figures 5(b), 5(d)). The serum levels of IL-6, IL-1 β , and TNF- α were increased in NAFLD model rats compared with rats receiving standard chow ($P < 0.01$; Figure 5(e)). The serum levels of IL-1 β and TNF- α were lower in the JGXZ low-dose group than those in the model group ($P < 0.05$ and $P < 0.01$, respectively; Figure 5(e)). High-dose JGXZ treatment decreased the serum levels of IL-6, IL-1 β , and TNF- α in NAFLD model rats ($P < 0.01$;

Figure 5(e)). Likewise, the gene expressions of *Il6*, *Il1b*, and *Tnfa* in the liver were upregulated in the model group compared with the control group ($P < 0.01$), whereas JGXZ treatment (8 and 16 g crude herb/kg) downregulated the gene expressions of *Il6* ($P < 0.05$ and $P < 0.01$, respectively), *Il1b* ($P < 0.01$), and *Tnfa* ($P < 0.01$; Figure 5(f)).

4. Discussion

In this study, we established a NAFLD rat model using HFD. Our results showed that the body weights and liver indices were increased in rats received HFD. Moreover, NAFLD model rats exhibited significant body weight gain, dyslipidemia, and hepatic steatosis, which are consistent with the pathological changes of NAFLD. In agreement with our previous study, JGXZ treatment (8 and 16 g crude herb/kg) showed remarkable therapeutic effects on NAFLD, manifesting as an improvement of body weight gain, liver index, dyslipidemia, and pathological changes in liver.

In addition, we investigated changes in gut microbiological composition using high-throughput sequencing. HFD has been shown previously to cause an increase in the alpha diversity of gut microbiota [20]. Likewise, our results showed a higher Shannon index in HFD-treated rats compared with the control group. JGXZ (16 g crude herb/kg) treatment reduced the alpha diversity of gut microbiota in NAFLD rats. PCoA analysis revealed significant distances between control and NAFLD model rats, indicating that the beta diversity of gut microbiota differed in HFD rats from

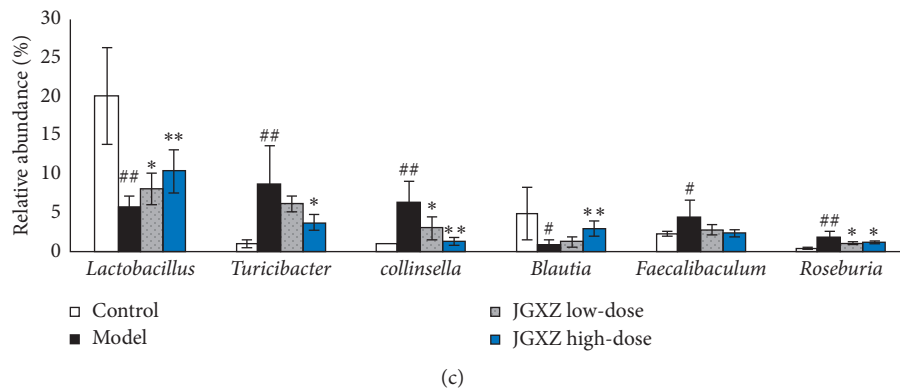
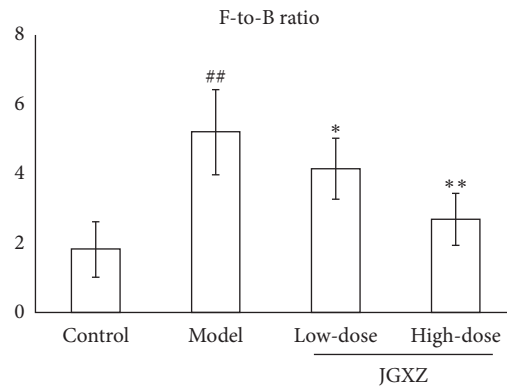
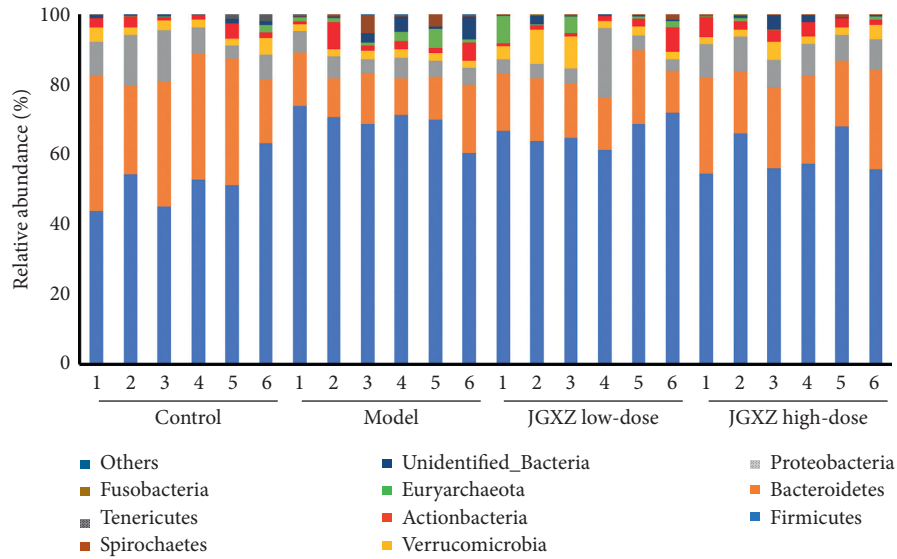
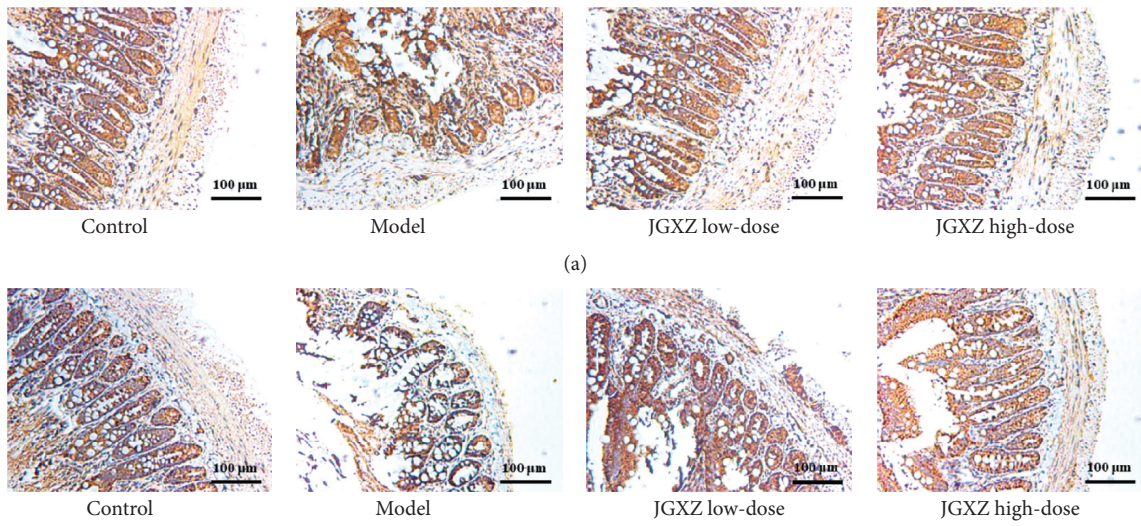


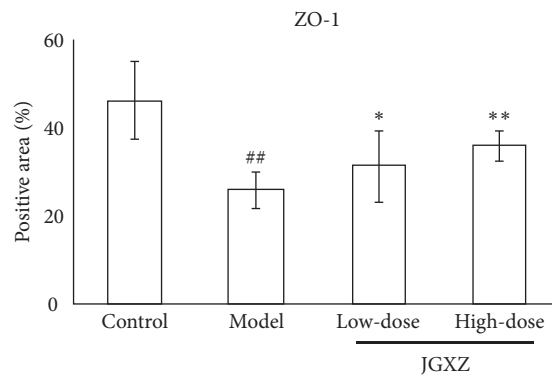
FIGURE 4: JGXZ treatment altered the abundances of gut microbiota in NAFLD model rats. (a, b) At the phylum level, JGXZ treatment decreased the *F-to-B* ratio in NAFLD model rats. (c) JGXZ treatment increased the abundances of *Lactobacillus* and *Blautia* and decreased the abundances of *Turicibacter*, *Collinsella*, and *Roseburia* in the gut. Control, model, JGXZ low-dose, and JGXZ high-dose groups ($n = 6$ per group). $^{\#}P < 0.05$ compared to the control group; $^{\#\#}P < 0.01$ compared to the control group; $*P < 0.05$ compared to the experimental model group; and $^{**}P < 0.01$ as compared to the experimental model group.

rats received standard chow. According to the system clustering tree, the beta diversity of the gut microbiota between JGXZ (16 g crude herb/kg)-treated rats and control rats were more similar than that between the NAFLD model rats and control rats. Accumulating numbers of studies show

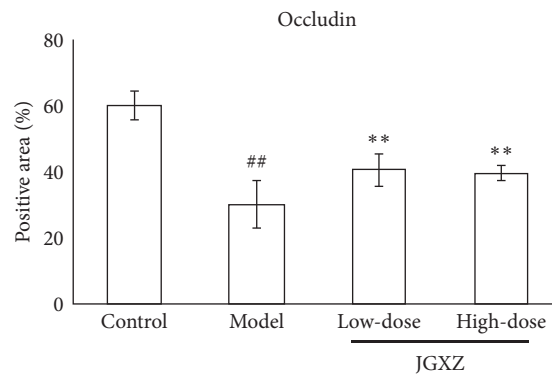
that the *Firmicutes-to-Bacteroidetes* ratio (*F-to-B* ratio) is closely related to many metabolic diseases, including obesity, type 2 diabetes, and NAFLD [21–23]. Compared with the healthy subjects, NAFLD patients show a significant increase in the relative abundance of *Firmicutes* and a remarkable



(b)



(c)



(d)

FIGURE 5: Continued.

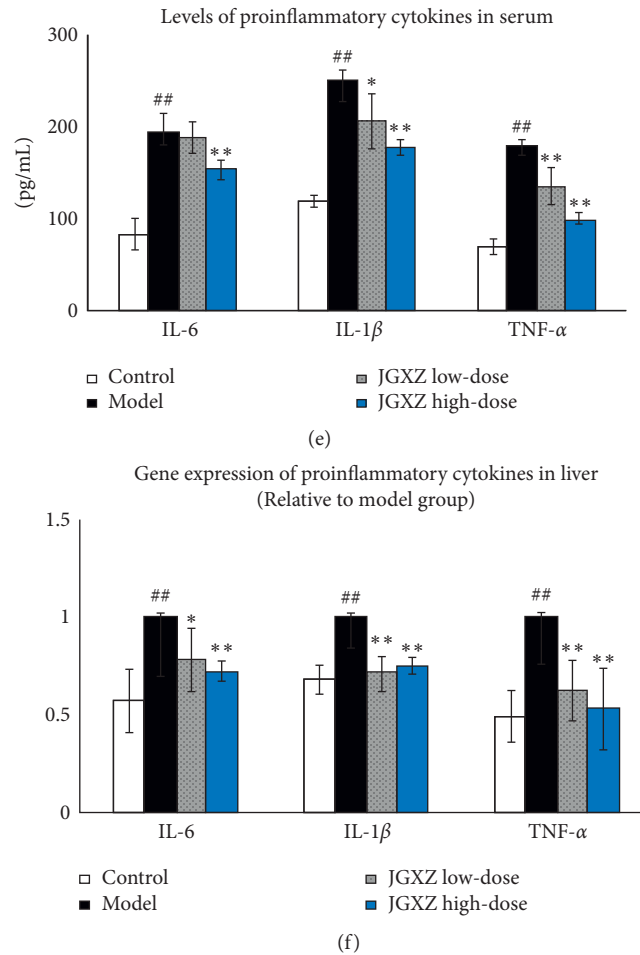


FIGURE 5: JGXZ treatment increased gut integrity and inhibited the inflammatory response in NAFLD model rats. (a–d) Immunostaining showed that the expression of ZO-1 (a, c) and occludin (b, d) in the colon was increased after JGXZ treatment. (e) The levels of IL-6, IL-1 β , and TNF- α in the serum were decreased after JGXZ treatment. (f) The gene expressions of *Il6*, *Il1b*, and *Tnfa* in the liver were decreased after JGXZ treatment. Control, model, JGXZ low-dose, and JGXZ high-dose groups ($n = 10$ per group). ^{*} $P < 0.05$ as compared to the control group; ^{##} $P < 0.01$ as compared to the control group; ^{*} $P < 0.05$ as compared to the experimental model group; ^{**} $P < 0.01$ as compared to the experimental model group.

decrease in *Bacteroidetes*, resulting in an increase in the *F-to-B* ratio [24, 25]. Decreasing *F-to-B* ratios in the gut microbiota demonstrated a superior clinical outcome in NAFLD patients [26]. Animal studies also showed the increase in *F-to-B* ratios in the NAFLD model; *Lonicera caerulea* L. berry polyphenols could decrease the *F-to-B* ratio in NAFLD mice [27]. In agreement to these prior studies, our results indicated a remarkable increase in the *F-to-B* ratio in the model group, with JGXZ treatment decreasing this increased *F-to-B* ratio.

At the genus level, the abundances of *Lactobacillus* and *Blautia* were increased in JGXZ-treated rats. Previous studies have demonstrated that *Lactobacillus* and *Blautia* were decreased in NAFLD patients [28, 29]. Mulberry leaf fiber and polyphenols mixture have been used to induce weight loss in obese rats through increasing the abundance of *Lactobacillus* [30]. Similarly, Xie-Xin-Tang has been shown to increase the abundance of *Blautia* and improve the hyperglycemia, dyslipidemia, and inflammation in type 2 diabetes rats [31]. The relative abundances of *Turicibacter*,

Collinsella, *Faecalibaculum*, and *Roseburia* were all increased in rats fed with HFD; JGXZ treatment decreased the gut abundances of *Turicibacter*, *Collinsella*, and *Roseburia*. Studies have shown that *Turicibacter* is positively correlated with metabolic phenotypes induced by HFD [32]. Ethanol extracts from marine microalga *Chlorella pyrenoidosa* have been shown to alleviate lipid metabolic disorders in HFD rats through decreasing the abundance of *Turicibacter* [33]. In addition, clinical studies have demonstrated that the abundance of *Collinsella* was significantly increased in atherosclerotic and nonalcoholic steatohepatitis (NASH) patients [34]. Additional correlation analysis indicated that *Collinsella* was positively related to the dysfunction of lipid metabolism in NASH patients [35]. *Collinsella* was also decreased in type 2 diabetic patients after they received a structured weight loss program [36]. Decreasing the abundances of *Turicibacter* and *Collinsella* might be the mechanism of JGXZ on dyslipidemia. Changes in dietary habits could be responsible for changes in *Faecalibaculum* abundance. For example, one study found that the

abundance of *Faecalibaculum* was increased in mice received whole-egg powder [37]. As for the changes in *Roseburia*, the abundance of *Roseburia* has been shown to increase in aged mice. However, few studies have demonstrated the role of *Faecalibaculum* or *Roseburia* in NAFLD, and further study is required before conclusions on their importance can be drawn. Furthermore, accumulated studies have demonstrated that compounds and herbs such as curcumin [38], *Astragalus membranaceus* polysaccharide [39], nuciferine [40], and *Radix Paeoniae Rubra* [41] in JGXZ could regulate gut microbiota. Further studies could be carried out to identify the critical compounds of JGXZ with regulatory effects on gut microbiota.

As the dysfunction in gut microbiota can disrupt the tight junction of intestinal epithelial cells, triggering an increase in gut permeability and contributing to inflammatory response [42], we studied whether JGXZ could enhance the integrity of the intestinal mucosa barrier and ameliorate inflammatory response in NAFLD model rats. ZO-1 and occludin were examined as indicators as they are tight junction proteins expressed in the intestinal epithelial cells [43]. Occludin can influence the tight junction of intestinal epithelial cells through regulating macromolecule flux [44]. ZO-1, also called tight junction protein 1, is a cytoplasmic plaque protein that connects the transmembrane proteins to cytoskeleton [45, 46]. Decreases in ZO-1 and occludin expression in the gut indicate a reduction of intestinal epithelial cell integrity [47]. Accordingly, reduced levels of ZO-1 and occludin were observed in HFD-treated rats compared with control rats, whereas JGXZ treatment increased the protein expressions of both ZO-1 and occludin. Moreover, JGXZ treatment attenuated the inflammatory response in NAFLD model rats, manifesting as mild lobular liver inflammation and reduced expression of proinflammatory cytokines (IL-6, IL-1 β , and TNF- α) in the serum and liver. Infiltration of inflammatory cells into the liver can induce excessive proinflammatory cytokine production, including IL-6, IL-1 β , and TNF- α , and induce hepatocyte injury, contributing to NASH [48]. These proinflammatory cytokines can also disrupt lipid metabolism and cause dyslipidemia [49]. Previous studies have demonstrated that the colonization of *Lactobacillus rhamnosus* GG can prevent liver injury by improving the gut integrity and ameliorating liver inflammation in an alcoholic liver disease model [50]. *Lactobacillus rhamnosus* GG was also shown to improve intestinal barrier dysfunction in patients with irritable bowel syndrome [51]. *Blautia* has been reported to reduce the inflammatory response in obesity-related complications. *In vitro* studies have shown that *Blautia* can inhibit the production of proinflammatory cytokines in the LPS-induced activation of peripheral blood mononuclear cells [52]. Based on these previous research studies, we postulate that the effects of JGXZ on gut permeability and liver inflammation occur via affecting the abundances of *Lactobacillus* and *Blautia*. In addition, several studies have shown that the dysbiosis of gut microbiota could cause intestinal inflammation and further contribute to the inflammatory response in the liver [53]. Modulating the gut microbiota to alleviate intestinal inflammation could

reduce liver inflammation in HFD-induced metabolic syndrome animal models [54]. The alternation of intestine-related inflammatory factors introduced by JGXZ treatment could be investigated in our future studies to demonstrate whether JGXZ has the potential to improve inflammatory response in the liver through modulating gut microbiota and alleviating intestinal inflammation.

5. Conclusion

In conclusion, our current study demonstrated that JGXZ could ameliorate NAFLD through modulating gut microbiota, decreasing gut permeability, and alleviating inflammatory response (sFigure1). Rats received high-dose JGXZ treatment exhibited superior therapeutic outcomes—more significant improvement in gut microbiota dysbiosis, lower grade of inflammation, and higher gut permeability—compared with low-dose JGXZ-treated rats, highlighting JGXZ's mechanisms and therapeutic potential against NAFLD in a dose-dependent manner.

Data Availability

The data sets used and/or analyzed during the current study are available from the corresponding author on reasonable request.

Ethical Approval

All animals were handled using experimental protocols outlined by the National Institutes of Health regulations and approved by the Ethics Committee and Use Committee of the Yunnan University of Traditional Chinese Medicine.

Conflicts of Interest

The authors declare no conflicts of interest.

Acknowledgments

This manuscript has been posted as a preprint on Research Square (<https://www.researchsquare.com/article/rs-122886/v1>). This work was funded by the National Science Foundation of China (81560772).

Supplementary Materials

sFigure1. Graphical abstract. JGXZ could ameliorate NAFLD through modulating gut microbiota, decreasing gut permeability, and alleviating liver inflammation. (*Supplementary Materials*)

References

- [1] P. Dibba, A. Li, G. Cholankeril et al., “Mechanistic potential and therapeutic implications of cannabinoids in nonalcoholic fatty liver disease,” *Medicines*, vol. 5, no. 2, p. 47, 2018.
- [2] S. Zelber-Sagi, J. Godos, and F. Salomone, “Lifestyle changes for the treatment of nonalcoholic fatty liver disease: a review of observational studies and intervention trials,” *Therapeutic Advances in Gastroenterology*, vol. 9, no. 3, pp. 392–407, 2016.

- [3] Y. Sumida and M. Yoneda, "Current and future pharmacological therapies for NAFLD/NASH," *Journal of Gastroenterology*, vol. 53, no. 3, pp. 362–376, 2018.
- [4] M. Cao, J. Miao, L. Wang, H. Z. Liu, H. T. Cui, and Y. H. Bian, "The advances of traditional Chinese medicine in the treatment of liver diseases in 2019," *Traditional Medicine Research*, vol. 5, no. 4, pp. 261–271, 2020.
- [5] J. Chen, H. Zhao, Y. Yang, B. Liu, J. Ni, and W. Wang, "Lipid-lowering and antioxidant activities of Jiang-Zhi-Ning in traditional Chinese medicine," *Journal of Ethnopharmacology*, vol. 134, no. 3, pp. 919–930, 2011.
- [6] J. Zhai, Z. Ren, Y. Wang et al., "Traditional Chinese patent medicine Zhixiong Capsule (ZXC) alleviated formed atherosclerotic plaque in rat thoracic artery and the mechanism investigation including blood-dissolved-component-based network pharmacology analysis and biochemical validation," *Journal of Ethnopharmacology*, vol. 254, p. 112523, 2020.
- [7] J. Fang, X. Sun, B. Xue, N. Fang, and M. Zhou, "Dahuang Zexie decoction protects against high-fat diet-induced NAFLD by modulating gut microbiota-mediated toll-like receptor 4 signaling activation and loss of intestinal barrier," *Evidence-Based Complementary and Alternative Medicine*, vol. 2017, Article ID 2945803, 13 pages, 2017.
- [8] X. H. Xie, J. B. Liao, F. Fang et al., "Jian-Gan-Xiao-Zhi decoction ameliorates high-fat high-carbohydrate diet-induced non-alcoholic fatty liver disease and insulin resistance by regulating the AMPK/JNK pathway," *Traditional Medicine Research*, vol. 6, no. 1, p. 4, 2021.
- [9] G. Ekhlasi, M. Zarrati, S. Agah et al., "Effects of symbiotic and vitamin E supplementation on blood pressure, nitric oxide and inflammatory factors in non-alcoholic fatty liver disease," *EXCLI Journal*, vol. 16, pp. 278–290, 2017.
- [10] C. Leung, L. Rivera, J. B. Furness, and P. W. Angus, "The role of the gut microbiota in NAFLD," *Nature Reviews Gastroenterology & Hepatology*, vol. 13, no. 7, pp. 412–425, 2016.
- [11] F. Del Chierico, V. Nobili, P. Vernocchi et al., "Gut microbiota profiling of pediatric nonalcoholic fatty liver disease and obese patients unveiled by an integrated meta-omics-based approach," *Hepatology*, vol. 65, no. 2, pp. 451–464, 2017.
- [12] Y. Lin, B. Li, X. Yang et al., "Non-hematopoietic STAT6 induces epithelial tight junction dysfunction and promotes intestinal inflammation and tumorigenesis," *Mucosal Immunology*, vol. 12, no. 6, pp. 1304–1315, 2019.
- [13] M. I. Bhat and R. Kapila, "Dietary metabolites derived from gut microbiota: critical modulators of epigenetic changes in mammals," *Nutrition Reviews*, vol. 75, no. 5, pp. 374–389, 2017.
- [14] Y. Ding, K. Yanagi, C. Cheng, R. C. Alaniz, K. Lee, and A. Jayaraman, "Interactions between gut microbiota and non-alcoholic liver disease: the role of microbiota-derived metabolites," *Pharmacological Research*, vol. 141, pp. 521–529, 2019.
- [15] Y. T. Li, H. T. Cui, Y. Lu et al., "Hua-Zhuo-Kai-Yu decoction inhibits apoptosis in nonalcoholic fatty liver disease," *Traditional Medicine Research*, vol. 6, no. 1, pp. 27–39, 2021.
- [16] H. T. Cui, Y. T. Li, M. Cao et al., "Untargeted metabolomic analysis of the effects and mechanism of nuciferine treatment on rats with nonalcoholic fatty liver disease," *Frontiers in Pharmacology*, vol. 11, p. 858, 2020.
- [17] J. C. Li, H. T. Cui, Y. Z. Cai et al., "Tong-Xie-Yao-Fang regulates 5-HT level in diarrhea predominant irritable bowel syndrome through gut microbiota modulation," *Frontiers in Pharmacology*, vol. 9, p. 1110, 2018.
- [18] L. Wang, H. T. Cui, Y. T. Li et al., "Kang-Xian pills inhibit inflammatory response and decrease gut permeability to treat carbon tetrachloride-induced chronic hepatic injury through modulating gut microbiota," *Evidence-Based Complementary and Alternative Medicine*, vol. 2020, Article ID 8890182, 14 pages, 2020.
- [19] K. J. Livak and T. D. Schmittgen, "Analysis of relative gene expression data using real-time quantitative PCR and the 2- $\Delta\Delta$ CT method," *Methods*, vol. 25, no. 4, pp. 402–408, 2001.
- [20] V. Lecomte, N. O. Kaakoush, C. A. Maloney et al., "Changes in gut microbiota in rats fed a high fat diet correlate with obesity-associated metabolic parameters," *PLoS One*, vol. 10, no. 5, Article ID e0126931, 2015.
- [21] C. M. D. S. P. Indiani, K. F. Rizzardi, P. M. Castelo, L. F. C. Ferraz, M. Darrieux, and T. M. Parisotto, "Childhood obesity and firmicutes/bacteroidetes ratio in the gut microbiota: a systematic review," *Childhood Obesity*, vol. 14, no. 8, pp. 501–509, 2018.
- [22] F. Magne, M. Gotteland, L. Gauthier et al., "The firmicutes/bacteroidetes ratio: a relevant marker of gut dysbiosis in obese patients?" *Nutrients*, vol. 12, no. 5, p. 1474, 2020.
- [23] A. Monga Kravetz, T. Testerman, B. Galuppo et al., "Effect of gut microbiota and PNPLA3 rs738409 variant on nonalcoholic fatty liver disease (NAFLD) in obese youth," *The Journal of Clinical Endocrinology & Metabolism*, vol. 105, no. 10, p. e3575, 2020.
- [24] Z. Pataky, L. Genton, L. Spahr et al., "Impact of hypocaloric hyperproteic diet on gut microbiota in overweight or obese patients with nonalcoholic fatty liver disease: a pilot study," *Digestive Diseases and Sciences*, vol. 61, no. 9, pp. 2721–2731, 2016.
- [25] C.-C. Chang, K.-Y. Lin, K.-Y. Peng, Y.-J. Day, and L.-M. Hung, "Resveratrol exerts anti-obesity effects in high-fat diet obese mice and displays differential dosage effects on cytotoxicity, differentiation, and lipolysis in 3T3-L1 cells," *Endocrine Journal*, vol. 63, no. 2, pp. 169–178, 2016.
- [26] D. S. H. Bell, "Changes seen in gut bacteria content and distribution with obesity: causation or association?" *Postgraduate Medicine*, vol. 127, no. 8, pp. 1–6, 2015.
- [27] S. Wu, R. Hu, H. Nakano et al., "Modulation of gut microbiota by *Lonicera caerulea* L. Berry polyphenols in a mouse model of fatty liver induced by high fat diet," *Molecules*, vol. 23, no. 12, p. 3213, 2018.
- [28] P. Vajro, G. Paoletta, and A. Fasano, "Microbiota and gut-liver axis: their influences on obesity and obesity-related liver disease," *Journal of Pediatric Gastroenterology & Nutrition*, vol. 56, no. 5, pp. 461–468, 2013.
- [29] H. Fukui, "Gut microbiota and host reaction in liver diseases," *Microorganisms*, vol. 3, no. 4, pp. 759–791, 2015.
- [30] Q. Li, F. Liu, J. Liu, S. Liao, and Y. Zou, "Mulberry leaf polyphenols and fiber induce synergistic antiobesity and display a modulation effect on gut microbiota and metabolites," *Nutrients*, vol. 11, no. 5, p. 1017, 2019.
- [31] X. Wei, J. Tao, S. Xiao et al., "Xiexin Tang improves the symptom of type 2 diabetic rats by modulation of the gut microbiota," *Sci Rep*, vol. 8, no. 1, p. 3685, 2018.
- [32] Y. Zhong, M. Nyman, and F. Fåk, "Modulation of gut microbiota in rats fed high-fat diets by processing whole-grain barley to barley malt," *Molecular Nutrition & Food Research*, vol. 59, no. 10, pp. 2066–2076, 2015.
- [33] X. Wan, T. Li, D. Liu et al., "Effect of marine microalgae *Chlorella pyrenoidosa* ethanol extract on lipid metabolism and gut microbiota composition in high-fat diet-fed rats," *Marine Drugs*, vol. 16, no. 12, p. 498, 2018.

- [34] F. H. Karlsson, F. Fåk, I. Nookaew et al., "Symptomatic atherosclerosis is associated with an altered gut metagenome," *Nat Commun*, vol. 3, p. 1245, 2012.
- [35] S. Astbury, E. Atallah, A. Vijay, P. A. Guruprasad, J. Grove, and A. M. Valdes, "Lower gut microbiome diversity and higher abundance of proinflammatory genus *Collinsella* are associated with biopsy-proven nonalcoholic steatohepatitis," *Gut Microbes*, vol. 11, pp. 569–580, 2019.
- [36] F. Frost, L. J. Storck, T. Kacprowski et al., "A structured weight loss program increases gut microbiota phylogenetic diversity and reduces levels of *Collinsella* in obese type 2 diabetics: a pilot study," *PLoS One*, vol. 14, no. 7, Article ID e0219489, 2019.
- [37] M. Fukunaga, K. Suriki, T. Kuda et al., "Typical indigenous bacteria in the cecum of ddY mice fed a casein-beef tallow diet or whole-egg diet," *Journal of Food Biochemistry*, vol. 43, no. 12, Article ID e13064, 2019.
- [38] W. Feng, H. Wang, P. Zhang et al., "Modulation of gut microbiota contributes to curcumin-mediated attenuation of hepatic steatosis in rats," *Biochimica et Biophysica Acta (BBA)—General Subjects*, vol. 1861, no. 7, pp. 1801–1812, 2017.
- [39] Y. Liu, W. Liu, J. Li et al., "A polysaccharide extracted from *Astragalus membranaceus* residue improves cognitive dysfunction by altering gut microbiota in diabetic mice," *Carbohydrate Polymers*, vol. 205, pp. 500–512, 2019.
- [40] Y. Yu, J. Lu, L. Sun et al., "Akkermansia muciniphila: a potential novel mechanism of nuciferine to improve hyperlipidemia," *Biomedicine & Pharmacotherapy*, vol. 133, Article ID 111014, 2021.
- [41] L.-J. Zhong, Z.-S. Xie, H. Yang, P. Li, and X.-J. Xu, "Moutan Cortex and *Paeoniae Radix Rubra* reverse high-fat-diet-induced metabolic disorder and restore gut microbiota homeostasis," *Chinese Journal of Natural Medicines*, vol. 15, no. 3, pp. 210–219, 2017.
- [42] M. Bulló, P. García-Lorda, I. Megias, and J. Salas-Salvadó, "Systemic inflammation, adipose tissue tumor necrosis factor, and leptin expression," *Obesity Research*, vol. 11, no. 4, pp. 525–531, 2012.
- [43] J. Zhang, G. Wu, A. Shan et al., "Dietary glutamine supplementation enhances expression of ZO-1 and occludin and promotes intestinal development in Min piglets," *Acta Agriculturae Scandinavica, Section A—Animal Science*, vol. 67, pp. 15–21, 2017.
- [44] R. Al-Sadi, K. Khatib, S. Guo, D. Ye, M. Youssef, and T. Ma, "Occludin regulates macromolecule flux across the intestinal epithelial tight junction barrier," *American Journal of Physiology-Gastrointestinal and Liver Physiology*, vol. 300, no. 6, pp. G1054–G1064, 2011.
- [45] M. Sheng and C. Sala, "PDZ domains and the organization of supramolecular complexes," *Annual Review of Neuroscience*, vol. 24, no. 1, p. 1, 2001.
- [46] R. Ranganathan and E. M. Ross, "PDZ domain proteins: scaffolds for signaling complexes," *Current Biology*, vol. 7, no. 12, pp. R770–R773, 1997.
- [47] X. N. Han, M. P. Fink, and R. L. Delude, "Inflammatory cytokines decrease ZO-1 and occludin expression in intestinal epithelial cells by increasing no center dot production," *Critical Care Medicine*, vol. 29, no. 12, p. A58, 2001.
- [48] C. Capurso and A. Capurso, "From excess adiposity to insulin resistance: the role of free fatty acids," *Vascular Pharmacology*, vol. 57, no. 2-4, pp. 91–97, 2012.
- [49] J. Liu, S. Yue, Z. Yang et al., "Oral hydroxysafflor yellow A reduces obesity in mice by modulating the gut microbiota and serum metabolism," *Pharmacological Research*, vol. 134, pp. 40–50, 2018.
- [50] J. P. Bruch-Bertani, C. Uribe-Cruz, A. Pasqualotto et al., "Hepatoprotective effect of probiotic *Lactobacillus rhamnosus* GG through the modulation of gut permeability and inflammasomes in a model of alcoholic liver disease in zebrafish," *Journal of the American College of Nutrition*, vol. 39, no. 3, pp. 163–170, 2019.
- [51] H. Xu, L. Allen, H. Sha et al., "*Lactobacillus rhamnosus* GG prevents epithelial barrier dysfunction induced by interferon-gamma and fecal supernatants from irritable bowel syndrome patients in human intestinal enteroids and colonoids," *Gut Microbes*, vol. 10, pp. 59–76, 2018.
- [52] A. Benítez-Páez, E. M. Gómez del Pugar, I. López-Almela, Á. Moya, P. Codoñer-Franch, and Y. Sanz, "Depletion of *Blautia* species in the microbiota of obese children relates to intestinal inflammation and metabolic phenotype worsening," *mSystems*, vol. 5, no. 2, pp. e00857–19, 2020.
- [53] Y. Mikami, S. Mizuno, N. Nakamoto et al., "Macrophages and dendritic cells emerge in the liver during intestinal inflammation and predispose the liver to inflammation," *PLoS One*, vol. 9, no. 1, p. e84619, 2014.
- [54] F. F. Anhê, D. Roy, G. Pilon et al., "A polyphenol-rich cranberry extract protects from diet-induced obesity, insulin resistance and intestinal inflammation in association with increased *Akkermansia* spp. population in the gut microbiota of mice," *Gut*, vol. 64, no. 6, pp. 872–883, 2015.

Research Article

Astragali Radix Contributes to the Inhibition of Liver Fibrosis via High-Mobility Group Box 1-Mediated Inflammatory Signaling Pathway

Jianxia Wen ^{1,2}, Dan Wang ^{1,2,3}, Jian Wang ², Ruilin Wang,⁴ Shizhang Wei,^{1,2} and Yanling Zhao ¹

¹Department of Pharmacy, The Fifth Medical Center of Chinese PLA General Hospital, Beijing 100039, China

²College of Pharmacy, Chengdu University of Traditional Chinese Medicine, Chengdu 611137, China

³Chongqing Academy of Chinese Materia Medica, Chongqing 400065, China

⁴Clinical Laboratory Medicine Center, The Fifth Medical Center of Chinese PLA General Hospital, Beijing 100039, China

Correspondence should be addressed to Yanling Zhao; zhaoyl2855@126.com

Received 9 January 2021; Revised 26 February 2021; Accepted 2 March 2021; Published 15 March 2021

Academic Editor: Chih-Yuan Ko

Copyright © 2021 Jianxia Wen et al. This is an open access article distributed under the Creative Commons Attribution License, which permits unrestricted use, distribution, and reproduction in any medium, provided the original work is properly cited.

Astragali Radix (AR), the dried root of *Astragali Radix membranaceus* (Fisch.) Bge. or *Astragali Radix membranaceus* (Fisch.) Bge. var. *mongholicus* (Bge) Hsiao, is a commonly used traditional Chinese medicine for the treatment of liver diseases. This study aimed to comprehensively evaluate the pharmacological action and explore the potential mechanism of AR on liver fibrosis. Rats were administered with carbon tetrachloride for eight weeks, followed by oral treatment with AR for six weeks. The efficacy was confirmed by measuring liver function and liver fibrosis levels. The underlying mechanisms were explored by detecting the expression of related proteins. AR significantly decreased the serum levels of alanine aminotransferase (ALT), aspartate aminotransferase (AST), collagen IV (COL-IV), hyaluronic acid (HA), laminin (LN), and precollagen type III (PCIII). In addition, AR inhibited the deposition of collagen and the activation of hepatic stellate cells. Those data strongly demonstrated that AR alleviated liver fibrosis by CCl₄. In order to illustrate the potential inflammatory, the mRNA levels of IL-6, TNF- α , and IL-1 β were detected. Subsequently, immunohistochemistry analysis was performed to further verify the expression of type I collagen. Finally, the expression of key proteins in the inflammatory signaling pathway was detected. AR significantly reduced the expression of high-mobility group box 1 (HMGB1), TLR4, Myd88, RAGE, and NF- κ B p65 genes and proteins. In addition, western blotting showed AR decreased the protein expression of RAGE, p-MEK1/2, p-ERK1/2, and p-c-Jun. Taken together, our data reveal that AR significantly inhibits liver fibrosis by intervening in the HMGB1-mediated inflammatory signaling pathway and secretion signaling pathway. This study will provide valuable references for the in-depth research and development of *Astragali Radix* against liver fibrosis.

1. Introduction

Liver fibrosis is a complex pathological process and an intermediate link between various liver diseases including cirrhosis and liver cancer [1, 2]. And prevention of malignant liver diseases by inhibiting the occurrence and development of liver fibrosis has attracted worldwide attention [3]. Numerous studies have revealed the pathogenesis of liver fibrosis, such as inflammatory response, activation of hepatic stellate cells, and excessive deposition of extracellular

matrix, but it has not yet been transformed into an effective and powerful treatment [4, 5]. There is still a lack of safe and effective means of treating liver fibrosis [6, 7].

It is necessary to develop new drugs for treating liver fibrosis [7]. Traditional Chinese medicine has potential advantages in the treatment of chronic diseases, so we tried to find effective drugs for the treatment of liver fibrosis. *Astragali Radix* (AR), the dried root of *Astragali Radix membranaceus* (Fisch.) Bge. or *Astragali Radix membranaceus* (Fisch.) Bge. var. *mongholicus* (Bge) Hsiao, is a

commonly used traditional Chinese medicine for the treatment of liver diseases [8]. And it has been proved that AR possesses hepatoprotective and anti-inflammatory properties and has been shown to exhibit immunomodulating and antioxidant activity, among others [9]. In traditional Chinese formula, AR is often used for the treatment of liver fibrosis [10]. Although the protective effects of AR on liver injury and related mechanisms have been reported [9, 11], the studies on the effect and mechanism of AR on liver fibrosis are still lacking. More importantly, toxicological study has confirmed the high safety of AR. No significant toxicity or side effects were observed when the dose administered to rats was set to 39.9 g/kg [12].

Experimental and clinical studies have found that the high-mobility group box-1 (HMGB1), recently discovered damage-associated molecular patterns (DAMPs), is substantially enriched in patients with hepatic fibrosis [13, 14]. HMGB1 is a late inflammatory mediator that plays an important role in the pathogenesis of many chronic inflammations, which is the main cause of liver fibrosis [15]. There is evidence that HMGB1 can directly stimulate hepatic stellate cells (HSCs) activation to accelerate the development of liver fibrosis [16]. More importantly, toll-like receptor 4 (TLR4) and the receptor of advanced glycation end products (RAGE) are the main receptors of HMGB1 [15]. It is reported that the binding of extracellular HMGB1 to TLR4 could activate NF- κ B signaling to induce inflammation and aggravate liver fibrosis. Studies have shown that extracellular HMGB1 binding to RAGE could phosphorylate c-Jun to induce a significant increase in type I collagen secretion [16, 17], which directly accelerates the development of liver fibrosis (c-Jun is a component of the heterodimeric AP1 and is a potent transactivating factor for the *collagen1a1* and *collagen1a2* genes [17, 18]).

Based on previous studies, this study aims to provide answers to the following questions: Does AR have therapeutic effect on carbon tetrachloride- (CCl_4 -) induced liver fibrosis in rats? What is the underlying mechanism? Is the mechanism related to downregulation of HMGB1?

2. Materials and Methods

2.1. Reagents. In this study, colchicine was purchased from Xishuangbanna Banna Pharmaceutical Co. Ltd. (Yunnan, China). CCl_4 was supplied by Tianjin Guangfu Chemical Research Institute (Tianjin, China). Alanine amino transferase (ALT, Cat. No.: 20180627), aspartate amino transferase (AST, Cat. No.: 20180607), collagen IV (COL-IV, Cat. No.: 201809), hyaluronic acid (HA, Cat. No.: 201808), laminin (LN, Cat. No.: 201809), and precollagen type III (PC III, Cat. No.: 201809) detection kits were provided by Nanjing Jiancheng Bioengineering Institute (Nanjing, China). The antibodies of phospho-c-Jun, phospho-MEK1/2, HMGB1, α -SMA, phospho-ERK1/2, and ERK1/2 were bought from Cell Signaling Technology (United States). The antibodies of MEK1/2 and COL-I were purchased from Abcam (United States) and the antibodies of RAGE and GAPDH were bought from ABclonal (China).

2.2. Plant Material. AR (the dried root of *AR membranaceus* (Fisch.) Bge.) was supplied by Beijing Lvye Pharmaceutical Co. Ltd. (Beijing, China). Ten times of water was used for the first extraction of AR for 2 h. Then, eight times of water was used to extract for 1.5 hours. The extract of *Astragalus membranaceus* was dried into powder by freeze vacuum drying oven. The final yield was about 40.08%. The Q-TOF LC/MS analysis showed that the main components of AR extract included 3,4-dihydroxybenzyl aldehyde (6.17%), calycosin-7-glucoside (0.69%), armillaripin (10.31%), rhodomollein III (7.05%), phthalic anhydride (1.76%), clavatine (6.46%), pterosin B (7.46%), D-cathinone (2.65%), formononetin (15.4%), Andrographolide (2.57%), and anemarrhenasaponin-I (4.55%) [19].

2.3. Animals and Administration. A total of 36 male Sprague Dawley rats weighting 180–200 g were obtained from the China Food and Drug Certification Research Institute (Permission No. SCXK (Jing)-2014-0013). Those rats were housed in the Central Animal Laboratory of the Fifth Medical Center of Chinese PLA General Hospital. The animals were maintained under controlled conditions of temperature $25^\circ\text{C} \pm 2^\circ\text{C}$, humidity $55\% \pm 5\%$, and with light and dark cycles.

All the animals were randomly divided into six groups with six rats in each group. Olive oil diluted CCl_4 in a ratio of 1:1. The model group, AR (2.7, 5.4, 10.8 g/kg/d) groups, and colchicine (as a positive control group) groups were given CCl_4 diluent (2 mL/kg) twice a week for 8 weeks [19]. At the same time, the control group was intraperitoneally injected with the same dose of olive oil. Eight weeks later, the AR (2.7, 5.4, and 10.8 g/kg/d) groups and colchicine group (0.2 mg/kg/d) were given the corresponding concentration of drugs [20]. The control group and model group were given equal volume of distilled water. All rats were treated by intragastric administration once a day for 6 weeks. All rats were deprived of food for 24 h before the last treatment but allowed free access to water. The animals were sacrificed 2 h after the last treatment and their liver and serum were harvested for the further studies. The blood samples were centrifuged at 3500 rpm for 15 min. The liver tissue was divided into 3 pieces and placed in the sample bottle. Serum and liver tissue were stored at -80°C . All animal experiments were approved by the Ethical Committee of the Fifth Medical Center of Chinese PLA General Hospital in China.

2.4. Biochemical Assay. The serum levels of ALT, AST, COL-IV, HA, LN, and PC III were measured. In brief, according to the manufacturer's protocols, the samples, 2,4-dinitrophenylhydrazine solution, and sodium hydroxide solution were added in turn. The final color was read at 510 nm, and the serum ALT and AST levels were determined according to the OD value. Similarly, according to the manufacturer's instructions, add the reagents in the kit in turn, read the final color at 450 nm, and obtain the serum

levels of COL-IV, HA, LN, and PC III according to the OD value.

2.5. Histological Examination. Liver tissue was fixed in 10% neutral buffered formalin for more than 48 h. All the livers were eluted with gradient ethanol solution and fixed and embedded in paraffin. Tissue sections about 4–5 μm in thickness were cut and stained with hematoxylin eosin (H&E) and Masson. The pathological changes in the liver tissues were observed under a Nikon microscope (Nikon Instruments Inc., Japan).

2.6. Quantitative Reverse Transcription Polymerase Chain Reaction (RT-PCR) Analyses. Quantitative RT-PCR was used to detect the mRNA expression of IL-6, TNF- α , IL-1 β , HMGB1, TLR4, Myd88, and RAGE in liver tissues. Total RNA was extracted from 90 mg frozen liver tissue by Trizol reagent (Life Technologies, CA, USA). The absorbance of the extracted mRNA was detected by spectrophotometer at 260 nm and 280 nm, respectively. The mRNA with purity (A260/A280) between 1.8 and 2.2 was selected as the qualified product for the follow-up study. RNA (2 μg) was transcribed into cDNA by PrimerScript RT reagent kit (Thermo Fisher Scientific, MA, USA). The cDNA was subsequently subjected to PCR amplification by ABI 7500 Real-Time PCR machine (Applied Biosystems Inc, Carlsbad, CA, USA). Data analysis was performed by the $2^{-\Delta\Delta\text{CT}}$ method. The primers are listed in Table 1.

2.7. Western Blotting. The mixture of ice-cold radio immunoprecipitation assay (RIPA) lysis buffer, phenylmethylsulfonyl fluoride (PMSF), and protein phosphatase inhibitor was used for protein extraction. Liver tissue (80 mg) was homogenized and lysed in the mixture, and then centrifuged at 12000 \times g and 4°C for 10 min. The supernatant was collected and BCA Protein Assay kit (Beijing Solarbio Science & Technology Co., Ltd. Beijing, China) was used to detect the total protein concentration. All protein samples were levelled to the same concentration. Then, reducing Laemmli SDS sample buffer was added and mixed well, and boiled in boiling water for 5 minutes. The prepared samples were western blotted with 10% sodium dodecyl sulfate-polyacrylamide gel electrophoresis (SDS-PAGE) and the blot was transferred to the polyvinylidene fluoride (PVDF) membrane. The PVDF membrane was sealed in 5% skimmed milk at room temperature for 2 hours and then placed in a mixture of 5% skimmed milk, Tris-buffered saline (TBS), and 0.05% Tween 20 with the corresponding primary antibody, and incubated overnight at 4°C. Antibodies, including rabbit Anti-NF- κB p65 (Cell Signaling Technology, dilution: 1:1000), RAGE (ABclonal technology, dilution: 1:1000), phospho-MEK1/2 (Cell Signaling Technology, dilution: 1:2000), MEK1/2 (Abcam, dilution: 1:10000), phospho-ERK1/2 (Cell Signaling Technology, dilution: 1:1000), ERK1/2 (Cell Signaling Technology, dilution: 1:10000), phospho-c-Jun (Abcam, dilution: 1:500), and GAPDH (ABclonal technology, dilution: 1:10000), were used at this step. GAPDH was used as

control for total protein extract. After incubation with appropriate secondary antibody for 2 hours at room temperature, the membrane was washed 3 times in TBS with 0.05% Tween 20 for 5 minutes each. Finally, the chemiluminescence system was used to measure immunoreactive proteins. All the western blotting was repeated 3 times.

2.8. Immunohistochemistry Analysis. To evaluate the effects of AR on the expression of α -SMA, HMGB1, and collagen I in liver tissue of fibrosis rats, immunohistochemical analysis was performed as described previously [21]. Paraffin sections of liver tissues were put in xylene and gradient ethanol for deparaffinization and dehydration, and then the sections were put into citric acid antigen retrieval solution for antigen retrieval. The sections were treated with 3% hydrogen peroxide solution to block endogenous peroxidase. The sections were then blocked with 1% BSA for 30 minutes at room temperature. Subsequently, the sections were incubated with α -SMA (Cell Signaling Technology, dilution: 1:100), Rabbit Anti-HMGB1 (Cell Signaling Technology, dilution: 1:200), and collagen type I (Abcam, dilution: 1:200) in a PBS solution at 4°C overnight. After incubating the sections with appropriate secondary antibodies for 1 hour at room temperature, they were stained with DAB staining solution and hematoxylin, and finally the slides were dehydrated and mounted. Nikon microscope (Nikon Instruments Inc., Japan) and NIS-Elements (F 4.0 version, Japan) software were used to observe the sections. Finally, Image-Pro Plus (version 6.0, Media Cybernetics, INC., Rockville, MD, USA) software was used to calculate and analyze the average integrated optical density (IOD) of the positive area of the immunohistochemical reaction image.

2.9. Statistical Analysis. Results were expressed as mean \pm standard deviation (SD). Data were evaluated by one-way ANOVA and Duncan's multirange test with the SPSS computer program (version 20.0, SPSS Inc., Chicago, IL, USA). $P < 0.05$ was considered statistically significant and $P < 0.01$ was considered highly significant.

3. Results

3.1. AR Has Therapeutic Effect on CCl_4 -Induced Liver Injury. As shown in Figures 1(a) and 1(b), the levels of ALT and AST in rats in the model group were significantly increased ($P < 0.01$) compared with those in the control group. And serum ALT and AST concentrations were significantly reduced after oral administration of AR 5.4 g/kg and 10.8 g/kg ($P < 0.01$). Subsequently, the serum levels of COL-IV, HA, LN, and PC III which could reflect the degree of hepatic fibrosis were examined [22]. As shown in Figures 1(c)–1(f), the serum levels of COL-IV, HA, LN, and PC III in the model group were significantly higher than those in the control group ($P < 0.01$). The inhibitory effect of AR on the levels of COL-IV, HA, LN, and PC III is dose-dependent. In particular, the serum levels of COL-IV, HA, LN, and PC III were significantly decreased in the 10.8 g/kg AR group ($P < 0.01$).

TABLE 1: Primers sequences for RT-PCR.

Gene	Sense primer (5'-3')	Antisense primer (5'-3')
IL-6	AGGAGTGGCTAAGGACCAAGACC	TGCCGAGTAGACCTCATAGTGACC
TNF- α	GCATGATCCGAGATGTGGAAGTGG	CGCCACGAGCAGGAATGAGAAG
IL-1 β	ATCTCACAGCAGCATCTCGACAAG	CACACTAGCAGGTCGTCATCATCC
HMGB1	ACAACACTGCTGCGGATGACAAG	CCTCCTCGTCTTCTCCTCTTCC
TLR4	GCTGCCAACATCATCCAGGAAGG	TGATGCCAGAGCGGCTACTCAG
Myd88	CGACGCCTTCATCTGCTACTGC	CCACCACCATGCGACGACAC
RAGE	CTGCCTCTGAACTCACAGCCAATG	GTGCCTCCTGGTCTCCTCCTTC
GAPDH	GTCCATGCCATCACTGCCACTC	GATGACCTTGCCACAGCCTTG

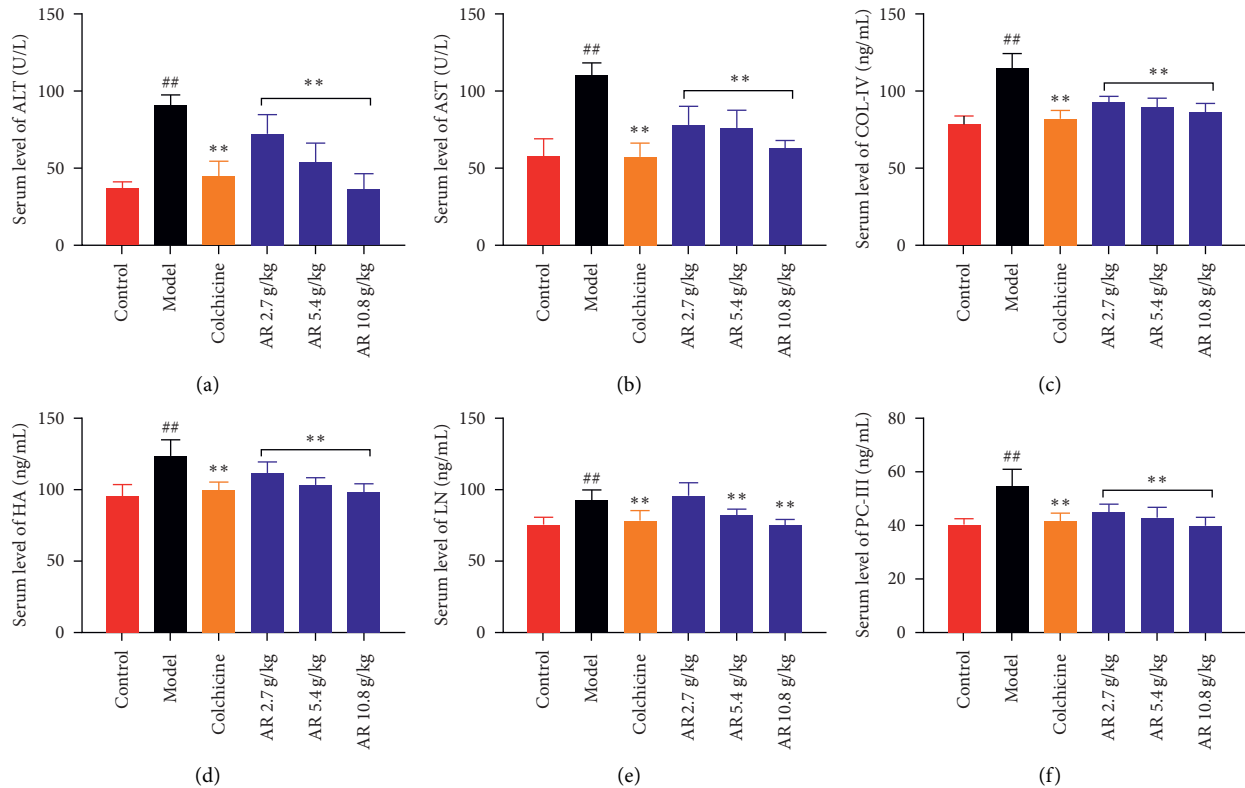


FIGURE 1: Effect of AR on CCl₄-induced liver fibrosis in rats in different groups. (a) Serum level of ALT, (b) serum level of AST, (c) serum level of COL-IV, (d) serum level of HA, (e) serum level of LN, and (f) serum level of PC-III. Values are expressed as mean \pm SD ($n = 6$). # $P < 0.05$ and ## $P < 0.01$ when compared with the control group. * $P < 0.05$ and ** $P < 0.01$ when compared with the model group.

3.2. *The Effect of AR on Liver Histopathological Changes and Liver Fibrosis.* Then, hematoxylin-eosin (HE) staining and Masson staining were used to observe the pathological changes of liver tissue [21, 23]. The results of HE showed that the liver tissue structure of the control group was normal without morphological changes. The long-term CCl₄-treated rats showed partial necrotic in their liver accompanied by severe steatosis and inflammatory cell infiltration around the central vein of hepatic lobules. In contrast, the degree of liver damage, steatosis, and inflammatory infiltration in the AR treatment groups were reduced to varied degrees in a dose-dependent manner (Figure 2(a)). In the liver section of Masson staining, the blue area represented the deposited collagen. The results show that a large amount of collagen was deposited around the hepatic sinus of the model group. AR can effectively reduce collagen deposition and improve

liver fibrosis (Figure 2(b)). The above results confirmed that the CCl₄-induced rat liver fibrosis model was successful, and AR could effectively ameliorate liver fibrosis in rats.

3.3. *Inflammatory Response in Rats Induced by CCl₄.* Clinical data suggest that inflammation is a key factor in the progression of liver fibrosis [24]. IL-6, as a classic proinflammatory cytokine biomarker, is used for clinical diagnosis of chronic liver fibrosis [25]. TNF- α can promote the survival of activated HSCs and promote the development of liver fibrosis [26]. It is reported that the serum IL-1 β in patients with liver fibrosis caused by schistosomiasis is significantly increased [24]. Therefore, we detected the expression of IL-6, TNF- α , and IL-1 β in rats by quantitative RT-PCR. The mRNA levels of IL-6, TNF- α , and IL-1 β were increased remarkably in

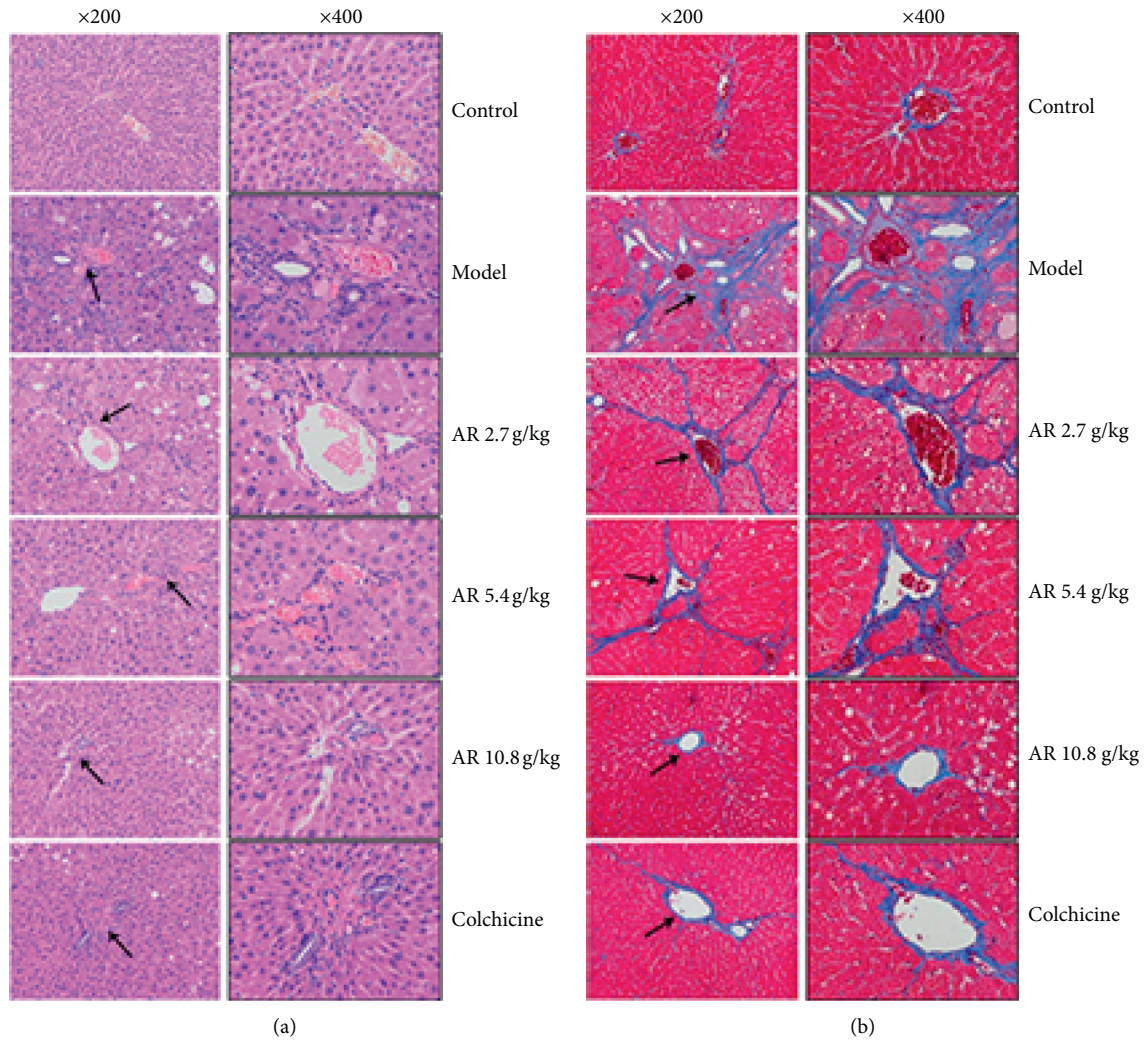


FIGURE 2: Histopathological observation of AR on improvement of liver fibrosis in rats. (a) Hematoxylin and eosin- (HE-) stained liver section in six groups (original magnification, $\times 200$, $\times 400$). (b) Histological examination of liver section with Masson stain (original magnification, $\times 200$, $\times 400$). Blue areas show collagen fibers and damaged liver tissue.

the CCl_4 -induced group compared with the control group ($P < 0.01$, Figure 3). After treatment with AR, the expression of related genes decreased in a dose-dependent manner ($P < 0.05$, $P < 0.01$). The results showed that AR had therapeutic effect on CCl_4 -induced liver inflammation in rats.

3.4. AR Downregulates CCl_4 -Induced Liver Inflammation. Literature research found that HMGB1, a cytokine abundantly enriched in patients with liver fibrosis, mediated TLR4//NF- κ B signaling pathway is one of the important pathways for liver aseptic inflammation. Therefore, we tested the expression levels of HMGB1, TLR4, Myd88, and NF- κ B p65, which are the key targets of this signaling pathway in liver fibrosis rats. Quantitative RT-PCR and immunohistochemistry (IHC) methods were used to detect the expression and subcellular localization of HMGB1. As shown in Figures 4(a)–4(e), in the control group, HMGB1 was mainly located in the nucleus of hepatocytes and rarely

in the cytoplasm or sinusoids. In the model group, the greater HMGB1 immunoreactivity was observed in the periportal and bridge fibrosis areas in the liver. In addition, computer-assisted semiquantitative analysis showed that AR treatment alleviated the expression of HMGB1 compared with the model group (Figure 4(f), $P < 0.05$, $P < 0.01$).

Furthermore, the mRNA expression of HMGB1 was also quantified by using the RT-PCR method. The results showed that high dose of AR could significantly reduce the mRNA expression of HMGB1, which is consistent with the result of the IHC method. Those results proved that AR could reduce the expression of HMGB1 (Figure 4(g)). Subsequently, quantitative RT-PCR was used to detect the TLR4, Myd88, and RAGE mRNA levels in the model group, which were significantly higher than those in the control group (Figures 4(h)–4(j), $P < 0.01$). After treatment with AR, the expression of related genes decreased in a dose-dependent manner ($P < 0.05$, $P < 0.01$). Western blotting was used to

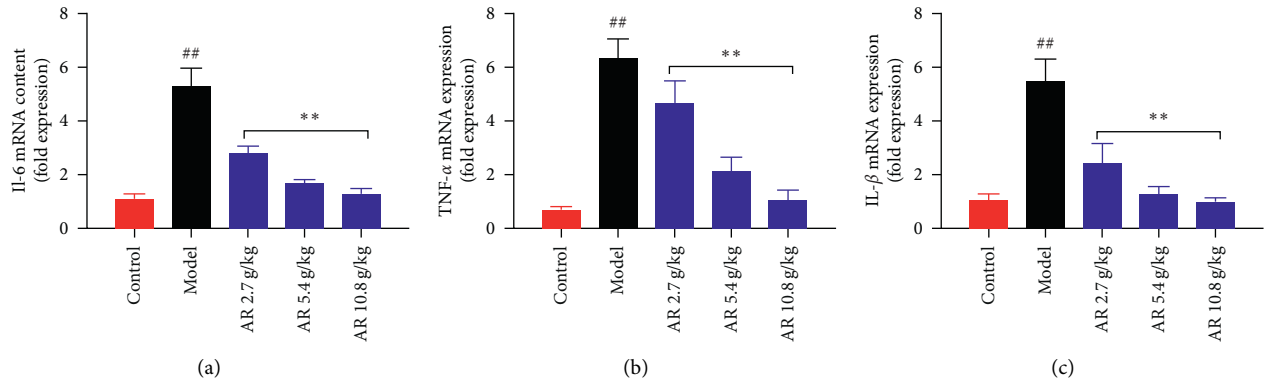


FIGURE 3: Effect of AR on inflammatory factors levels in liver fibrosis induced by CCl₄. (a) IL-6 mRNA level. (b) TNF-α mRNA level. (c) IL-1β mRNA level. Values are expressed as mean ± SD (n = 6). # P < 0.05 and ## P < 0.01 when compared with the control group. * P < 0.05 and ** P < 0.01 when compared with the model group.

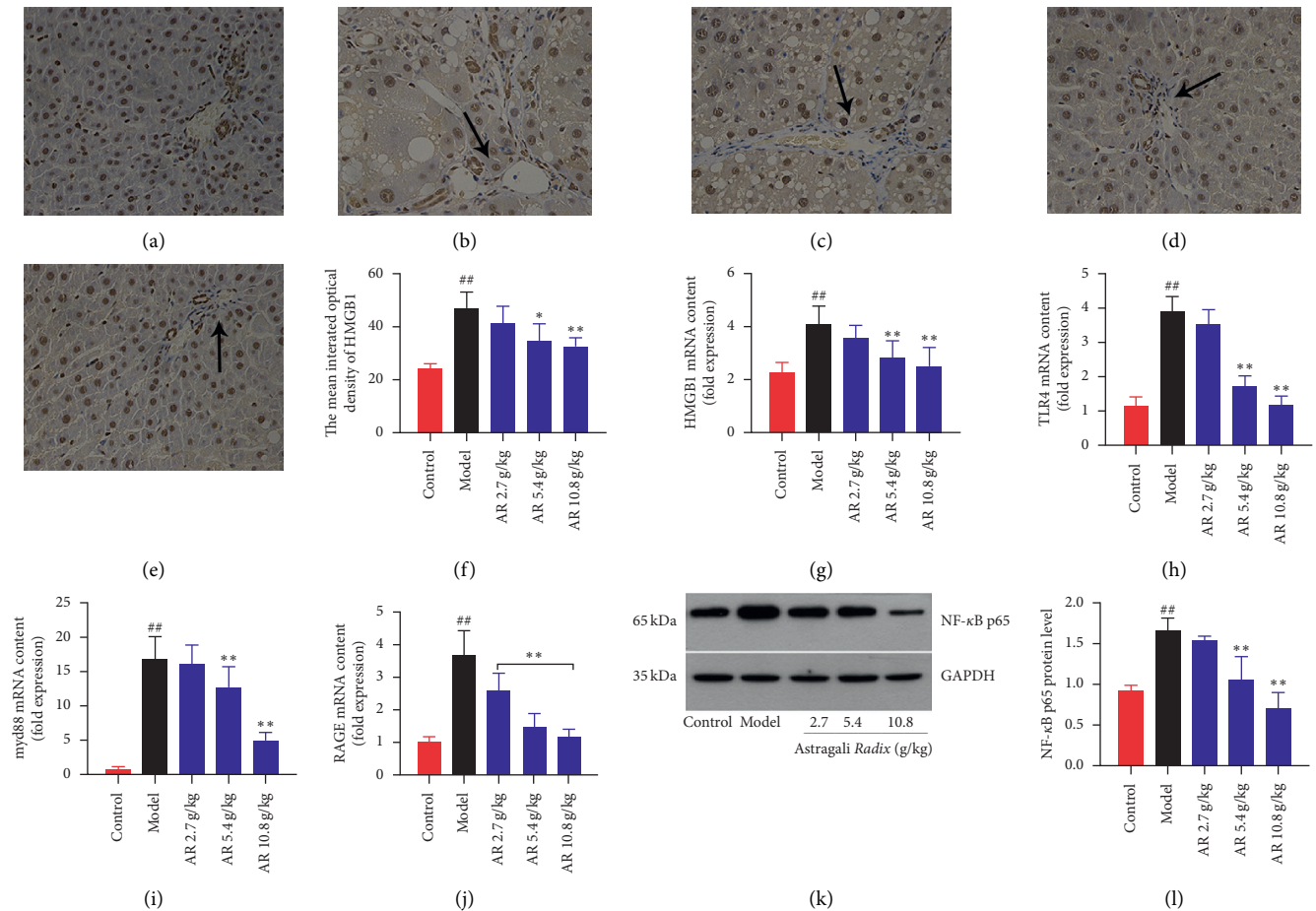


FIGURE 4: Effect of AR on HMGB1/TLR4/NF-κB signaling pathway in liver fibrosis induced by CCl₄. (a–e) Immunohistochemistry analysis for the effect of AR on HMGB1 localization (original magnification, ×400; n = 3; (a) control group; (b) model group; (c) 2.7 g/kg AR group; (d) 5.4 g/kg AR group; (e) 10.8 g/kg AR group). (f) The mean integrated optical density of HMGB1. (g) HMGB1 mRNA level. (h) TLR4 mRNA level. (i) Myd88 mRNA level. (j) RAGE mRNA level. (k) Western blot images of NF-κB p65. (l) NF-κB p65 protein level. Values are expressed as mean ± SD (n = 6). # P < 0.05 and ## P < 0.01 when compared with the control group. * P < 0.05 and ** P < 0.01 when compared with the model group.

detect the expression level of NF-κB p65 in the liver of rats with liver fibrosis. As shown in Figures 4(k)–4(l), the immunoblotting band of NF-κB p65 in the model group was

significantly thicker than that of the control group, and the statistical results showed significant differences (P < 0.01). After AR treatment, the expression of NF-κB p65 decreased in

a dose-dependent manner, especially in the 5.4 g/kg AR group and 10.8 g/kg AR group ($P < 0.01$). These results suggest that AR may improve liver inflammation by downregulating HMGB1/TLR4/NF- κ B signaling pathway.

3.5. AR Inhibits the Activation of HSCs. HSCs are the core cells of liver fibrosis. It is reported that HMGB1 can directly activate HSCs [16]. Therefore, we speculate that AR can play a protective role in liver fibrosis by reducing the activation of HSCs. α -smooth muscle actin (α -SMA) is a special marker of activated HSCs [27]. Here, the ratio of activated HSCs was measured by using IHC method through detecting α -SMA in the liver tissues (Figure 5). In the control group, only a small amount of α -SMA-positive cells was found in the portal area, which might be the hepatic arteries. More α -SMA-positive cells were observed in the CCl₄-induced group compared with control group, and the α -SMA-positive cells were significantly reduced after AR treatment. By computer-assisted semi-quantitative analysis, the mean integrated optical density (IOD) of the α -SMA-positive area of the AR treatment group was confirmed to be significantly reduced in a dose-dependent manner compared to model group (Figure 5, $P < 0.01$). Those results revealed that AR could reduce the activation of HSCs, a key cell of liver fibrosis.

3.6. AR Has an Effect on the Type I Collagen Secretion Signaling Pathway Mediated by HMGB1. Next, IHC method was used to detect the expression of collagen type I. In Figures 6(a)–6(e), type I collagen deposition around the hepatic lobular portal vein in rats treated with CCl₄ alone was significantly increased. After treatment with AR, the expression and deposition of type I collagen in the liver were significantly inhibited, especially in the group with the dose of 10.8 g/kg. The semiquantitative analysis of type I collagen immunopositive region further confirmed the above results (Figure 6(f)). The mean IOD of type I collagen in the AR administered group was significantly reduced in a dose-dependent manner compared to the model group ($P < 0.01$). It was previously reported that HMGB1 interacted with the receptor of RAGE to regulate the expression of type I collagen [17]. Therefore, we explored the effects of AR on the expression of downstream targets of HMGB1, such as RAGE, p-MEK1/2, p-ERK1/2, p-cJun, and type I collagen. Western blot method was used to detect the expression of RAGE, p-MEK1/2, p-ERK1/2, and p-cJun protein after administration of AR (Figures 6(g)–6(k)). The proteins of RAGE, p-MEK1/2, p-ERK1/2, and p-cJun were increased remarkably only in the CCl₄-induced group compared with the control group ($P < 0.05$, $P < 0.01$). Compared with the model group, the high-dose administration group of AR significantly reduced the expression of RAGE, p-MEK1/2, p-ERK1/2, and p-cJun (Figures 6(h)–6(k), $P < 0.05$, $P < 0.01$).

4. Discussion

In this study, the aqueous extract of AR was used, which is consistent with the clinical use of traditional Chinese

medicine. And the research results are more valuable. To determine whether AR has a protective effect on liver fibrosis, CCl₄-induced liver fibrosis model was performed in rats. Consistent with clinical observations, AR could improve liver function to some extent to alleviate liver injury [28, 29]. In this study, the results demonstrated that AR could reduce serum markers of liver fibrosis, including COL-IV, HA, LN, and PC-III. The examination of serum levels and liver histopathology exhibited that AR showed obvious anti-liver fibrosis effect and the anti-liver fibrosis effect of AR at the dose of 10.8 g/kg is comparable to that of colchicine. In order to apply AR more scientifically, the potential mechanism of AR on alleviating liver fibrosis was further explored.

Previous reports and the results of this study confirmed that AR has definite hepatoprotective effect and can effectively improve liver fibrosis [19, 30, 31]. However, how to exert the therapeutic effect is still unclear. Previous studies have reported that AR has strong anti-inflammatory activity and can effectively reduce the expression of inflammatory factors such as iNOS, cyclooxygenase-2 (COX-2), IL-6, TNF- α , and IL-1 β [32, 33]. Long-term inflammatory response is the key to the occurrence of liver fibrosis [34]. Therefore, we detected the effect of AR on the expression of inflammatory factors in liver fibrosis rats. The results showed that AR could significantly downregulate the expression of IL-1 β , TNF- α , and IL-6. It suggested that AR might improve liver fibrosis by inhibiting the inflammatory response in rats.

Pathogen-free inflammatory liver disease is considered “sterile” [35]. Studies have reported that DAMP is the key to aseptic inflammation after liver injury, and HMGB1 is the key point [36]. Extracellular HMGB1 is a multifunctional cytokine, which induces inflammation by binding with specific cell surface receptor TLR4 [37]. Thus, we detected the expression of HMGB1 in rats to explore whether AR had effect on regulating HMGB1 expression via improving the inflammatory response. The results showed that the expression of HMGB1 decreased in the AR treatment group compared with the model group. The TLR4 signaling pathway is the most studied pathway. TLR4, as a pattern recognition receptor, recruits Myd88 under the action of the endogenous activator HMGB1, which causes the activation of the NF- κ B inflammatory pathway and promotes the transcription of inflammatory cytokines IL-1 β , TNF- α , and IL-6 [38, 39]. Therefore, we detected the expression of TLR4, Myd88, and NF- κ B p65. The results showed that the expression levels of TLR4, Myd88, and NF- κ B p65 in AR treatment group were significantly lower than those in the model group. The above results suggest that AR might reduce CCl₄-induced liver inflammatory by downregulating the expression of HMGB1/TLR4/NF- κ B signaling pathway.

In experimental and human liver injury, activated HSCs (myofibroblasts) are recognized as the driving factors of liver fibrosis [40]. It has been reported that HSCs activated by inflammatory factors are the main source of myofibroblasts in the liver [34]. And HMGB1 could directly stimulate the activation of HSCs [16]. The pharmacodynamic results show that AR can effectively improve the liver fibrosis in rats induced by CCl₄. The study also found that AR can not only

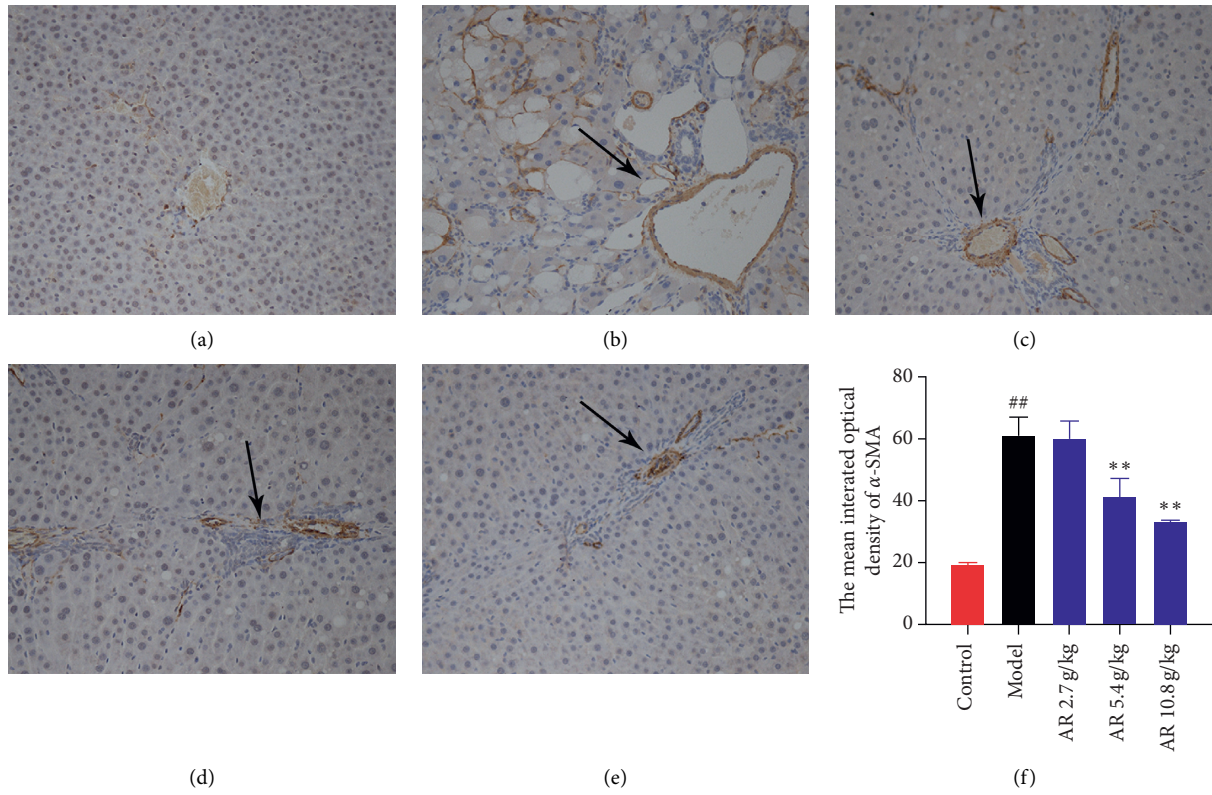


FIGURE 5: Immunohistochemistry analysis for the effect of AR on α -SMA localization (original magnification, $\times 200$; $n = 3$; (a) control group; (b) model group; (c) 2.7 g/kg AR group; (d) 5.4 g/kg AR group; (e) 10.8 g/kg AR group). (f) Quantitative analysis of α -SMA localization by immunohistochemistry.

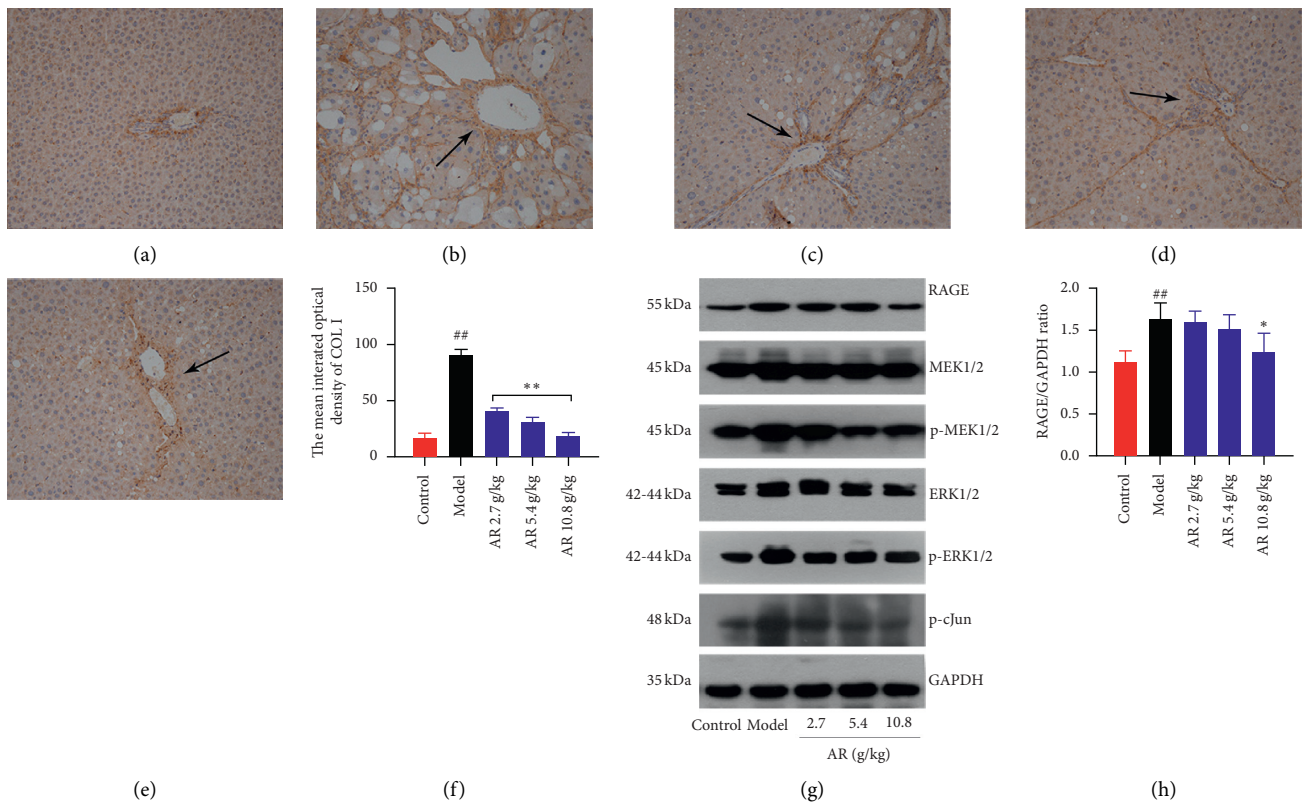


FIGURE 6: Continued.

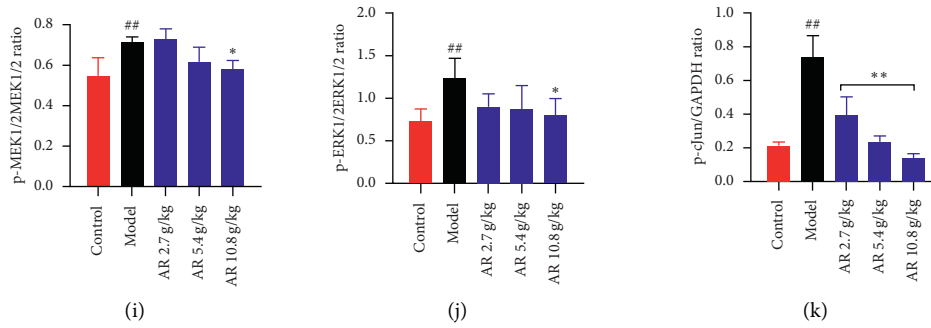


FIGURE 6: Effect of RA on type 1 collagen level and HMGB1/RAGE/c-Jun pathway in liver fibrosis induced by CCl₄. (a–e) Immunohistochemistry analysis for the effect of AR on type 1 collagen expression (original magnification, ×200; n = 3); (a): control group; (b): model group; (c): 2.7 g/kg AR group; (d) 5.4 g/kg AR group; (e) 10.8 g/kg AR group.) (f) The mean integrated optical density of COL-I. (g) Western blot images of RAGE, MEK1/2, p-MEK1/2, ERK1/2, p-ERK1/2, and p-cJun. (h) RAGE protein level. (i) p-MEK1/2 protein level. (j) p-ERK1/2 protein level. (k) p-cJun protein level.

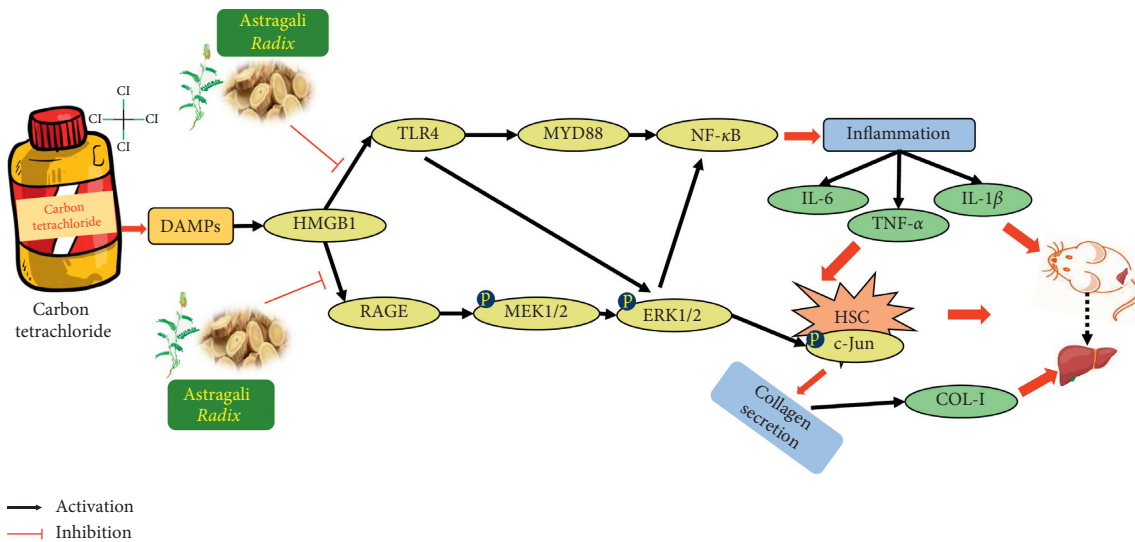


FIGURE 7: Schematic diagram of signal pathway which mediates CCl₄-induced liver fibrosis and the ameliorative effects of AR on rat.

downregulate the expression of HMGB1, but also reduce the transcription of inflammatory cytokine IL-1 β , TNF- α , and IL-6 by regulating HMGB1/TLR4/NF- κ B signaling pathway. Therefore, we speculate that AR can inhibit the activation of rat HSCs. The detection of α -SMA, a marker protein of HSCs activation, further confirmed our hypothesis: AR can significantly inhibit the activation of rat HSCs induced by CCl₄ (Figure 7).

Liver fibrosis or scar deposition caused by chronic injury is similar in all forms of liver disease [41]. In the sub-endothelial space between hepatocytes and endothelial cells, fibrillar or type I collagen aggregates to replace the low-density basement membrane-like matrix containing type IV collagen. The conversion of the subendothelial matrix to fibril-rich collagen is a key event, which mediates the loss of differentiation function characteristic of progressive liver disease [42]. Myofibroblasts are the main source of type I collagen accumulated during tissue fibrosis [43]. It was found that the activation of HSCs was decreased in AR-treated group, and we speculated that the expression of type I

collagen in the liver of rats would also be reduced accordingly. In addition, the latest research reports that HMGB1 activates the paracrine system and upregulates the secretion of type 1 collagen by binding to the receptor RAGE on the surface of fibroblasts, thereby triggering and/or maintaining scar formation [17]. Therefore, we detected the expression of type I collagen in the liver of rats, as well as the expression of RAGE, p-MEK1/2, p-ERK1/2, and p-c-Jun in liver tissues. The results showed that AR can significantly reduce the expression of type 1 collagen in rats, which may be related to the decrease of HSCs activation and the downregulation of collagen secretion mediated by HMGB1-RAGE-c-Jun.

5. Conclusion

In conclusion, biochemical tests and histological assessments were used to reveal the function of AR. The study also demonstrated that AR was potent for downregulating the expression of HMGB1/RAGE/cJun pathway and HMGB1/TLR4/NF- κ B pathway, thus protecting rats against CCl₄-

induced liver fibrosis. Therefore, this study will provide scientific evidence and theoretical basis for the development of AR as a potential drug candidate for liver fibrosis.

Abbreviations

AR:	<i>Astragali Radix</i>
ALT:	Alanine aminotransferase
AST:	Aspartate aminotransferase
CCL ₄ :	Carbon tetrachloride
COL-IV:	Collagen IV
DAMPs:	Damage-associated molecular patterns
ECM:	Extracellular matrix
HA:	Hyaluronic acid
HMGB1:	High-mobility group box 1
HSCs:	Hepatic stellate cells
H&E:	Hematoxylin-eosin
IHC:	Immunohistochemistry
IOD:	Integrated optical density
LN:	Laminin
PCR:	Polymerase chain reaction
PC III:	Precollagen type III
RAGE:	The receptor of advanced glycation end products
SD:	Standard deviation
α -SMA:	α -smooth muscle actin.

Data Availability

The data used to support the findings of this study are available from the corresponding author upon reasonable request.

Conflicts of Interest

The authors declare that there are no conflicts of interest.

Authors' Contributions

Jianxia Wen and Dan Wang contributed equally to this study. Jianxia Wen and Dan Wang conducted the experiments and wrote the manuscript. Ruilin Wang and Shizhang Wei analyzed the data. Yanling Zhao and Jian Wang designed the study and guided the experiment.

Acknowledgments

This work was supported by the project of Capital's Funds for Health Improvement and Research (no. 2018-2-5032).

References

- [1] G. Zhang, Y. Liu, and P. Liu, "Active components from sea buckthorn (*Hippophae rhamnoides* L.) regulate hepatic stellate cell activation and liver fibrogenesis," *Journal of Agricultural and Food Chemistry*, vol. 66, no. 46, pp. 12257–12264, 2018.
- [2] Y. Liu, Y. Bi, C. Mo et al., "Betulinic acid attenuates liver fibrosis by inducing autophagy via the mitogen-activated protein kinase/extracellular signal-regulated kinase pathway," *Journal of Natural Medicines*, vol. 73, no. 1, pp. 179–189, 2019.
- [3] F. Alegre, P. Pelegrin, and A. Feldstein, "Inflammasomes in liver fibrosis," *Seminars in Liver Disease*, vol. 37, no. 2, pp. 119–127, 2017.
- [4] D. Schuppan, M. Ashfaq-Khan, A. T. Yang, and Y. O. Kim, "Liver fibrosis: direct antifibrotic agents and targeted therapies," *Matrix Biology*, vol. 68–69, pp. 435–451, 2018.
- [5] Y. Yoon, Y. Lee, and S. Friedman, "Antifibrotic therapies: Where are we now?" *Seminars in Liver Disease*, vol. 36, no. 1, pp. 087–098, 2016.
- [6] F. Tacke and C. Trautwein, "Mechanisms of liver fibrosis resolution," *Journal of Hepatology*, vol. 63, no. 4, pp. 1038–1039, 2015.
- [7] L. Campana and J. Iredale, "Regression of liver fibrosis," *Seminars in Liver Disease*, vol. 37, no. 1, pp. 1–10, 2017.
- [8] A. Gong, R. Duan, H. Wang et al., "Evaluation of the pharmaceutical properties and value of *Astragali radix*," *Medicines*, vol. 5, no. 2, p. 46, 2018.
- [9] J. Fu, Z. Wang, L. Huang et al., "Review of the botanical characteristics, phytochemistry, and pharmacology of *astragalus membranaceus* (huangqi)," *Phytotherapy Research*, vol. 28, no. 9, pp. 1275–1283, 2014.
- [10] S. He, Y. Yang, X. Liu et al., "Compound astragalus and salvia miltiorrhiza extract inhibits cell proliferation, invasion and collagen synthesis in keloid fibroblasts by mediating transforming growth factor- β /smad pathway," *British Journal of Dermatology*, vol. 166, no. 3, pp. 564–574, 2012.
- [11] L. Li, W. Huang, S. Wang et al., "Astragaloside IV attenuates acetaminophen-induced liver injuries in mice by activating the Nrf2 signaling pathway," *Molecules*, vol. 23, no. 8, p. 2032, 2018.
- [12] S.-Y. Yu, H.-T. Ouyang, J.-Y. Yang et al., "Subchronic toxicity studies of *Radix Astragali* extract in rats and dogs," *Journal of Ethnopharmacology*, vol. 110, no. 2, pp. 352–355, 2007.
- [13] J. Li, F.-P. Wang, W.-M. She et al., "Enhanced high-mobility group box 1 (HMGB1) modulates regulatory T cells (Treg)/T helper 17 (Th17) balance via toll-like receptor (TLR)-4-interleukin (IL)-6 pathway in patients with chronic hepatitis B," *Journal of Viral Hepatitis*, vol. 21, no. 2, pp. 129–140, 2014.
- [14] J. Li, C. Zeng, B. Zheng et al., "HMGB1-induced autophagy facilitates hepatic stellate cells activation: a new pathway in liver fibrosis," *Clinical Science*, vol. 132, no. 15, pp. 1645–1667, 2018.
- [15] P. Qiu, L. Wang, J. Ni, and Y. Zhang, "Associations between HMGB1 gene polymorphisms and susceptibility and clinical outcomes in Chinese Han sepsis patients," *Gene*, vol. 687, pp. 23–29, 2019.
- [16] H. Gaskell, X. Ge, and N. Nieto, "High-mobility group box-1 and liver disease," *Hepatology Communications*, vol. 2, no. 9, pp. 1005–1020, 2018.
- [17] X. Ge, E. Arriazu, F. Magdaleno et al., "High mobility group box-1 drives fibrosis progression signaling via the receptor for advanced glycation end products in mice," *Hepatology*, vol. 68, no. 6, pp. 2380–2404, 2018.
- [18] S. Leppa, R. Saffrich, and W. Ansorge, "Differential regulation of c-Jun by ERK and JNK during PC12 cell differentiation," *The EMBO Journal*, vol. 17, no. 15, pp. 4404–4413, 1998.
- [19] D. Wang, R. Li, and S. Wei, "Metabolomics combined with network pharmacology exploration reveals the modulatory properties of *Astragali Radix* extract in the treatment of liver fibrosis," *Chinese Medicine*, vol. 14, p. 30, 2019.
- [20] Q. Yao, Y. Lin, X. Li, X. Shen, J. Wang, and C. Tu, "Curcumin ameliorates intrahepatic angiogenesis and capillarization of

- the sinusoids in carbon tetrachloride-induced rat liver fibrosis,” *Toxicology Letters*, vol. 222, no. 1, pp. 72–82, 2013.
- [21] Y. Yang, P. Zhang, and Y. Wang, “Hepatoprotective effect of san-cao granule on con a-induced liver injury in mice and mechanisms of action exploration,” *Frontiers in Pharmacology*, vol. 9, p. 624, 2018.
- [22] X. Feng, G. J. Zhong, D. J. Yang, L. Chen, and S. Du, “Hepatoprotective effect of *Herpetospermum caudigerum* wall. On carbon tetrachloride-induced hepatic fibrosis in rats,” *Journal of Cellular and Molecular Medicine*, vol. 22, no. 7, pp. 3691–3697, 2018.
- [23] E. Ramos-Tovar, E. Hernandez-Aquino, S. Casas-Grajales et al., “Stevia prevents acute and chronic liver injury induced by carbon tetrachloride by blocking oxidative stress through Nrf2 upregulation,” *Oxidative Medicine and Cellular Longevity*, vol. 2018, Article ID 3823426, 12 pages, 2018.
- [24] H.-J. Zhangdi, S.-B. Su, F. Wang et al., “Crosstalk network among multiple inflammatory mediators in liver fibrosis,” *World Journal of Gastroenterology*, vol. 25, no. 33, pp. 4835–4849, 2019.
- [25] M. Yakut, H. Özkan, M. F. Karakaya, and H. Erdal, “Diagnostic and prognostic role of serum interleukin-6 in malignant transformation of liver cirrhosis,” *Euroasian Journal of Hepato-Gastroenterology*, vol. 8, no. 1, pp. 23–30, 2018.
- [26] J.-P. Pradere, J. Kluwe, S. De Minicis et al., “Hepatic macrophages but not dendritic cells contribute to liver fibrosis by promoting the survival of activated hepatic stellate cells in mice,” *Hepatology*, vol. 58, no. 4, pp. 1461–1473, 2013.
- [27] J. Sun, Y. Wu, C. Long et al., “Anthocyanins isolated from blueberry ameliorates CCl₄ induced liver fibrosis by modulation of oxidative stress, inflammation and stellate cell activation in mice,” *Food and Chemical Toxicology*, vol. 120, pp. 491–499, 2018.
- [28] R. Simeonova, V. M. Bratkov, M. Kondeva-Burdina, V. Vitcheva, V. Manov, and I. Krasteva, “Experimental liver protection of n-butanol extract of *Astragalus monspessulanus* L. on carbon tetrachloride model of toxicity in rat,” *Redox Report*, vol. 20, no. 4, pp. 145–153, 2015.
- [29] Y. Zhou, X. Tong, S. Ren et al., “Synergistic anti-liver fibrosis actions of total astragalus saponins and glycyrrhizic acid via TGF- β 1/smads signaling pathway modulation,” *Journal of Ethnopharmacology*, vol. 190, pp. 83–90, 2016.
- [30] Y. Li, C. Wang, Y. Jin et al., “Huang-Qi San improves glucose and lipid metabolism and exerts protective effects against hepatic steatosis in high fat diet-fed rats,” *Biomedicine & Pharmacotherapy*, vol. 126, Article ID 109734, 2020.
- [31] M. Hao, Z. Guan, Y. Gao et al., “Huang-Qi San ameliorates hyperlipidemia with obesity rats via activating brown adipocytes and converting white adipocytes into brown-like adipocytes,” *Phytomedicine*, vol. 78, Article ID 153292, 2020.
- [32] M. Ryu, E. H. Kim, M. Chun et al., “*Astragalus Radix* elicits anti-inflammation via activation of MKP-1, concomitant with attenuation of p38 and Erk,” *Journal of Ethnopharmacology*, vol. 115, no. 2, pp. 184–193, 2008.
- [33] Y. S. Lee, O. K. Han, C. W. Park et al., “Pro-inflammatory cytokine gene expression and nitric oxide regulation of aqueous extracted *Astragalus Radix* in RAW 264.7 macrophage cells,” *Journal of Ethnopharmacology*, vol. 100, no. 3, pp. 289–294, 2005.
- [34] Y. Koyama and D. A. Brenner, “Liver inflammation and fibrosis,” *Journal of Clinical Investigation*, vol. 127, no. 1, pp. 55–64, 2017.
- [35] S. Mihm, “Danger-associated molecular patterns (DAMPs): molecular triggers for sterile inflammation in the liver,” *International Journal of Molecular Sciences*, vol. 19, no. 10, p. 3104, 2018.
- [36] P. Huebener, J.-P. Pradere, C. Hernandez et al., “The HMGB1/RAGE axis triggers neutrophil-mediated injury amplification following necrosis,” *Journal of Clinical Investigation*, vol. 125, no. 2, pp. 539–550, 2015.
- [37] A. Vicentino, V. Carneiro, and D. Allonso, “Emerging role of HMGB1 in the pathogenesis of schistosomiasis liver fibrosis,” *Frontiers in Immunology*, vol. 9, no. 1979, 2018.
- [38] T. Trotta, C. Porro, and R. Calvello, “Biological role of toll-like receptor-4 in the brain,” *Journal of Neuroimmunology*, vol. 268, no. 1–2, pp. 1–12, 2014.
- [39] Z. Zhang, Q. Liu, M. Liu et al., “Upregulation of HMGB1-TLR4 inflammatory pathway in focal cortical dysplasia type II,” *Journal of Neuroinflammation*, vol. 15, no. 1, p. 27, 2018.
- [40] T. Tsuchida and S. L. Friedman, “Mechanisms of hepatic stellate cell activation,” *Nature Reviews Gastroenterology & Hepatology*, vol. 14, no. 7, pp. 397–411, 2017.
- [41] S. L. Friedman, “Molecular regulation of hepatic fibrosis, an integrated cellular response to tissue injury,” *Journal of Biological Chemistry*, vol. 275, no. 4, pp. 2247–2250, 2000.
- [42] E. Olaso, K. Ikeda, F. J. Eng et al., “DDR2 receptor promotes MMP-2-mediated proliferation and invasion by hepatic stellate cells,” *Journal of Clinical Investigation*, vol. 108, no. 9, pp. 1369–1378, 2001.
- [43] N. C. Henderson, T. D. Arnold, Y. Katamura et al., “Targeting of α v integrin identifies a core molecular pathway that regulates fibrosis in several organs,” *Nature Medicine*, vol. 19, no. 12, pp. 1617–1624, 2013.

Review Article

Hepatocardiac or Cardiohepatic Interaction: From Traditional Chinese Medicine to Western Medicine

Yaxing Zhang ^{1,2} and Xian-Ming Fang ³

¹Department of Physiology, School of Basic Medical Sciences, Guangzhou University of Chinese Medicine, Guangzhou, Guangdong, China

²Issue 12 of the Master-Apprentice Education of Guangxi Traditional Chinese Medicine, College of Continuing Education, Guangxi University of Chinese Medicine, Nanning, Guangxi, China

³Department of Cardiology, Ruikang Hospital Affiliated to Guangxi University of Chinese Medicine/Ruikang Clinical Faculty of Guangxi University of Chinese Medicine/Guangxi Hospital of Integrated Chinese and Western Medicine, Guangxi University of Chinese Medicine, Nanning, Guangxi, China

Correspondence should be addressed to Xian-Ming Fang; fxm621@126.com

Received 2 October 2020; Revised 18 January 2021; Accepted 5 February 2021; Published 13 March 2021

Academic Editor: Michał Tomczyk

Copyright © 2021 Yaxing Zhang and Xian-Ming Fang. This is an open access article distributed under the Creative Commons Attribution License, which permits unrestricted use, distribution, and reproduction in any medium, provided the original work is properly cited.

There is a close relationship between the liver and heart based on “zang-xiang theory,” “five-element theory,” and “five-zang/five-viscus/five-organ correlation theory” in the theoretical system of Traditional Chinese Medicine (TCM). Moreover, with the development of molecular biology, genetics, immunology, and others, the Modern Medicine indicates the existence of the essential interorgan communication between the liver and heart (the heart and liver). Anatomically and physiologically, the liver and heart are connected with each other primarily via “blood circulation.” Pathologically, liver diseases can affect the heart; for example, patients with end-stage liver disease (liver failure/cirrhosis) may develop into “cirrhotic cardiomyopathy,” and nonalcoholic fatty liver disease (NAFLD) may promote the development of cardiovascular diseases via multiple molecular mechanisms. In contrast, heart diseases can affect the liver, heart failure may lead to cardiogenic hypoxic hepatitis and cardiac cirrhosis, and atrial fibrillation (AF) markedly alters the hepatic gene expression profile and induces AF-related hypercoagulation. The heart can also influence liver metabolism via certain nonsecretory cardiac gene-mediated multiple signals. Moreover, organokines are essential mediators of organ crosstalk, e.g., cardiomyokines link the heart to the liver, while hepatokines link the liver to the heart. Therefore, both TCM and Western Medicine, and both the basic research studies and the clinical practices, all indicate that there exist essential “heart-liver axes” and “liver-heart axes.” To investigate the organ interactions between the liver and heart (the heart and liver) will help us broaden and deepen our understanding of the pathogenesis of both liver and heart diseases, thus improving the strategies of prevention and treatment in the future.

1. Introduction

In the theoretical system of Traditional Chinese Medicine (TCM), there are close relationships/interactions between the liver and heart (the heart and liver) according to the first records in the original literature Huang-Di-Nei-Jing (The Yellow Emperor’s Canon of Medicine), the earliest existing TCM classics, which summarized the medical achievements and treatment experience before China Spring and Autumn,

Warring State Period (770 B.C.–221 B.C.). Huang-Di-Nei-Jing established the unique theoretical system of TCM and became the basis of TCM. Moreover, the “five-zang (also known as five-viscus or five-organ) correlation theory, 五脏相关学说/理论” established by the National Chinese Medical Science Master (Guo-Yi Master) Deng Tietao (邓铁涛) in the 1960s also contains the “liver-heart correlation theory (or heart-liver correlation theory)” [1–4]. These interactions between the liver and heart (the heart and liver)

have been extensively used by doctors of TCM to guide the clinical diagnosis, prevention, and treatment of both hepatic and cardiovascular diseases (CVDs) for more than 2200 years in China.

In Modern Medicine (Western Medicine), most notably from Claude Bernard in the 19th century, it is first suggested that a system involving chemical messengers ensures the communication between the different organs of the body [5]. Since the discovery of cardiac natriuretic peptides (NPs) by de Bold in 1981, it is well known that the heart has an endocrine function [6, 7]. Now, the biological and medical scientists found that the heart can secrete other proteins besides NPs, they are termed as “cardiomyokines” [8, 9], and the liver is also an endocrine organ that secretes “hepatokines” [10–12]. These “organokines” are essential mediators of organ interaction between the liver and heart (the heart and liver) [8, 10, 11, 13–16].

In modern anatomy and physiology, the heart is central to hemodynamics of many organs both in the form of distributing the oxygenated blood and delivering deoxygenated blood in order to send it to the lungs [17]. The liver, which has high metabolic activities, receives up to 25% of cardiac output, coming by two systems of blood vessels: the hepatic artery and the portal vein [18]. The venous drainage occurs by hepatic veins and the inferior vena cava, which have no valves, resulting in direct transmission of the rise of right heart filling pressures to the liver [18]. Moreover, accumulating basic and clinical evidences indicate that acute as well as chronic heart disease can directly contribute to an acute or chronic worsening of liver function and vice versa [19].

Therefore, there exist the essential interorgan crosstalk between the heart and liver (the liver and heart). The aim of this review is to comprehensively summarize and discuss the hepatocardiac or the cardiohepatic interaction from the perspective of TCM and Western/Modern Medicine. These will broaden and deepen our understanding of the hepatic and cardiovascular physiology, and the pathogenesis of liver diseases and heart diseases, thus helping us improve the prevention and treatment strategies in the future.

2. Hepatocardiac or Cardiohepatic Interaction in Traditional Chinese Medicine

2.1. The Physiological Relationship between the Liver and Heart Based on “Zang-Xiang Theory”. The words “zang-xiang” were firstly recorded in the TCM literature *Su wen-Liu jie zang xiang lun*, which is a section of *Huang-Di-Nei-Jing*. The word “zang” refers to the internal organs hidden in the body, while “xiang” refers to the physiological and pathological phenomena that appear outside. The “zang-xiang theory” investigates the physiological functions and pathological changes of “zang-fu” and their relationship. Based on the physiological function of “zang-fu,” they are divided into “five-zang” (liver, heart, spleen, lung, and kidney), “six-fu” (gallbladder, small intestine, stomach, large intestine, bladder, and san-jiao), and “qi-heng-zhi-fu” (brain, marrow, bone, vessels (mai), gallbladder, and nv-zi-bao (also known as the uterus)). Among these, the heart is considered as the “official of monarch” according to the TCM literature *Su wen-Ling lan*

mi dian lun. Heart governs the blood and vessels (mai, also known as “xin zhu xue-mai”) and controls “shen-zhi,” also known as heart controlling “shen-ming” or heart storing “shen.” Generally, “shen” refers to the external performance of the life activities of the whole human body. Narrowly, “shen” refers to spirit, consciousness, and thinking activities. The liver is considered as the “organ of general” according to the TCM literature *Su wen-Ling lan mi dian lun*, physiologically, the liver governs “shu-xie,” also known as “liver-governing free flow of Qi” or “liver-controlling dispersion,” and the liver is also capable of storing blood and regulating the distribution of blood volume in all parts of the human body and capable of storing soul based on “liver storing blood and blood housing soul.” Therefore, there is a functional relationship between the heart and liver (the liver and heart) mediated by “blood movement” and “qing-zhi regulation.”

2.2. The Relationship between the Liver and Heart Based on “Five-Element Theory”. The “five-element theory” in TCM refers to the “zang-fu,” “five-guan,” “five-ti,” “five-ye,” “five-zhi,” and “jing-luo (meridians and collaterals),” and others of the human body into the five elements: wood, fire, soil/earth (known as “Tu” in Chinese), gold (known as “Jin” in Chinese), and water. The application of “five-element theory” in TCM is mainly to analyze and study the five-element attribute of “zang-fu,” “jing-luo,” and others according to the characteristics of five elements, to investigate the relationships in “zang-fu,” in “jing-luo” and in others, and in their physiological functions based on the “generation-inhibition” of five elements, to explain the mutual influence of the diseases according to the “cheng-wu” (“cheng,” domineer over the weak by being strong; “wu,” reverse restriction in five elements) of five elements. Therefore, the “five-element theory” in TCM is not only used as a theoretical exposition but also has the significance in clinical practices.

In this theory, the liver belongs to wood as the mother of heart, and the heart belongs to fire as the son of liver; therefore, the “wood inducing fire” is equaled to the “liver inducing heart.” The “mother-child relationship of the liver and heart” is a physiological description of mutual promotion and mutual restriction relationship in the liver and heart according to “five-element theory” in TCM [20]. If the “mother-child relationship of the liver and heart” was destroyed, the pathological phenomena of “mother-organ disorder involving its child-organ” (which indicates that liver disease may induce heart disease) and “illness of the child-organ involving its mother-organ” (which indicates that heart disease may induce liver disease) would occur [20] (Figure 1). Thus, the liver and heart influence each other under normal or pathophysiological conditions.

2.3. Liver and Heart in “Five-Zang Correlation Theory”. The five visceral systems are interrelated, which is one of the basic characteristics of TCM academic ideologies since the ancient times in China, for example, “five-zang xiang-tong” recorded in *Su wen-Yu ji zhen zang lun*, “five-zang diseases theory” by Zhang Zhongjing (China Han Dynasty), “five-yun zhu-bing/diseases” by Liu Wansu (China Jin Dynasty),

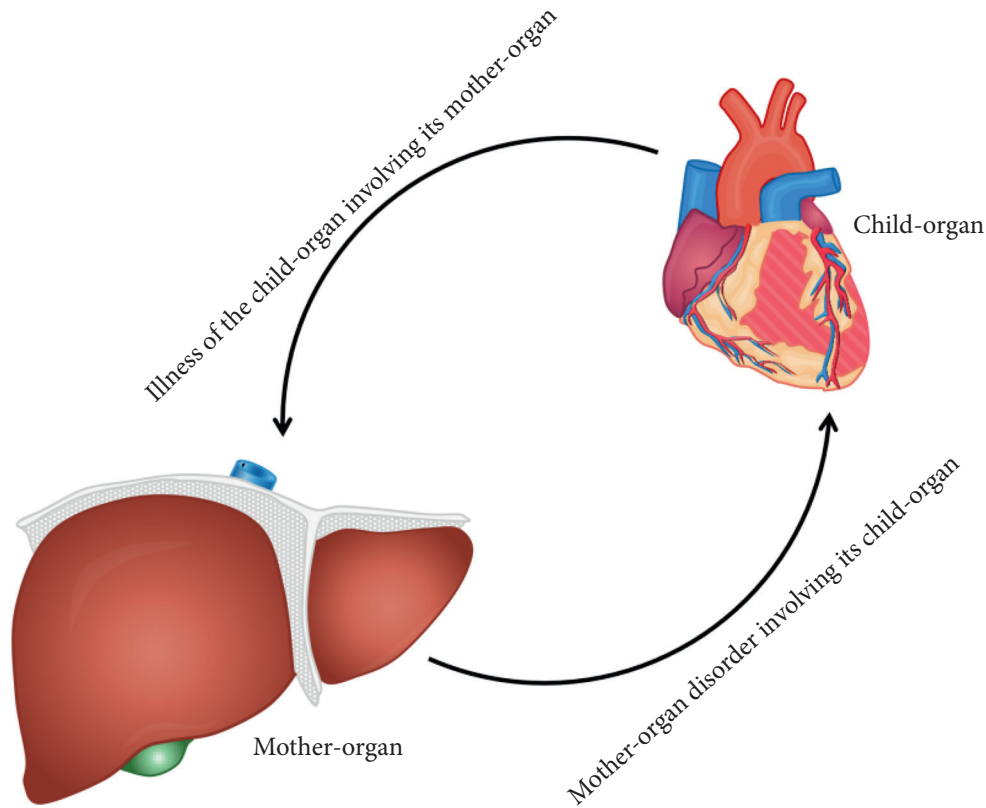


FIGURE 1: The disturbance of liver-heart homeostasis in TCM. In TCM, the liver is the mother-organ and the heart is the child-organ. The mother-child relationship of the liver and heart is essential for modulating both organs' homeostasis. The "mother-organ disorder involving its child-organ" refers to the transformation of the disease from the mother viscera to the child viscera; therefore, liver diseases may trigger heart diseases. The "illness of the child-organ involving its mother-organ" indicates that the diseases can be transformed from the child viscera to the mother viscera; therefore, heart diseases may induce liver diseases. For example, the insufficiency of heart blood involves the liver and induces blood deficiency of the liver, thus forming "heart-liver blood deficiency." The effulgent heart fire conversely involves the liver and triggers liver fire, thus inducing "hyperactivity of heart fire and liver fire."

"five-element hu-han" recorded in Fu-xing-jue (Dunhuang Legacy), "five-zang pang-tong" by Sun Simiao (China Tang Dynasty), "five-zang chuan-zao" by Li Ting (China Ming Dynasty), "five-element hu-cang" by Zhang Jiebin (China Ming Dynasty), "five-zang mutually guan-she" by He Mengyao (China Qing Dynasty), and others [21]. Based on the classic "five-element theory," the theories mentioned above, and the long-term clinical practice, Deng Tietao established the "five-zang correlation theory" in 1961 [3]. The theory refers to that in the large system of the human body, the "five-zang" and their corresponding "six-fu," limbs, skin, hair, tendons (jin), vessels (mai), meat, five-guan, nine orifices, etc. constitute the five visceral systems, and there are horizontal, vertical, and cross multidimensional connections within the visceral system, between the visceral system and the visceral system, between the visceral system and the human body system, between the visceral system and the nature and society [1, 2]. They promote and restrict each other in order to play different functions and coordinate the normal activities of the body [1]. Moreover, the five

visceral systems interact with each other under the pathological conditions [1]. In short, the "five-zang" organs are related [1], which highlight the importance of "five-zang" system communication in modulating body homeostasis; for example, the coronary heart disease is related to "Qi deficiency of five-zang" [22] and can be treated by "Yi-Qi-Chu-Tan-Fang" [23].

Based on zang-xiang, yin-yang, five-element, qi-blood, jing-luo, and qing-zhi (seven emotions) theory according to Huang-Di-Nei-Jing and based on "five-zang correlation theory" by Deng Tietao, there are close physiological and pathological relationships/interactions between the liver and heart (the heart and liver) in TCM theories [1–4]. Clinically, these TCM theories have been extensively used to treat both the heart diseases and liver diseases. For example, the methods of "Shu-Liver, 疏肝" and "Rou-Liver, 柔肝" based on "treating the heart disease from the liver" have been extensively used for treating coronary heart disease [24–26], and the methods of "Xing-Qi-Huo-Xue, 行气活血" and "Bu-Xue, 补血" have been used for treating nonalcoholic fatty liver disease (NAFLD) [27–30]. These

connections between the liver and heart (the heart and liver) have also been confirmed by the Western Medicine.

3. Organ Interaction in Western Medicine

Organ interaction, also known as organ crosstalk or interorgan communication, can be defined as the complex and mutual biological communication between different tissues/organs of multicellular organisms via multiple signals [5, 31]. Normally, the maintenance of systemic homeostasis and the adaptation to external conditions, such as nutritional and environmental challenges, require a finely tuned system of interorgan communication; however, sudden or chronic dysfunction in any organ causes dysregulation in another organ [5, 31–33]. Interorgan communication has been shown to play essential roles in orchestrating metabolic health [5, 33]. Mechanistically, bioactive peptides and proteins (e.g., hormones and cytokines), extracellular vesicles (EVs, e.g., exosome and migrasome), and certain nonsecretory genes are the key messengers in modulating the interorgan communication [5, 34–43]. Moreover, organokines are the novel players mediating the interorgan communication, they are proteins exclusively or predominantly produced by and secreted from a specific tissue (e.g., the functional proteins released from adipose tissue are termed as “adipokines” and skeletal muscle-derived proteins are known as “myokines”), but they are not simply markers of the function of their source tissue, and all organokines have the paracrine or endocrine actions, or both [13]. Similar to that in TCM, the interorgan communication of Western Medicine also supports the organ interaction between the liver and heart (the heart and liver), and there exist the liver-heart axis and the heart-liver axis (Figure 2).

3.1. The Liver-Heart Axis in Modern Medicine

3.1.1. Liver Diseases Affecting the Heart. The close interaction and connection between the cardiac and hepatic functions are well known, for example, “hepatic/cirrhotic cardiomyopathy” is an important clinical entity which best describes the mutual pathogenical influence between these two organs [44]. Patients with end-stage liver disease (liver failure/cirrhosis) displayed hyperdynamic circulation characterized by low systemic vascular resistance and high cardiac output state [45, 46]. However, the cardiac response to physiological, pathophysiological, or pharmacological stimuli (such as exercise, hemorrhage, infection, and surgery) is abnormal with systolic and diastolic dysfunction, as well as electromechanical abnormalities in the absence of other known causes of cardiac disease, a condition termed “cirrhotic cardiomyopathy” [45, 47–53]. Moreover, in patients with liver cirrhosis, the elevated parameters of myocardial edema and fibrosis were observed at magnetic resonance imaging (MRI), these were more abnormal with greater severity of liver disease [54].

Bile duct ligation (BDL)-induced advanced liver fibrosis is a suitable mouse model to investigate the pathophysiology of hepatic/cirrhotic cardiomyopathy at a preclinical level, as it resembles the characteristics of the

clinical syndrome seen in patients [55]. One of the main contributors to the BDL-induced liver fibrosis is tissue inflammation, which contributes, as liver failure develops, to the production and excretion of several inflammatory cytokines, such as tumor necrosis factor- α (TNF- α), into the blood, culminating in a general inflammatory response and subsequent oxidative stress, and the heart is one of the major organs involved [55, 56]. Cannabinoid-2 receptor (CB₂-R), a negative regulator of ischemia/reperfusion (I/R)-induced liver injury and carbon tetrachloride-induced hepatic fibrosis, is upregulated in the liver and heart of BDL mice [55, 57–59]. Treatment BDL mice with a selective CB₂-R agonist HU910 alleviated hepatic inflammation and fibrosis, restored the hepatic microcirculation, reduced serum levels of TNF- α , and improved cardiac dysfunction, myocardial inflammation, and oxidative stress [55]. These beneficial effects of HU910 indicated that controlling the liver and/or myocardial inflammation may delay or prevent the development of cardiomyopathy in severe liver disease [55]. Thus, the liver-heart inflammatory axis has a pivotal pathophysiological role in the pathogenesis of hepatic cardiomyopathy [55].

The liver is a central hub for lipid metabolism and endogenous glucose production; therefore, the liver is crucial for systemic glucose and lipid homeostasis [60]. Fatty liver disease (FLD), which primarily includes alcoholic liver disease (ALD) and NAFLD, encompasses a broad spectrum of pathological changes of the liver, ranging from simple steatosis to steatohepatitis, and liver fibrosis, with eventual progression to cirrhosis and hepatocellular carcinoma (HCC) [61–64]. Moreover, FLD is also associated with extrahepatic manifestations, such as fatal and nonfatal CVDs, leading to an increased morbidity and mortality [65–69]. Although debate continues over the causal relationship between NAFLD and CVDs, many mechanistic and longitudinal studies have indicated that NAFLD is one of the major driving forces for CVDs, and NAFLD should be recognized as an independent risk factor for CVDs apart from other metabolic disorders [66–68, 70–72]. Mechanistically, dysfunction of the glucose and lipid metabolism, activation of low-grade systemic inflammation and oxidative stress, disturbance of immunologic and neuroendocrine homeostasis, activation of the prothrombotic system, intestinal dysbiosis, and some genetic and epigenetic factors for liver diseases, such as NAFLD, may contribute to CVDs [65, 66]. Therefore, the contribution of FLD to CVDs also establishes the liver-heart axis.

3.1.2. Hepatokines Link the Liver to Heart. Besides the mentioned mechanisms above, changes in protein secretions from the fatty liver also contribute to the pathogenesis of CVDs [16, 65, 67, 73–76]. The liver has recently been recognized as an endocrine organ that secretes hepatokines, which are proteins secreted by hepatocytes that can influence metabolic processes through autocrine, paracrine, and endocrine signaling [10–12]. The hepatocyte protein secretome undergoes marked changes in response to liver

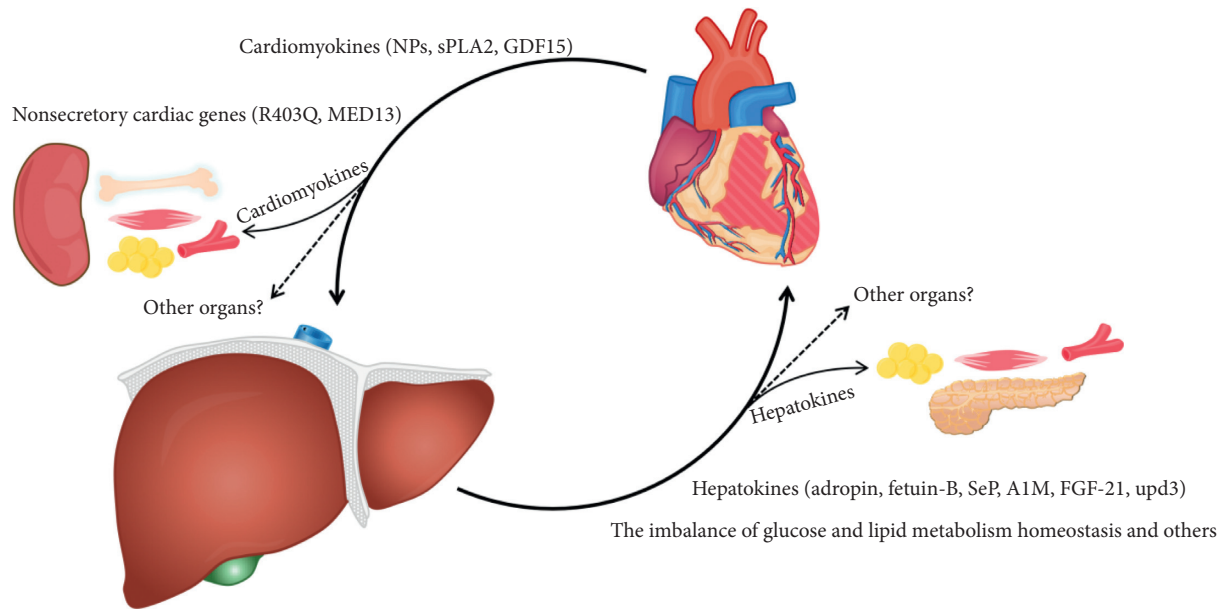


FIGURE 2: The modern molecular biological basis of liver-heart axis and heart-liver axis. The liver is sensitive to hemodynamic changes, the liver and heart are connected via blood circulation, pathologically, certain liver disease may cause heart diseases and vice versa. In molecular biology, cardiomyokines secreted from cardiomyocytes, such as natriuretic peptides (NPs), secreted phospholipase A2 (sPLA2), and growth differentiation factor 15 (GDF15), link the heart to liver. Besides the heart, blood vessels, and liver, several cardiomyokines also target other remote organs, for example, kidneys, bone, skeletal muscles, and adipose tissues. The nonsecretory cardiac genes, such as familial hypertrophic cardiomyopathy-(HCM-) causing mutation in myosin (R403Q) and Mediator complex subunit 13 (MED13), may also influence liver metabolism. Conversely, the hepatokines, for example, adropin, fetuin-B, selenoprotein P (SeP), α 1-microglobulin (A1M), fibroblast growth factor-21 (FGF-21), and unpaired 3 (upd3), act as novel linkers connecting the liver to heart. Additionally, some hepatokines also link the liver to adipose tissue, skeletal muscle, blood vessels, pancreas, and others. Moreover, the imbalance of hepatic glycolipid metabolism homeostasis, as well as other factors involved in liver diseases, may also contribute to cardiovascular diseases (CVDs).

steatosis, for example, Meex et al. have identified 168 hepatokines, of which 32 were differentially secreted in steatotic versus nonsteatotic hepatocytes, thus promoting insulin resistance and other metabolic complications [11, 77]. Increased intrahepatic levels of triglyceride (TG) induce the changes in hepatokine transcription and endoplasmic reticulum processing, leading to decrease the secretion of some hepatokines (such as sex hormone-binding globulin (SHBG), angiopoietin-like protein 4 (ANGPTL4), and adropin) during steatosis and increase the secretion of other hepatokines (such as fetuin-A, fetuin-B, hepassocin, leukocyte cell-derived chemotaxin 2 (LECT2), retinol-binding protein 4 (RBP4), and selenoprotein P (SeP)) [11]. Key hepatokines can induce either negative (fetuin-A, fetuin-B, hepassocin, LECT2, RBP4, and SeP) or positive (SHBG, fibroblast growth factor-21 (FGF-21), ANGPTL4, and adropin) metabolic effects [11, 78]. In addition to signaling to hepatocytes, most importantly, hepatokines function systemically through transporting to and communicating with distant target tissues, including the skeletal muscle, adipose tissue, pancreas, blood vessels, and heart [10, 11, 13, 16, 79] (Figure 2, right).

Adropin is a nutritionally regulated peptide hormone, secreted primarily by the liver and brain, and it is central to the control of cardiac fuel metabolism [80, 81]. Its expression was declined in the liver with genetically induced obesity or high-fat diet (HFD)-induced obesity, transgenic overexpression or systemic adropin treatment protects against

hepatic steatosis, and hyperinsulinemia associated with obesity; therefore, adropin acts as a positive factor governing glucose and lipid homeostasis [80, 81]. Altamimi et al. showed that adropin has an important role in regulating cardiac energy substrate preference through enhancing insulin signaling, stimulating glucose oxidation and inhibiting fatty acid oxidation in the heart of C57Bl/6 mice [82]. They proposed signaling pathways that are modulated by adropin: adropin, possibly via a plasma membrane receptor, such as G-protein coupled receptor 19 (GPR19) or some other mediators, reduces pyruvate dehydrogenase kinase 4 (PDK4) protein levels and stimulates ERK1/2 MAPK, which is also known to regulate PDK4 expression, resulting in a decrease in the inhibitory phosphorylation of pyruvate dehydrogenase (PDH), the rate limiting glucose oxidation enzyme, leading to its activation and enhancement of glucose oxidation [82]. On the other hand, adropin treatment appears to reduce JNK phosphorylation, which otherwise inhibits insulin receptor substrate 1 (IRS-1) signaling, thus resulting in an overall stimulation of insulin signaling including phosphorylation of Akt (protein kinase B), FOXO1 (forkhead box O1, further reduces PDK4 expression), and AS160 (Akt substrate of 160 kDa, increases glucose transporter 4 (GLUT4) plasmalemmal translocation and glucose uptake), and inhibitory phosphorylation of GSK3 β (glycogen synthase kinase 3 beta, enhances glycogen synthesis) [82]. All these above lead to a net enhancement of insulin sensitivity and glucose metabolism and utilization [82]. The

beneficial effect of adropin exposure on the impaired cardiac glucose oxidation was also confirmed in prediabetic obese mice under HFD conditions [83]. In detail, adropin reduces the expression of mitochondrial acetyltransferase enzyme general control of amino acid synthesis 5 like 1 (GCN5L1), which results in decreasing the fuel metabolism enzyme PDH lysine acetylation, thus increasing the activity of PDH to favor cardiac glucose utilization in HFD-induced prediabetic obese mice [83]. In addition, adropin has the antiatherosclerotic effects by suppressing monocyte-endothelial cell adhesion and smooth muscle cell proliferation [84]. These studies all used the exogenous adropin to evaluate its role in the heart; however, the physiological and pathological roles of endogenous adropin in heart homeostasis still need further investigation.

α 1-Microglobulin (A1M) is a 26 kDa plasma and tissue protein, which is mainly synthesized in the liver, but also in smaller amounts in peripheral organs [85–87]. A cross-sectional study showed a significant association between urinary A1M-creatinine ratio and NAFLD [88]. Hakuno et al. have identified A1M as an Akt-activating hepatokine by screening the effects of conditioned media on doxorubicin- or hypoxia-induced cardiomyocytes stress in vitro, and the in vivo study also confirmed that A1M is produced by the liver rather than the heart [89]. A1M is secreted into the blood stream, from the liver, and found in blood as complexes with IgA, albumin, and prothrombin (1 μ M) and in its free form (1 μ M) [86, 90, 91]. After secretion from the liver, A1M is transiently distributed in the infarct and border zones via infiltrated macrophages (MQs) and cardiac fibroblasts during the acute phase of mouse myocardial infarction (MI) [89]. Functionally, A1M enhances MQs migration as well as the proinflammatory response in cardiac fibroblasts and MQs in vitro, intramyocardial administration of recombinant murine A1M augment MQs infiltration, inflammation, and matrix metalloproteinase-9 (MMP-9) mRNA expression in the infarct and border zones, disturbs fibrotic repair, and drives cardiac rupture during the acute phase of MI in vivo [89]. These actions of A1M were partly mediated by its binding to phosphatidic acid (PA) [89]. Therefore, short-term, systemic delivery of CU-3, a selective inhibitor of diacylglycerol kinase alpha (DGK α) mediated PA biosynthesis, reduced MQs infiltration, inflammation, and MMP activity during the acute phase, and further mitigated left ventricular remodeling during the chronic phase in mouse MI [89]. This study indicates that targeting hepatic A1M expression and the MQs A1M signaling could be the promising options to mitigate adverse left ventricular remodeling in MI.

SeP (encoded by SELENOP in humans) contains ten selenocysteine residues and functions as a selenium supply protein, and it is primarily produced and secreted by liver [92–95]. SeP causes insulin resistance, at least partly, by dephosphorylating adenosine monophosphate-activated protein kinase (AMPK) [92]. A recent study using SeP knockout (KO) mice and hepatic overexpression of SeP in SeP KO mice indicated that the endogenous SeP mediates the deleterious effect of myocardial I/R injury [96]. SeP gene deletion reduces I/R-induced myocardial apoptosis by

increasing the phosphorylation of insulin-like growth factor 1 (IGF1) receptor, Akt, ERK, and S6K, which were reversed by overexpressing SeP in the liver of SeP KO mice [96]. Thus, SeP serves as a hepatokine that contributes to myocardial I/R injury.

Fetuin-B, also a secreted hepatocyte factor, was upregulated in humans with liver steatosis and patients with type 2 diabetes, and it impairs insulin action in myotubes and hepatocytes and causes glucose intolerance in mice, while silencing of fetuin-B in obese mice improves glucose tolerance [77]. The increased expression of fetuin-B in diabetic liver exacerbates myocardial I/R injury and cardiac dysfunction, while suppression of fetuin-B exerts cardiac protective effects [16]. Mechanistically, fetuin-B interacts with insulin receptor- β subunit, impairs cardiac insulin signaling, and consequently causes myocardial I/R injury [16]. Therefore, this study confirmed that fetuin-B is a novel linker from the liver to heart I/R injury.

In contrast to the disturbed effects of hepatic A1M, SeP, and fetuin-B for heart repair after myocardial I/R injury, FGF-21 is beneficial for cardiac repair after MI [97]. In 2000, murine and human FGF-21 were identified by Nishimura et al., and they found that FGF-21 mRNA was most abundantly expressed in the liver and also expressed in the thymus at lower levels [98]. Studies in the past few years indicated that FGF-21 is also synthesized in several other tissues, such as pancreas, skeletal muscle, and adipose tissue [99–103]. The pharmacological effects of FGF-21 are mediated by both its central and peripheral actions and by its fine-tuning of interorgan metabolic crosstalk [78]. Recently, during investigating the cardiac effect and mechanism of interleukin (IL)-22 after MI, Tang et al. found that IL-22 promoted hepatocyte-derived FGF-21 production depending on hepatic signal transducer and activator of transcription-3 (STAT-3) activation [97]. Subsequently, FGF-12 arrived at the heart and bound its functional receptor fibroblast growth factor receptor 1 (FGFR-1) in cardiomyocytes, thus modulating the expression of genes that are involved in cholesterol homeostasis, DNA repair, peroxisome, oxidative phosphorylation, glycolysis, apoptosis, and steroid responses, all of which contributed to the survival of cardiomyocytes [97]. Therefore, hepatic STAT3-FGF-21 axis modulated by IL-22 contributes to liver-heart crosstalk and is an essential mechanism for injury repair after MI [97].

Recently, Huang et al. demonstrated an IL-6-like proinflammatory cytokine unpaired 3 (upd3) expressed in *Drosophila* oenocytes (a hepatocyte-like tissue) mediated interorgan communication between the liver and heart [104]. They found that the impaired peroxisomal import in aged *Drosophila* oenocytes promotes ROS production and JNK activation and then induces upd3 as a peroxikine in aged oenocytes, this peroxikine signals to the heart and nonautonomously activates the JAK-STAT pathway in cardiomyocytes, and thus, it causes arrhythmia [104]. This study indicates that peroxisome is a central regulator of inflammaging and liver-heart communication via mediating hepatic peroxikine (also can be termed as “hepatokine”)

production. However, the roles of hepatic peroxisomes in age-related heart diseases in human and other mammalian animals are not clear.

Therefore, hepatokines act as essential linkers from the liver to heart in the pathological conditions not limited to NAFLD-related CVDs, but also in myocardial I/R injury and in ageing-related heart diseases, thus establishing a set of liver-heart axes.

3.2. The Heart-Liver Axis in Modern Medicine

3.2.1. Heart Diseases Affecting the Liver. Heart failure leads to a chronic inability to meet metabolic requirements of the end organs or skeletal muscle; therefore, the syndrome of heart failure is characterized by organ crosstalks, for example, the well-established “cardiorenal syndrome” [17, 105]. The liver is an organ sensitive to hemodynamic changes, and hepatic involvement in the form of cardiohepatic interaction has been described in patients with acute and chronic heart failure [17, 18, 52, 53]. The mechanisms underlying the cardiac hepatopathy are reduced arterial perfusion, whose deleterious effects are amplified by concomitant hypoxia, and passive congestion secondary to increased systemic venous pressure [53]. The arterial hypoperfusion predominates in acute heart failure leading to hypoxic hepatitis, while chronic passive congestion prevails in congestive hepatopathy secondary to chronic heart failure, and the chronic passive congestion leads to sinusoidal hypertension, centrilobular fibrosis, and ultimately, cirrhosis (“cardiac cirrhosis”) and HCC after several decades of ongoing injury [53, 106]. These forward and backward factors often coexist and potentiate each other [53].

Atrial fibrillation (AF) is the most common among the severe cardiac arrhythmias, which is associated with a high risk of thromboembolism and stroke [107]. AF activates the coagulation system, leading to prothrombotic or hypercoagulable state [107, 108]. The liver is an essential organ synthesizing many coagulation factors and other prothrombotic molecules [108]. Using rapid atrial pacing (RAP) rat model, Yaegashi et al. found that short-term RAP mimicking paroxysmal AF markedly altered the hepatic gene expression profile, and hepatic mRNA levels of prothrombotic molecules, including fibrinogen chains, prothrombin, coagulation factor X, and anti-thrombin III, were augmented by short-term RAP [108]. The activation of the IL-6/STAT3 signaling pathway is responsible for the augmented fibrinogen and coagulation factor X production by RAP [108]. Therefore, IL-6 neutralizing antibody pretreatment inhibited RAP-mediated hepatic STAT3 phosphorylation and fibrinogen and coagulation factor X expression [108]. This indicated that the cardiohepatic interactions are also involved in AF-related hypercoagulation.

3.2.2. Cardiomyokines Link the Heart to Liver. The breakthrough discovery of cardiac NPs by de Bold provided the first direct evidence that the heart has an endocrine function

[6, 7]. They found that the extracts derived from atrial muscle (atrial natriuretic peptide, ANP) caused a rapid, more than 30-fold increase of sodium and chloride excretions, while urine volume rose 10-fold, and potassium excretion doubled [7]. They concluded that the atrial extract contained an extremely powerful inhibitor of renal tubular NaCl reabsorption [7]. In 1988, Sudoh et al. discovered a new natriuretic peptide of 26 amino-acid residues in porcine brain, eliciting possesses diuretic-natriuretic (e.g., increase in urine output, Na⁺, K⁺, and Cl⁻ excretion) and hypotensive (decrease in mean blood pressure) responses similar to that of ANP, and they have designated the peptide “brain natriuretic peptide” (BNP) [6, 109], which is also localized in the secretory granules of human atrium that contain ANP [110]. Therefore, cardiac ANP- and BNP-mediated communications between the heart and kidney are essential for maintaining sodium and volume homeostasis in health and disease [6, 7, 111].

An emerging concept is that the heart not only regulates blood pressure homeostasis and water-salt balance but also acts as a regulator of whole body metabolism [14, 112–115]. The cardiac NPs are modulators of metabolism, and they induce human fat cell lipolysis and the “browning” of white adipocytes, favor blood glucose control and insulin sensitivity by increasing glucose uptake in human adipocytes, and enhance mitochondrial oxidative metabolism and fat oxidation in human skeletal muscle [14, 116–119]. Moreover, ANP was shown to increase hepatic gluconeogenesis and inhibit glycolysis, in part by inhibiting pyruvate kinase activity, and the effects of ANP are mediated via activation of guanylyl cyclase-linked ANF receptors which elevate cGMP production [15]. It is clear that ANP can protect against hepatic I/R injuries [120, 121]. On the molecular mechanism, ANP activates cGMP-dependent heat shock protein 70 (HSP70) expression and correlates with enhanced binding of HSP70 to inhibitory factor kappa B ($I\kappa B$) [122], thus attenuating the activation of the proinflammatory transcription factor nuclear factor kappa B (NF- κB) and the expression of TNF- α [123, 124]; ANP also attenuates necrotic (mainly in hepatocytes and endothelial cells) and apoptotic (mainly in hepatocytes) cell death [125–127]; ANP increases the phosphorylation of p38 MAPK during liver I/R [128–130]. However, a p38 MAPK inhibitor fails to abolish ANP-mediated antiapoptotic action in the cold I/R liver [126]; the antiapoptotic effect of ANP is primarily mediated via protein kinase A (PKA) and PI-3-kinase (PI3K)-Akt pathways [125–127]. In addition, ANP prevents dimethylnitrosamine (DMN)-induced hepatic fibrosis in rats [131] and antagonizes endothelin-1 (ET-1)-induced calcium increase and cell contraction in cultured human hepatic stellate cells (HSCs) [132]. Therefore, NPs act as an endocrine linker between the heart and liver.

Besides NPs, cardiomyocytes also secrete other peptide hormones through secretory granules, and these proteins are referred as “cardiomyokines” [8, 9]. Most of such cardiomyokines function as autocrine or paracrine factors, and several cardiomyokines target remote organs as endocrine factors, which act on not only blood vessels and kidneys, but also skeletal muscles, bone, adipose tissues, and liver

[8, 14, 15, 133] (Figure 2, left). These cardiomyokines are essential cardiometabolic hormones, for example, the cardiac-specific FGF-21 overexpression mice display upregulation of plasma FGF-21 levels and show a reduction in body weight and lean body mass, whereas increasing fat mass [134]; the osteocrin secreted from the heart contributes to bone formation in zebrafish [133]. Therefore, the heart is a central regulator of metabolism and energy homeostasis in noncardiac tissues, including the liver, and this further highlights the important roles of the crosstalk between the heart and liver [117, 135].

Carlos Fernandez-Patron group has identified a unique heart secreted phospholipase A2 (sPLA2), and MMP-2 is a negative regulator of sPLA2 activity [136, 137]. Under physiological conditions, MMP-2 activity maintains low levels of certain chemokines, such as monocyte chemoattractant protein-3 (MCP-3, encoded by *Ccl7*, an agonist of cardiac sPLA2), by cleavage of MCP-3 at a glycine/isoleucine bond [136]. Cleaved MCP-3 binds to CC-chemokine receptors-1, -2, and -3, but no longer induces calcium fluxes or promotes chemotaxis, and instead acts as a general chemokine antagonist that dampens inflammation [136, 138]. MMP-2 deficiency (functional blockade or genetic deletion) or MCP-3 may trigger cardiac sPLA2 release from the heart, which leads to cardiac inflammation and disturb cardiac metabolic homeostasis [136, 137]. Moreover, MMP-2 deficiency causes excess sPLA2 activity, which, in turn, elevates hepatic PGE2 [137]. PGE2 is a kind of vasodilatory prostanooids, treatment with either varespladib (sPLA2 inhibitor) or indomethacin inhibited PGE2-triggered acute hypertension selectively in MMP-2^{-/-}, but not in wild-type mice [137]. The cardiac sPLA2 circulates in the plasma, reaching distant target organs (e.g., the liver), contributes to the hepatic inflammatory and lipid metabolic phenotype in the liver of MMP-2 deficiency, for example, increasing liver TG and plasma very low-density lipoprotein (VLDL) TG levels [136]. Therefore, MMP-2/cardiac sPLA2 system may serve multiple purposes including signaling to the liver to modulate hepatic inflammation and lipid metabolism, and maintaining systemic blood pressure homeostasis [136].

It is known that growth hormone (GH)-IGF1 signaling is a dominant mechanism regulating postnatal mammalian growth [139–144]. GH secreted from the pituitary signals to the liver to stimulate the production of IGF1, IGF binding protein 3 (IGFBP3), and IGFBP acid-labile subunit (IGFALS) via the JAK2-STAT5 pathway [139, 145]. Circulating IGF1 forms a ternary complex with IGFBP3 and IGFALS and is a major mediator of GH's effect on mammalian postnatal body growth [139, 140, 142, 146]. Recently, Wang et al. have revealed that the levels of growth differentiation factor 15 (GDF15) in the heart and plasma are elevated in a mice model of primary pediatric cardiomyopathy with secondary failure to thrive (FTT), and the plasma GDF15 levels are elevated in children with concomitant heart disease and FTT [139]. They showed that pediatric heart disease induces GDF15 synthesis and secretion by cardiomyocytes, circulating GDF15 in turn acts on the liver to inhibit GH signaling, and specifically knockdown GDF15 in Cre⁺ cardiomyocytes by AAV9-

Sico-mouse *Gdf15* shRNA normalizes the circulating GDF15 levels and restores liver GH signaling, establishing GDF15 as a bona fide heart-derived hormone that negatively regulates pediatric body growth via heart-liver axis mediated to suppress hepatic GH signaling [139]. In addition, hepatic and serum GDF15 levels are increased in the nonalcoholic steatohepatitis (NASH) mouse model and in patients with NASH or advanced fibrosis [147, 148]. Using GDF15-knockout mice and liver-specific GDF15-transgenic mice, Kim et al. revealed that induction of endogenous GDF15 is a compensatory mechanism to protect against the progression of NASH [147]. However, the influence of cardiac GDF15 on NAFLD/NASH is not clear.

3.2.3. *The Nonsecretory Cardiac Genes Influence Liver Metabolism.*

There is a clear link between liver dysfunction, specifically NAFLD, and cardiac dysfunction, but new evidence suggests that the reverse is also true, such as those discussed in Section 3.2.1 [66, 135, 149]. Magida and Leinwand had demonstrated that decreased left ventricular contractile function in male, but not in female, familial hypertrophic cardiomyopathy (HCM) mice (contained two mutations, a point mutation, R403Q, and a deletion of 59 amino acids in the actin-binding site bridged by the addition of nine nonmyosin amino acids), is associated with reduced capacity for ventricular fatty acid release and uptake, thus diminishing myocardial lipid (TG and fatty acid) and ATP content [150]. However, the basis for the phenotypic gender differences in HCM mice is unclear, and whether this is related to the protective effects of estrogen (E₂) on cardiac energetics as well as liver metabolism still needs further investigation [135]. Since the heart is a principal lipolytic organ, the proposed defects in lipid clearance by the HCM heart result in elevated the levels of oleic acid and TG in circulating VLDLs and the liver [150]. Mechanistically, the reduced expression of cardiac fatty acid translocase (CD36), lipoprotein lipase, and VLDL receptor, and the decreased activities of CD36 and its regulator AMPK in the heart are responsible for these metabolic defects in HCM mice [150]. Moreover, as the activator of CD36 expression and fatty acid uptake, the expression of myocardial transcription factor FOXO1 was also reduced in the male HCM mice [150]. HCM-induced oleic acid accumulation and PKC α -mediated p38 MAPK activation in the liver facilitated the phosphorylation and stabilization of hepatic peroxisome proliferator-activated receptor- γ coactivator-1 α (PGC-1 α) [150–152]. PGC-1 α drove hepatocyte nuclear factor-4 and phosphoenolpyruvate carboxykinase (PEPCK) expression in the liver and subsequently induced PEPCK-mediated gluconeogenesis and increased blood glucose levels [150, 152]. Importantly, features of ventricular architecture and contractile dysfunction in HCM mice can be rescued either by restoring the energetic deficit at the level of the cardiomyocyte via AMPK agonist, or by blocking the deleterious elevation in hepatic glucose output using the PEPCK inhibitor 3-mercaptopicolinic acid (3-MPA) [135, 150]. Certainly, the relationship between the heart and liver is not monogamous, and other tissues, such as skeletal muscle,

adipose, and pancreas, are likely to be directly affected by the elevated circulating oleic acid and VLDL TG levels [135]. Therefore, these findings raise the interesting concept that the lack of use of a specific metabolic substrate by one tissue directly affects another, perhaps revealing an intertissue homeostatic feedback mechanism [135].

The subunits of Mediator (MED) are key molecules maintaining metabolic homeostasis [40, 153]. Mediator is a multiprotein complex that acts as a bridge between DNA-bound transcription factors and RNA polymerase II (RNAPII) [153]. Mediator contains 25 (yeast) or 30 (human) subunits organized into four modules: head, middle, tail, and kinase [154, 155]. The head module together with the middle module plays an essential role during the preinitiation complex assembly, contacting the RNAPII and stabilizing its interaction with the general transcription factors, while the tail interacts with sequence-specific transcription factors [153–156]. The kinase module associates reversibly with Mediator and has negative and positive regulatory roles in transcription [154, 155]. MED1 is required for peroxisome proliferator-activated receptor (PPAR) α -regulated gene (including those involved in fatty acid oxidation) expression in the liver [157], and for PPAR γ -mediated differentiation of mouse embryonic fibroblasts to adipocytes [158]; moreover, it plays important roles in regulating glucose and energy metabolism in skeletal muscle [159]. MED15 is a key effector of sterol regulatory element binding protein (SREBP)-dependent gene regulation and lipid homeostasis in metazoans [160]. Grueter et al. had revealed that heart regulates systemic energy homeostasis via MED13; MED13, in turn, is negatively regulated by a heart-specific microRNA, miR-208a [153]. They also find that MED13-dependent signaling from the heart confers leanness by enhancing metabolism in the adipose tissue and liver [40]. The interorgan communication in transgenic mice with enhanced cardiac MED13 expression (MED13cTg mice) is controlled by circulating factors that enhance white adipose tissue and liver metabolism [40]. However, the circulating factors responsible for this phenotype still need further investigation.

4. Perspective

In Modern Medicine, the liver and heart are anatomically and physiologically connected with each other primarily via “blood circulation.” Moreover, organokines are essential mediators of organ crosstalk between the liver and heart (the heart and liver) (Figure 2). The pathophysiological interactions between the liver and heart (the heart and liver) can be classified into three groups in Modern Medicine [17, 18, 52, 53, 106, 108]: (1) liver disease resulting from the heart disease; (2) heart disease resulting from the liver disease; (3) conditions, e.g., systemic amyloidosis, affecting the heart and the liver at the same time. In TCM, the liver and heart are physiologically connected with each other primarily via “blood movement” and “qing-zhi regulation.” Heart can modulate the pathophysiology of the liver based on the TCM theory of “illness of the child-organ involving the mother-organ,” and liver can influence the pathophysiology of the heart based on the TCM theory of “mother-

organ disorder involving its child-organ,” respectively (Figure 1). Thus, the coronary heart disease can be treated from the liver based on the TCM theory of “treating the heart disease from the liver” [24–26], and NAFLD can be treated by the methods of “Xing-Qi-Huo-Xue” and “Bu-Xue” in the clinical practice of TCM [27–30]. Therefore, the evidences from TCM to Modern Medicine, and from basic research studies to clinical investigations, show that there exists interorgan crosstalk between the liver and heart (the heart and liver).

The interorgan communication between the liver and heart (the heart and liver) improves our understandings on the physiological or pathophysiological phenomena of these two organs. However, human body is a complex living organism. In addition to monogenic inherited disease, most liver and heart diseases are regulated by the complex internal environment of the body and the external environment. Therefore, both identified and unidentified cardiomyokines and hepatokines might have the interactive network during modulating liver and heart homeostasis. Besides these organokines, EVs (e.g., exosome and migrasome) are the key messengers in interorgan communication, and certain nonsecretory gene-mediated multiple signals are also important in mediating interorgan communication [5, 34–42]. However, the network and detail roles of these mediators in modulating hepatocardiac or cardiohepatic interaction still need further investigation.

TCM emphasizes steady-state balance (homeostasis) and systematization/integrity, and its treatment principle tends to individualized medicine. The basic characteristics of the theoretical system of TCM are holistic concept and treatment based on the differentiation of syndrome. How to use the philosophical thinking of TCM to promote the progress of Western Medicine is worth pondering. Moreover, it is also interesting to investigate whether the relationships between the liver and heart (the heart and liver) in TCM can be explained by Modern Medicine. Therefore, we hope that the integrated Traditional Chinese and Western Medicine will contribute to the research of the liver-heart (the heart-liver) interaction network and promote the future medical progress.

Data Availability

The data supporting this review are from previously reported studies and datasets, which have been cited.

Conflicts of Interest

The authors declare that they have no conflicts of interest.

Acknowledgments

The authors thank the Research Center for Integrative Medicine of Guangzhou University of Chinese Medicine (Key Laboratory of Chinese Medicine Pathogenesis and Therapy Research) for Traditional Chinese Medicine information/reference support. This work was supported by the National Natural Science Foundation of China (grant no.

81900376), the Natural Science Foundation of Guangdong Province (grant no. 2018A030313657), and the Project funded by China Postdoctoral Science Foundation (grant no. 2019M653238).

References

- [1] T. Deng, "Five-viscera correlation theory replacing five-element theory," *Journal of Guangzhou University of Traditional Chinese Medicine*, vol. 5, no. 2, pp. 65–68, 1988.
- [2] T. Deng and H. Zheng, "Study on the theory of five organs correlation—from five elements to five organs correlation," *Strategic Study of CAE*, vol. 10, no. 2, pp. 7–13, 2008.
- [3] S. Qiu, J. Chen, and B. Cheng, "The discuss on Chinese medical science theory about correlation of five viscera," *Journal of Hubei Institute for Nationalities (Medical Edition)*, vol. 24, no. 1, pp. 1–5, 2007.
- [4] H. Sun and S. Qiu, "Research on heart-liver correlation in Yin-Yang, Qi-blood, meridians from the Yellow Emperor's Canon of medicine," *Journal of Liaoning University of Traditional Chinese Medicine*, vol. 14, no. 4, pp. 110–112, 2012.
- [5] J. Castillo-Armengol, L. Fajas, and I. C. Lopez-Mejia, "Inter-organ communication: a gatekeeper for metabolic health," *EMBO Reports*, vol. 20, no. 9, p. e47903, 2019.
- [6] E. Hardy-Rando and C. Fernandez-Patron, "Emerging pathways of communication between the heart and non-cardiac organs," *Journal of Biomedical Research*, vol. 33, no. 3, pp. 145–155, 2019.
- [7] A. J. de Bold, H. B. Borenstein, A. T. Veress, and H. Sonnenberg, "A rapid and potent natriuretic response to intravenous injection of atrial myocardial extract in rats," *Life Sciences*, vol. 28, no. 1, pp. 89–94, 1981.
- [8] A. Chiba, H. Watanabe-Takano, T. Miyazaki, and N. Mochizuki, "Cardiomyokines from the heart," *Cellular and Molecular Life Sciences*, vol. 75, no. 8, pp. 1349–1362, 2018.
- [9] C. C. Glembotski, "Functions for the cardiomyokine, MANF, in cardioprotection, hypertrophy and heart failure," *Journal of Molecular and Cellular Cardiology*, vol. 51, no. 4, pp. 512–517, 2011.
- [10] S. O. Jensen-Cody and M. J. Potthoff, "Hepatokines and metabolism: deciphering communication from the liver," *Molecular Metabolism*, vol. 44, p. 101138, 2020.
- [11] R. C. R. Meex and M. J. Watt, "Hepatokines: linking non-alcoholic fatty liver disease and insulin resistance," *Nature Reviews Endocrinology*, vol. 13, no. 9, pp. 509–520, 2017.
- [12] M. J. Watt, P. M. Miotto, W. De Nardo, and M. K. Montgomery, "The liver as an endocrine organ-linking NAFLD and insulin resistance," *Endocrine Reviews*, vol. 40, no. 5, pp. 1367–1393, 2019.
- [13] N. Stefan and H. U. Haring, "The role of hepatokines in metabolism," *Nature Reviews Endocrinology*, vol. 9, no. 3, pp. 144–152, 2013.
- [14] V. Cannone, A. Cabassi, R. Volpi, and J. C. Burnett Jr., "Atrial natriuretic peptide: a molecular target of novel therapeutic approaches to cardio-metabolic disease," *International Journal of Molecular Sciences*, vol. 20, no. 13, p. 3265, 2019.
- [15] H. M. Rashed, B. G. Nair, and T. B. Patel, "Regulation of hepatic glycolysis and gluconeogenesis by atrial natriuretic peptide," *Archives of Biochemistry and Biophysics*, vol. 298, no. 2, pp. 640–645, 1992.
- [16] W. Xing, Y. Tan, K. Li, P. Tian, F. Tian, and H. Zhang, "Upregulated hepatokine fetuin B aggravates myocardial ischemia/reperfusion injury through inhibiting insulin signaling in diabetic mice," *Journal of Molecular and Cellular Cardiology*, vol. S0022-2828, no. 20, pp. 30057–30062, 2020.
- [17] M. B. Yilmaz, M. Nikolaou, and A. Mebazaa, "Cardiohepatic interactions in heart failure," *Anadolu Kardiyoloji Dergisi*, vol. 13, no. 7, pp. 731–732, 2013.
- [18] O. M. Silvestre, F. Bacal, R. O. Ximenes, F. J. Carrilho, L. A. D'Albuquerque, and A. Q. Farias, "Cardiohepatic interactions—from humoral theory to organ transplantation," *Arquivos Brasileiros de Cardiologia*, vol. 102, no. 6, pp. e65–e67, 2014.
- [19] G. Poelzl and J. Auer, "Cardiohepatic syndrome," *Current Heart Failure Reports*, vol. 12, no. 1, pp. 68–78, 2015.
- [20] G. Zhao, F. Tang, Y. Dai et al., "Analysis of the physiology, pathology, clinic of "mother-child relationship of liver and heart" in TCM five elements theory," *Journal of Traditional Chinese Medicine University of Hunan*, vol. 38, no. 4, pp. 413–416, 2018.
- [21] X. Liu, S. Qiu, H. Zheng, and T. Deng, "Research on Deng Tietao's "five-zang correlation theory" (邓铁涛"五脏相关"理论研究)," *Journal of Basic Chinese Medicine*, vol. 14, no. 1, pp. 20–22, 2008.
- [22] X. Fang, "Theory of phlegm and blood stasis and syndrome differentiation and treatment of coronary heart disease (痰瘀学说与冠心病辨治)," *Guangxi Journal of Traditional Chinese Medicine*, vol. 36, no. 5, pp. 50–51, 2013.
- [23] X. Fang and T. Deng, "Clinical observation on 52 cases of coronary heart disease treated by Yi-Qi-Chu-Tan-Fang (益气除痰方治疗冠心病52例疗效观察)," *Guangxi Journal of Traditional Chinese Medicine*, vol. 11, no. 6, pp. 1–3, 1988.
- [24] D. Fu, "The summary of treatment heart disease from liver (心病治肝举要)," *Acta Chinese Medicine and Pharmacology*, no. 3, pp. 8–9, 1987.
- [25] Z. Zhao, "Professor Lu Zhizheng's experience in treating Xin-Bi from liver (路志正教授从肝论治心痹的经验)," *Journal of New Chinese Medicine*, no. 9pp. 5–6, 1991.
- [26] Y. Zhao, H. Wu, X. Ruan, and T. Deng, "Treatment of coronary heart disease from five viscera correlation (从五脏相关论治冠心病)," *Journal of Sichuan of Traditional Chinese Medicine*, vol. 17, no. 11, pp. 12–13, 1999.
- [27] Y. Zhang, G. Zhou, Z. Chen et al., "Si-Wu-Tang alleviates nonalcoholic fatty liver disease via blocking TLR4-JNK and caspase-8-GSDMD signaling pathways," *Evidence-based Complementary and Alternative Medicine*, vol. 2020, Article ID 8786424, 11 pages, 2020.
- [28] H. F. Chiu, Y. H. Wu, Y. C. Shen, S. J. Wang, K. Venkatakrishnan, and C. K. Wang, "Antioxidant and physiological effects of Si-Wu-Tang on skin and liver: a randomized, double-blind, placebo-controlled clinical trial," *Chinese Medicine*, vol. 11, p. 30, 2016.
- [29] J. Zheng and B. Lu, "Effect of the Xingqi Huoxue Qushi prescription on mice model of nonalcoholic steatohepatitis," *Chinese Journal of Integrated Traditional and Western Medicine on Liver Diseases*, vol. 30, no. 6, pp. 527–530+554, 2020.
- [30] X. Bao, "Clinical observation on 26 cases of nonalcoholic steatohepatitis treated with Shugan Xingqi Huoxue Decoction (疏肝行气活血汤治疗非酒精性脂肪性肝炎26例临床观察)," *Hunan Journal of Traditional Chinese Medicine*, vol. 30, no. 7, pp. 56–58, 2014.
- [31] F. Armutcu, "Organ crosstalk: the potent roles of inflammation and fibrotic changes in the course of organ

- interactions,” *Inflammation Research*, vol. 68, no. 10, pp. 825–839, 2019.
- [32] M. Plauth, A. Raible, M. Gregor, and F. Hartmann, “Inter-organ communication between intestine and liver in vivo and in vitro,” *Seminars in Cell Biology*, vol. 4, no. 3, pp. 231–237, 1993.
- [33] C. Priest and P. Tontonoz, “Inter-organ cross-talk in metabolic syndrome,” *Nature Metabolism*, vol. 1, no. 12, pp. 1177–1188, 2019.
- [34] Y. Zhang, J. Wang, Y. Ding et al., “Migrasome and tetraspanins in vascular homeostasis: concept, present, and future,” *Frontiers in Cell and Developmental Biology*, vol. 8, p. 438, 2020.
- [35] M. A. Rogers and E. Aikawa, “MicroRNA extracellular vesicle stowaways in cell-cell communication and organ crosstalk,” *Arteriosclerosis, Thrombosis, and Vascular Biology*, vol. 39, no. 12, pp. 2448–2450, 2019.
- [36] D. Jiang, Z. Jiang, D. Lu et al., “Migrasomes provide regional cues for organ morphogenesis during zebrafish gastrulation,” *Nature Cell Biology*, vol. 21, no. 8, pp. 966–977, 2019.
- [37] B. Gao, M. F. Ahmad, L. E. Nagy, and H. Tsukamoto, “Inflammatory pathways in alcoholic steatohepatitis,” *Journal of Hepatology*, vol. 70, no. 2, pp. 249–259, 2019.
- [38] M. Nawaz, N. Shah, B. R. Zanetti et al., “Extracellular vesicles and matrix remodeling enzymes: the emerging roles in extracellular matrix remodeling, progression of diseases and tissue repair,” *Cells*, vol. 7, no. 10, p. 167, 2018.
- [39] M. Nakamura and J. Sadoshima, “Heart over mind: metabolic control of white adipose tissue and liver,” *EMBO Molecular Medicine*, vol. 6, no. 12, pp. 1521–1524, 2014.
- [40] K. K. Baskin, C. E. Grueter, C. M. Kusminski et al., “MED13-dependent signaling from the heart confers leanness by enhancing metabolism in adipose tissue and liver,” *EMBO Molecular Medicine*, vol. 6, no. 12, pp. 1610–1621, 2014.
- [41] L. Yu, “Migrasomes: the knowns, the known unknowns and the unknown unknowns: a personal perspective,” *Science China Life Sciences*, vol. 64, no. 1, pp. 162–166, 2021.
- [42] M. Zhu, Q. Zou, R. Huang et al., “Lateral transfer of mRNA and protein by migrasomes modifies the recipient cells,” *Cell Research*, vol. 31, no. 2, pp. 237–240, 2021.
- [43] B. da Rocha-Azevedo and S. L. Schmid, “Migrasomes: a new organelle of migrating cells,” *Cell Research*, vol. 25, no. 1, pp. 1–2, 2015.
- [44] R. S. Miftode, I. L. Şerban, A. S. Timpau et al., “Syndecan-1: a review on its role in heart failure and chronic liver disease patients’ assessment,” *Cardiology Research and Practice*, vol. 2019, Article ID 4750580, 7 pages, 2019.
- [45] M. Izzy, L. B. VanWagner, G. Lin et al., “Redefining cirrhotic cardiomyopathy for the modern era,” *Hepatology*, vol. 71, no. 1, pp. 334–345, 2020.
- [46] T. Horvatits, A. Drolz, K. Rutter, K. Roedl, S. Kluge, and V. Fuhrmann, “[Hepatocardiic disorders: interactions between two organ systems],” *Medizinische Klinik-Intensivmedizin und Notfallmedizin*, vol. 111, no. 5, pp. 447–452, 2016.
- [47] Y. M. Fouad and R. Yehia, “Hepato-cardiac disorders,” *World Journal of Hepatology*, vol. 6, no. 1, pp. 41–54, 2014.
- [48] N. Elleuch, S. Mrabet, A. Ben Slama et al., “Cirrhotic cardiomyopathy,” *La Tunisie medicale*, vol. 98, no. 3, pp. 206–210, 2020.
- [49] M. V. H. Carvalho, P. C. Kroll, R. T. M. Kroll, and V. N. Carvalho, “Cirrhotic cardiomyopathy: the liver affects the heart,” *Brazilian Journal of Medical and Biological Research*, vol. 52, no. 2, p. e7809, 2019.
- [50] S. Wiese, J. D. Hove, F. Bendtsen, and S. Moller, “Cirrhotic cardiomyopathy: pathogenesis and clinical relevance,” *Nature Reviews Gastroenterology & Hepatology*, vol. 11, no. 3, pp. 177–186, 2014.
- [51] E. M. Zardi, A. Abbate, D. M. Zardi et al., “Cirrhotic cardiomyopathy,” *Journal of the American College of Cardiology*, vol. 56, no. 7, pp. 539–549, 2010.
- [52] S. Moller, C. W. Dumcke, and A. Krag, “The heart and the liver,” *Expert Review of Gastroenterology & Hepatology*, vol. 3, no. 1, pp. 51–64, 2009.
- [53] S. Moller and M. Bernardi, “Interactions of the heart and the liver,” *European Heart Journal*, vol. 34, no. 36, pp. 2804–2811, 2013.
- [54] A. Isaak, M. Praktikno, C. Jansen et al., “Myocardial fibrosis and inflammation in liver cirrhosis: MRI study of the liver-heart axis,” *Radiology*, vol. 297, no. 1, pp. 51–61, 2020.
- [55] C. Matyas, K. Erdelyi, E. Trojnar et al., “Interplay of liver-heart inflammatory axis and cannabinoid 2 receptor signaling in an experimental model of hepatic cardiomyopathy,” *Hepatology*, vol. 71, no. 4, pp. 1391–1407, 2020.
- [56] Y. Y. Yang, H. Liu, S. W. Nam, G. Kunos, and S. S. Lee, “Mechanisms of TNF α -induced cardiac dysfunction in cholestatic bile duct-ligated mice: interaction between TNF α and endocannabinoids,” *Journal of Hepatology*, vol. 53, no. 2, pp. 298–306, 2010.
- [57] B. Horvath, L. Magid, P. Mukhopadhyay et al., “A new cannabinoid CB2 receptor agonist HU-910 attenuates oxidative stress, inflammation and cell death associated with hepatic ischaemia/reperfusion injury,” *British Journal of Pharmacology*, vol. 165, no. 8, pp. 2462–2478, 2012.
- [58] S. Batkai, D. Osei-Hyiaman, H. Pan et al., “Cannabinoid-2 receptor mediates protection against hepatic ischemia/reperfusion injury,” *FASEB Journal*, vol. 21, no. 8, pp. 1788–1800, 2007.
- [59] B. Julien, P. Grenard, F. Teixeira-Clerc et al., “Antifibrogenic role of the cannabinoid receptor CB2 in the liver,” *Gastroenterology*, vol. 128, no. 3, pp. 742–755, 2005.
- [60] Y. Zhang, J. Xu, and H. Yang, “Hydrogen: an endogenous regulator of liver homeostasis,” *Frontiers in Pharmacology*, vol. 11, p. 877, 2020.
- [61] B. Gao and R. Bataller, “Alcoholic liver disease: pathogenesis and new therapeutic targets,” *Gastroenterology*, vol. 141, no. 5, pp. 1572–1585, 2011.
- [62] R. Parker, S. J. Kim, and B. Gao, “Alcohol, adipose tissue and liver disease: mechanistic links and clinical considerations,” *Nature Reviews Gastroenterology & Hepatology*, vol. 15, no. 1, pp. 50–59, 2018.
- [63] J. Zhou, F. Zhou, W. Wang et al., “Epidemiological features of NAFLD from 1999 to 2018 in China,” *Hepatology*, vol. 71, no. 5, pp. 1851–1864, 2020.
- [64] J. Cai, M. Xu, X. Zhang, and H. Li, “Innate immune signaling in nonalcoholic fatty liver disease and cardiovascular diseases,” *Annual Review of Pathology*, vol. 14, pp. 153–184, 2019.
- [65] A. Ismaiel and D. L. Dumitraşcu, “Cardiovascular risk in fatty liver disease: the liver-heart axis-literature review,” *Frontiers in Medicine (Lausanne)*, vol. 6, p. 202, 2019.
- [66] J. Cai, X. J. Zhang, Y. X. Ji, P. Zhang, Z. G. She, and H. Li, “Nonalcoholic fatty liver disease pandemic fuels the upsurge in cardiovascular diseases,” *Circulation Research*, vol. 126, no. 5, pp. 679–704, 2020.
- [67] L. Zhang, Z. G. She, H. Li, and X. J. Zhang, “Non-alcoholic fatty liver disease: a metabolic burden promoting

- atherosclerosis," *Clinical Science (London)*, vol. 134, no. 13, pp. 1775–1799, 2020.
- [68] A. Mantovani, "Nonalcoholic fatty liver disease (NAFLD) and risk of cardiac arrhythmias: a new aspect of the liver-heart axis," *Journal of Clinical and Translational Hepatology*, vol. 5, no. 2, pp. 134–141, 2017.
- [69] Y. Zhang, S. Tan, J. Xu, and T. Wang, "Hydrogen therapy in cardiovascular and metabolic diseases: from bench to bedside," *Cellular Physiology and Biochemistry*, vol. 47, no. 1, pp. 1–10, 2018.
- [70] T. Takahashi, T. Watanabe, T. Shishido et al., "The impact of non-alcoholic fatty liver disease fibrosis score on cardiac prognosis in patients with chronic heart failure," *Heart Vessels*, vol. 33, no. 7, pp. 733–739, 2018.
- [71] Y. C. Zhao, G. J. Zhao, Z. Chen, Z. G. She, J. Cai, and H. Li, "Nonalcoholic fatty liver disease: an emerging driver of hypertension," *Hypertension*, vol. 75, no. 2, pp. 275–284, 2020.
- [72] Q. M. Anstee, A. Mantovani, H. Tilg, and G. Targher, "Risk of cardiomyopathy and cardiac arrhythmias in patients with nonalcoholic fatty liver disease," *Nature Reviews Gastroenterology & Hepatology*, vol. 15, no. 7, pp. 425–439, 2018.
- [73] R. Y. Jiang and L. Yang, "The role of hepatokines in NAFLD-related extrahepatic diseases: culprit or accomplice?" *Gut*, vol. 67, no. 3, p. 590, 2018.
- [74] H. S. Chung and K. M. Choi, "Organokines in disease," *Advances in Clinical Chemistry*, vol. 94, pp. 261–321, 2020.
- [75] H. J. Yoo and K. M. Choi, "Hepatokines as a link between obesity and cardiovascular diseases," *Diabetes & Metabolism Journal*, vol. 39, no. 1, pp. 10–15, 2015.
- [76] T. W. Jung, H. J. Yoo, and K. M. Choi, "Implication of hepatokines in metabolic disorders and cardiovascular diseases," *BBA Clinical*, vol. 5, pp. 108–113, 2016.
- [77] R. C. Meex, A. J. Hoy, A. Morris et al., "Fetuin B is a secreted hepatocyte factor linking steatosis to impaired glucose metabolism," *Cell Metabolism*, vol. 22, no. 6, pp. 1078–1089, 2015.
- [78] L. Geng, K. S. L. Lam, and A. Xu, "The therapeutic potential of FGF21 in metabolic diseases: from bench to clinic," *Nature Reviews Endocrinology*, vol. 16, no. 11, pp. 654–667, 2020.
- [79] K. Huang and H. Bai, "Liver hepatokines and peroxisomes as therapeutic targets for cardiovascular diseases," *Future Cardiology*, 2020.
- [80] B. A. Mushala and I. Scott, "Adropin: a hepatokine modulator of vascular function and cardiac fuel metabolism," *American Journal of Physiology: Heart and Circulatory Physiology*, vol. 320, no. 1, pp. H238–H244, 2021.
- [81] K. G. Kumar, J. L. Trevisan, D. D. Lam et al., "Identification of adropin as a secreted factor linking dietary macronutrient intake with energy homeostasis and lipid metabolism," *Cell Metabolism*, vol. 8, no. 6, pp. 468–481, 2008.
- [82] T. R. Altamimi, S. Gao, Q. G. Karwi et al., "Adropin regulates cardiac energy metabolism and improves cardiac function and efficiency," *Metabolism*, vol. 98, pp. 37–48, 2019.
- [83] D. Thapa, B. Xie, M. Zhang et al., "Adropin treatment restores cardiac glucose oxidation in pre-diabetic obese mice," *Journal of Molecular and Cellular Cardiology*, vol. 129, pp. 174–178, 2019.
- [84] K. Sato, T. Yamashita, R. Shirai et al., "Adropin contributes to anti-atherosclerosis by suppressing monocyte-endothelial cell adhesion and smooth muscle cell proliferation," *International Journal of Molecular Sciences*, vol. 19, no. 5, p. 1293, 2018.
- [85] T. Bratt and B. Akerstrom, "Expression of rat alpha 1-microglobulin-bikunin in baculovirus-transformed insect cells," *Protein Expression and Purification*, vol. 6, no. 4, pp. 431–438, 1995.
- [86] J. Bergwik and B. Akerstrom, "Alpha1-microglobulin binds illuminated flavins and has a protective effect against sublethal riboflavin-induced damage in retinal epithelial cells," *Frontiers in Physiology*, vol. 11, p. 295, 2020.
- [87] T. Berggard, T. D. Oury, I. B. Thogersen, B. Akerstrom, and J. J. Enghild, "Alpha1-microglobulin is found both in blood and in most tissues," *Journal of Histochemistry and Cytochemistry*, vol. 46, no. 8, pp. 887–894, 1998.
- [88] J. Zhang, X. Zhang, Y. Zhao, and G. Lv, "Association between urinary alpha1-microglobulin levels and nonalcoholic fatty liver disease: a cross-sectional study," *Annals of Nutrition and Metabolism*, vol. 72, no. 1, pp. 30–36, 2018.
- [89] D. Hakuno, M. Kimura, S. Ito et al., "Hepatokine alpha1-microglobulin signaling exacerbates inflammation and disturbs fibrotic repair in mouse myocardial infarction," *Scientific Reports*, vol. 8, no. 1, p. 16749, 2018.
- [90] T. Berggard, N. Thelin, C. Falkenberg, J. J. Enghild, and B. Akerstrom, "Prothrombin, albumin and immunoglobulin A form covalent complexes with alpha1-microglobulin in human plasma," *European Journal of Biochemistry*, vol. 245, no. 3, pp. 676–683, 1997.
- [91] D. D. DeMars, J. A. Katzmann, T. K. Kimlinger, J. D. Calore, and R. P. Tracy, "Simultaneous measurement of total and IgA-conjugated alpha 1-microglobulin by a combined immunoenzyme/immunoradiometric assay technique," *Clinical Chemistry*, vol. 35, no. 5, pp. 766–772, 1989.
- [92] H. Misu, T. Takamura, H. Takayama et al., "A liver-derived secretory protein, selenoprotein P, causes insulin resistance," *Cell Metabolism*, vol. 12, no. 5, pp. 483–495, 2010.
- [93] R. F. Burk and K. E. Hill, "Selenoprotein P: an extracellular protein with unique physical characteristics and a role in selenium homeostasis," *Annual Review of Nutrition*, vol. 25, pp. 215–235, 2005.
- [94] B. A. Carlson, S. V. Novoselov, E. Kumaraswamy et al., "Specific excision of the selenocysteine tRNA[Ser]Sec (Trsp) gene in mouse liver demonstrates an essential role of selenoproteins in liver function," *Journal of Biological Chemistry*, vol. 279, no. 9, pp. 8011–8017, 2004.
- [95] Y. Saito and K. Takahashi, "Characterization of selenoprotein P as a selenium supply protein," *European Journal of Biochemistry*, vol. 269, no. 22, pp. 5746–5751, 2002.
- [96] H. Chadani, S. Usui, O. Inoue et al., "Endogenous selenoprotein P, a liver-derived secretory protein, mediates myocardial ischemia/reperfusion injury in mice," *International Journal of Molecular Sciences*, vol. 19, no. 3, p. 878, 2018.
- [97] T. T. Tang, Y. Y. Li, J. J. Li et al., "Liver-heart crosstalk controls IL-22 activity in cardiac protection after myocardial infarction," *Theranostics*, vol. 8, no. 16, pp. 4552–4562, 2018.
- [98] T. Nishimura, Y. Nakatake, M. Konishi, and N. Itoh, "Identification of a novel FGF, FGF-21, preferentially expressed in the liver," *Biochimica et Biophysica Acta*, vol. 1492, no. 1, pp. 203–206, 2000.
- [99] E. Hondares, R. Iglesias, A. Giral et al., "Thermogenic activation induces FGF21 expression and release in brown adipose tissue," *Journal of Biological Chemistry*, vol. 286, no. 15, pp. 12983–12990, 2011.
- [100] S. Keipert, M. Ost, K. Johann et al., "Skeletal muscle mitochondrial uncoupling drives endocrine cross-talk through the induction of FGF21 as a myokine," *American Journal of*

- Physiology: Endocrinology*, vol. 306, no. 5, pp. E469–E482, 2014.
- [101] S. Keipert, M. Kutschke, D. Lamp et al., “Genetic disruption of uncoupling protein 1 in mice renders brown adipose tissue a significant source of FGF21 secretion,” *Molecular Metabolism*, vol. 4, no. 7, pp. 537–542, 2015.
- [102] K. C. Coate, G. Hernandez, C. A. Thorne et al., “FGF21 is an exocrine pancreas secretagogue,” *Cell Metabolism*, vol. 25, no. 2, pp. 472–480, 2017.
- [103] M. Klein Hazebroek and S. Keipert, “Adapting to the cold: a role for endogenous fibroblast growth factor 21 in thermoregulation?” *Frontiers in Endocrinology (Lausanne)*, vol. 11, p. 389, 2020.
- [104] K. Huang, T. Miao, K. Chang et al., “Impaired peroxisomal import in *Drosophila* oenocytes causes cardiac dysfunction by inducing upd3 as a peroxikine,” *Nature Communications*, vol. 11, no. 1, p. 2943, 2020.
- [105] M. D. Samsky, C. B. Patel, T. A. DeWald et al., “Cardiohepatic interactions in heart failure: an overview and clinical implications,” *Journal of the American College of Cardiology*, vol. 61, no. 24, pp. 2397–2405, 2013.
- [106] J. I. Fortea, A. Puente, A. Cuadrado et al., “Congestive hepatopathy,” *International Journal of Molecular Sciences*, vol. 21, no. 24, p. 9420, 2020.
- [107] T. Watson, E. Shantsila, and G. Y. Lip, “Mechanisms of thrombogenesis in atrial fibrillation: virchow’s triad revisited,” *Lancet*, vol. 373, no. 9658, pp. 155–166, 2009.
- [108] T. Yaegashi, T. Kato, S. Usui et al., “Short-term rapid atrial pacing alters the gene expression profile of rat liver: cardiohepatic interaction in atrial fibrillation,” *Heart Rhythm*, vol. 13, no. 12, pp. 2368–2376, 2016.
- [109] T. Sudoh, K. Kangawa, N. Minamino, and H. Matsuo, “A new natriuretic peptide in porcine brain,” *Nature*, vol. 332, no. 6159, pp. 78–81, 1988.
- [110] S. Nakamura, M. Naruse, K. Naruse et al., “Atrial natriuretic peptide and brain natriuretic peptide coexist in the secretory granules of human cardiac myocytes,” *American Journal of Hypertension*, vol. 4, no. 11, pp. 909–912, 1991.
- [111] K. Horky and J. Widimsky Jr., “Role of the heart as an endocrine organ,” *Cor et Vasa*, vol. 33, no. 6, pp. 441–450, 1991.
- [112] M. Forte, M. Madonna, S. Schiavon et al., “Cardiovascular pleiotropic effects of natriuretic peptides,” *International Journal of Molecular Sciences*, vol. 20, no. 16, p. 3874, 2019.
- [113] F. Theilig and Q. Wu, “ANP-induced signaling cascade and its implications in renal pathophysiology,” *American Journal of Physiology-Renal Physiology*, vol. 308, no. 10, pp. F1047–F1055, 2015.
- [114] P. De Vito, “Atrial natriuretic peptide: an old hormone or a new cytokine?” *Peptides*, vol. 58, pp. 108–116, 2014.
- [115] A. M. Vollmar, “The role of atrial natriuretic peptide in the immune system,” *Peptides*, vol. 26, no. 6, pp. 1086–1094, 2005.
- [116] C. Sengenès, A. Zakaroff-Girard, A. Moulin et al., “Natriuretic peptide-dependent lipolysis in fat cells is a primate specificity,” *American Journal of Physiology-Regulatory, Integrative and Comparative Physiology*, vol. 283, no. 1, pp. R257–R265, 2002.
- [117] M. Bordicchia, D. Liu, E. Z. Amri et al., “Cardiac natriuretic peptides act via p38 MAPK to induce the brown fat thermogenic program in mouse and human adipocytes,” *Journal of Clinical Investigation*, vol. 122, no. 3, pp. 1022–1036, 2012.
- [118] S. Engeli, A. L. Birkenfeld, P. M. Badin et al., “Natriuretic peptides enhance the oxidative capacity of human skeletal muscle,” *Journal of Clinical Investigation*, vol. 122, no. 12, pp. 4675–4679, 2012.
- [119] M. Coue, V. Barquissau, P. Morigny et al., “Natriuretic peptides promote glucose uptake in a cGMP-dependent manner in human adipocytes,” *Scientific Reports*, vol. 8, no. 1, p. 1097, 2018.
- [120] M. Bilzer, R. Witthaut, G. Paumgartner, and A. L. Gerbes, “Prevention of ischemia/reperfusion injury in the rat liver by atrial natriuretic peptide,” *Gastroenterology*, vol. 106, no. 1, pp. 143–151, 1994.
- [121] T. Yamada, Y. Kotake, H. Nagata, and J. Takeda, “Atrial natriuretic peptide reduces hepatic ischemia-reperfusion injury in rabbits,” *Journal of Anesthesia*, vol. 27, no. 6, pp. 901–908, 2013.
- [122] A. K. Kiemer, A. L. Gerbes, M. Bilzer, and A. M. Vollmar, “The atrial natriuretic peptide and cGMP: novel activators of the heat shock response in rat livers,” *Hepatology*, vol. 35, no. 1, pp. 88–94, 2002.
- [123] A. K. Kiemer, A. M. Vollmar, M. Bilzer, T. Gerwig, and A. L. Gerbes, “Atrial natriuretic peptide reduces expression of TNF-alpha mRNA during reperfusion of the rat liver upon decreased activation of NF-kappaB and AP-1,” *Journal of Hepatology*, vol. 33, no. 2, pp. 236–246, 2000.
- [124] A. L. Gerbes, A. M. Vollmar, A. K. Kiemer, and M. Bilzer, “The guanylate cyclase-coupled natriuretic peptide receptor: a new target for prevention of cold ischemia-reperfusion damage of the rat liver,” *Hepatology*, vol. 28, no. 5, pp. 1309–1317, 1998.
- [125] T. Gerwig, H. Meissner, M. Bilzer et al., “Atrial natriuretic peptide preconditioning protects against hepatic preservation injury by attenuating necrotic and apoptotic cell death,” *Journal of Hepatology*, vol. 39, no. 3, pp. 341–348, 2003.
- [126] S. Kulhanek-Heinze, A. L. Gerbes, T. Gerwig, A. M. Vollmar, and A. K. Kiemer, “Protein kinase A dependent signalling mediates anti-apoptotic effects of the atrial natriuretic peptide in ischemic livers,” *Journal of Hepatology*, vol. 41, no. 3, pp. 414–420, 2004.
- [127] U. Grutzner, M. Keller, M. Bach et al., “PI 3-kinase pathway is responsible for antiapoptotic effects of atrial natriuretic peptide in rat liver transplantation,” *World Journal of Gastroenterology*, vol. 12, no. 7, pp. 1049–1055, 2006.
- [128] A. K. Kiemer, S. Kulhanek-Heinze, T. Gerwig, A. L. Gerbes, and A. M. Vollmar, “Stimulation of p38 MAPK by hormonal preconditioning with atrial natriuretic peptide,” *World Journal of Gastroenterology*, vol. 8, no. 4, pp. 707–711, 2002.
- [129] K. Kobayashi, K. Oshima, M. Muraoka et al., “Effect of atrial natriuretic peptide on ischemia-reperfusion injury in a porcine total hepatic vascular exclusion model,” *World Journal of Gastroenterology*, vol. 13, no. 25, pp. 3487–3492, 2007.
- [130] M. Keller, A. L. Gerbes, S. Kulhanek-Heinze et al., “Hepatocyte cytoskeleton during ischemia and reperfusion—Influence of ANP-mediated p38 MAPK activation,” *World Journal of Gastroenterology*, vol. 11, no. 47, pp. 7418–7429, 2005.
- [131] N. Ishigaki, N. Yamamoto, H. Jin, K. Uchida, S. Terai, and I. Sakaida, “Continuous intravenous infusion of atrial natriuretic peptide (ANP) prevented liver fibrosis in rat,” *Biochemical and Biophysical Research Communications*, vol. 378, no. 3, pp. 354–359, 2009.
- [132] M. N. Gorbic, P. Gines, R. Bataller et al., “Atrial natriuretic peptide antagonizes endothelin-induced calcium increase and cell contraction in cultured human hepatic stellate cells,” *Hepatology*, vol. 30, no. 2, pp. 501–509, 1999.

- [133] A. Chiba, H. Watanabe-Takano, K. Terai et al., "Osteocrin, a peptide secreted from the heart and other tissues, contributes to cranial osteogenesis and chondrogenesis in zebrafish," *Development*, vol. 144, no. 2, pp. 334–344, 2017.
- [134] M. K. Brahma, R. C. Adam, N. M. Pollak et al., "Fibroblast growth factor 21 is induced upon cardiac stress and alters cardiac lipid homeostasis," *Journal of Lipid Research*, vol. 55, no. 11, pp. 2229–2241, 2014.
- [135] K. K. Baskin, A. L. Bookout, and E. N. Olson, "The heart-liver metabolic axis: defective communication exacerbates disease," *EMBO Molecular Medicine*, vol. 6, no. 4, pp. 436–438, 2014.
- [136] S. Hernandez-Anzaldo, E. Berry, V. Brglez et al., "Identification of a novel heart-liver axis: matrix metalloproteinase-2 negatively regulates cardiac secreted phospholipase A2 to modulate lipid metabolism and inflammation in the liver," *Journal of the American Heart Association*, vol. 4, no. 11, p. e002553, 2015.
- [137] E. Berry, S. Hernandez-Anzaldo, F. Ghomashchi et al., "Matrix metalloproteinase-2 negatively regulates cardiac secreted phospholipase A2 to modulate inflammation and fever," *Journal of the American Heart Association*, vol. 4, no. 4, p. e001868, 2015.
- [138] G. A. McQuibban, J. H. Gong, E. M. Tam, C. A. McCulloch, I. Clark-Lewis, and C. M. Overall, "Inflammation dampened by gelatinase A cleavage of monocyte chemoattractant protein-3," *Science*, vol. 289, no. 5482, pp. 1202–1206, 2000.
- [139] T. Wang, J. Liu, C. McDonald et al., "GDF15 is a heart-derived hormone that regulates body growth," *EMBO Molecular Medicine*, vol. 9, no. 8, pp. 1150–1164, 2017.
- [140] I. Pilecka, A. Whatmore, R. Hooft van Huijsduijnen, B. Destenaves, and P. Clayton, "Growth hormone signalling: sprouting links between pathways, human genetics and therapeutic options," *Trends in Endocrinology and Metabolism: TEM*, vol. 18, no. 1, pp. 12–18, 2007.
- [141] M. Baik, J. H. Yu, and L. Hennighausen, "Growth hormone-STAT5 regulation of growth, hepatocellular carcinoma, and liver metabolism," *Annals of the New York Academy of Sciences*, vol. 1229, pp. 29–37, 2011.
- [142] M. O. Savage, V. Hwa, A. David, R. G. Rosenfeld, and L. A. Metherell, "Genetic defects in the growth hormone-IGF-I axis causing growth hormone insensitivity and impaired linear growth," *Frontiers in Endocrinology (Lausanne)*, vol. 2, p. 95, 2011.
- [143] P. Rotwein, "Mapping the growth hormone-Stat5b-IGF-I transcriptional circuit," *Trends in Endocrinology and Metabolism: TEM*, vol. 23, no. 4, pp. 186–193, 2012.
- [144] S. Milman, D. M. Huffman, and N. Barzilai, "The somatotropic axis in human aging: framework for the current state of knowledge and future research," *Cell Metabolism*, vol. 23, no. 6, pp. 980–989, 2016.
- [145] J. M. Wit and F. de Luca, "Atypical defects resulting in growth hormone insensitivity," *Growth Hormone IGF Research*, vol. 28, pp. 57–61, 2016.
- [146] H. M. Domene, V. Hwa, J. Argente et al., "Human acid-labile subunit deficiency: clinical, endocrine and metabolic consequences," *Hormone Research*, vol. 72, no. 3, pp. 129–141, 2009.
- [147] K. H. Kim, S. H. Kim, D. H. Han, Y. S. Jo, Y. H. Lee, and M. S. Lee, "Growth differentiation factor 15 ameliorates nonalcoholic steatohepatitis and related metabolic disorders in mice," *Scientific Reports*, vol. 8, no. 1, p. 6789, 2018.
- [148] B. K. Koo, S. H. Um, D. S. Seo et al., "Growth differentiation factor 15 predicts advanced fibrosis in biopsy-proven non-alcoholic fatty liver disease," *Liver International*, vol. 38, no. 4, pp. 695–705, 2018.
- [149] L. S. Bhatia, N. P. Curzen, P. C. Calder, and C. D. Byrne, "Non-alcoholic fatty liver disease: a new and important cardiovascular risk factor?" *European Heart Journal*, vol. 33, no. 10, pp. 1190–1200, 2012.
- [150] J. A. Magida and L. A. Leinwand, "Metabolic crosstalk between the heart and liver impacts familial hypertrophic cardiomyopathy," *EMBO Molecular Medicine*, vol. 6, no. 4, pp. 482–495, 2014.
- [151] Q. F. Collins, Y. Xiong, E. G. Lupo Jr., H. Y. Liu, and W. Cao, "p38 mitogen-activated protein kinase mediates free fatty acid-induced gluconeogenesis in hepatocytes," *Journal of Biological Chemistry*, vol. 281, no. 34, pp. 24336–24344, 2006.
- [152] P. Puigserver and B. M. Spiegelman, "Peroxisome proliferator-activated receptor-gamma coactivator 1 alpha (PGC-1 alpha): transcriptional coactivator and metabolic regulator," *Endocrine Reviews*, vol. 24, no. 1, pp. 78–90, 2003.
- [153] C. E. Grueter, E. van Rooij, B. A. Johnson et al., "A cardiac microRNA governs systemic energy homeostasis by regulation of MED13," *Cell*, vol. 149, no. 3, pp. 671–683, 2012.
- [154] A. Verger, D. Monte, and V. Villeret, "Twenty years of mediator complex structural studies," *Biochemical Society Transactions*, vol. 47, no. 1, pp. 399–410, 2019.
- [155] C. Jeronimo and F. Robert, "The mediator complex: at the nexus of RNA polymerase II transcription," *Trends in Cell Biology*, vol. 27, no. 10, pp. 765–783, 2017.
- [156] M. Carrer, N. Liu, C. E. Grueter et al., "Control of mitochondrial metabolism and systemic energy homeostasis by microRNAs 378 and 378*," *Proceedings of the National Academy of Sciences of the United States of America*, vol. 109, no. 38, pp. 15330–15335, 2012.
- [157] Y. Jia, C. Qi, P. Kashireddi et al., "Transcription coactivator PBP, the peroxisome proliferator-activated receptor (PPAR)-binding protein, is required for PPARalpha-regulated gene expression in liver," *Journal of Biological Chemistry*, vol. 279, no. 23, pp. 24427–24434, 2004.
- [158] K. Ge, M. Guermah, C. X. Yuan et al., "Transcription coactivator TRAP220 is required for PPAR gamma 2-stimulated adipogenesis," *Nature*, vol. 417, no. 6888, pp. 563–567, 2002.
- [159] W. Chen, X. Zhang, K. Birsoy, and R. G. Roeder, "A muscle-specific knockout implicates nuclear receptor coactivator MED1 in the regulation of glucose and energy metabolism," *Proceedings of the National Academy of Sciences of the United States of America*, vol. 107, no. 22, pp. 10196–10201, 2010.
- [160] F. Yang, B. W. Vought, J. S. Satterlee et al., "An ARC/Mediator subunit required for SREBP control of cholesterol and lipid homeostasis," *Nature*, vol. 442, no. 7103, pp. 700–704, 2006.

Research Article

Network Pharmacology-Based Study on the Molecular Biological Mechanism of Action for Qingdu Decoction against Chronic Liver Injury

Chongyang Ma,¹ Mengpei Zhao,² Yuqiong Du ,¹ Shuang Jin,³ Xiaoyi Wu,¹ Haiyan Zou,¹ Qiuyun Zhang,¹ and Lianyin Gao ¹

¹School of Traditional Chinese Medicine, Capital Medical University, Beijing 10069, China

²Kaifeng Second Hospital of Traditional Chinese Medicine, Kaifeng 475000, China

³Yanqing County Hospital of Traditional Chinese Medicine, Beijing 102100, China

Correspondence should be addressed to Lianyin Gao; 19950032@ccmu.edu.cn

Received 24 December 2020; Revised 5 January 2021; Accepted 4 February 2021; Published 4 March 2021

Academic Editor: Chih-Yuan Ko

Copyright © 2021 Chongyang Ma et al. This is an open access article distributed under the Creative Commons Attribution License, which permits unrestricted use, distribution, and reproduction in any medium, provided the original work is properly cited.

Background. Qingdu Decoction (QDD) is a traditional Chinese medicine formula for treating chronic liver injury (CLI). **Materials and methods.** A network pharmacology combining experimental validation was used to investigate potential mechanisms of QDD against CLI. We firstly screened the bioactive compounds with pharmacology analysis platform of the Chinese medicine system (TCMSP) and gathered the targets of QDD and CLI. Then, we constructed a compound-target network and a protein-protein interaction (PPI) network and enriched core targets in Kyoto Encyclopedia of Genes and Genomes (KEGG) signaling pathways. At last, we used a CLI rat model to confirm the effect and mechanism of QDD against CLI. Enzyme-linked immunosorbent assay (ELISA), western blot (WB), and real-time quantitative polymerase chain reaction (RT-qPCR) were used. **Results.** 48 bioactive compounds of QDD passed the virtual screening criteria, and 53 overlapping targets were identified as core targets of QDD against CLI. A compound-CLI related target network containing 94 nodes and 263 edges was constructed. KEGG enrichment of core targets contained some pathways related to CLI, such as hepatitis B, tumor necrosis factor (TNF) signaling pathway, apoptosis, hepatitis C, interleukin-17 (IL-17) signaling pathway, and hypoxia-inducible factor (HIF)-1 signaling pathway. Three PPI clusters were identified and enriched in hepatitis B and tumor necrosis factor (TNF) signaling pathway, apoptosis and hepatitis B pathway, and peroxisome pathway, respectively. Animal experiment indicated that QDD decreased serum concentrations of alanine aminotransferase (ALT), aspartate aminotransferase (AST), endotoxin (ET), and IL-17 and increased prothrombin time activity (PTA) level. WB and RT-qPCR analyses indicated that, compared with the model group, the expression of cysteinyl aspartate specific proteinase-9 (caspase-9) protein, caspase-3 protein, B-cell lymphoma-2 associated X protein (Bax) mRNA, and cytochrome c (Cyt c) mRNA was inhibited and the expression of B-cell lymphoma-2 (Bcl-2) mRNA was enhanced in the QDD group. **Conclusions.** QDD has protective effect against CLI, which may be related to the regulation of hepatocyte apoptosis. This study provides novel insights into exploring potential biological basis and mechanisms of clinically effective formula systematically.

1. Introduction

Chronic liver disease (CLD) usually results from iterative liver injury, such as excessive alcohol consumption, viral hepatitis, nonalcoholic fatty liver disease, autoimmune hepatitis, primary biliary cholangitis, and primary sclerosing cholangitis, and causes approximately 2 million deaths per

year worldwide [1]. Current treatments for CLD mainly lie in combined medications and artificial liver support, and liver transplant is the only recommended treatment to patients diagnosed with liver failure. Chronic liver injury (CLI), that leads to apoptosis, inflammation, matrix deposition, hyper-bilirubinemia, angiogenesis, and progressive fibrosis, is the hallmark of all types of CLDs, and targeting

molecular pathways in chronic liver injury would help the development of clinical therapies to prevent or improve the prognosis of CLDs.

Traditional Chinese medicine has been around for thousands of years. There is increasing evidence that certain Chinese medicine prescriptions have beneficial effects on experimental liver injury [2]. Qingdu Decoction (QDD), a traditional Chinese medicine preparation containing *Rheum palmatum* L., *Citrus aurantium* L., *Magnolia officinalis* Rehder and E.H. Wilson, *Rehmannia glutinosa* (Gaertn.) DC., and *Rubia cordifolia* L., has notable effects on patients with CLI. Our previous clinical studies have confirmed that the prescription has a good effect on improving clinical symptoms, protecting liver function, and reducing endotoxin absorption in CLI patients [3, 4]. And our previous experiments have shown that, in TAA-induced model rats, QDD can reduce the level of inflammatory factors and eliminate endotoxin to improve the state of liver damage [5]. We even made some efforts on the mechanisms of QDD against CLI, and a holistic understanding of its molecular mechanisms needs to be further explored.

In the present study, network pharmacology was employed to establish a compound-target network to understand the potential mechanisms of QDD against CLI. The flowchart of the whole study design is illustrated in Figure 1. Firstly, we screened bioactive compounds of QDD and mined their targets using available online databases, and then, targets related to CLI were also obtained. After intersecting these two parts of targets, targets related to both QDD and CLI were obtained and were used for further gene ontology enrichment analysis. Finally, animal experiments were used to confirm the mechanisms predicted through this *in silico* approach.

2. Materials and Methods

2.1. Reagent Supplies. Thioacetamide (TAA) was purchased from Keao Co., Ltd (Beijing, China). Rat ET Enzyme-linked immunoassay (ELISA) kit was from Jiancheng Inst. Biotechnology (Nanjing, China). Rat IL-17 ELISA kit was from eBioscience (Santiago, CA, USA). Primary antibodies used were rabbit caspase-9 and caspase-3 antibody (Santa cruz, Dallas, TX, USA) and mouse β -actin antibody (Zhongshan Jinqiao, Beijing, China). Secondary antibodies used were horseradish peroxidase-conjugated goat anti-rabbit IgG and anti-mouse IgG (Jackson, Lancaster, PA, USA). Total RNA kit was purchased from Tian Gen Biotech (Beijing, China).

2.2. Preparation of QDD. QDD is composed of five Chinese herbs. All the medicinal plants were provided by Beijing Tongrentang Chinese Medicine Co. Ltd. (Beijing, China). Samples were authenticated by a Prof. Zhang Qiuyun from Capital Medical University, China. Every dose of QDD contains *Rheum palmatum* L. (10 g), *Citrus aurantium* L. (10 g), *Magnolia officinalis* Rehder and E.H. Wilson (10 g), *Rehmannia glutinosa* (Gaertn.) DC. (12 g), and *Rubia cordifolia* L. (9 g). The mixture of herbal materials (51 g) was decocted with distilled water (2×1 h, 1:10 for the first

extraction and 1 : 8 for the second extraction, w/v). The water extract was filtered and concentrated under reduced pressure to give the aqueous extract of QDD (34 mL). One milliliter of the extract corresponds to 1.5 g of crude drug. The decoction was stored at -20°C and heated in a 37°C water bath before gavage.

2.3. Animal Model and Treatment. Specific pathogen-free (SPF) grade male Wistar rats (190–210 g) were provided by Charles River Experimental Animals Technology Co. Ltd (Beijing, China). Laboratory animal use and experimental protocols have been reviewed and approved by the Ethics Committee of Capital Medical University (ethics number: AEEI-2017-109). The rats were maintained on a 12 h light/dark cycle at constant room temperature ($22\text{--}25^{\circ}\text{C}$) and humidity (50–70%), and they have free access to standard rodent food and water.

After 7 days of adaptive feeding, 72 rats were randomly divided into six groups and each group had 12 rats: normal group, model group, lactulose (LA) group, and QDD in a low, moderate, or high dosage (QDDL, QDDM, and QDDH). The normal group was given physiological saline by gavage. The other groups were pretreated with TAA at a dose of 12 mg/kg for 8 weeks and at an increased dose of 36 mg/kg from the 9th to the 12th week [6]. In addition, the LA group was fed lactulose solution once a day as a positive control at a dose of 3.5 mL/kg. Each QDD group was given QDD concentrate (QDDL, QDDM, and QDDH: 5.08, 10.17, and 20.33 g/kg) daily. The whole experiment lasted 12 weeks. After intraperitoneal injection of 3% sodium pentobarbital anesthetic (30 mg/kg), all rats were sacrificed by abdominal aorta extraction.

2.4. Serum Biochemical Assay and Plasma Coagulation Analysis. The content of alanine transaminase (ALT) and aspartate transaminase (AST) were measured by automatic biochemical analyzer (Hitachi, Tokyo, Japan). The prothrombin time activity (PTA) was determined with coagulation by an automatic coagulation analyzer (Beckman, LAX, CA, USA).

2.5. Enzyme-Linked Immunoassay (ELISA) Analysis. The content of endotoxin (ET) and IL-17 in serum was measured by multiscan spectrum (Thermo, Waltham, MA, USA) using ET and IL-17 ELISA kits according to the kit's specifications.

2.6. Western Blot Analysis. Total protein was extracted from the liver tissues using cell lysis buffer and analyzed with bicinchoninic acid protein assay kit. Protein samples were separated on sodium dodecyl sulfate (SDS)-polyacrylamide gels and transferred onto a polyvinylidene fluoride membrane. After blocked with 5% nonfat dry milk in Tris-buffered saline containing 0.05% Tween-20 (TBST) buffer, membranes were incubated with primary antibody followed by the corresponding horseradish peroxidase-conjugated secondary antibodies. Antibodies and dilutions included the following: rabbit caspase-9 antibody (1:500), mouse

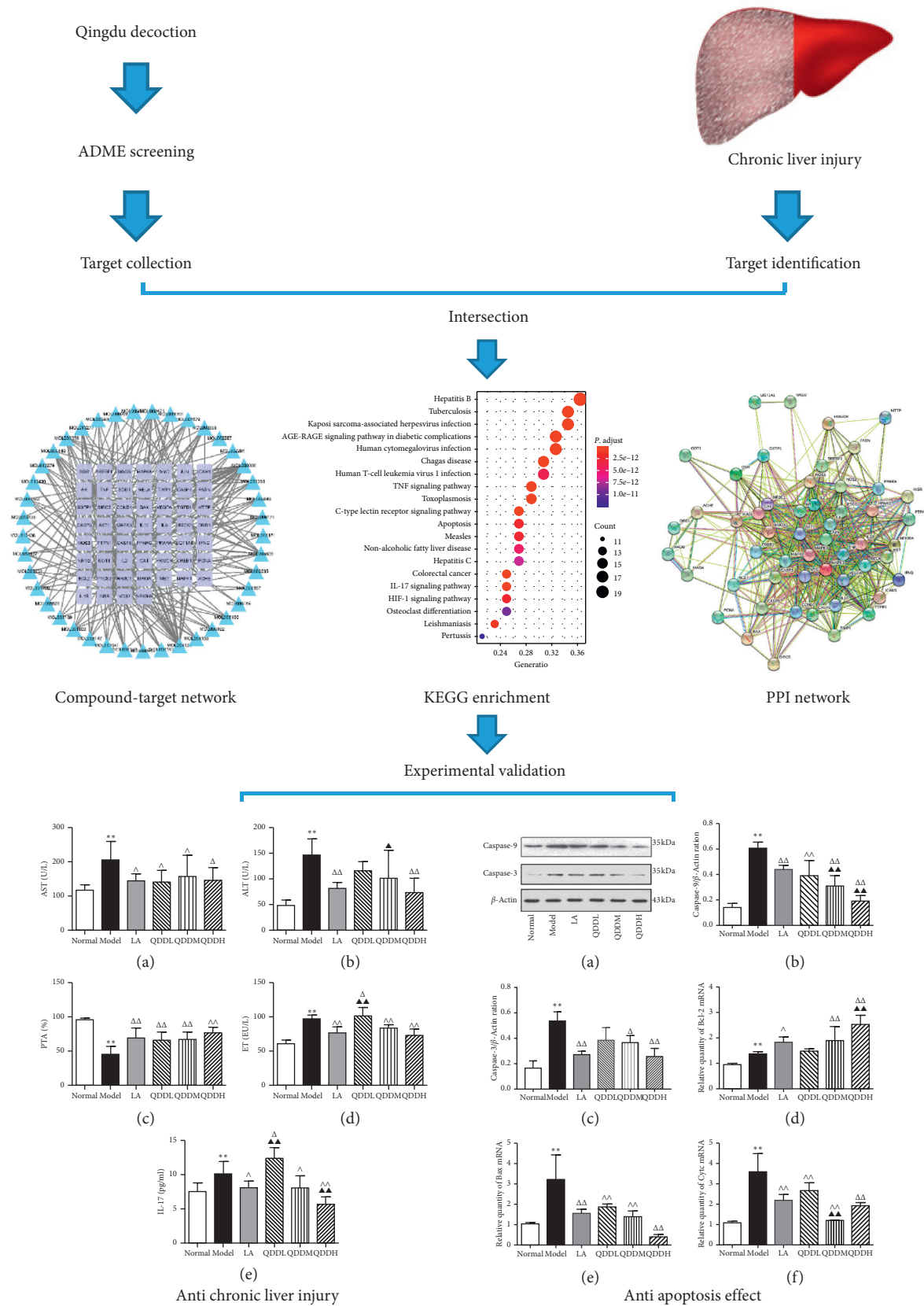


FIGURE 1: The flowchart of the whole study design.

caspase-3 antibody (1:500), mouse β -actin antibody (1:1,000), horseradish peroxidase-conjugated goat anti-rabbit IgG (1:10,000), and horseradish peroxidase-conjugated goat anti-mouse IgG (1:10,000).

2.7. Real-Time Quantitative PCR Analysis. Total RNA was extracted from liver tissues using RNA isolation kit according to the manufacturer's specification. Each sample was reverse transcribed into complementary DNA (cDNA) using the HiFi-MMLV cDNA first chain synthesis kit. Gene expression was quantified by means of the comparative Ct method ($\Delta\Delta C_t$), and the relative expressions were calculated by the $2^{-\Delta\Delta C_t}$ method.

2.8. Screening of Active Compounds. All compounds contained in QDD were searched for in the Traditional Chinese Medicine Systems Pharmacology Database and Analysis Platform (TCMSP; <http://lsp.nwu.edu.cn/tcmsp.php>), containing detailed pharmacological properties of each compound. In the present study, oral bioavailability (OB) > 30%, CACO-2 permeability > -0.4, and drug likeness (DL) > 0.18 were used for bioactive compounds screening for further analyses.

2.9. Identification of Targets Associated with QDD and CLI. To predict the target proteins of identified bioactive compounds in QDD, we used an approach integrated with two Chinese medicine databases, including integrative database of traditional Chinese medicine enhanced by symptom mapping (SymMap) and TCMSP [7, 8]. Comparative Toxicogenomics Database (CTD) was used for genes associated with CLI identification [9]. Only genes with Inference Score > 20 were chosen for further analysis. All these targets were transformed into gene symbols using the UniProt knowledge database (<http://www.uniprot.org>) with the selected species as *Homo sapiens*. Subsequently, the intersection of QDD targets and CLI targets was identified as core targets using Draw Venn Diagram online (<http://bioinfogp.cnb.csic.es/tools/venny/index.html>). Cytoscape 3.7.1 software was used for construction of compound-CLI related target network.

2.10. Construction of PPI Network of Core Targets. The protein-protein interaction (PPI) data of core targets were obtained from STRING database (<https://string-db.org/>). K-means algorithm was used for PPI cluster identification with default parameters supplied in STRING database. Also, PPI clusters were constructed using Cytoscape 3.7.1 software (National Resource for Network Biology, USA).

2.11. Pathway Enrichment Analysis of Core Targets. To identify the potential biological pathways regulated by QDD against CLI, the ClusterProfiler package of R 3.5.0 was adopted to conduct Kyoto Encyclopedia of Genes and Genomes (KEGG) pathway enrichment analysis of core targets [10]. Adjust P value < 0.05 was thought to be significant. The top 20

significantly results were further processed to produce a high-level bubble map and an enrichment map of pathways. KEGG Mapper (<https://www.kegg.jp/kegg/mapper.html>) was used for pathway visualization.

2.12. Statistical Analysis. All data were presented as means \pm standard error. One-way analysis of variance (ANOVA) was performed using SPSS 19.0 (IBM Corp. Released 2010. IBM SPSS Statistics for Windows, Version 19.0. Armonk, NY, USA) to test the differences between groups. The least-significant difference (LSD) test was used for homogeneity of variance and Tamhane's T2 test for heterogeneity of variance. A value of $P < 0.05$ was considered statistically significant.

3. Results

3.1. Therapeutic Effect of QDD against CLI. AST and ALT in serum were considered as important indicators of liver injury, and PTA was used to evaluate liver function. As shown in Figures 2(a)–2(c), compared to normal group, AST and ALT levels in the model group were significantly increased ($P < 0.01$), from 115.50 U/L to 205.30 U/L and from 47.58 U/L to 145.67 U/L, respectively; and PTA was significantly decreased ($P < 0.01$), from 96.00% to 45.67%. Compared with the model group, the content of AST in the LA group and each QDD group showed different degrees of reductions ($P < 0.05$), and the content of ALT of LA and QDDH groups were significantly decreased ($P < 0.01$). PTA was significantly increased in each intervention group ($P < 0.01$). Compared with the normal group, endotoxin (ET) and interleukin (IL)-17 levels were increased in the model group ($P < 0.01$). Compared with the model group, the ET and IL-17 levels of the LA group, the QDDM group, and the QDDH group were significantly lower ($P < 0.05$ or $P < 0.01$), and these results were shown in Figures 2(d) and 2(e).

3.2. Screening Bioactive Compounds of QDD. To understand the potential mechanisms of QDD against CLI, a network approach was used as we previous mentioned [11]. After pharmacological properties screening, 48 bioactive compounds were identified for further analysis. As shown in Supplementary Table 1, 9 compounds were found in Dahaung, 19 compounds were found in Zhishi, 2 compounds were found in Houpo, 2 compounds were found in Dihuang, and 18 compounds were found in Qiancao.

3.3. Core Targets of QDD against CLI Using Network Pharmacology Approach. As shown in Supplementary Table 2 and Supplementary Table 3, a total of 813 targets associated with CLI pathogenesis and 172 targets of QDD were obtained from our integrative approach. Furthermore, 53 overlapping targets were identified via mapping targets of QDD into targets related to CLI, which were regarded as the core therapeutic targets of QDD against CLI (Figure 3(a)). Then, a compound-CLI-related target network containing

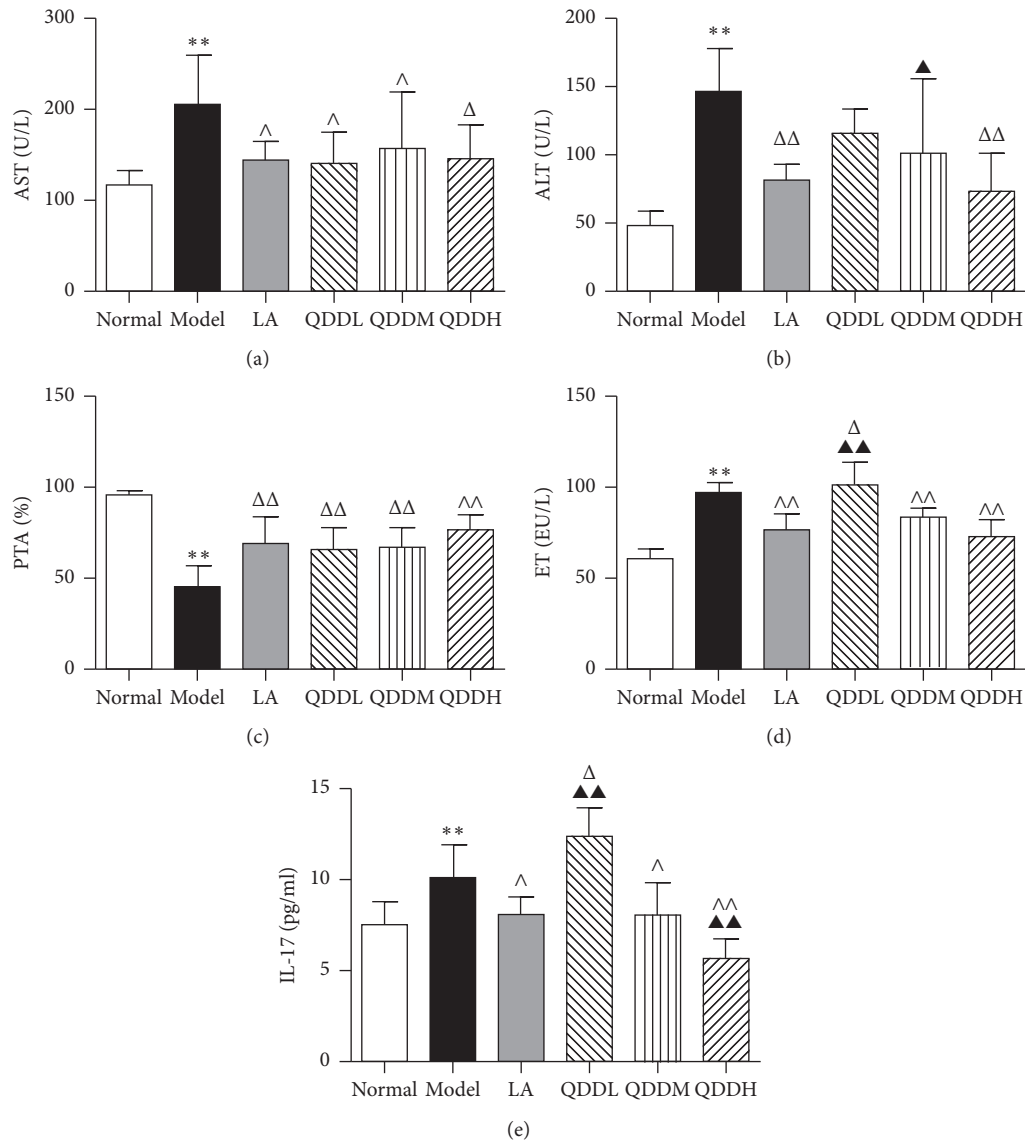


FIGURE 2: Effects of QDD on blood related indicators: (a) change in serum AST level in each group; (b) change in serum ALT level in each group; (c) change in plasma PTA level in each group; (d) change in serum ET level in each group; (e) change in serum IL-17 level in each group. Values are expressed as mean \pm SEM, $n = 6$ for each group, ** $P < 0.01$ vs normal group; $\Delta P < 0.05$ and $\Delta\Delta P < 0.01$ vs model group; $\blacktriangle P < 0.05$ and $\blacktriangle\blacktriangle P < 0.01$ vs LA group.

94 nodes and 263 edges was constructed (Figure 3(b)), and top 5 important compounds were identified based on degree values, including luteolin (degree: 27), naringenin (degree: 22), aloë-emodin (degree: 14), nobiletin (degree: 13), and beta-sitosterol (degree: 10).

3.4. KEGG Pathway Enrichment and PPI Network Construction. To understand the related signaling pathways of core targets of QDD against CLI, KEGG pathway enrichment analysis was employed via *R* package. A total of 165 pathways were enriched and top 20 pathways ranked by adjust *P* value were visualized in a bubble plot (Figure 4(a)). In detail, some pathways related to CLI were obtained, including hepatitis B, TNF signaling pathway, apoptosis, hepatitis C, IL-17 signaling pathway,

and hypoxia-inducible factor (HIF-1) signaling pathway. Enrichment map showed that top 20 pathways could be constructed as a network (Figure 4(b)). We focused on the multiple target effect of QDD on apoptosis pathway and visualized these target data in a KEGG diagram. Red nodes represented core targets of QDD against CLI (Figure 4(c)). PPI network of core targets containing 53 nodes and 620 targets was constructed with STRING website (Figure 5(a)). Also, based on topological analysis through K-means algorithm, three PPI clusters were identified (Figures 5(b)–5(d)). After KEGG pathway enrichment, we found that cluster 1 was enriched in the hepatitis B and TNF signaling pathway, cluster 2 was enriched in the apoptosis and hepatitis B pathway, and cluster 3 was enriched in the peroxisome pathway.

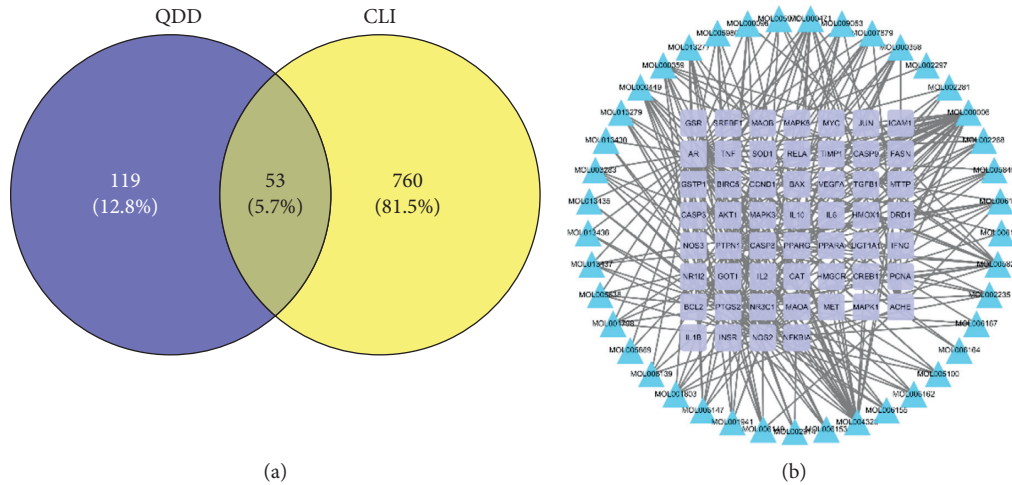


FIGURE 3: Identification of core targets of Qingdu decoction against chronic liver injury: (a) the Venn diagram of QDD targets and CLI targets; (b) compound-CLI related target network.

3.5. Antiapoptosis Effect of QDD against CLI. The above network pharmacology approach indicated a multiple target effect of QDD on apoptosis pathway, caspase-3, caspase-9, and their upstream signals including Bcl2 and Bax. Western blot analysis showed that the relative expression level of the caspase-9 protein in the model group was significantly increased ($P < 0.01$) compared with the normal group (Figures 6(a) and 6(b)). The relative expression of caspase-9 protein was decreased after treatment with QDD and LA ($P < 0.01$). Compared with the LA group, the relative expression of caspase-9 protein in the QDDM group and the QDDH group was significantly lower ($P < 0.01$). Also, the relative expression level of the caspase-3 protein in the model group was significantly increased ($P < 0.01$) compared with the normal group (Figures 6(a) and 6(c)). The relative expression of caspase-3 protein was decreased after treatment with middle ($P < 0.05$) and high dose ($P < 0.01$) of QDD. Bcl-2 and Bax are core members of the Bcl-2 family of proteins and play a crucial role in mitochondrial apoptosis [12]. Cyt *c* is a specific protein that activates caspase-9 [13]. As shown in Figures 6(c) and 6(d), the relative expression levels of Bcl-2, Bax, and Cyt *c* genes in the model group were significantly increased by RT-qPCR ($P < 0.01$). Compared with the model group, the relative expression levels of the Bcl-2 gene were increased in all treatment groups ($P < 0.05$ or $P < 0.01$) except the QDDL group; the relative expression levels of Bax and Cyt *c* genes were significantly lower in each treatment group ($P < 0.01$).

4. Discussion

Our previously research showed that QDD treatment inhibited CLI induced by TAA and decreased TLR4 signal activation [5]. For QDD was a multiple target preparation, it is necessary to reveal the potential mechanisms in a system level. In the present study, we used a network pharmacology approach to reveal the potential mechanisms of QDD against CLI in a system level. Compound-target network construction indicated that luteolin, naringenin, alo-

emodin, nobiletin, and beta-sitosterol were the most important compounds in the network. Literature evidence supported that all these compounds showed a very good protective effect in various CLI experimental models [14–18]. Evidence supported the ability of alo-emodin to inhibit diverse events involved in cell apoptosis [19]. Mol-lugin was a potential nuclear factor kappa-B (NF κ B) inhibitor and decreased expression of inflammatory molecules respond to TNF signal [20, 21]. Rhein was reported to protect liver cells from methotrexate-induced injury through modulating apoptosis-related proteins, such as caspase-3 and Bcl-2 family [22]. On the contrary, some studies reported that all the above compounds could induce apoptosis in many cancer models with different doses [23–25]. Therefore, future studies should explore the differences in drug targets and involve discussion about the relationship between dose and bidirectional effect.

Core targets of QDD against CLI enriched in four categories of pathways, including disease pathways, apoptosis-related pathway, inflammatory pathway, and fibrosis-related pathway. According to KEGG enrichment analysis, these core targets were also enriched in two diseases pathways, including hepatitis B and hepatitis C. Evidence shows that hepatitis B and hepatitis C are common causes of CLI, and management of these etiologies leads to a prevention of liver inflammation and fibrosis progression [26, 27]. Both core targets of QDD against CLI and PPI cluster two were enriched in the apoptosis pathway. According to a reconstructed KEGG map, we found that core targets of QDD against CLI involved in both of the upstream and midstream of apoptosis pathway, such as TNF- α , Bcl-2, Bax, and Caspase-9. Our previous study has found that serum level of TNF- α was significantly decreased by QDD in the same CLI model [5]. Therefore, we focused on other targets in this pathway. Besides apoptosis pathway, two inflammatory pathways were obtained, including IL-17 and TNF. TNF pathway activation was the most common phenomenon in kinds of CLI animal models [28–30]. IL-17 is mainly produced from Th17 cells and upregulated in

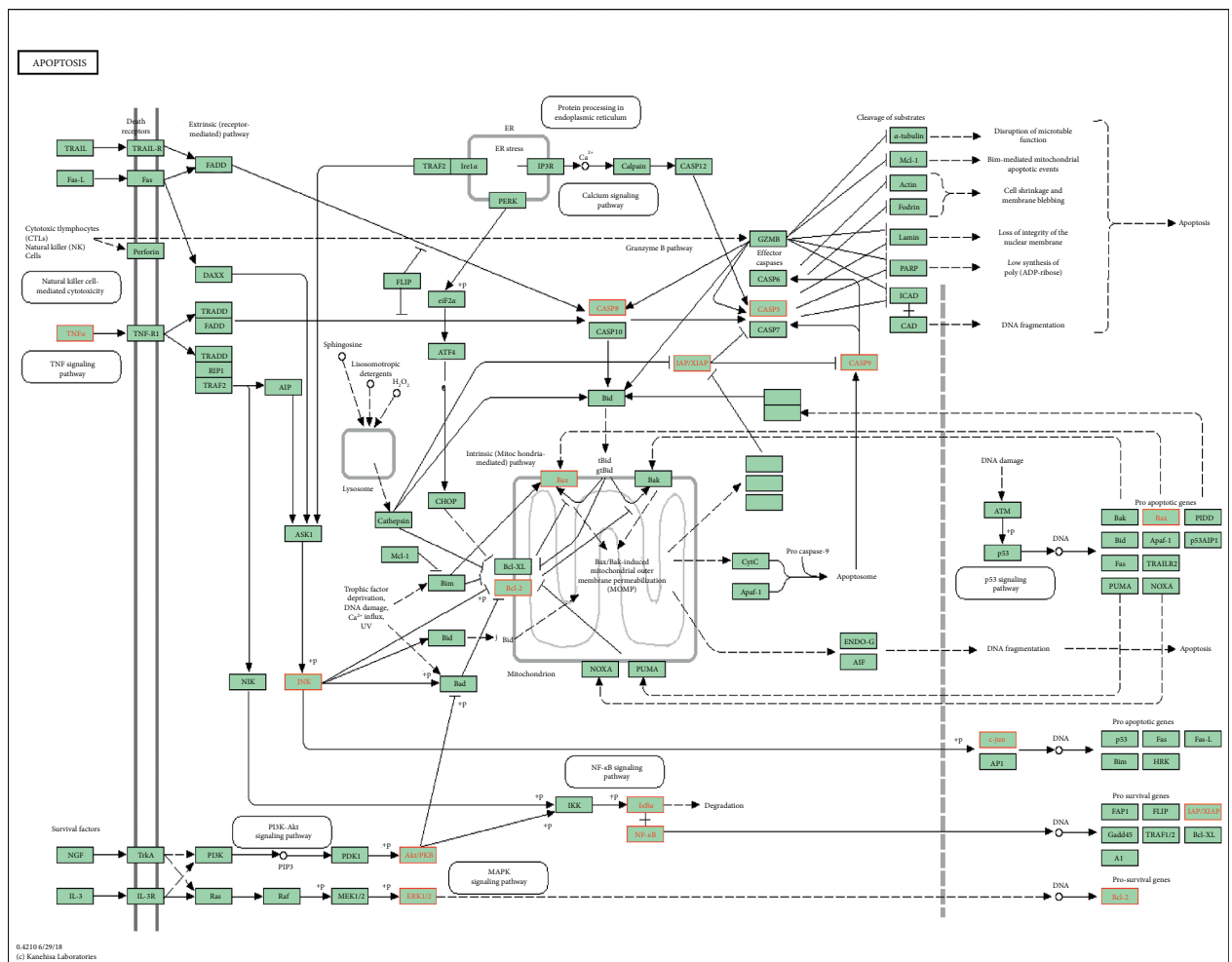
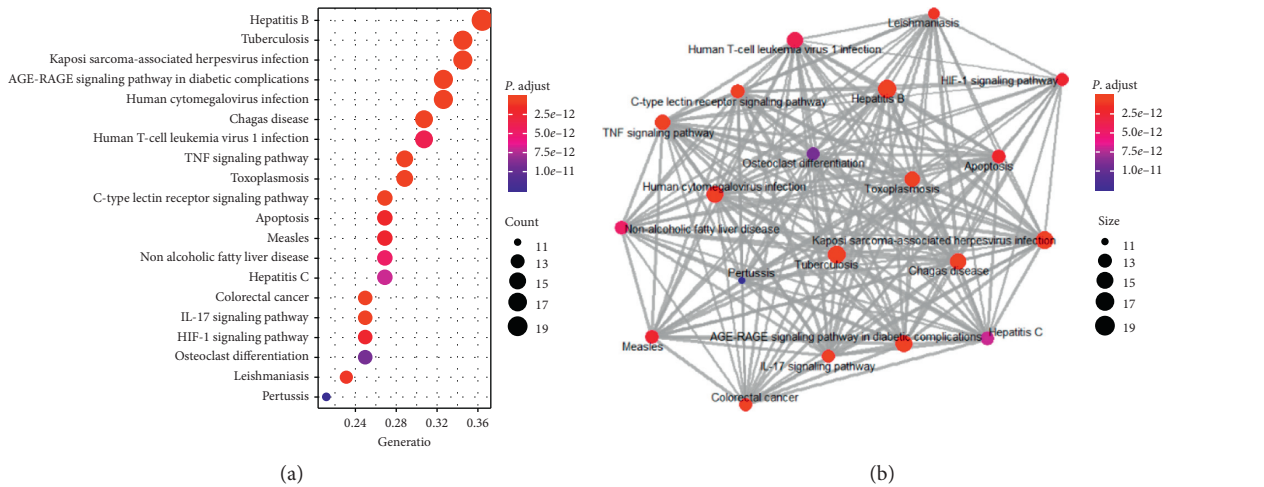


FIGURE 4: KEGG pathway enrichment analysis of core targets of Qingdu decoction against chronic liver injury: (a) bubble plot of top 20 enriched pathways; (b) enrichment map of top 20 enriched pathways; (c) modulating diagram of QDD on the apoptosis pathway. Red nodes represented core targets of QDD against CLI and green nodes represented proteins in the pathway.

hepatitis B and C, alcoholic liver disease, and autoimmune hepatitis [31]. Literature evidence showed that inhibiting IL-17 pathway led to a resistance to CLI-induced liver fibrosis [27]. HIF-1 signaling pathway was also identified, and

HIF-1 was confirmed as a critical regulator of profibrotic mediator production during the development of CLI-induced liver fibrosis [32]. The present study focused on the effect of QDD on apoptosis, and we designed a biological

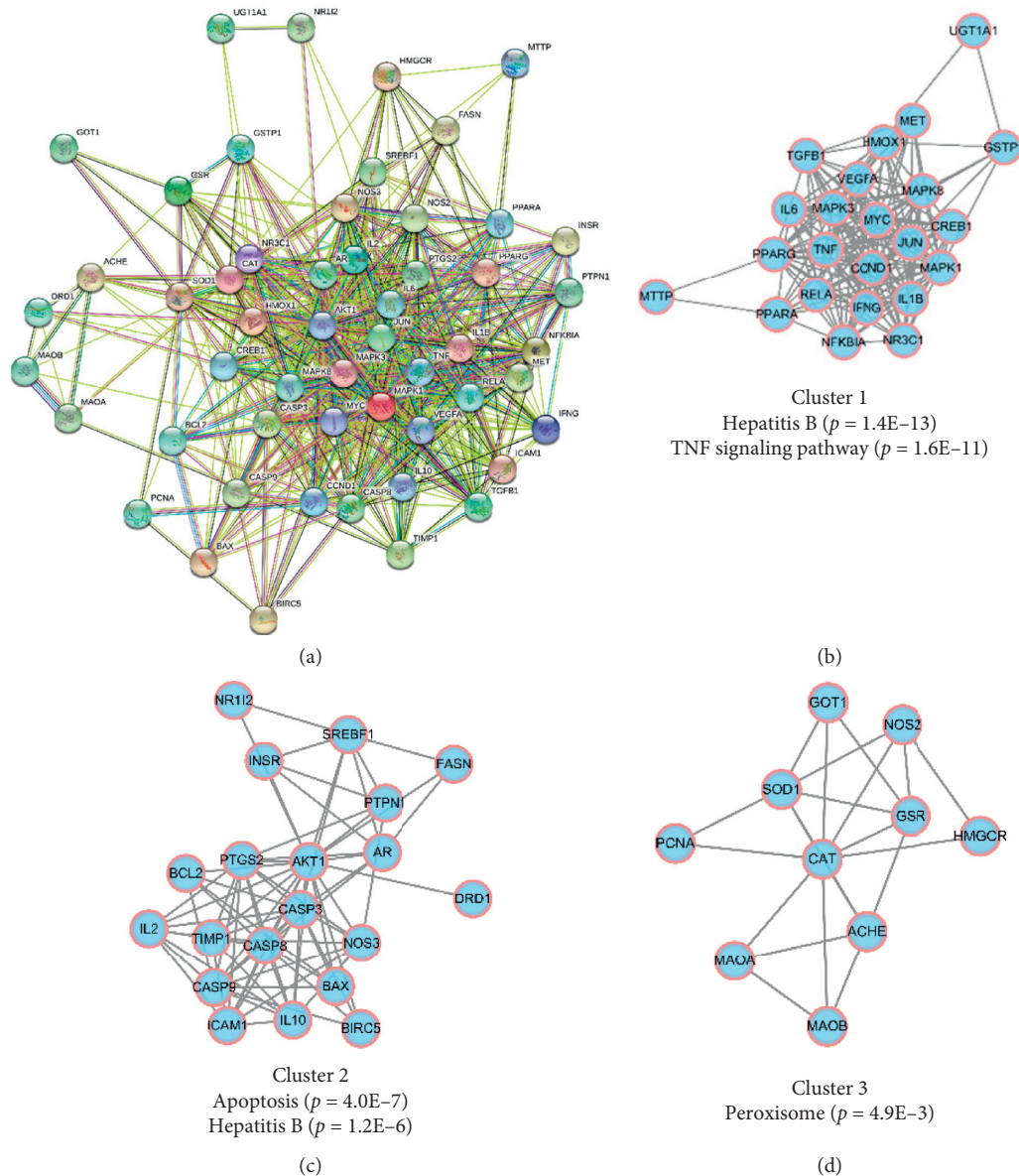


FIGURE 5: Protein-protein interaction (PPI) analysis of core targets of Qingdu decoction against chronic liver injury: (a) PPI network of core targets; (b) cluster 1 of the core PPI network; (c) cluster 2 of the core PPI network; (d) cluster 3 of the core PPI network.

molecular experiment to reveal the potential mechanisms of QDD on the apoptosis pathway.

Similar to our previously reported study, we found protective effect of QDD against CLI. AST is mainly distributed in the mitochondria of cells, and ALT is mainly distributed in the cytoplasm of cells [33]. Therefore, the sensitivity of ALT in liver injury is higher than that of AST, and the amplitude of increase is also higher than AST [34]. On the contrary, when AST elevation exceeds ALT, it often indicates that hepatocyte injury is more serious and is a sign of aggravation of chronic disease. Plasma PTA levels mainly reflect the status of liver coagulation function and are also sensitive indicators, reflecting the degree of liver cell damage and prognosis [35].

After confirming the potential anti-CLI effect of QDD, we try to focus on the effects and mechanisms of DQQ

against apoptosis. Apoptosis is one of the important causes of liver cell damage, and it is known that endotoxin is the second blow to CLI and induces chronic liver disease progression via gut-liver axis [36, 37] and directly damage liver cells and induce hepatocyte apoptosis [38, 39]. Pre-clinical evidence showed that LA reduced liver injury and decreased oxidative stress response, excessive inflammatory response, and fibrotic progression via downregulating endotoxin levels [40, 41]. Therefore, LA was used as positive control in the present study. By observing the ultrastructure of hepatocytes and mitochondria, it was found that the mitochondria of hepatocytes in the model group were severely swollen, accompanied by mitochondrial cristae rupture or disappearance. In severe cases, vacuolization or even rupture of the outer membrane was observed. After the

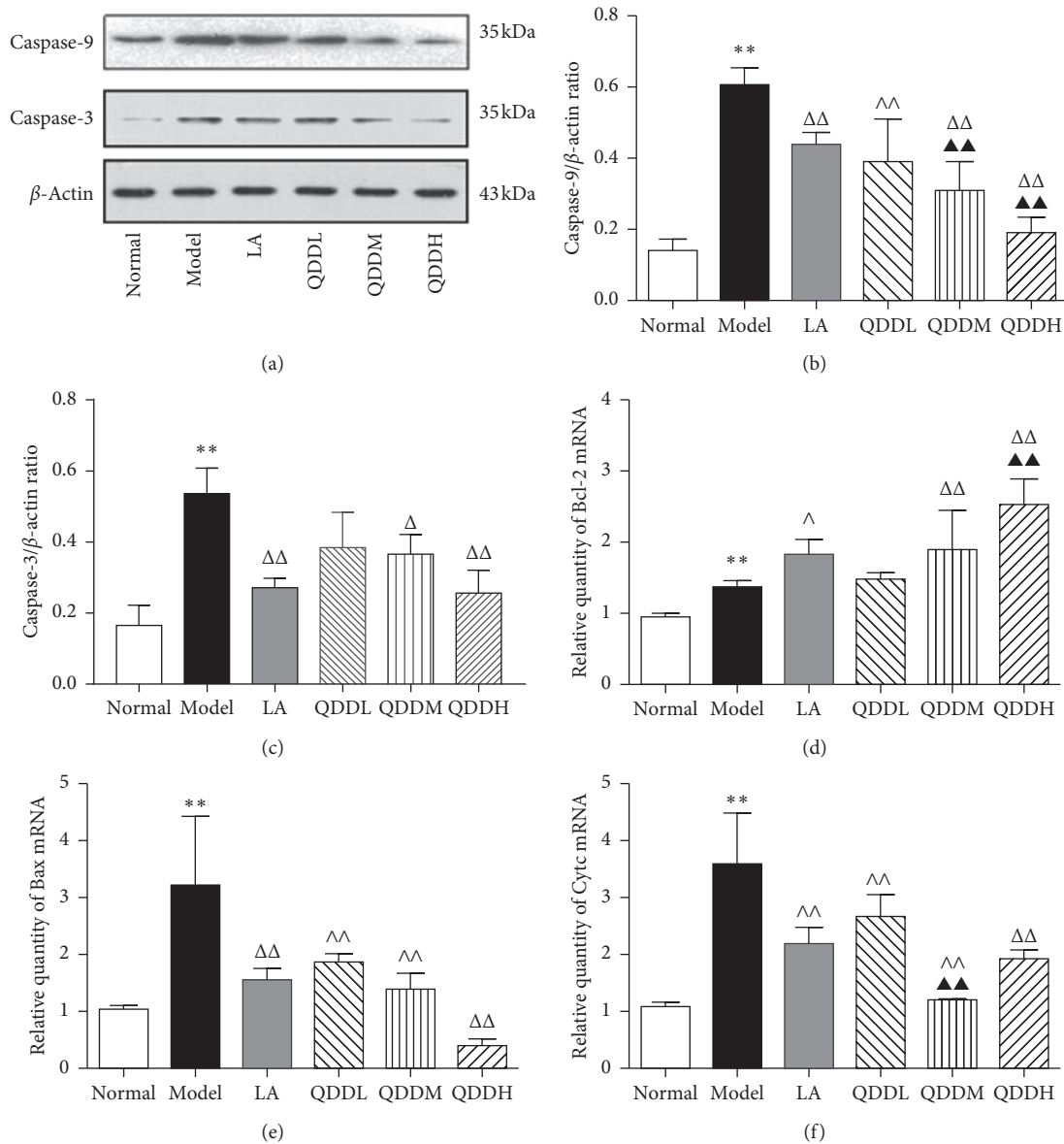


FIGURE 6: Effects of QDD on hepatocyte apoptosis. (a) Representative results of caspase-9 and caspase-3 protein; (b) the quantitative results of caspase-9 protein; (c) the quantitative results of caspase-3 protein; (d–f) quantification of Bcl-2, Bax, and Cyt c mRNA. Values are expressed as mean \pm SEM, $n = 5$ for each group. ** $P < 0.01$ vs normal group; $\Delta P < 0.05$, $\Delta\Delta P < 0.01$ vs model group; $\blacktriangle\blacktriangle P < 0.01$ vs LA group.

intervention of QDD, the apoptosis rate of mitochondria in liver cells was significantly reduced, and the degree of mitochondrial swelling was alleviated. At the same time, it was found that QDD can effectively reduce serum endotoxin level, which was similar to LA treatment.

Inflammatory factor is another inducer of apoptosis activation. Our previous studies confirmed that previously mentioned cytokines via target prediction of QDD, such as TNF- α , IL-6, and IL-1 β , were significantly induced by QDD in the same CLI model [5, 42]. The present study, we tested the serum level of IL-17 following QDD treatment, and the result indicated the potential of IL-17 as a target of QDD. Transcriptomic analysis found that luteolin had a synergistic effect on the expression level of IL-17 pathway-related genes [43], naringenin had a property of T-cell-suppressive activity

[44], and nobiletin was also reported to reduce IL-17 level upregulated in inflammatory model [45]. These compounds could be the biological basis of QDD on IL-17 pathway.

Under above stimulating factors, the mitochondrial membrane permeability increased, the membrane potential decreased to gradually disappear, and then, the mitochondrial morphological structure changed, leading to the release of various proapoptotic factors, which in turn leads to apoptosis. Our study found that, during the chronic liver injury, Cyt c was released and activated caspase-9, while Bax expression increased. After QDD intervention, Bax, Cyt c, caspase-9, and caspase-3 were downregulated. The experimental results also showed that the expression of anti-apoptosis factor Bcl-2 mRNA was not inhibited, but increased. The role of Bcl-2 family proteins in mitochondrial

apoptosis is well known [46]. As a core member of Bcl-2 family proteins, the antiapoptotic effect of Bcl-2 is mainly through the stabilization of mitochondrial membrane and regulation of intracellular Ca^{2+} concentration [47]. Bax, another core member of Bcl-2 family, can promote the release of various proapoptotic factors in mitochondria and can also form specific pores leading to the specific release of Cyt c [48]. Cyt c is a water-soluble protein located in the membrane gap of mitochondria, which is electrostatically stable in physiological conditions and bound to the inner membrane of mitochondria [49]. When stimulated by an apoptosis stimulating factor, Cyt c is released through the mitochondrial outer membrane, which promotes the binding of caspase-9 precursor to the amino terminus of apoptotic protease activating factor-1 (Apaf-1) to form an apoptotic body, further activating caspase-9 [50]. Activated caspase-9 activates the apoptotic executor caspase-3, which ultimately leads to apoptosis [51]. Back to the compound-target network, aloe-emodin, naringenin, and sitosterol were found to influence these tested targets directly, future studies should recognize the role of these compound in QDD, and pharmacokinetic parameters should be calculated in both healthy and disease individuals.

5. Conclusions

In conclusion, our study demonstrated that QDD can effectively reduce CLI, which is related to regulate hepatocyte apoptosis. The present study provides a new basis for the application of QDD for the treatment of CLI, which is worthy of further study.

Abbreviations

QDD:	Qingdu decoction
LA:	Lactulose
ALT:	Alanine aminotransferase
AST:	Aspartate aminotransferase
ET:	Endotoxin
IL-17:	Interleukin-17
PTA:	Prothrombin time activity
ELISA:	Enzyme-linked immunoassay
HE:	Hematoxylin-eosin
TEM:	Transmission electron microscopy
WB:	Western blot
qPCR:	Quantitative polymerase chain reaction
Bcl-2:	B-cell lymphoma-2
Bax:	Bcl-2-associated X protein
Cyt c:	Cytochrome c
Caspase-9:	Cysteiny aspartate specific proteinase-9
TNF- α :	Tumor necrosis factor- α
IL-6:	Interleukin-6
CLI:	Chronic liver injury.

Data Availability

The data used to support the findings of this study are available from the corresponding author upon request.

Ethical Approval

All experimental animal procedures were performed in strict accordance with Ethics Committee of Capital Medical University.

Consent

The consent for publication is not applicable.

Conflicts of Interest

The authors declare that they have no conflicts of interest.

Authors' Contributions

LG and QZ conceived and designed the study. CM, MZ, YD, SJ, and HZ performed the study. CM, MZ, YD, SJ, and HZ analyzed the data. CM, MZ, YD, and XW wrote the paper. LG supported the funding. All authors read and approved the final manuscript. Chongyang Ma and Mengpei Zhao contributed equally to this work.

Acknowledgments

The work was supported by the Beijing Municipal Commission of Education (Grant numbers 16ZY01 and KM201810025001).

Supplementary Materials

Supplementary Table 1. Bioactive compound information of Qingdu Decoction. Supplementary Table 2. Target information of Qingdu Decoction. Supplementary Table 3. Targets associated with chronic liver injury. (*Supplementary Materials*)

References

- [1] A. M. Moon, A. G. Singal, and E. B. Tapper, "Contemporary epidemiology of chronic liver disease and cirrhosis," *Clinical Gastroenterology and Hepatology*, vol. 18, no. 12, pp. 2650–2666, 2020.
- [2] J. B. Wang et al., "A systems pharmacology-oriented discovery of a new therapeutic use of the TCM formula Liuweiwuling for liver failure," *Scientific Reports*, vol. 8, no. 1, p. 5645, 2018.
- [3] L. Y. Gao and R. B. Wang, "Qingdu decoction with western medicine treatment of severe hepatitis endotoxemia in 30 cases," *Journal of Traditional Chinese Medicine*, vol. 44, no. 5, pp. 366–367, 2003.
- [4] R. B. Wang, Y. Z. Wu, Y. Y. Jiang et al., "Clinical observation of qingdu decoction in the treatment of enterogenous endotoxin in liver disease," *Chinese Journal of Integrated Traditional and Western Medicine on Liver Diseases*, vol. 14, no. 3, pp. 135–137, 2004.
- [5] W. Cao, Y. Du, L. Gao et al., "Lipopolysaccharide/Toll-like receptor 4 signaling pathway involved Qingdu decoction treating severe liver injury merging with endotoxemia," *Journal of Traditional Chinese Medicine = Chung I Tsa Chih Ying Wen pan*, vol. 37, no. 3, pp. 371–377, 2017.
- [6] M. Wallace, K. Hamesch, M. Lunova et al., "Standard operating procedures in experimental liver research:

- thioacetamide model in mice and rats,” *Laboratory Animals*, vol. 49, no. 1_suppl, pp. 21–29, 2015.
- [7] C. Lin, F. Wu, T. Zheng, X. Wang, Y. Chen, and X. Wu, “Kaempferol attenuates retinal ganglion cell death by suppressing NLRP1/NLRP3 inflammasomes and caspase-8 via JNK and NF- κ B pathways in acute glaucoma,” *Eye*, vol. 33, no. 5, p. 777, 2019.
 - [8] J. Ru, B. Li, P. Li et al., “TCMSP: a database of systems pharmacology for drug discovery from herbal medicines,” *Journal of Cheminformatics*, vol. 6, p. 13, 2014.
 - [9] A. P. Davis, C. J. Grondin, R. J. Johnson et al., “The comparative toxicogenomics database: update 2019,” *Nucleic Acids Research*, vol. 47, no. D1, pp. D948–d954, 2019.
 - [10] G. Yu, L.-G. Wang, Y. Han, and Q.-Y. He, “clusterProfiler: an R package for comparing biological themes among gene clusters,” *OMICS: A Journal of Integrative Biology*, vol. 16, no. 5, pp. 284–287, 2012.
 - [11] C. Ma, C. Zhai, T. Xuo et al., “A systems pharmacology-based study of the molecular mechanisms of san cao decoction for treating hypertension,” *Evid Based Complementary Alternative Medicine*, vol. 2019, Article ID 3171420, 10 pages, 2019.
 - [12] A. Panasiuk, J. Dzieciol, B. Panasiuk, and D. Prokopowicz, “Expression of p53, Bax and Bcl-2 proteins in hepatocytes in non-alcoholic fatty liver disease,” *World Journal of Gastroenterology*, vol. 12, no. 38, pp. 6198–6202, 2006.
 - [13] Y. Hu, M. A. Benedict, L. Ding, and G. Nunez, “Role of cytochrome c and dATP/ATP hydrolysis in Apaf-1-mediated caspase-9 activation and apoptosis,” *The EMBO Journal*, vol. 18, no. 13, pp. 3586–3595, 1999.
 - [14] H. Zhang, X. Tan, D. Yang et al., “Dietary luteolin attenuates chronic liver injury induced by mercuric chloride via the Nrf2/NF- κ B/P53 signaling pathway in rats,” *Oncotarget*, vol. 8, no. 25, pp. 40982–40993, 2017.
 - [15] L. Zhao, D. Yan, F. Zhao et al., “Protective effects of five structurally diverse flavonoid subgroups against chronic alcohol-induced hepatic damage in a mouse model,” *Nutrients*, vol. 10, no. 11, 2018.
 - [16] S. W. Woo, J.-X. Nan, S. H. Lee, E.-J. Park, Y. Z. Zhao, and D. H. Sohn, “Aloe emodin suppresses myofibroblastic differentiation of rat hepatic stellate cells in primary culture,” *Pharmacology and Toxicology*, vol. 90, no. 4, pp. 193–198, 2002.
 - [17] N. M. Morrow, A. C. Burke, J. P. Samsoumar et al., “The citrus flavonoid nobiletin confers protection from metabolic dysregulation in high-fat-fed mice independent of AMPK,” *Journal of Lipid Research*, vol. 61, no. 3, pp. 387–402, 2020.
 - [18] E. Devaraj, A. Roy, G. Royapuram Veeraragavan et al., “ β -Sitosterol attenuates carbon tetrachloride-induced oxidative stress and chronic liver injury in rats,” *Naunyn-Schmiedeberg’s Archives of Pharmacology*, vol. 393, no. 6, pp. 1067–1075, 2020.
 - [19] X. Dong, Y. Zeng, Y. Liu et al., “Aloe-emodin: a review of its pharmacology, toxicity, and pharmacokinetics,” *Phytotherapy Research*, vol. 34, no. 2, pp. 270–281, 2020.
 - [20] K. J. Kim, J. S. Lee, M. -K. Kwak et al., “Anti-inflammatory action of mollugin and its synthetic derivatives in HT-29 human colonic epithelial cells is mediated through inhibition of NF- κ B activation,” *European Journal of Pharmacology*, vol. 622, no. 1-3, pp. 52–57, 2009.
 - [21] Z. Wang, M. Y. Li, M. Chunliu, K. S. Wang, J. Ma, and X. Jin, “Mollugin has an anti-cancer therapeutic effect by inhibiting TNF- α -induced NF- κ B activation,” *International Journal of Molecular Sciences*, vol. 18, no. 8, 1619 pages, 2017.
 - [22] T. Bu, C. Wang, Q. Meng et al., “Hepatoprotective effect of rhein against methotrexate-induced liver toxicity,” *European Journal of Pharmacology*, vol. 834, pp. 266–273, 2018.
 - [23] X. Jiang, Y. Ma, M. Ma et al., “Aloe-emodin induces breast tumor cell apoptosis through upregulation of miR-15a/miR-16-1 that suppresses BCL2,” *Evidence Based Complementary Alternative Medicine*, vol. 2020, Article ID 5108298, 2020.
 - [24] L. Zhang, H. Wang, J. Zhu, J. Xu, and K. Ding, “Mollugin induces tumor cell apoptosis and autophagy via the PI3K/AKT/mTOR/p70S6K and ERK signaling pathways,” *Biochemical and Biophysical Research Communications*, vol. 450, no. 1, pp. 247–254, 2014.
 - [25] A. KoraMagazi, D. Wang, B. Yousef, M. Guerram, and F. Yu, “Rhein triggers apoptosis via induction of endoplasmic reticulum stress, caspase-4 and intracellular calcium in primary human hepatic HL-7702 cells,” *Biochemical and Biophysical Research Communications*, vol. 473, no. 1, pp. 230–236, 2016.
 - [26] G. Sebastiani, K. Gkouvatsos, and K. Pantopoulos, “Chronic hepatitis C and liver fibrosis,” *World Journal of Gastroenterology*, vol. 20, no. 32, pp. 11033–11053, 2014.
 - [27] E. Seki and D. A. Brenner, “Recent advancement of molecular mechanisms of liver fibrosis,” *Journal of Hepato-Biliary-Pancreatic Sciences*, vol. 22, no. 7, pp. 512–518, 2015.
 - [28] V. Rachakonda, D. Ahmed, N. Shah et al., “M1 muscarinic receptor deficiency attenuates azoxymethane-induced chronic liver injury in mice,” *Scientific Reports*, vol. 5, p. 14110, 2015.
 - [29] F. J. Cubero, A. Singh, E. Borkham-Kamphorst et al., “TNFR1 determines progression of chronic liver injury in the IKK γ /Nemo genetic model,” *Cell Death and Differentiation*, vol. 20, no. 11, pp. 1580–1592, 2013.
 - [30] B. Knight and G. C. Yeoh, “TNF/LT? double knockout mice display abnormal inflammatory and regenerative responses to acute and chronic liver injury,” *Cell and Tissue Research*, vol. 319, no. 1, pp. 61–70, 2005.
 - [31] L. Hammerich, F. Heymann, and F. Tacke, “Role of IL-17 and Th17 cells in liver diseases,” *Clin Dev Immunol*, vol. 2011, p. 345803, 2011.
 - [32] J.-O. Moon, T. P. Welch, F. J. Gonzalez, and B. L. Copple, “Reduced liver fibrosis in hypoxia-inducible factor-1 α -deficient mice,” *American Journal of Physiology-Gastrointestinal and Liver Physiology*, vol. 296, no. 3, pp. G582–G592, 2009.
 - [33] A. Deghady, A. Abdou, W. A. EL-Neanaey, and I. Diab, “Association of genetic polymorphism –670A>G in the fas gene and serum markers AST/platelet ratio index, AST/ALT with significant fibrosis and cirrhosis in chronic hepatitis C,” *Genetic Testing and Molecular Biomarkers*, vol. 16, no. 6, pp. 531–535, 2012.
 - [34] P. Rief, M. Pichler, R. Raggam et al., “The AST/ALT (De-Ritis) ratio: a novel marker for critical limb ischemia in peripheral arterial occlusive disease patients,” *Medicine (Baltimore)*, vol. 95, no. 24, Article ID e3843, 2016.
 - [35] X. Q. Che, Z. Q. Li, Z. Chen et al., “Plasma exchange combining with plasma bilirubin adsorption effectively removes toxic substances and improves liver functions of hepatic failure patients,” *European Review for Medical and Pharmacological Sciences*, vol. 22, no. 4, pp. 1118–1125, 2018.
 - [36] S. De Minicis, C. Rychlicki, L. Agostinelli et al., “Dysbiosis contributes to fibrogenesis in the course of chronic liver injury in mice,” *Hepatology*, vol. 59, no. 5, pp. 1738–1749, 2014.
 - [37] A. Albillos, A. de Gottardi, and M. Rescigno, “The gut-liver axis in liver disease: pathophysiological basis for therapy,” *Journal of Hepatology*, vol. 72, no. 3, pp. 558–577, 2020.

- [38] M. Xiao, W. Chen, C. Wang et al., "Senescence and cell death in chronic liver injury: roles and mechanisms underlying hepatocarcinogenesis," *Oncotarget*, vol. 9, no. 9, pp. 8772–8784, 2018.
- [39] H. Zhou et al., "Fc-apelin fusion protein attenuates lipopolysaccharide-induced liver injury in mice," *Scientific Reports*, vol. 8, no. 1, p. 11428, 2018.
- [40] B. Taskin, M. A. Erdogan, G. Yiğittürk, D. Güneç, and O. Erbaş, "Antifibrotic effect of lactulose on a methotrexate-induced liver injury model," *Gastroenterology Research and Practice*, vol. 2017, Article ID 7942531, , 2017.
- [41] F. B. Kasravi, D. Adawi, G. Molin, S. Bengmark, and B. Jeppsson, "Effect of oral supplementation of lactobacilli on bacterial translocation in acute liver injury induced by D-galactosamine," *Journal of Hepatology*, vol. 26, no. 2, pp. 417–424, 1997.
- [42] G. L. Luo Jiajia, S. Jin, N. Che, Q. Zhang, Y. Du, and X. Fu, "Effect of Qingdu decoction on intestinal mucosal permeability in rats with severe liver injury," *Global Traditional Chinese Medicine*, vol. 10, no. 3, pp. 261–264, 2017.
- [43] T. J. Lin, Y. Shu-Yi, H. Pei-Wen, and Y. Ning-Sun, I.- Jen Wang, "Transcriptomic analysis reveals a controlling mechanism for NLRP3 and IL-17A in dextran sulfate sodium (DSS)-induced colitis," *Scientific Reports*, vol. 8, no. 1, p. 14927, 2018.
- [44] X. Niu, C. Wu, M. Li et al., "Naringenin is an inhibitor of T cell effector functions," *The Journal of Nutritional Biochemistry*, vol. 58, pp. 71–79, 2018.
- [45] G. Yang, S. Li, Y. Yang et al., "Nobiletin and 5-Hydroxy-6,7,8,3',4'-pentamethoxyflavone ameliorate 12-O-Tetradecanoylphorbol-13-acetate-Induced psoriasis-like mouse skin lesions by regulating the expression of ki-67 and proliferating cell nuclear antigen and the differentiation of CD4+ T cells through mitogen-activated protein kinase signaling pathways," *Journal of Agricultural and Food Chemistry*, vol. 66, no. 31, pp. 8299–8306, 2018.
- [46] R. Wang, H. Zhang, Y. Wang, F. Song, and Y. Yuan, "Inhibitory effects of quercetin on the progression of liver fibrosis through the regulation of NF- κ B/I κ B α , p38 MAPK, and Bcl-2/Bax signaling," *International Immunopharmacology*, vol. 47, pp. 126–133, 2017.
- [47] S. Shimamoto, M. Tsuchiya, F. Yamaguchi, Y. Kubota, H. Tokumitsu, and R. Kobayashi, "Ca²⁺/S100 proteins inhibit the interaction of FKBP38 with Bcl-2 and Hsp90," *Biochemical Journal*, vol. 458, no. 1, pp. 141–152, 2014.
- [48] J. C. Goldstein, N. J. Waterhouse, P. Juin, G. I. Evan, and D. R. Green, "The coordinate release of cytochrome c during apoptosis is rapid, complete and kinetically invariant," *Nature Cell Biology*, vol. 2, no. 3, pp. 156–162, 2000.
- [49] S. Snigdha, E. D. Smith, G. A. Prieto, and C. W. Cotman, "Caspase-3 activation as a bifurcation point between plasticity and cell death," *Neuroscience Bulletin*, vol. 28, no. 1, pp. 14–24, 2012.
- [50] S. B. Bratton and G. S. Salvesen, "Regulation of the apaf-1-caspase-9 apoptosome," *Journal of Cell Science*, vol. 123, no. Pt 19, pp. 3209–3214, 2010.
- [51] M. Saikia, R. Jobava, M. Parisien et al., "Angiogenin-cleaved tRNA halves interact with cytochrome c, protecting cells from apoptosis during osmotic stress," *Molecular and Cellular Biology*, vol. 34, no. 13, pp. 2450–2463, 2014.

Research Article

The Association between Metabolic Syndrome and Elevated Alanine Aminotransferase Levels in an Indigenous Population in Northern Taiwan: A Community-Based and Cross-Sectional Study

Yi-Fang Chen ¹, Yen-An Lin ¹, Wei-Chung Yeh ¹, Yu-Chung Tsao ^{2,3},
Wen-Cheng Li ^{1,3,4}, Wei-Ching Fang ¹, I-Ju Chen ¹, and Jau-Yuan Chen ^{1,3}

¹Department of Family Medicine, Chang-Gung Memorial Hospital, Linkou Branch, Taoyuan City 33305, Taiwan

²Department of Occupational Medicine, Chang Gung Memorial Hospital, Linkou Branch, Taoyuan City 33305, Taiwan

³Chang Gung University College of Medicine, Taoyuan City 33302, Taiwan

⁴Department of Health Management, Xiamen Chang-Gung Hospital, Xiamen 361028, China

Correspondence should be addressed to Jau-Yuan Chen; welins@cgmh.org.tw

Received 16 October 2020; Revised 18 November 2020; Accepted 26 November 2020; Published 9 December 2020

Academic Editor: Chih-Yuan Ko

Copyright © 2020 Yi-Fang Chen et al. This is an open access article distributed under the Creative Commons Attribution License, which permits unrestricted use, distribution, and reproduction in any medium, provided the original work is properly cited.

Our study aims to determine the prevalence of metabolic syndrome (MetS) among the Northern Taiwanese indigenous population and to explore the relationship between MetS and liver enzyme, especially serum alanine transaminase (ALT). This is an observational and cross-sectional study that was conducted in remote villages of an indigenous community in Northern Taiwan between 2010 and 2015. MetS was defined based on the revised NCEP/ATPIII criteria from Taiwan Health Promotion Administration. A total of 454 participants were included in the analysis. There were 277 people with MetS and 177 people without. The prevalence of MetS was 61.01%. The average age was 49.50 years. People with MetS had a significantly higher liver enzyme (ALT) level than those without MetS. In addition, the study showed that participants with higher ALT had a tendency towards a higher prevalence of MetS (76.7% vs. 57.3%, $p = 0.001$). The adjusted odds ratio (OR) of ALT levels >36 U/L for MetS was 2.79 (95% CI = 1.24–6.27, $p = 0.01$). The area under the ROC curve (AUC) of the ALT level was 0.63 (95% CI = 0.58–0.68, $p < 0.001$), which showed that the ALT level was positively associated with MetS. The overall prevalence of MetS was 61.01% in the highland indigenous population in Northern Taiwan; this study indicated that higher serum ALT levels were associated with an increased risk of MetS.

1. Introduction

Metabolic syndrome (MetS), a serious global health concern, is a constellation of different metabolic abnormalities in an individual, including central obesity, hyperglycemia, hypertension, elevated triglyceride levels, and low high-density lipoprotein cholesterol levels [1]. These abnormalities result in an increased risk of cardiovascular events, type II diabetes, and chronic kidney disease [2, 3]. Therefore, the identification of risk factors associated with MetS is vital.

According to the Taiwan national survey, the Nutrition and Health Survey in Taiwan (NAHSIT), the prevalence of MetS increased from 13.6% (1993–1996) to 30% (2013–2016). Taking the regional and ethnic diversity in

Taiwan into consideration, the NAHSIT 2005–2008 investigated the regional differences and showed that the indigenous area had the highest prevalence (52.1%) compared to the prevalence in the densely populated areas, the Off-shore island and the Hakka area. Additionally, up to 71.6% of indigenous peoples were overweight or obese [4, 5]. Furthermore, two cross-sectional studies demonstrated a high prevalence of MetS among indigenous populations in Taiwan between 2010 and 2011 [6, 7]. Nevertheless, there are still limited studies on MetS among indigenous peoples in Taiwan. A hospital-based study showed the prevalence of metabolic syndrome in aboriginals in Southeastern Taiwan was 58.7%, with a higher prevalence (68.5%) in women than in men (50.3%) ($p < 0.001$) [6]. Thus, we decided to design a

real world and community-based study to figure out whether the indigenous population in northern part of Taiwan has the same high prevalence or not. We intend to assess MetS status in an indigenous tribe, the Atayal tribe, which is widely distributed in the northern part of the Central Mountain Range of Taiwan.

Alanine transaminase (ALT) is an enzyme that mainly exists in hepatocytes, and when the liver is injured due to conditions such as viral hepatitis, ALT will be released, resulting in elevated serum ALT levels [8]. A large community study in Taiwan from 2003 to 2004 illustrated that the prevalence of elevated ALT in an adult population was 11.4%, and nonalcoholic fatty liver disease (NAFLD) seemed to be the most common cause of elevated ALT [9]. Moreover, there were 16.5% adults with abnormal ALT levels in an Atayal indigenous community [10]. Previous cross-sectional studies have reported a positive association between serum ALT level and MetS [11, 12]. A systemic review and meta-analysis and a large cohort study both showed that the increase in serum ALT levels increased the risk of MetS [13, 14]. In addition, the Taiwan indigenous groups have high prevalence of alcoholism, hepatitis B, and hepatitis C, and the prevalence of abnormal ALT level was also high in the Atayal tribe [10]. Therefore, our study aimed to determine the association and the prevalence of MetS with higher serum ALT levels among the Northern Taiwanese indigenous population.

2. Materials and Methods

2.1. Study Design and Study Population. This is an observational and cross-sectional study. Before this study, the minimum sample size for this study was calculated at the initial stage of the study. After previewing a relatively smaller population, considering 80% power, 95% confidence level, and 0.59 as the metabolic syndrome prevalence rate among indigenous population, we calculated that 276 participants were required to detect at least 2 odds ratios. We collected data from three remote villages in an indigenous community in Northern Taiwan from 2010 through 2015. Subjects were residents who had lived in the community for more than 6 months, aged over 18, and were able to walk to the health station. Every subject completed a questionnaire containing questions regarding basic personal data and medical conditions, including race, age, sex, occupation, and history of hypertension, diabetes, and hyperlipidemia. The questionnaires were completed after detailed explanations were provided by the trained interviewers in in-person interviews. Additionally, urine and blood samples were collected. Anthropometric measurements were performed by trained research assistants or nurses under the supervision of a medical doctor. After the exclusion of subjects who were pregnant or who had incomplete, missing, or repeated data, 454 participants were eligible for the analysis. The flow chart diagram (Figure 1) shows a gradual selection of individuals who comprised the subjects for final analysis. The study was approved by the Chang Gung Medical Foundation Institutional Review Board (99-0231B, 101-4156A3, 104-7978A3), and written informed consent was provided by all the subjects before enrollment.

2.2. Definition of Metabolic Syndrome and Abnormal ALT Level. MetS was defined by the revised NCEP/ATPIII criteria from Taiwan Health Promotion Administration [15]. In detail, a diagnosis of MetS requires the presence of three or more of the following factors: (1) waist circumference (WC) ≥ 90 cm in men or ≥ 80 cm in women, (2) systolic blood pressure (SBP) ≥ 130 mmHg or diastolic blood pressure (DBP) ≥ 85 mmHg or current use of anti-hypertensive drugs, (3) serum HDL-C < 40 mg/dl in men or < 50 mg/dl in women, (4) serum triglycerides ≥ 150 mg/dl or triglycerides-lowering drugs, and (5) fasting plasma glucose ≥ 100 mg/dl or current use of antihyperglycemic drugs. An abnormal ALT level was defined as a level > 36 U/L according to the laboratory method used in Chang Gung Memorial Hospital.

2.3. Definition of Hypertension, Diabetes Mellitus, Hyperlipidemia, Smoking, and Alcohol Drinking. Hypertension was defined by a SBP ≥ 140 mmHg or DBP ≥ 90 mmHg or use of antihypertensive drugs. Diabetes mellitus was defined as a fasting plasma glucose ≥ 126 mg/dL, or glycated hemoglobin (HbA1c) ≥ 6.5 , or the use of oral hypoglycemic agents or insulin therapy. Hyperlipidemia was defined as LDL-C ≥ 130 mg/dL, or triglycerides (TGs) ≥ 150 mg/dL, or total cholesterol (TC) ≥ 200 mg/dL, or use of lipid-lowering medications. Smoking was defined as at least 3 days a week in the recent month. Alcohol drinking habit was defined as more than 3 times a week.

2.4. Anthropometric and Laboratory Measurements. Each subject's blood pressure (BP) was measured on the upper arm while they were in a seated position after at least 5 minutes of rest with a standardized electronic sphygmomanometer. WC was measured at the level midway between the iliac crests and the lowest rib margin with the subjects in a standing position. Height was determined by a height-measuring machine while subjects were barefoot and standing in an erect position with their arms by their side and their feet together. Weight measurements were performed with subjects standing at the center of the weighing scale in light clothing without shoes or socks. Body mass index (BMI) was defined as the weight in kilograms divided by the square of the height in meters (kg/m^2). Then, we classified the BMI values into 3 main categories according to the definition published by Taiwan Health Promotion Administration: (1) underweight (BMI < 18.5), (2) normal weight ($18.5 \leq \text{BMI} < 24$), and (3) overweight or obesity (BMI ≥ 24) [16].

Blood samples were obtained from the antecubital vein after a 12 h overnight fast. All blood analyses were carried out at the clinical laboratory department of the Linkou Chang Gung Memorial Hospital, which is certified by the College of American Pathologists. Biochemical markers were analyzed on a Hitachi 7600-210 autoanalyzer (Hitachi, Tokyo, Japan); the biochemical markers included serum TC, HDL-C, TGs, fasting plasma glucose (FPG), ALT, high-sensitivity C-reactive protein (HS-CRP), HbA1c, and uric acid. In detail, the ALT levels were measured by an enzymatic

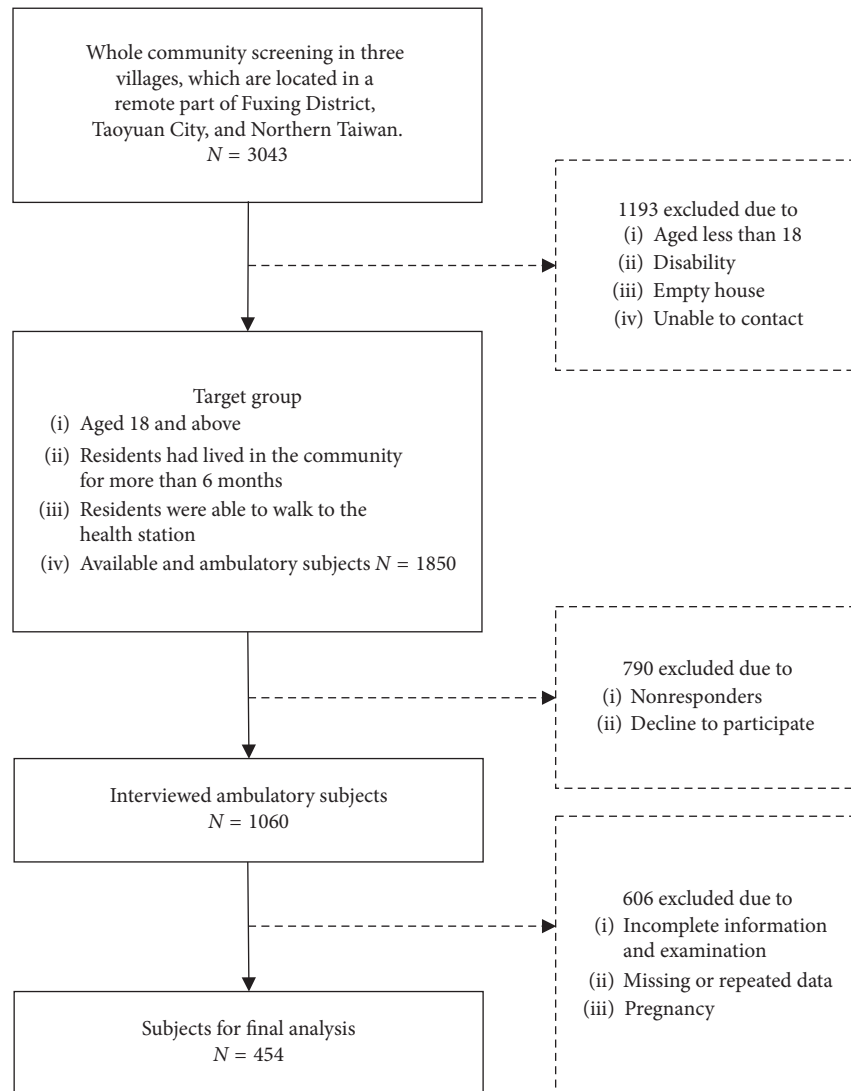


FIGURE 1: Flow chart of the study subjects.

method with a matched instrument application (Hitachi, Tokyo, Japan) in the Linkou Chang Gung Memorial Hospital.

2.5. Statistical Analysis. Data are presented as the mean and standard deviation for continuous variables or numbers and percentages for categorical variables. For variables with nonnormal distributions, the data are log-transformed for analysis and shown as median (interquartile range). In univariate analysis, independent sample *t*-tests and chi-square tests were used to compare MetS and non-MetS subjects. The chi-square test was also performed to determine the differences in two categorical variables and the prevalence of MetS in different serum ALT level groups. Correlations between different cardiometabolic risk factors and serum ALT levels were assessed with Pearson's correlation coefficient. The odds ratios (ORs) and their 95% confidence intervals (CIs) were determined for the association between cardiometabolic risk factors and MetS with

adjustment for potential confounders, such as age, sex, alcohol drinking, and uric acid level. The receiver operating characteristic (ROC) curve was produced to acquire the values of the area under the curve (AUC) with 95% CIs and sensitivity and specificity values for the serum ALT level as a predictor of MetS. The analyses mentioned above were performed with SPSS Statistics version 22 (IBM, SPSS Armonk, NY, IBM Corp.). A *p* value of <5% was considered to indicate a statistically significant result.

3. Results

The baseline characteristics of the study population according to MetS diagnosis are presented in Table 1. A total of 454 participants were enrolled in the analysis, including 215 (47.36%) men and 239 (52.64%) women. There were 277 people with MetS and 177 people without. The prevalence of MetS was 61.01%. The average age was 49.50 years. People with MetS had a significantly higher ALT level (24.00 (17–36) U/L vs. 19.00 (15–26) U/L,

$p < 0.001$) than those without MetS (Table 1). Also, the prevalence of antihypertensive, antilipidemic, and antidiabetic medication was 50% ($86/172 = 50\%$), 23.48% ($85/362 = 23.48\%$), and 44.58% ($37/83 = 44.58\%$), respectively.

Furthermore, people with MetS had significantly higher levels of SBP, DBP, WC, BMI, FPG, serum HbA1c, TC, HS-CRP, TGs, and uric acid than those without MetS (Table 1). People with MetS were also older, more likely to be male, and had a higher prevalence of hypertension, diabetes, and hyperlipidemia but lower serum HDL-C levels. However, there were no statistically significant differences in the percentages of alcohol drinkers, smokers, and serum total bilirubin levels between the two groups.

The comparisons of the prevalence of MetS in different ALT levels >36 U/L and ≤ 36 U/L groups and the total study group are shown in Figure 2(a). The chi-square comparison showed that participants with ALT levels >36 U/L had a tendency towards a higher prevalence of MetS (76.7% vs. 57.3%, $p = 0.001$) compared with the prevalence of those with ALT levels ≤ 36 U/L. The bar chart illustrates that the ALT levels >36 U/L group had the highest MetS prevalence among the groups (Figure 2(b)). The chi-square comparison also showed that female participants with ALT levels >36 U/L had a tendency towards a higher prevalence of MetS (88.9% vs. 61.1%, $p = 0.001$) compared with the prevalence of those with ALT levels ≤ 36 U/L (Figure 2(b)).

The correlations between the serum ALT level and cardiometabolic risk factors are displayed in Table 2. The age-adjusted Pearson's coefficients of BMI, SBP, DBP, WC, FPG, and HS-CRP were 0.21 ($p < 0.001$), 0.14 ($p = 0.01$), 0.18 ($p < 0.001$), 0.26 ($p < 0.001$), 0.11 ($p = 0.03$), and 0.14 ($p = 0.01$), respectively, which indicated positive linear relationships with serum ALT levels (Table 2). The age-adjusted Pearson's coefficient of HDL-C was -0.12 ($p = 0.02$), which indicated a weak negative linear relationship with serum ALT levels. The serum Hb-1Ac, TC, TG, and uric acid levels had no statistically significant correlations with the serum ALT level.

The ORs of cardiometabolic risk factors for MetS are shown in Table 3. In the univariate logistic regression model, the crude ORs of ALT levels >36 U/L, each additional year of age, sex (men versus women), alcohol drinking (yes versus no), $\text{BMI} \geq 24 \text{ kg/m}^2$, serum HS-CRP, and uric acid levels for MetS were 2.46 (95% CI = 1.43–4.22, $p = 0.001$), 1.04 (95% CI = 1.03–1.05, $p < 0.001$), 1.46 (95% CI = 1.00–2.13, $p = 0.05$), 1.36 (95% CI = 0.77–2.39, $p = 0.29$), 7.31 (95% CI = 4.72–11.32, $p < 0.001$), 1.04 (95% CI = 0.99–1.09, $p = 0.14$), and 1.25 (95% CI = 1.12–1.40, $p < 0.001$), respectively. In the univariate logistic regression model, the adjusted ORs of ALT levels >36 U/L, each additional year of age, sex (men versus women), alcohol drinking (yes versus no), $\text{BMI} \geq 24 \text{ kg/m}^2$, serum HS-CRP, and uric acid levels for MetS were 2.79 (95% CI = 1.24–6.27, $p = 0.01$), 1.06 (95% CI = 1.04–1.08, $p < 0.001$), 2.88 (95% CI = 1.57–5.29, $p = 0.001$), 2.19 (95% CI = 1.09–4.41, $p = 0.03$), 9.40 (95% CI = 4.90–18.01, $p < 0.001$), 1.00 (95% CI = 0.94–1.05, $p = 0.86$), and 1.22 (95% CI = 1.02–1.45, $p = 0.03$), respectively (Table 3). The adjusted ORs of $\text{BMI} < 18.5 \text{ kg/m}^2$ for MetS were not statistically significant.

Finally, the AUC of the serum ALT level was 0.63 (95% CI = 0.58–0.68, $p < 0.001$), which showed that the serum ALT level was positively associated with MetS, and the cut-off point was 20.50 U/L (Table 4, Figure 3).

4. Discussion

The main finding of the present study is the high prevalence of MetS in a Taiwanese indigenous population, and there was an association between serum ALT levels and MetS. Higher serum ALT levels, especially over 36 U/L, were associated with an increased risk of MetS.

The results were consistent with the findings of several previous studies. A hospital-based study showed that more than half of the indigenous adults in southeastern Taiwan had MetS [6], and two community-based studies revealed that the prevalence of MetS in indigenous populations in Northern Taiwan was over 48% [7, 17]. In contrast, without regard to regional difference, the data from the Taiwan Health Promotion Administration revealed that the overall prevalence of MetS in Taiwanese adults above the age of 20 was 19.7% in 2007 [15]. According to a cross-sectional survey, the MetS prevalence in a Taiwan metropolitan area was 33.32% among adults aged over 40 years in 2007 [18]. Therefore, it seems that the prevalence of MetS is higher in the Atayal tribe than in the metropolitan or overall population in Taiwan. This inference was in line with the results of the 2005–2008 NAHSIT, which revealed that the highest prevalence of MetS was found in the indigenous area (mountains) compared to the prevalence in other places in Taiwan [4]. Additionally, this idea was supported by a cross-sectional study illustrating that indigenous groups in Taiwan had a markedly higher prevalence of MetS than the Taiwanese and Hakka groups [19].

The reasons for the above phenomenon could be multifactorial. First, there were some health disparities between indigenous individuals and the general population in Taiwan [20]. For example, the lifetime prevalence of alcoholism according to ICD or DSM in four Taiwanese indigenous groups was 40–60% [21], and a large prospective cohort study revealed that heavy alcohol consumption is associated with an increased risk of the MetS [22]. In addition, a study suggested that 6% of inhabitants in Kaohsiung, the second-largest city of Taiwan, were current betel chewers, whereas 42% of the indigenous individuals aged over 15 years in southern Taiwan were current chewers [23]. Although areca nut chewing is deeply rooted in indigenous culture and symbolizes social belonging in Taiwan [24], chronic areca nut chewing is one of the independent risk factors for MetS and contributes to metabolic derangements via the involvement of tumor necrosis factor- α , leptin, and leukocyte count [25].

Second, there is a socioeconomic gap between the indigenous people and the general public in Taiwan. According to the economic status survey from the Council of Indigenous Peoples in Taiwan, the indigenous household income was approximately 61% of the average household income of Taiwan in 2014, and only 6.58% of primary income earners had a university education or above [26]. However, a study suggested that good socioeconomic status

TABLE 1: Study population characteristics according to the presence of MetS.

Variables	Total (<i>n</i> = 454)	Metabolic syndrome		<i>p</i> value
		No (<i>n</i> = 177)	Yes (<i>n</i> = 277)	
Age (year)	49.50 ± 16.01	43.83 ± 16.97	53.12 ± 14.26	<0.001
SBP (mmHg)	133.03 ± 21.26	123.45 ± 18.21	139.15 ± 20.84	<0.001
DBP (mmHg)	83.80 ± 13.85	78.82 ± 12.53	86.97 ± 13.74	<0.001
WC (cm)	88.62 ± 11.00	81.23 ± 9.08	93.37 ± 9.40	<0.001
ALT (U/L) ^a	22.00 (16–32)	19.00 (15–26)	24.00 (17–36)	<0.001
FPG (mg/dL) ^a	93.00 (86–104.25)	87.00 (83–92)	99.00 (90–117)	<0.001
HbA1c (%) ^a	5.90 (5.6–6.2)	5.70 (5.5–5.9)	6.00 (5.7–6.5)	<0.001
HDL-C (mg/dL)	50.47 ± 13.05	56.40 ± 11.79	46.68 ± 12.41	<0.001
HS-CRP (mg/L) ^a	1.48 (0.72–2.94)	0.88 (0.4–2.2)	1.90 (0.96–3.52)	<0.001
TC (mg/dL)	194.28 ± 39.79	184.14 ± 33.21	200.75 ± 42.27	<0.001
Total bilirubin (mg/dL) ^a	0.50 (0.40–0.70)	0.50 (0.4–0.7)	0.50 (0.4–0.7)	0.24
TG (mg/dL) ^a	114.00 (80–183)	85.00 (62.0–115.5)	143.00 (103.5–215.0)	<0.001
Uric acid (mg/dL)	6.36 ± 1.88	5.91 ± 1.78	6.65 ± 1.88	<0.001
Men, <i>n</i> (%)	215 (47.36%)	94 (53.11%)	121 (43.68%)	0.0498
ALT				0.001
≤36 U/L	368 (81.06%)	157 (88.70%)	211 (76.17%)	
>36 U/L	86 (18.94%)	20 (11.30%)	66 (23.83%)	
BMI				<0.001
<18.5	10 (2.21%)	8 (4.55%)	2 (0.72%)	
18.5–24	152 (33.55%)	103 (58.52%)	49 (17.69%)	
≥24	291 (64.24%)	65 (36.93%)	226 (81.59%)	
HTN, <i>n</i> (%)	172 (38.05%)	35 (19.89%)	137 (49.64%)	<0.001
DM, <i>n</i> (%)	94 (20.70%)	5 (2.82%)	89 (32.13%)	<0.001
Hyperlipidemia, <i>n</i> (%)	362 (79.74%)	96 (54.24%)	266 (96.03%)	<0.001
Smoking, <i>n</i> (%)	43 (13.78%)	14 (12.28%)	29 (14.65%)	0.56
Alcohol drinking, <i>n</i> (%)	71 (22.61%)	22 (19.30%)	49 (24.50%)	0.29

Notes: clinical characteristics are presented as mean ± SD for continuous variables and *n* (%) for categorical variables. Variables with nonnormal distributions are log-transformed for analysis and shown as median (interquartile range). *p* values were derived from the independent *t*-test for continuous variables and chi-square test for categorical variables. ^a is considered as log-transformed variables. SBP, systolic blood pressure; DBP, diastolic blood pressure; WC, waist circumference; ALT, alanine aminotransferase; FPG, fasting plasma glucose; HbA1c, glycated hemoglobin; HDL-C, high-density lipoprotein cholesterol; HS-CRP, high-sensitivity C-reactive protein; TC, total cholesterol; TG, triglyceride; BMI, body mass index; HTN, hypertension; DM, diabetes mellitus.

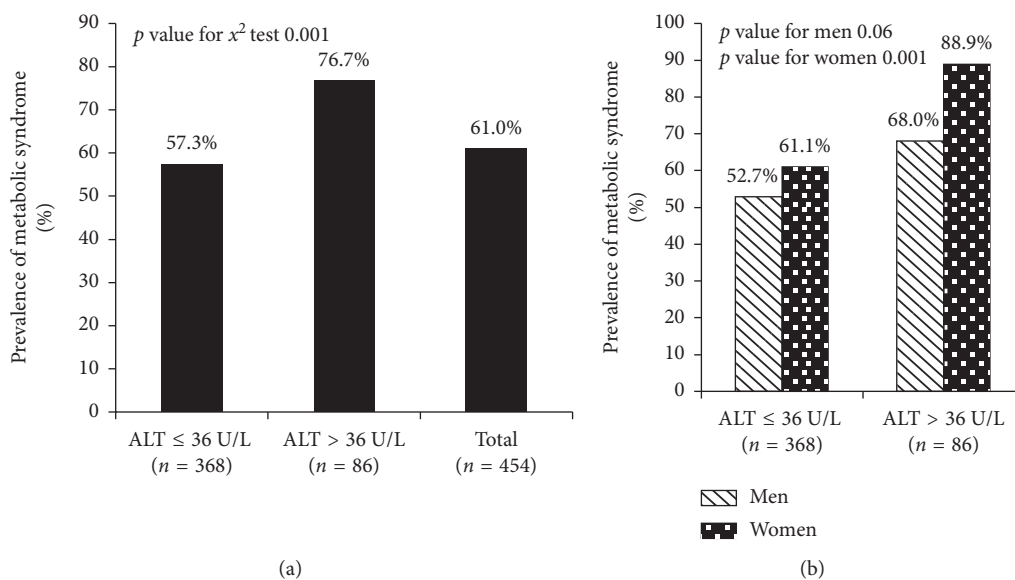


FIGURE 2: The comparisons of the prevalence of MetS in different ALT level groups and the total study group (a) and the prevalence of MetS of men and women in different ALT level groups (b).

TABLE 2: The correlations between ALT and cardiometabolic risk factors.

Variables	ALT U/L (<i>n</i> = 454)			
	Unadjusted		Adjusted for age	
	Pearson's coefficient	<i>p</i> value	Pearson's coefficient	<i>p</i> value
Age (year)	-0.07	0.147	NA	NA
BMI (kg/m ²)	0.24	<0.001	0.21	<0.001
SBP (mmHg)	0.11	0.02	0.14	0.01
DBP (mmHg)	0.16	<0.001	0.18	<0.001
WC (cm)	0.26	<0.001	0.26	<0.001
FPG (mg/dL)	0.09	0.04	0.11	0.03
HbA1c (%)	0.08	0.08	0.09	0.10
HDL-C (mg/dL)	-0.12	0.01	-0.12	0.02
HS-CRP (mg/L)	0.15	0.001	0.14	0.01
TC (mg/dL)	0.02	0.60	0.01	0.82
Total bilirubin (mg/dL)	0.19	<0.001	0.23	<0.001
TG (mg/dL)	0.11	0.02	0.09	0.09
Uric acid (mg/dL)	0.10	0.03	0.10	0.05

ALT, alanine aminotransferase; BMI, body mass index; SBP, systolic blood pressure; DBP, diastolic blood pressure; WC, waist circumference; FPG, fasting plasma glucose; HbA1c, glycated hemoglobin; HDL-C, high-density lipoprotein cholesterol; HS-CRP, high-sensitivity C-reactive protein; TC, total cholesterol; TG, triglyceride.

TABLE 3: Univariate and multivariate logistic regression on the cardiometabolic risk factors related to MetS among the study population.

Variables	Crude odds ratio	(95% CI)	<i>p</i> value	Adjusted odds ratio	(95% CI)	<i>p</i> value
ALT (>36 U/L versus ≤36 U/L)	2.46	(1.43–4.22)	0.001	2.79	(1.24–6.27)	0.01
Age (year)	1.04	(1.03–1.05)	<0.001	1.06	(1.04–1.08)	<0.001
Sex (men versus women)	1.46	(1.00–2.13)	0.05	2.88	(1.57–5.29)	0.001
Alcohol drinking (yes versus no)	1.36	(0.77–2.39)	0.29	2.19	(1.09–4.41)	0.03
BMI (kg/m ²)						
<18.5	0.53	(0.11–2.57)	0.43	1.53	(0.19–12.32)	0.69
18.5–24	1.00	—	—	1.00	—	—
≥24	7.31	(4.72–11.32)	<0.001	9.40	(4.90–18.01)	<0.001
HS-CRP (mg/L)	1.04	(0.99–1.09)	0.14	1.00	(0.94–1.05)	0.86
Uric acid (mg/dL)	1.25	(1.12–1.40)	<0.001	1.22	(1.02–1.45)	0.03

ALT, alanine aminotransferase; BMI, body mass index; HS-CRP, high-sensitivity C-reactive protein.

TABLE 4: The areas under ROC curve (AUC) and sensitivity, specificity by the optimized cut-off points for ALT in predicting metabolic syndrome.

Variables	AUC (95% CI)	<i>p</i> value	Cut-off point	Sensitivity	Specificity
ALT (U/L)	0.63 (0.58–0.68)	<0.001	20.500	0.643	0.559

ALT, alanine aminotransferase; ROC curve, receiver operating characteristic curve; CI, confidence interval.

could protect against MetS [27], and a study with a large sample size also implied that a higher education level was related to a lower risk of MetS [28]. In other words, low socioeconomic status could negatively impact the health of indigenous people. Third, the indigenous population in our study was located in the mountains without adequate healthcare resources, and the lack of medical accessibility caused them to delay seeking care to improve their health outcomes. In summary, differences in health behaviors, low socioeconomic status, and limited access to healthcare in remote areas all impacted the health inequality between the Atayal tribe and individuals from metropolitan areas.

In the present study, the second major finding was that baseline serum ALT level and MetS were positively

associated with the cut-off point of 20.50 U/L based on the AUC, and the adjusted OR of ALT levels >36 U/L for MetS was 2.79 after correction for age, sex, alcohol drinking, BMI, serum HS-CRP, and uric acid levels. These results corroborate the findings from a large-population, community-based study conducted in China, which verified a positive correlation between normal serum ALT levels and the morbidity rate of MetS after age and BMI correction. The optimal ALT boundary value based on the ROC curve was 24.5 for men and 14.5 U/L for women [29]. In short, an elevated ALT level, even at a level still within the reference interval, may reflect early metabolic changes.

On the other hand, our study also implied that an ALT level >36 U/L was associated with a tendency towards a

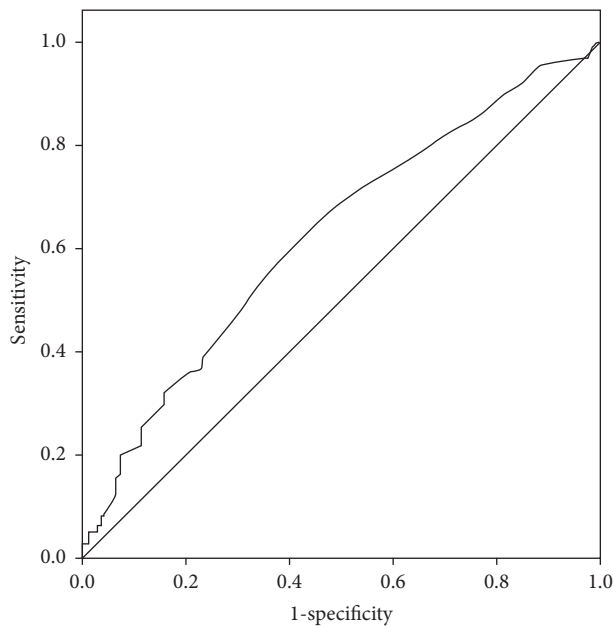


FIGURE 3: ROC curve and AUC for ALT as a predictor of MetS.

higher prevalence of MetS compared to the prevalence associated with ALT levels ≤ 36 U/L. The finding was similar to the results of prior studies. A systematic review and meta-analysis revealed that the baseline circulating ALT level is associated with the risk of MetS and exhibits a linear dose-response relationship [14], which was identical to the results of a cross-sectional study including over 15000 adults and a longitudinal study with 7 years of follow-up from China [12, 13]. Taken together, these research studies have indicated that people with higher ALT levels have a higher risk of MetS.

In addition, a Korean study also confirmed that serum ALT levels were positively associated with MetS and its components (FPG, TGs, BP, and WC) [11], and we also found weak positive linear relationships between serum ALT levels and cardiometabolic risk factors (BMI, SBP, DBP, WC, FPG, and HS-CRP) in our study. Although the present study only included adults aged over 18, a nationwide study conducted in Iran indicated that MetS and some cardiometabolic risk factors were significantly associated with ALT levels in children and adolescents aged 7–18 years [30].

Although the mechanisms underlying the association between serum ALT levels and MetS are not entirely understood, a study from the Netherlands shed light on a possible mechanism. Insulin resistance acts as a major mediator of the association between the MetS and ALT level, while inflammatory adipokines, endothelial dysfunction, and nonesterified fatty acids also play minor roles but to a lesser extent [31]. ALT is a catalyzer that is involved in the transfer of the amino group of alanine to α -ketoglutarate [32], and a study from Argentina proposed that abnormal ALT levels are related to a dysregulation of normal amino acid metabolism in the liver, and aberrant liver metabolism could lead to MetS and insulin resistance [33]. Further studies are required to better clarify the pathophysiology.

5. Conclusions

In the present study, the overall prevalence of MetS was high in an indigenous population in Northern Taiwan, and higher serum ALT levels, especially those over 36 U/L, were associated with an increased risk of MetS. Further studies need to be performed with regard to this serious health problem in indigenous communities of Taiwan.

Abbreviations

MetS:	Metabolic syndrome
NCEP:	National Cholesterol Education Program Expert Panel
ATP III:	Adult treatment panel III
NAFLD:	Nonalcoholic fatty liver disease
SBP:	Systolic blood pressure
DBP:	Diastolic blood pressure
WC:	Waist circumference
ALT:	Alanine aminotransferase
FPG:	Fasting plasma glucose
HbA1c:	Glycated hemoglobin
HDL-C:	High-density lipoprotein cholesterol
HS-CRP:	High-sensitivity C-reactive protein
TC:	Total cholesterol
TG:	Triglyceride
BMI:	Body mass index
HTN:	Hypertension
DM:	Diabetes mellitus.

Data Availability

The data used to support the findings of this study are available from the corresponding author upon request.

Additional Points

Strengths and Limitations. A key strength of this study is that to the best of our knowledge, there were few community-based studies demonstrating the association between serum ALT levels and MetS, especially targeting the Northern Taiwan indigenous population. Furthermore, it demonstrated high prevalence of MetS and the positive association between baseline serum ALT levels and MetS in the Taiwan Atayal tribe. Accordingly, the result of the study enhanced the knowledge of the Northern Taiwan indigenous population in public health scopes and may improve the indigenous health-care in clinical practice. There were also four limitations in this study: first, the cross-sectional design inherently limited the ability to effectively determine the causal relationship between MetS and serum ALT levels. Second, the serum ALT is a sensitive marker for liver dysfunction and affected by heavy alcohol consumption [34] and some medications [35], but some of the study population had several risk factors, including hypertension and dyslipidemia. Hence, we could not eliminate the possible effect of underlying diseases and medications used for these diseases on the present findings. There was also no clear

personal history for viral hepatitis and NAFLD. Third, there were more female subjects than male subjects. The participants in the study were from three remote villages of Taoyuan City and had lived in these villages for over 6 months. The shift from rural low-wage labor to metropolitan higher-paying jobs reduced the available number of indigenous men in the mountain region. Fourth, there are selection bias and limited external validity in the study because the data were originated from 3 villages. Our study population just represented highland indigenous population in the northern part of Taiwan. Therefore, more comprehensive and meticulous consideration should be used in future studies. Further prospective population-based studies are needed to investigate the mechanisms in order to improve the above problems.

Disclosure

The manuscript was presented as a preprint according to the following link: “<https://www.researchsquare.com/article/rs-15642/v2>.”

Conflicts of Interest

The authors declare that there are no conflicts of interest regarding the publication of this paper.

Authors' Contributions

Yi-Fang Chen was involved in writing of the manuscript. Yen-An Lin, Wei-Chung Yeh, Yu-Chung Tsao, Wen-Cheng Li, Wei-Ching Fang, and I-Ju Chen provided opinions about the study designs and helped collect data. Jau-Yuan Chen contributed to, conceived, designed, and performed the experiments and collected and analyzed the data, revising it critically for important intellectual content and final approval of the version to be submitted.

Acknowledgments

The authors appreciate Chang Gung Memorial Hospital (grant nos. CMRPG3F0761, CMRPG3F0762, and CMRPG3F0763) for supporting this study.

References

- [1] K. G. Alberti, R. H. Eckel, S. M. Grundy et al., “Harmonizing the metabolic syndrome: a joint interim statement of the international diabetes federation task force on epidemiology and prevention; national heart, lung, and blood institute; American heart association; world heart federation; international atherosclerosis society; and international association for the study of obesity,” *Circulation*, vol. 120, no. 16, pp. 1640–1645, 2009.
- [2] A. S. Gami, B. J. Witt, D. E. Howard et al., “Metabolic syndrome and risk of incident cardiovascular events and death: a systematic review and meta-analysis of longitudinal studies,” *Journal of the American College of Cardiology*, vol. 49, no. 4, pp. 403–414, 2007.
- [3] C. Ding, Z. Yang, S. Wang, F. Sun, and S. Zhan, “The associations of metabolic syndrome with incident hypertension, type 2 diabetes mellitus and chronic kidney disease: a cohort study,” *Endocrine*, vol. 60, no. 2, pp. 282–291, 2018.
- [4] C. J. Yeh, H. Y. Chang, and W. H. Pan, “Time trend of obesity, the metabolic syndrome and related dietary pattern in Taiwan: from NAHSIT 1993–1996 to NAHSIT 2005–2008,” *Asia Pacific Journal of Clinical Nutrition*, vol. 20, no. 2, pp. 292–300, 2011.
- [5] W.-H. Pan, “The report of the nutrition and health survey in Taiwan (NASHIT) from 2013 to 2016,” 2019, https://www.hpa.gov.tw/Pages/ashx/File.ashx?FilePath=~/File/Attach/10443/File_11960.pdf.
- [6] Y.-C. Hsiao, K. Wang, and M.-J. Bair, “Prevalence of obesity and metabolic syndrome in aboriginals in southeastern Taiwan—a hospital-based study,” *Journal of Internal Medicine of Taiwan*, vol. 22, pp. 48–56, 2011.
- [7] C.-I. Ho, Y.-C. Tsao, J.-Y. Chen et al., “Gamma-glutamyl transpeptidase and the metabolic syndrome in a Taiwanese aboriginal population,” *International Journal of Diabetes in Developing Countries*, vol. 33, no. 3, pp. 147–154, 2013.
- [8] Z. Liu, S. Que, J. Xu, and T. Peng, “Alanine aminotransferase-old biomarker and new concept: a review,” *International Journal of Medical Sciences*, vol. 11, no. 9, pp. 925–935, 2014.
- [9] C. H. Chen, M. H. Huang, J. C. Yang et al., “Prevalence and etiology of elevated serum alanine aminotransferase level in an adult population in Taiwan,” *Journal of Gastroenterology and Hepatology*, vol. 22, no. 9, pp. 1482–1489, 2007.
- [10] C.-F. Lin, T.-J. Shiau, Y.-C. Ko, P.-H. Chen, and J.-D. Wang, “Prevalence and determinants of biochemical dysfunction of the liver in atayal aboriginal community of Taiwan: is betel nut chewing a risk factor?” *BMC Gastroenterology*, vol. 8, no. 1, p. 13, 2008.
- [11] S.-H. Lee, D.-Y. Cho, N.-S. Joo, K.-M. Kim, and K.-N. Kim, “The relationship of alanine aminotransferase to metabolic syndrome in a Korean population,” *The Turkish Journal of Gastroenterology*, vol. 29, no. 1, p. 52, 2018.
- [12] P. Wu, Q. Chen, L. Chen et al., “Dose-response relationship between alanine aminotransferase levels within the reference interval and metabolic syndrome in Chinese adults,” *Yonsei Medical Journal*, vol. 58, no. 1, pp. 158–164, 2017.
- [13] H. Sun, Q. Liu, X. Wang et al., “The longitudinal increments of serum alanine aminotransferase increased the incidence risk of metabolic syndrome: a large cohort population in China,” *Clinica Chimica Acta*, vol. 488, pp. 242–247, 2019.
- [14] S. K. Kunutsor and D. Seddoh, “Alanine aminotransferase and risk of the metabolic syndrome: a linear dose-response relationship,” *PLoS One*, vol. 9, no. 4, Article ID e96068, 2014.
- [15] M. O. H. A. W. Health Promotion Administration, R. O. C., “The criteria of adult metabolic syndrome 2007,” 2007, <https://www.hpa.gov.tw/Pages/Detail.aspx?nodeid=639&pid=1219>.
- [16] M. O. H. A. W. Health Promotion Administration, R. O. C., “BMI calculation,” https://health99.hpa.gov.tw/OnlinkHealth/Onlink_BMI.aspx.
- [17] W.-C. Yeh and S.-S. Chang, “Relationship between manual labor and metabolic syndrome in aboriginal community,” *Chinese Journal of Occupational Medicine*, vol. 23, no. 2, pp. 101–110, 2016.
- [18] C.-C. Lin, C.-S. Liu, M.-M. Lai et al., “Metabolic syndrome in a Taiwanese metropolitan adult population,” *BMC Public Health*, vol. 7, no. 1, p. 239, 2007.
- [19] H.-P. Huang, H.-Y. Hsu, T.-C. Chung, C.-A. Sun, C.-M. Chu, and T. Yang, “An investigation of metabolic syndrome indicators among different ethnic groups—a case study from a health screening in pingtung area,” *Taiwan Journal of Public Health*, vol. 27, no. 3, pp. 250–258, 2008.

- [20] S.-C. Juan, T. Awerbuch-Friedlander, and R. Levins, "Ethnic density and mortality: aboriginal population health in Taiwan," *Public Health Reviews*, vol. 37, no. 1, p. 11, 2016.
- [21] A. T. Cheng and W. J. Chen, "Alcoholism among four aboriginal groups in Taiwan: high prevalences and their implications," *Alcoholism: Clinical and Experimental Research*, vol. 19, no. 1, pp. 81–91, 1995.
- [22] I. Baik and C. Shin, "Prospective study of alcohol consumption and metabolic syndrome," *The American Journal of Clinical Nutrition*, vol. 87, no. 5, pp. 1455–1463, 2008.
- [23] Y. C. Ko, T. A. Chiang, S. J. Chang, and S. F. Hsieh, "Prevalence of betel quid chewing habit in Taiwan and related sociodemographic factors," *Journal of Oral Pathology & Medicine*, vol. 21, no. 6, pp. 261–264, 1992.
- [24] W.-F. Ma, C.-I. Li, E. R. Gritz, I. Tamí-Maury, C. Lam, and C.-C. Lin, "A symbol of connectedness between the self and the tribal home: betel quid in the lives of indigenous Taiwanese," *Hu Li Za Zhi the Journal of Nursing*, vol. 64, no. 3, pp. 65–73, 2017.
- [25] F.-M. Chung, D.-M. Chang, M.-P. Chen et al., "Areca nut chewing is associated with metabolic syndrome: role of tumor necrosis factor- α , leptin, and white blood cell count in betel nut chewing-related metabolic derangements," *Diabetes Care*, vol. 29, no. 7, p. 1714, 2006.
- [26] R. O. C. Council of Indigenous Peoples, "Economic status survey of indigenous peoples in Taiwan," 2014, https://srda.sinica.edu.tw/srda_freedownload.php?recid=703&fileid=204.
- [27] C.-M. Liao and C.-M. Lin, "Life course effects of socioeconomic and lifestyle factors on metabolic syndrome and 10-year risk of cardiovascular disease: a longitudinal study in taiwan adults," *International Journal of Environmental Research and Public Health*, vol. 15, no. 10, p. 2178, 2018.
- [28] H. F. Wu, T. Tam, L. Jin et al., "Age, gender, and socioeconomic gradients in metabolic syndrome: biomarker evidence from a large sample in Taiwan, 2005–2013," *Annals of Epidemiology*, vol. 27, no. 5, pp. 315–322.e2, 2017.
- [29] H. Shen, J. Lu, T.-T. Shi et al., "Correlation between normal range of serum alanine aminotransferase level and metabolic syndrome: a community-based study," *Medicine*, vol. 97, no. 41, Article ID e12767, 2018.
- [30] R. Kelishadi, M. Qorbani, R. Heshmat et al., "Association of alanine aminotransferase concentration with cardiometabolic risk factors in children and adolescents: the CASPIAN-V cross-sectional study," *Sao Paulo Medical Journal*, vol. 136, no. 6, pp. 511–519, 2018.
- [31] M. Jacobs, M. M. Van Greevenbroek, C. J. Van Der Kallen et al., "The association between the metabolic syndrome and alanine amino transferase is mediated by insulin resistance via related metabolic intermediates (the cohort on diabetes and atherosclerosis maastricht [CODAM] study)," *Metabolism*, vol. 60, no. 7, pp. 969–975, 2011.
- [32] J. M. Berg, J. L. Tymoczko, and L. Stryer, *Biochemistry*, W. H. Freeman and Company, New York, NY, USA <https://www.ncbi.nlm.nih.gov/books/NBK22475/>, 5th edition., 2002
- [33] S. Sookoian and C. J. Pirola, "Alanine and aspartate aminotransferase and glutamine-cycling pathway: their roles in pathogenesis of metabolic syndrome," *World Journal of Gastroenterology: WJG*, vol. 18, no. 29, pp. 3775–3781, 2012.
- [34] P. Alatalo, H. Koivisto, K. Puukka et al., "Biomarkers of liver status in heavy drinkers, moderate drinkers and abstainers," *Alcohol & Alcoholism*, vol. 44, no. 2, pp. 199–203, 2008.
- [35] E. Bjornsson, "Drug-induced liver injury in clinical practice," *Alimentary Pharmacology & Therapeutics*, vol. 32, pp. 3–13, 2010.

Research Article

Identification of Bioactive Components from *Ruellia tuberosa* L. on Improving Glucose Uptake in TNF- α -Induced Insulin-Resistant Mouse FL83B Hepatocytes

Jian-Hua Xu,¹ Yangming Martin Lo,² Wen-Chang Chang,³ Da-Wei Huang,⁴ James Swi-Bea Wu,⁵ Yu-Yuan Jhang,⁶ Wen-Chung Huang,⁷ Chih-Yuan Ko ,^{8,9,10,11} and Szu-Chuan Shen ⁶

¹Department of Tumor Surgery, The Second Affiliated Hospital of Fujian Medical University, Quanzhou 362000, China

²Institute for Advanced Study, Shenzhen University, Shenzhen 518060, China

³Department of Food Science, National Chiayi University, Chiayi City 60004, Taiwan

⁴Department of Biotechnology and Food Technology, Southern Taiwan University of Science and Technology, Tainan City 71005, Taiwan

⁵Graduate Institute of Food Science and Technology, National Taiwan University, Taipei 10672, Taiwan

⁶Graduate Program of Nutrition Science, National Taiwan Normal University, Taipei 10610, Taiwan

⁷Graduate Institute of Health Industry Technology, Chang Gung University of Science and Technology, Taoyuan 33303, Taiwan

⁸Department of Respiratory and Critical Care Medicine, The Second Affiliated Hospital of Fujian Medical University, Quanzhou 362000, China

⁹Department of Clinical Nutrition, The Second Affiliated Hospital of Fujian Medical University, Quanzhou 362000, China

¹⁰School of Public Health, Fujian Medical University, Fuzhou 350122, Fujian, China

¹¹Respiratory Medicine Center of Fujian Province, Quanzhou 362000, China

Correspondence should be addressed to Chih-Yuan Ko; yuanmomoko@gmail.com and Szu-Chuan Shen; scs@ntnu.edu.tw

Received 21 October 2020; Revised 11 November 2020; Accepted 18 November 2020; Published 1 December 2020

Academic Editor: Armando Zarrelli

Copyright © 2020 Jian-Hua Xu et al. This is an open access article distributed under the Creative Commons Attribution License, which permits unrestricted use, distribution, and reproduction in any medium, provided the original work is properly cited.

Ruellia tuberosa L. (RTL) has been used as a folk medicine to cure diabetes in Asia. RTL was previously reported to alleviate hyperglycemia, insulin resistance (IR), abnormal hepatic detoxification, and liver steatosis. However, the potential bioactive compounds of RTL have still not been identified. The aim of this study was to investigate the bioactive compounds in RTL ethyl acetate (EA) fractions by using a glucose uptake assay in TNF- α -treated mouse FL83B hepatocytes to discover a mechanism by which to improve IR. The bioactive compounds were identified by the high-performance liquid chromatography (HPLC) assay. Using the Sephadex LH20 gel packing chromatography column, the EAF5 fraction was isolated from RTL and significantly increased glucose uptake in TNF- α -treated FL83B cells. Moreover, the MCI gel packing chromatography column separated EAF5 into five subfractions and had no significant cytotoxic effect in FL83B cells when treated at the concentration of 25 μ g/ml. Among the subfractions, EAF5-5 markedly enhanced glucose uptake in TNF- α -treated FL83B cells. The possible bioactive compounds of the EAF5-5 fraction that were identified by the HPLC assay include syringic acid, *p*-coumaric acid, and cirsimaritin. The bioactive compound with the best effect of increasing glucose uptake was *p*-coumaric acid, but its effect alone was not as good as the combined effect of all three compounds of the EAF5-5 fraction. Thus, we speculate that the antidiabetic effect of RTL may be the result of multiple active ingredients.

1. Introduction

Type 2 diabetes mellitus (T2DM) is characterized by insulin resistance (IR), which is caused by insufficient production of insulin or by the ineffectiveness of insulin activity to maintain constant blood sugar. In response to hyperglycemia, the presence of high levels of blood sugar, the body compensatively secretes more blood insulin in increasing concentrations, causing hyperinsulinemia. Once the body presents hyperglycemia and hyperinsulinemia, it can be prone to many complications [1]. Diabetic control and therapy can consist of three parts, including dietary therapy, exercise, and medications. Unfortunately, most T2DM patients will depend on drug treatments, which have adverse side effects. Diabetic drugs have been reported to cause nausea, abdominal pain, or weight gain [2, 3]. Recently, researchers have turned to natural plant ingredients containing phenolic acids or flavonoids. Moreover, various ingredients have been proven to alleviate hyperglycemia or antidiabetic effects [4–6].

Ruellia tuberosa L. (RTL) is a herb plant that has been used as folk medicine to cure diabetes in Asian countries for decades. Our previous studies have demonstrated that RTL aqueous or ethanolic extracts can significantly improve glucose uptake in C2C12 myoblasts, alleviate the tumor necrosis factor (TNF)- α -induced IR in skeletal muscles, and ameliorate hyperglycemia, IR indices, and aorta dysfunction in high-fat-diet-fed streptozotocin-induced T2DM rats [7, 8]. Additionally, RTL ameliorated abnormal hepatic detoxification, nonalcoholic fatty liver disease, and lipid accumulation in the liver of T2DM rats [9, 10].

Previous studies have identified more than sixty compounds in RTL. The compounds obtained by separation and purification are mainly flavonoids, triterpenes, and steroids also containing long-chain fatty acids, alkaloids, and lignans [11–13]. However, there remains a void in the literature regarding the role of these potent RTL compounds alleviating hepatic glucose uptake. Therefore, we aimed to screen the best glucose uptake activity of TNF- α -induced IR in FL83B hepatocytes with ethyl acetate (EA) fractions of RTL by using thin-layer chromatography (TLC) and high-performance liquid chromatography (HPLC) to identify and characterize the specific potent compounds.

2. Materials and Methods

2.1. Preparation of RTL Extracts. The extraction protocol was based on our previous methods, with slight modifications [7, 9]. One gram of RTL stems and leaves were extracted with 6 ml distilled water and methanol (1 : 6, *w/v*) at 4°C for 72 h and filtered using a cheese cloth. The filtrate was filtered twice through a Whatman No. 1 filter paper and centrifuged at 7,000 \times g for 20 min. The supernatant was vacuum concentrated using a rotary evaporator below 40°C. The concentrated methanol extract was dissolved in 400 ml water and subsequently extracted with an equal volume of hexane and EA solvent, and the EA layers were divided through column chromatography using a Sephadex LH-20 column with 200 ml of 50–100% methanol sequentially. The different

fractions were then collected from the EA layer (EAF1 to EAF8). The best of glucose uptake hepatocytes of fractions was evaluated and screened, and the EAF5 fractions were divided through column chromatography using an MCI gel column with 200 ml of 20–100% methanol sequentially. The different fractions were then collected from the EAF5 layer (EAF5-1 to EAF5-5), as shown in Figure 1.

2.2. TLC. The supernatants were placed onto a silica gel precoated plate (Kieselgel 60 F254, 0.20 mm, Merck, Darmstadt, Germany). The TLC plates were added with a solvent mixture of dichloromethane : methanol : water : acetic acid (10 : 1 : 0.1 : 0.2, *v/v*), followed by immersion into 10% sulfuric acid, and then the mixture was heated. Using the color distribution state of TLC, similar effluents were gathered, and the solvent was drained through a rotary evaporator. Different concentrates were freeze-dried into a powder and kept at -80°C until use.

2.3. Cell Culture. The experiments were performed on FL83B mouse hepatocytes (ATCC, Rockville, MD, USA) incubated in F12K medium containing 10% fetal bovine serum (Invitrogen Corporation, Camarillo, CA, USA) in 10 cm Petri dishes at 37°C and 5% CO₂. The experiments were conducted on cells that were 80–90% confluent.

2.4. TNF- α Induction of IR in FL83B Cells. IR was induced according to a method described previously [7, 14]. FL83B cells were seeded in 10 cm dishes and incubated at 37°C for 48 h to reach 80% confluences. Serum-free medium containing recombinant mouse TNF- α and different RTL fractions (25 $\mu\text{g}/\text{ml}$) was incubated for 16 h at 37°C to induce IR.

2.5. Uptake of Fluorescent 2-[N-(7-Nitrobenz-2-oxa-1,3-diazol-4-yl) amino]-2-deoxy-d-glucose (2-NBDG) in FL83B cells. The FL83B cells were seeded in 10 cm dishes and then incubated at 37°C for 48 h to achieve 80% confluences. Serum-free medium containing 20 ng/ml recombinant mouse TNF- α was added before incubating for 16 h to induce IR. The cells were then transferred to another F12K medium containing 5 mm glucose, without (basal) or with 200 μm insulin and 10 μl different RTL fractions and incubated for 30 min at 37°C. An assay of glucose uptake was then performed as described previously [7]. The fluorescence intensity of the cell suspension was evaluated using flow cytometry (FACScan, Becton Dickinson, Bellport, NY, USA) at an excitation wavelength of 488 nm and an emission wavelength of 542 nm. Fluorescence intensity reflected the cellular uptake of 2-NBDG.

2.6. Chemical Profiles. The total phenolic and flavonoid contents of EA extracts were determined by the HPLC assay [15, 16]. Gallic acid, protocatechuic acid, vanillic acid, syringic acid, caffeic acid, sinapic acid, ferulic acid, *p*-coumaric acid, and cinnamic acid were chosen as standards for

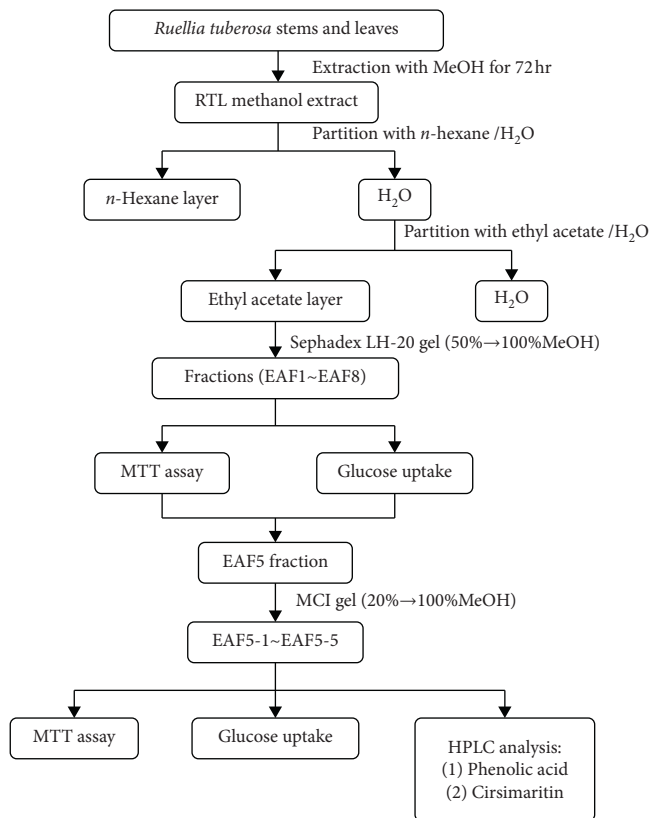


FIGURE 1: The flowchart for fractionation of *Ruellia tuberosa* Linn. (RTL) extraction.

phenols, whereas cirsimaritin was chosen as the standard for flavonoids. The samples (10 mg) were dissolved in 1 ml methanol and filtered through a 0.22 μm filter. The HPLC system was equipped with a diode array detector (Shimadzu, Kyoto, Japan) and Varian Polaris C18 column (5 μm , 250 mm \times 4.6 mm; Agilent, CA, USA). The injection volume was 10 μl with a flow rate of 1.0 ml/min. For the phenolic acid assay, the mobile phases were methanol (eluent A) and acetic acid (eluent B) in the following gradient elutions: 5% (A), 95% (B) in 0–5 min; 5%–20% (A), 95%–90% (B) in 5–10 min; 20%–40% (A), 90%–60% (B) in 10–20 min; 40%–60% (A), 60%–40% (B) in 20–30 min; and 60%–100% (A), 40%–0% (B) in 30–40 min. The samples were detected by a UV detector (280 nm). For the flavonoid assay, the mobile phases were methanol (eluent A) and acetic acid (eluent B) in the following gradient elutions: 50%–100% (A), 50%–0% (B) in 0–25 min. The samples were detected by using a UV detector (270 nm). The standards for phenolic acids and cirsimaritin (purchased from Sigma, St Louis, MO, USA) had a coefficient of determination (r^2) that was greater than 0.995.

2.7. Statistical Analyses. Values are presented as the mean \pm standard deviation using SPSS version 22.0 (SPSS Inc., Chicago, IL, USA) by one-way analysis of variance (ANOVA) and Duncan's new multiple range tests. $P < 0.05$ was considered statistically significant.

3. Results

3.1. Effect of Different EA Fractions from RTL on Glucose Uptake in FL83B Mouse Hepatocytes. The different RTL fractions from the EA layers (EAF1 to EAF8) were collected through TLC analysis (Supplementary Figure S1). When the concentration of each fraction was less than 25 $\mu\text{g/ml}$, the cell survival rate was greater than 80% and did not inhibit cell growth (Supplementary Figure S2). Thus, the concentration of 25 $\mu\text{g/ml}$ was used for the follow-up glucose uptake evaluation.

An evaluation of the 2-NBDG uptake was performed to assess the improvement of glucose uptake in FL83B hepatocytes. Compared with the TNF- α -treated group, the fluorescence content of the two fractions of EAF5 and EAF7 was significantly increased, and the fluorescence intensity was $93.3 \pm 5.4\%$ and $88.9 \pm 2.8\%$ ($P < 0.05$), respectively. The EAF5-treated group demonstrated the best improvement in glucose uptake in the IR-induced FL83B hepatocytes. Thus, EAF5 was used for the following examinations (Figure 2).

3.2. Effect of Different EAF5 Fractions from RTL on Glucose Uptake in FL83B Mouse Hepatocytes. The different EAF5 fractions (EAF5-1–EAF5-5) were collected through TLC analysis (Supplementary Figure S3). MTT assay showed that the optimal concentration was 25 $\mu\text{g/ml}$ for cell survival of EAF5 subfractions (Supplementary Figure S4). The EAF5-5 fraction significantly increased fluorescence intensity of hepatocytes ($108.4 \pm 7.7\%$), compared with the TNF- α -induced IR group ($P < 0.05$; Figure 3).

3.3. Bioactive Components of RTL. Nine standards of phenolic acid, including gallic acid, protocatechuic acid, vanillic acid, syringic acid, caffeic acid, sinapic acid, ferulic acid, *p*-coumaric acid, and cinnamic acid, and retention time (10.66, 17.15, 23.06, 23.66, 24.09, 27.70, 28.24, 28.78, and 35.27 min, respectively) are shown in Supplementary Figure S5. The standard of cirsimaritin was examined by HPLC, and the retention time was 16.91 min, detail shown in Supplementary Figure S6. EAF5-5 contains $27.3 \pm 1.4 \mu\text{g/g}$ syringic acid, $95.0 \pm 2.5 \mu\text{g/g}$ *p*-coumaric acid, and $805.5 \pm 24.8 \mu\text{g/g}$ cirsimaritin (Table 1).

3.4. Evaluation of Bioactive Components from RTL on Glucose Uptake in IR of FL83B Hepatocytes. The fluorescence intensity of syringic acid, *p*-coumaric acid, and cirsimaritin was $97.4 \pm 20.8\%$, $98.8 \pm 13.7\%$, and $87.1 \pm 4.3\%$, respectively, and among them, *p*-coumaric acid has the most significant ability to improve glucose uptake, which can increase by about 22%, compared with the TNF- α group ($P < 0.05$; Figure 4).

The fluorescence intensity of the three bioactive components mixed (the mixing ratio was equal to the ratio contained in EAF5-5) and EAF5-5 was $120.9 \pm 5.1\%$ and $118.1 \pm 16.5\%$, which were significantly increased by 45% and 42%, respectively, compared to the TNF- α group ($P < 0.05$; Figure 4).

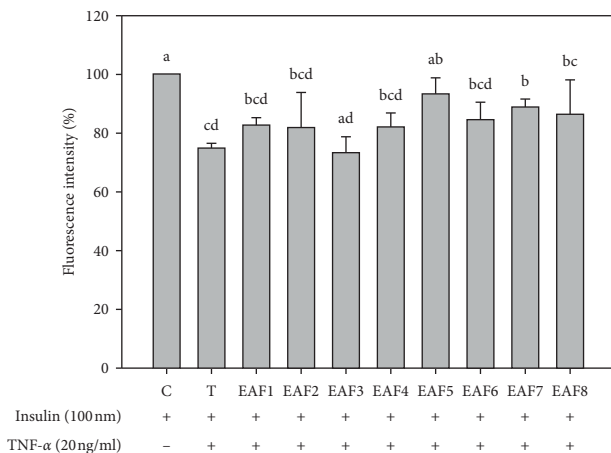


FIGURE 2: Effects of RTL-EA fractions on glucose uptake in mouse FL83B hepatocytes. Each value is mean \pm SD ($n = 3$). C (control): FL83B cells incubated with F-12K medium. T (TNF- α treatment): FL83B cells incubated with F-12K medium containing TNF- α (20 ng/ml) for 16 hours to induce insulin resistance. EAFs: TNF- α induced insulin resistance and then coincubated with RTL-EA fractions (25 μ g/ml) for 30 min. *Significantly different from control ($P < 0.05$).

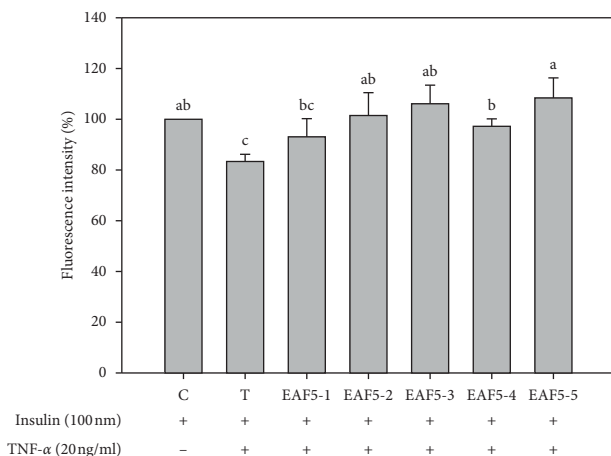


FIGURE 3: Effect of RTL-EAF5 fractions on glucose uptake in mouse FL83B hepatocytes. Each value is mean \pm SD ($n = 3$). C (control): FL83B cells incubated with F-12K medium. T (TNF- α treatment): FL83B cells incubated with F-12K medium containing TNF- α (20 ng/ml) for 16 hours to induce insulin resistance. EAF5s: TNF- α induced insulin resistance and then coincubated with RTL-EAF5 fractions (25 μ g/ml) for 30 min. *Significantly different from control ($P < 0.05$).

TABLE 1: Retention time and contents of phenolic acid and flavanoid from the RTL-EAF5 fraction.

Standard	Retention time (min)	EAF5-1 (μ g/g)	EAF5-2 (μ g/g)	EAF5-3 (μ g/g)	EAF5-4 (μ g/g)	EAF5-5 (μ g/g)
Phenolic acid						
Syringic acid	23.66	—	—	—	6.7 \pm 0.9	27.3 \pm 1.4
<i>p</i> -Coumaric acid	28.78	—	—	—	—	95.0 \pm 2.5
Flavanoid						
Cirsimaritin	16.91	—	—	—	—	805.5 \pm 24.8

—, not detected. Each value is mean \pm SD ($n = 3$).

4. Discussion

In this study, two columns, Sephadex LH-20 gel and MCI gel, were used to separate the bioactive components of the EA layer of RTL. The IR-induced FL83B hepatocytes model was used to screen out the distinguishing substances in the RTL that may improve glucose uptake, and then the active ingredients were identified by HPLC. Our results showed that in the first

chromatography column of the EA layer of RTL, the EAF5 fraction significantly increased the glucose uptake of liver cells that induce IR by TNF- α ; thus, EAF5 was selected for the second chromatography column. EAF5-5 demonstrated the best potential activity for improving cellular glucose uptake based on the activity evaluation of the three types of bioactive phenolic acid and flavonoid compounds—syringic acid, *p*-coumaric acid, and cirsimaritin—which were identified by

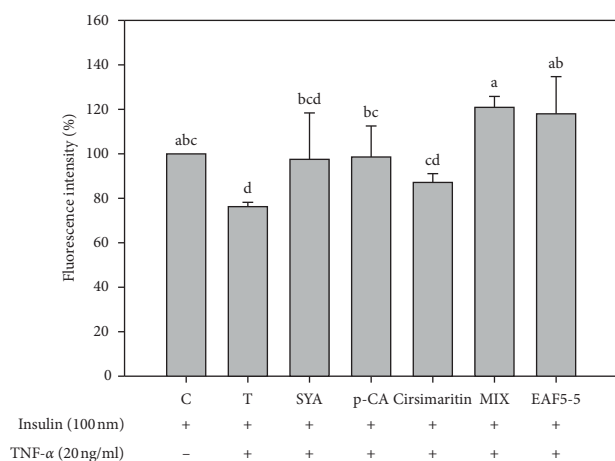


FIGURE 4: Effects of bioactive components in RTL on glucose uptake in mouse FL83B hepatocytes. Each value is mean \pm SD ($n = 3$). C (control): FL83B cells incubated with F-12K medium. T (TNF- α treatment): FL83B cells incubated with F-12K medium containing TNF- α (20 ng/ml) for 16 hours to induce insulin resistance. SYA: syringic acid; p-CA: *p*-coumaric acid; MIX: syringic acid + *p*-coumaric acid + cirsimaritin. *Significantly different from control ($P < 0.05$).

HPLC analysis. It has been suggested that phenolic compounds can significantly improve the activity of cellular glucose uptake, at least partially. Our results show that among the three active ingredients, *p*-coumaric acid is the most effective for increasing glucose uptake, but its effect is not as good as the combined activity of all three compounds and the EAF5-5 fraction.

An investigation of the cytotoxicity of the EA fractions in the cells was necessary before evaluating the cellular glucose uptake activity. In this study, when the concentration of all EA fractions from RTL was greater than 200 μ g/ml, it significantly inhibited cell growth in FL83B mouse hepatocytes. However, when the concentration was less than 25 μ g/ml of each fraction, the cell survival rate was more than 80%, which indicates that there was no significant inhibition of cell growth (Supplementary Figures S2 and S4). Hence, a concentration of 25 μ g/ml was used for each EAF fraction during the subsequent glucose uptake evaluation. Similarly, it was evident in our previous study that the concentration of RTL improved glucose uptake in mouse C2C12 myoblasts [7].

Administration of RTL fractions of n-hexane and EA in diabetic rabbits lowered the animals' blood sugar levels [17]. Moreover, the best antioxidant activity result was reported from an evaluation of RTL extraction using methanol and EA [18]. RTL fractions of EA can effectively improve the blood sugar level in diabetes through their antioxidant capacity, as EA fractions speculatively contain high amounts of polyphenols and triterpenoids [17]. Another study indicated that the active compound of the EA fraction may be a polyphenol called cirsimaritin [19]. Our findings seem to be consistent with the above studies.

In this study, two phenolic acids, syringic acid and *p*-coumaric acid, were identified by HPLC, which had not been identified from RTL in the past. Previously, vanillic acid was isolated from an RTL extraction utilizing EA [20]. However,

our present study did not identify vanillic acid from the fractions of RTL. It is speculated that when this compound cannot be identified, it is due to too little content or the extraction method that was used.

However, previous studies have confirmed that syringic acid and *p*-coumaric acid have many physiological activities, such as antioxidation, anticancer, and antibacterial [21–25]. Moreover, the effects of both of these compounds in treating diabetes have been demonstrated [26]. The administration of syringic acid in alloxan-induced diabetic rats for 30 days showed increased insulin, glycogen, glucose 6-phosphate dehydrogenase, and C-peptide contents, as well as decreased blood sugar, HbA1c, and glucokinase, which are associated with an improvement in diabetic symptoms. Additionally, in histopathological sections, syringic acid was found to reduce pancreatic damage caused by alloxan and stimulate β -cell regeneration, thus demonstrating its potential to treat diabetes [27, 28].

Yoon et al. [29] demonstrated that *p*-coumaric acid can improve IR and the lipid metabolism of skeletal muscle cells. The administration of *p*-coumaric (100 mg/kg BW) in streptozotocin-induced diabetic rats for 30 days can reduce the fasting blood glucose level and HbA1c, as well as increase the insulin level. In addition, *p*-coumaric has been found to have excellent antioxidant ability and can enhance the activity of antioxidant enzymes (catalase, superoxide dismutase, and glutathione peroxidase) of the kidney and liver [23].

Based on the above results, it is speculated that the two phenolic acids—syringic acid and *p*-coumaric acid—may be the active ingredients for the EAF5-5 fraction to improve glucose uptake in mouse FL83B liver cells and will therefore be developed into drugs or dietary supplements for the treatment of diabetes in the future.

On the other hand, flavonoids isolated from natural substances have been proven to have a variety of physiological effects, such as antioxidation, lowering blood lipids, or antidiabetics [30–32]. RTL contains a variety of flavonoids, such as cirsimaritin, cirsimarin, cirsiliol 4'-glucoside, sorbifolin, or pedalitin [13, 20]. At present, there are no animal experiments to explore the hypoglycemic effect of cirsimaritin, but cirsimaritin has been found in many natural products with antidiabetic properties [33, 34]. It is speculated that cirsimaritin may be one of the main active ingredients of flavonoids from the EAF5-5 fraction to improve the glucose uptake capacity of insulin-resistant FL83B hepatocytes.

In this study, three components (syringic acid, *p*-coumaric acid, and cirsimaritin) that were isolated from the EAF5-5 fraction were shown to improve cellular glucose uptake, with *p*-coumaric acid demonstrating the best effect. However, the increase in cellular glucose uptake is highest when all three compounds were used. We speculated that the hypoglycemic effect of RTL may be the result of multiple active ingredients. One theory has pointed out that if plants can be used to treat diabetes, then their effects can be multiplied by using them in higher concentrations and in combination with the chemical components that are contained in a variety of medicinal plants to cure diabetes

through distinct mechanisms [35]. Thus, the mechanisms by which RTL improves glucose uptake needs further study.

5. Conclusions

Sephadex LH20 gel and MCI gel were used to separate the EA layer of RTL. An evaluation of the glucose uptake in IR-induced FL83B hepatocytes showed that EAF5-5 demonstrated the best activity for improving cell glucose uptake. These activities were eventually linked by HPLC to two phenolic compounds—syringic acid and *p*-coumaric acid—and the flavonoid compound cirsimaritin. Among the three compounds that significantly improved the activity of cellular glucose uptake, *p*-coumaric acid was the active ingredient with the best effect of increasing glucose uptake although its effect was still not as good as the combined effect of all three compounds and the EAF5-5 fraction. Thus, we speculate that the antidiabetic effect of RTL may be the result of multiple active ingredients, but additional research is needed to confirm this.

Data Availability

All the data used to support the findings of this study are included within the article.

Conflicts of Interest

The authors declare that they do not have any conflicts of interest.

Authors' Contributions

SCS and CYK participated in the design of the study and wrote the protocol and the manuscript. YML participated in the design and discussion of the experiments and the writing of the manuscript. JHX analyzed the results and jointly wrote the manuscript. WCH and JSBW conducted literature searches. WCC, DWH, and YYJ carried out cell experiments as well as TLC and HPLC analysis.

Acknowledgments

The authors would like to thank the Ministry of Science and Technology of the Republic of China (ROC), Taiwan, for financially supporting this research under contract No. MOST 107-2320-B-003-004-MY3 and academic funding of the Second Affiliated Hospital of Fujian Medical University (serial No. BS201902). Special thanks are due to Professor Y. C. Huang of the Graduate Institute of Pharmacognosy at Taipei Medical University for his guidance in column chromatography analysis.

Supplementary Materials

Figure S1: thin layer chromatography of eight fractions from RTL-EA by Sephadex LH20 gel column chromatography. Figure S2: concentration effect of RTL-EA fractions on the cell viability of mouse FL83B hepatocytes. Figure S3: thin

layer chromatography of five fractions from RTL-EAF5 by MCI gel column chromatography. Figure S4: concentration effect of RTL-EAF5 fractions on the cell viability of mouse FL83B hepatocytes. Figure S5: HPLC chromatogram of phenolic acids from RTL-EAF5-5 fraction. Figure S6: HPLC chromatogram of RTL-EAF5-5 fraction. (*Supplementary Materials*)

References

- [1] American Diabetes Association (ADA), "Classification and diagnosis of diabetes: standards of medical care in diabetes-2020," *Diabetes Care*, vol. 43, no. 1, pp. S14–S31, 2020.
- [2] D. Sola, L. Rossi, G. P. C. Schianca et al., "State of the art paper Sulfonylureas and their use in clinical practice," *Archives of Medical Science*, vol. 4, no. 4, p. 840, 2015.
- [3] F. Alam, M. A. Islam, M. A. Kamal, and S. H. Gan, "Updates on managing type 2 diabetes mellitus with natural products: towards antidiabetic drug development," *Current Medicinal Chemistry*, vol. 25, no. 39, pp. 5395–5431, 2016.
- [4] S. Elavarasi, K. Saravanan, and C. Renuka, "A systematic review on medicinal plants used to treat diabetes mellitus," *International Journal of Pharmaceutical, Chemical and Biological Sciences*, vol. 3, no. 3, pp. 983–992, 2013.
- [5] A. N. M. Mamun-or-Rashid, M. S. Hossain, B. Naim Hassan, M. Kumar Dash, A. Sapon, and M. K. Sen, "A review on medicinal plants with antidiabetic activity," *Journal of Pharmacognosy and Phytochemistry*, vol. 3, no. 4, pp. 149–159, 2014.
- [6] A. N. Singab, F. S. Youssef, and M. L. Ashour, "Medicinal plants with potential antidiabetic activity and their assessment," *Medicinal and Aromatic Plant*, vol. 3, no. 151, pp. 2167–0412, 2014.
- [7] C.-Y. Ko, R.-H. Lin, Y.-M. Zeng et al., "Ameliorative effect of *Ruellia tuberosa* L. on hyperglycemia in type 2 diabetes mellitus and glucose uptake in mouse C2C12 myoblasts," *Food Science & Nutrition*, vol. 6, no. 8, pp. 2414–2422, 2018.
- [8] C. Y. Ko, R. H. Lin, Y. M. Lo et al., "Effect of *Ruellia tuberosa* L. on aorta endothelial damage-associated factors in high-fat diet and streptozotocin-induced type 2 diabetic rats," *Food Science & Nutrition*, vol. 7, no. 11, pp. 3742–3750, 2019.
- [9] W.-C. Chang, D.-W. Huang, J.-A. Chen, Y.-F. Chang, J. Swi-Bea Wu, and S.-C. Shen, "Protective effect of *Ruellia tuberosa* L. extracts against abnormal expression of hepatic detoxification enzymes in diabetic rats," *RSC Advances*, vol. 8, no. 38, pp. 21596–21605, 2018.
- [10] D. W. Huang, Y. M. Lo, W. C. Chang et al., "Alleviative effect of *Ruellia tuberosa* L. on NAFLD and hepatic lipid accumulation via modulating hepatic de novo lipogenesis in high-fat diet plus streptozotocin-induced diabetic rats," *Food Science & Nutrition*, vol. 8, no. 10, pp. 1–7, 2020.
- [11] C. Phakeovilay, W. Disadee, P. Sahakitpichan et al., "Phenylethanoid and flavone glycosides from *Ruellia tuberosa* L.," *Journal of Natural Medicines*, vol. 67, no. 1, pp. 228–233, 2013.
- [12] V. R. Mohan and K. Vasantha, "GC-MS analysis of bioactive components of tubers of *Ruellia tuberosa* L. (Acanthaceae)," *American Journal of Phytomedicine and Clinical Therapeutics*, vol. 2, no. 2, pp. 209–216, 2014.
- [13] M. N. Samy, S. Sugimoto, K. Matsunami, H. Otsuka, and M. S. Kamel, "Chemical constituents and biological activities of genus *Ruellia*," *International Journal of Pharmacognosy*, vol. 2, no. 6, pp. 270–279, 2015.
- [14] J.-J. Chang, M.-J. Hsu, H.-P. Huang, D.-J. Chung, Y.-C. Chang, and C.-J. Wang, "Mulberry anthocyanins inhibit

- oleic acid induced lipid accumulation by reduction of lipogenesis and promotion of hepatic lipid clearance,” *Journal of Agricultural and Food Chemistry*, vol. 61, no. 25, pp. 6069–6076, 2013.
- [15] T. Minh, D. Khang, P. Tuyen et al., “Phenolic compounds and antioxidant activity of phalaenopsis orchid hybrids,” *Antioxidants*, vol. 5, no. 3, p. 31, 2016.
- [16] M. F. Beer, F. M. Frank, O. Germán Elso et al., “Trypanocidal and leishmanicidal activities of flavonoids isolated from *Stevia satureiifolia* var. *satueiifolia*,” *Pharmaceutical Biology*, vol. 54, no. 10, pp. 2188–2195, 2016.
- [17] D. Shahwara, S. Ullah, M. Ahmad, S. Ullah, N. Ahmad, and M. A. Khan, “Hypoglycemic activity of *Ruellia tuberosa* linn (Acanthaceae) in normal and alloxan-induced diabetic rabbits,” *Indian Journal of Pharmaceutical Sciences*, vol. 7, pp. 107–115, 2011.
- [18] F.-A. Chen, A.-B. Wu, P. Shieh, D.-H. Kuo, and C.-Y. Hsieh, “Evaluation of the antioxidant activity of *Ruellia tuberosa*,” *Food Chemistry*, vol. 94, no. 1, pp. 14–18, 2006.
- [19] D. R. Wulan, E. P. Utomo, and C. Mahdi, “Antidiabetic activity of *Ruellia tuberosa* L., role of α -amylase inhibitor: *in silico*, *in vitro*, and *in vivo* approaches,” *Biochemistry Research International*, vol. 2015, Article ID 349261, 9 pages, 2015.
- [20] C. F. Lin, Y. L. Huang, L. Y. Cheng, S. J. Sheu, and C. C. Chen, “Bioactive flavonoids from *Ruellia tuberosa*,” *The Journal of Chinese Medicine*, vol. 17, no. 3, pp. 103–109, 2006.
- [21] O. Cikman, O. Soylemez, O. F. Ozkan et al., “Antioxidant activity of syringic acid prevents oxidative stress in l-arginine-Induced acute pancreatitis: an experimental study on rats,” *International Surgery*, vol. 100, no. 5, pp. 891–896, 2015.
- [22] S. H. Sharma, D. R. Chellappan, P. Chinnaswamy, and S. Nagarajan, “Protective effect of *p*-coumaric acid against 1,2 dimethylhydrazine induced colonic preneoplastic lesions in experimental rats,” *Biomedicine & Pharmacotherapy*, vol. 94, pp. 577–588, 2017.
- [23] M. DellaGreca, L. Previtera, R. Purcaro, and A. Zarrelli, “Cinnamic ester derivatives from *Oxalis pes-caprae* (Bermuda buttercup)#,” *Journal of Natural Products*, vol. 70, no. 10, pp. 1664–1667, 2007.
- [24] M. DellaGreca, A. Fiorentino, P. Monaco, L. Previtera, and A. Zarrelli, “A new dimeric 9,10-dihydrophenanthrenoid from the rhizome of *Juncus acutus*,” *Tetrahedron Letters*, vol. 43, no. 14, pp. 2573–2575, 2002.
- [25] M. DellaGreca, A. Fiorentino, M. Isidori, L. Previtera, F. Temussi, and A. Zarrelli, “Benzocoumarins from the rhizomes of *Juncus acutus*,” *Tetrahedron*, vol. 59, no. 26, pp. 4821–4825, 2003.
- [26] R. Vinayagam, M. Jayachandran, and B. Xu, “Antidiabetic effects of simple phenolic acids: a comprehensive review,” *Phytotherapy Research*, vol. 30, no. 2, pp. 184–199, 2016.
- [27] J. Muthukumaran, S. Srinivasan, R. S. Venkatesan, V. Ramachandran, and U. Muruganathan, “Syringic acid, a novel natural phenolic acid, normalizes hyperglycemia with special reference to glycoprotein components in experimental diabetic rats,” *Journal of Acute Disease*, vol. 2, no. 4, pp. 304–309, 2013.
- [28] S. Srinivasan, J. Muthukumaran, U. Muruganathan, R. S. Venkatesan, and A. M. Jalaludeen, “Antihyperglycemic effect of syringic acid on attenuating the key enzymes of carbohydrate metabolism in experimental diabetic rats,” *Biomedicine & Preventive Nutrition*, vol. 4, no. 4, pp. 595–602, 2014.
- [29] S.-A. Yoon, S.-I. Kang, H.-S. Shin et al., “*p*-Coumaric acid modulates glucose and lipid metabolism via AMP-activated protein kinase in L6 skeletal muscle cells,” *Biochemical and Biophysical Research Communications*, vol. 432, no. 4, pp. 553–557, 2013.
- [30] V. Amalan and N. Vijayakumar, “Antihyperglycemic effect of *p*-coumaric acid on streptozotocin induced diabetic rats,” *Indian Journal of Applied Research*, vol. 5, pp. 10–13, 2015.
- [31] X. Wang, Q. Liu, H. Zhu et al., “Flavonols from the *Camellia sinensis* var. *assamica* and their hypoglycemic and hypolipidemic activities,” *Acta Pharmaceutica Sinica B*, vol. 7, no. 3, pp. 342–346, 2017.
- [32] M. Abbas, F. Saeed, F. M. Anjum et al., “Natural polyphenols: an overview,” *International Journal of Food Properties*, vol. 20, no. 8, pp. 1689–1699, 2017.
- [33] E. G. E. Helal, N. Abou-Aouf, and A. S. M. Khatib, “A possible hypoglycemic and antioxidant effect of herbal mixture extraction in diabetic rats,” *The Egyptian Journal of Hospital Medicine*, vol. 58, pp. 109–119, 2015.
- [34] H. Y. Al Ati, G. A. Fawzy, A. A. El Gamal et al., “Phytochemical and biological evaluation of *Buddleja polystachya* growing in Saudi Arabia,” *Pakistan Journal of Pharmaceutical Sciences*, vol. 28, no. 4, pp. 1533–1540, 2015.
- [35] U. F. Ezuruike and J. M. Prieto, “The use of plants in the traditional management of diabetes in Nigeria: pharmacological and toxicological considerations,” *Journal of Ethnopharmacology*, vol. 155, no. 2, pp. 857–924, 2014.